AD NUMBER
AD338333
CLASSIFICATION CHANGES
TO: unclassified
FROM: confidential
LIMITATION CHANGES
TO: Approved for public release, distribution unlimited
FROM: Distribution authorized to DoD only; Administrative/Operational Use; JUN 1956. Other requests shall be referred to Armed Forces Special Weapons Project, Washington, DC.
AUTHORITY
3 Nov 1980, dna/doe per document marking; dna ltr 12 dec 1980

AD NUMBER

AD338333

CLASSIFICATION CHANGES

TO

confidential

FROM

secret

AUTHORITY

30 Jun 1967, DoDD 5200.10, GP-3

AD-338333

[redacted]

This document consists of 166 pages

No. 174 of 220 copies, Series A

AD-338333

OPERATION CASTLE

Project 6.2a

[redacted]

BLAST AND THERMAL EFFECTS ON B-36 AIRCRAFT IN FLIGHT

REPORT TO THE TEST DIRECTOR

G. C. Miller
and
E. J. Schlei
C. R. Andrews

June 1956

[redacted]

This [redacted] contains restricted data as [redacted] Atomic Energy Act of 1954. [redacted] for the disclosure of its [redacted] any manner to an unauthorized person is prohibited.

Classification (Cancelled) [redacted]
By Authority of [redacted]
By [redacted] Date 3 MAY 80

[redacted]

Aircraft Laboratory
Wright Air Development Center
Dayton, Ohio

[redacted]

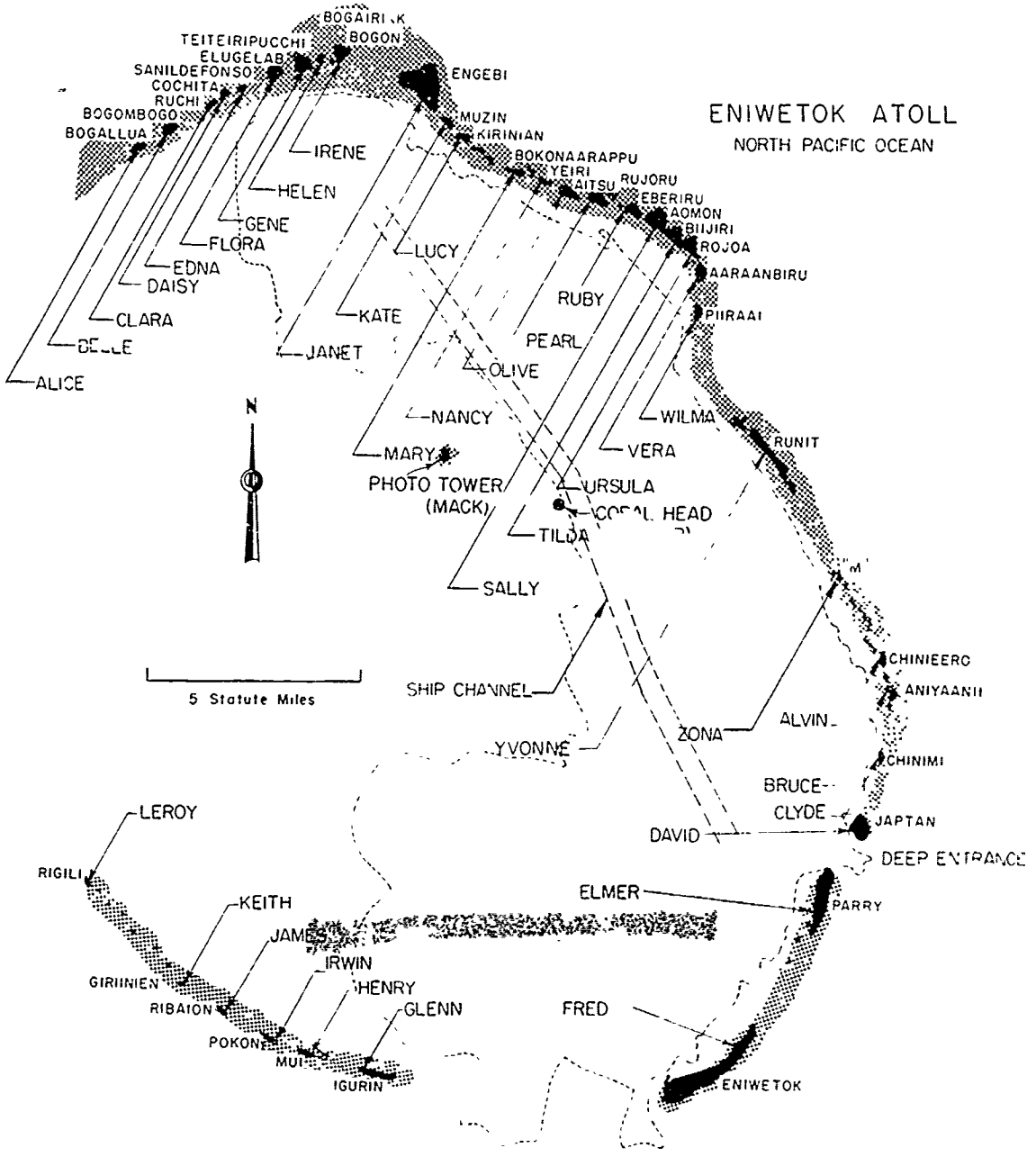
ENIWETOK ATOLL
NORTH PACIFIC OCEAN
BOGAIRIK
BOGON
TEITEIRIPUCCHI
ELUGELAB
SANILDEFONSO
COCHITA
RUCHI
BOGOMBOGO
BOGALLUA
ENGEBI
MUZIN
KIRINIAN
IRENE
BOKONAARAPPU
YEIRI
AITSU
RUJORU
EBERIRU
AOMON
BIJIRI
ROJOA
AARAANBIRU
PIIRAAI
HELEN
GENE
FLORA
EDNA
DAISY
CLARA
BELLE
ALICE
JANET
LUCY
KATE
RUBY
PEARL
OLIVE
NANCY
MARY
PHOTO TOWER
(MACK)
WILMA
VERA
URSULA
CORAL HEAD
TILDA
SALLY
RUNIT
N
5 Statute Miles
SHIP CHANNEL
YVONNE
ZONA
ALVIN
CHINIEERC
ANIYAANII
CHINIMI
BRUCE
CLYDE
JAPTAN
DAVID
DEEP ENTRANCE
LEROY
RIGILI
KEITH
ELMER
PARRY
JAMES
IRWIN
HENRY
GLENN
FRED
GIRIINIEN
RIBAION
POKON
MUI
IGURIN
ENIWETOK

GENERAL SHOT INFORMATION

	Shot 1	Shot 2	Shot 3	Shot 4	Shot 5	Shot 6
DATE	1 March	27 March	7 April	26 April	5 May	14 May
CODE NAME (Unclassified)	Bravo	Romeo	Koon	Union	Yankee	Nectar
TIME*	06:40	06:25	06:15	06:05	06:05	06:15
LOCATION	Bikini, West of Charlie (Namu) on Reef	Bikini, Shot 1 Crater	Bikini, Tare (Enimman)	Bikini, on Barge at Intersection of Arcs with Radii of 6900' from Dog (Yurochi) and 3 Statute Miles from Fox (Aomoen).		Eniwetok, IVY Mike Crater, Flora (Elugelab)
TYPE	Land	Barge	Land	Barge	Barge	Barge
HOLMES & NARVER COORDINATES	N 170,617 17 E 76,163.98	N 170,635 05 E 75,950.46	N 100,154 50 E 109,799 00	N 161,698 83 E 116,800 27	N 161,424 43 E 116,688,15	N 147,750.00 E 67,790 00

* APPROXIMATE

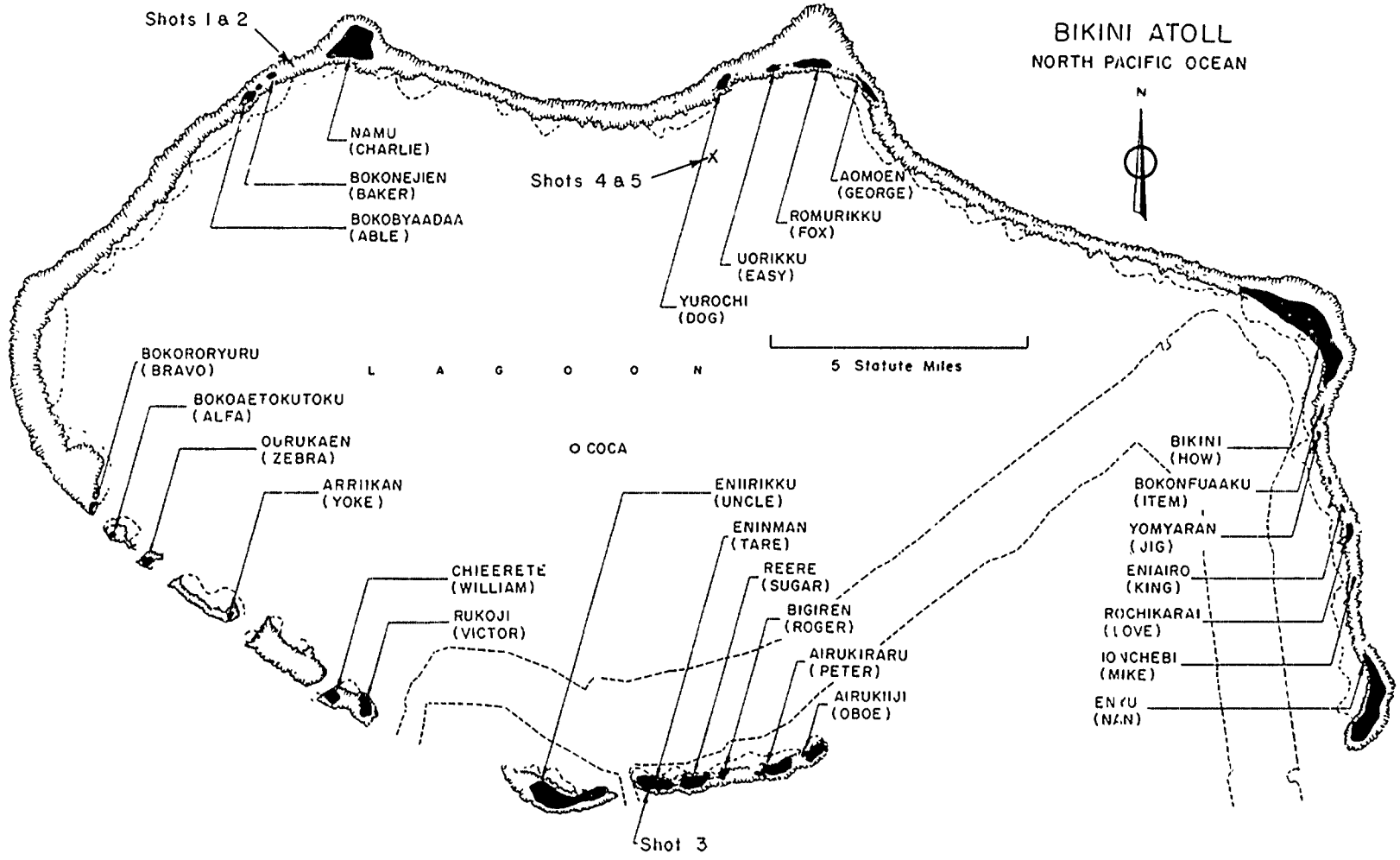
BIKINI ATOLL
NORTH PACIFIC OCEAN
N
Shots 1 & 2
Shots 4 & 5
NAMU (CHARLIE)
BOKONEJIEN (BAKER)
BOKOBYAADAA (ABLE)
AOMOEN (GEORGE)
ROMURIKKU (FOX)
UORIKKU (EASY)
YUROCHI (DOG)
5 Statute Miles
L A G O O N
BOKORORYURU (BRAVO)
BOKOAETOKUTOKU (ALFA)
OURUKAEN (ZEBRA)
ARRIIKAN (YOKE)
O COCA
ENIIRIKKU (UNCLE)
ENINMAN (TARE)
REERE (SUGAR)
BIGIREN (ROGER)
AIRUKIRARU (PETER)
AIRUKIIJI (OBOE)
CHIEERETE (WILLIAM)
RUKOJI (VICTOR)
Shot 3
BIKINI (HOW)
BOKONFUAAKU (ITEM)
YOMYARAN (JIG)
ENIAIRO (KING)
ROCHIKARAI (LOVE)
IONCHEBI (MIKE)
ENYU (NAN)

3

ABSTRACT

Project 6.2a was established to determine the responses of a B-36 aircraft to the effects of a nuclear detonation at levels approaching the thermal and blast limitations of the aircraft. The data obtained were used to verify, and to modify where necessary, the theoretical techniques used to predict the B-36 responses. Accurate prediction methods are essential for the determination of the maximum delivery capabilities of the B-36.

A B-36D aircraft was instrumented and flown in the vicinity of each of the six shots of the CASTLE sequence. Time-history input and response measurements constituted the main instrumentation effort. For the first five shots, the aircraft was positioned at predicted near-limiting inputs in a simulated delivery configuration, that is, flying away from the explosion. On Shot 6, the aircraft was headed toward the explosion to obtain initial experimental data for this orientation.

On five of the shots, the yields of the detonations were such that good results were obtained; the unexpected low yield of Shot 3 provided no useful information. Shot 5 provided the highest thermal and gust loading responses experienced by the aircraft, these being 64 per cent and 76 per cent of the theoretical safe limits for thermal and blast, respectively. One hundred per cent of the limiting overpressure was attained on Shot 1 resulting in significant damage to the sheet metal components of the aircraft. In addition to the measured data, together with photographs and descriptions of the damage, this report contains pertinent observations as reported by the flight crew.

Sufficient data were obtained to fulfill the specific objective of the project. A comparison between the experimental data and theoretically-predicted responses is made in the Discussion.

In addition, the data and information obtained from this experiment should be useful to agencies exploring the problems of capabilities, vulnerabilities, or lethalities of other aircraft with respect to the effects of a nuclear detonation.

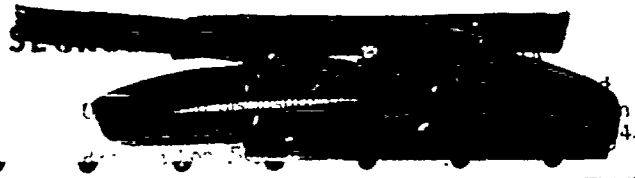

FOREWORD

This report is one of the reports presenting the results of the 34 projects participating in the Military Effects Tests Program of Operation CASTLE, which included six test detonations. For readers interested in other pertinent test information, reference is made to ITR-934, Summary of Weapons Effects Tests, Military Effects Program. This summary report includes the following information of possible general interest.

a. An over-all description of each detonation, including yield, height of burst, ground zero location, time of detonation, ambient atmospheric conditions at detonation, etc., for the six shots.
b. Discussion of all project results.
c. A summary of each project, including objectives and results.
d. A complete listing of all reports covering the Military Effects Test Program.

PREFACE

This publication is the final report of Project 6.2a, Operation CASTLE. The data and information pertain, for the most part, to specific exposures of a B-36D aircraft to the effects of several nuclear detonations. Caution should be exercised in applying these data to other types of aircraft and conditions of exposure. The theories and equations presented here are those utilized for this particular experiment and may not necessarily represent current or future thinking in this field. For detailed application of the data, the reader is referenced to WADC Technical Note, WCLS-55-10, entitled Data Results, Project 6.2a, Operation CASTLE, which contains graphical representations of the measured data in which the minute variations of the functions are depicted with a high degree of definition.

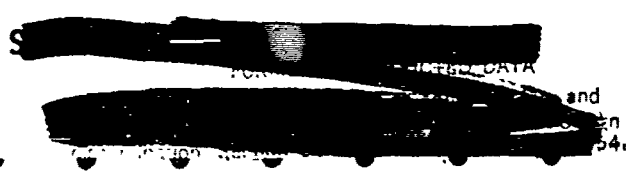

ACKNOWLEDGEMENTS

In presenting a report of the results of a project with the scope and magnitude of Project 6.2a, it cannot be overemphasized that the success that was achieved may be attributed to a vast amount of coordinated effort and cooperation by many organizations and many individuals. Specifically acknowledged in the following paragraphs are the direct contributions of a few of these individuals and groups.

Col. L. E. Richardson, commander of the SAC Test Detachment for maintenance and flight operations, whose personalized interest in the project contributed to the successful completion of the planned participation.

Lt. Col. G. J. Savage, aircraft commander and his crew, for the intense interest and effort given in attaining the desired positions in space at the moment of detonation.

Lt. Col. D. I. Prickett, Director of Program 6, through a consistent understanding of the project background and objectives, contributed the extra effort required to successfully complete the test missions.

Dr. W. B. Plum and Mr. R. P. Day, representatives of Naval Radiological Defense Laboratory, for the many hours of work put forth in support of the project thermal measurements.

The San Antonio Air Materiel Area at Kelly Air Force Base while conducting a major overhaul of the aircraft gave indispensable help to the University of Dayton instrumentation crew.

The cooperation of the Consolidated Vultee Aircraft Corporation at Fort Worth in supplying advice and data as required and in accepting the delicate problem of calibrating a radioactive aircraft was greatly appreciated.

Finally, the authors wish to express their special indebtedness to all members of Project 6.2a and, in particular, to Capt. W. R. Lounsbery, the Assistant Project Officer; Mr. J. R. Westerheide, the University of Dayton Project Engineer; and Messrs. G. W. Mills, W. J. Hovey and D. H. Whitford, for significant contributions to the project.

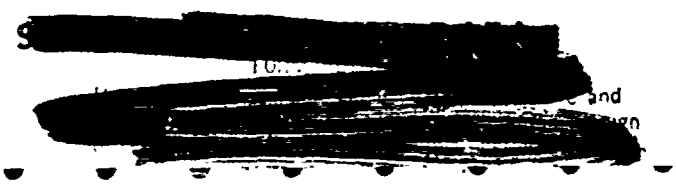

CONTENTS

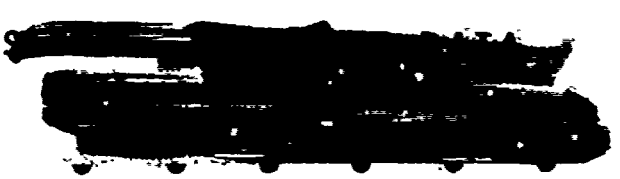

TABLES

APPENDIX A

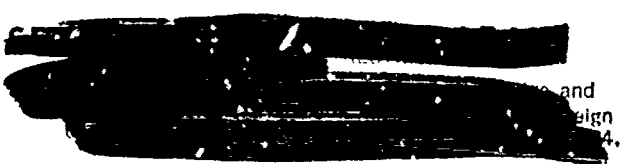

[redacted]

CHAPTER 1

OBJECTIVE

The studies conducted by Project 6.2a in Operation CASTLE are a part of the Wright Air Development Center's (WADC) research and development program devoted to the study of nuclear-weapon effects on aircraft systems. This program has as its ultimate objective the establishment of operational and design criteria concerning nuclear-weapon effects for present-day and future aircraft. The effective use of existing aircraft is dependent on knowledge of the effects of nuclear radiation and of thermal and blast properties of atomic explosions on the aircraft. The destructive power of the warhead may limit the delivery capabilities of bomber aircraft if the aircraft is to escape serious damage. In like manner, fighters, transports, liaison, and other aircraft may be restricted in their operations near the scene of an atomic detonation. A knowledge of the effects of atomic detonations on aircraft is also useful in specifying modifications of current aircraft, as well as in designing aircraft of the future, so that they will be less vulnerable to atomic explosions. Thus, the capabilities of aircraft of the United States Air Force will continue to be maintained for the performance of any required mission.

The specific objective of this project was to determine the responses of a B-36 aircraft to a nuclear detonation at response levels approaching the thermal and blast limitations of the aircraft and, in this manner, to assist in defining the most-powerful weapon that could be dropped from a B-36 type aircraft and detonated without serious danger to the aircraft.

[redacted]

CHAPTER 2

BACKGROUND AND THEORY

2.1 BACKGROUND

The effects of a bomb detonation upon aircraft have been a matter for consideration by military organizations since the initial use of aircraft by the Armed Forces but not a matter of paramount importance until the creation of new problem areas by the successful development of nuclear and thermonuclear weapons. A thorough knowledge and understanding of all the parameters associated with the effects of a nuclear detonation, as related to both parked and in-flight aircraft, are essential for the proper design of current and future aircraft, as well as for the intelligent planning of modern military tactics. One phase of this overall problem with regard to in-flight aircraft is the effect of a bomb explosion on the delivery aircraft. Prior to Operation IVY, aircraft design and performance were advanced to such a state with respect to the destructive power of bombs that the aircraft could escape the danger region for any type and size of explosive load that the aircraft could carry. The far-reaching destructive ability of high-yield nuclear devices reduced the altitude-speed advantage of aircraft; thus, the problem of bomb delivery assumed profound importance.

The agency responsible for the determination of nuclear-weapon effects on aircraft systems for the Air Force is the Wright Air Development Center of the Air Research and Development Command. As early as 1946, WADC participated in the atomic tests of Operation CROSSROADS, where a limited amount of vertical-acceleration data were obtained. In 1948, four drone aircraft were instrumented for structural response data and flown during Operation SANDSTONE. The principal value of these data was the indication of the magnitude and nature of the problems involved. In 1949, WADC contracted the Massachusetts Institute of Technology (MIT) to conduct theoretical studies concerning aircraft structural response to the loads imposed by the shock wave. With planning based on the preliminary work of the MIT group, extensive ground and air instrumentation programs were undertaken by WADC during Operation GREENHOUSE in the spring of 1951. The data obtained indicated an urgent need for additional studies and experiments, especially in the field of response to thermal energy. The University of California at Los Angeles

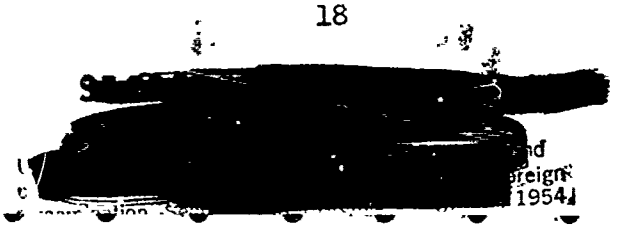

(UCLA) was contracted by WADC to study the thermal problem. In 1952, WADC contracted Allied Research Associates, Inc. (ARA) to correlate the experimental effects data with the results of the studies of MIT and UCLA. Participation in Operation IVY in the fall of 1952 provided the first experimental data on the effects of high-yield nuclear explosions on in-flight aircraft, viz., a B-36D and a B-47B. The effects on aircraft were studied further by the participation of both ground and air programs in the relatively low-yield atomic tests of Operation UPSHOT-KNOTHOLE in the spring of 1953. The ground program was concerned primarily with basic research on thermoelastic response and on the coupling effects of the two primary inputs, thermal and blast; the air program utilized the B-36D and one B-50 aircraft to obtain blast-response data and thermal inputs.

The B-36D was flown during Operation CASTLE to obtain data on both thermal and blast responses at input levels approaching the design limits of the aircraft, and is the subject of this report.

Additional background information can be obtained from reports written by agencies that have contributed to the overall objective; some of these reports are listed in references 1 through 5.

2.2 THEORY

In order to comprehend the usefulness of the data obtained during CASTLE, it is necessary to consider the theoretical aspects of a nuclear detonation and the effects on aircraft flying near the explosion. Much has been written on the subject; however, it is beyond the scope of this report to present a complete summary of the work that has been done. Nevertheless, an attempt will be made in the following paragraphs to present the more-important considerations. It should be realized that procedures set forth in this chapter were the best available prior to Operation CASTLE and that some of the methods have been superseded by more recent evaluations.

Nuclear detonations are characterized by the sudden release of energy involving many different phenomena, the most important of which, with respect to aircraft, are nuclear and thermal radiations and an air-blast wave.

2.2.1 Nuclear Radiation

Nuclear radiation is produced in a variety of forms by a nuclear detonation. With regard to the immediate effects on an aircraft and, in particular, the effects on the human occupants of an aircraft, the most-important part of the nuclear radiation is gamma-ray exposure. Although there is considerable variation among individuals insofar as sensitivity to nuclear radiation is concerned, it is generally accepted that the human body can withstand a dose of 25 roentgen equivalents without obvious injury.

An aircraft and its occupants may be contaminated by proximity to the explosion at burst time, by envelopment in the radioactive cloud that rises rapidly after the explosion, or by contact with the radioactive material from the atomic cloud. At ranges critical for a B-36

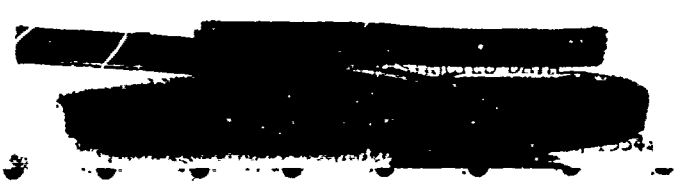

with regard to thermal and blast effects of weapons in the MT yield category, it has been shown that nuclear radiation effects, due to proximity to the explosion at burst time, are negligible. Previous experience and a preliminary evaluation of available data indicate that radiation danger due to envelopment and fall-out of the cloud is not a serious problem for the B-36 at ranges where thermal and blast effects are limiting.

2.2.2 Thermal Radiation

The fireball produced by a nuclear explosion radiates thermal energy in all directions. The irradiance varies with time and is characterized by a fast rise to a peak value followed by a relatively slow decrease to zero. The effective duration of the thermal irradiance varies with the yield. For 10 MT bombs this time is approximately 15 seconds. Radiant exposure is the energy per unit area that reaches a receiver as a result of a detonation. In equation form, considering only specular transmittance:

$$Q = C \frac{W}{D^2} e^{-kD} \qquad (2.1)$$

where Q = radiant exposure on a surface normal to the radiation, cal/sq cm,
W = total yield of source, KT,
k = atmospheric attenuation coefficient, $(\text{kilofeet})^{-1}$,
D = distance between source and receiver, kilofeet,
C = constant.

Since W is the total yield, that fraction of the total yield that appears as thermal energy must be known and included in the constant C. The thermal yield is accepted as being approximately a third of the total yield, but this figure is subject to a degree of uncertainty.

The equation, as given, does not include that energy received which is due to the reflectivity of clouds, water, and the earth's surface and to the back-scattering properties of the atmosphere. The energy lost due to selective absorption in the infrared by water vapor and carbon dioxide is also neglected. These effects are not negligible but are difficult to evaluate.

For radiant exposure predictions during CASTLE, the following formula, a modification of equation 2.1, was used.

$$Q = 36 \frac{W^{0.94}}{D^2} e^{-0.008D} \qquad (2.2)$$

The constants 36 and 0.008 were based upon unpublished correlation by UCLA, ARA, and WADC of thermal and attenuation measurements made by UCLA and ranges determined by WADC during IVY. The constant 0.94 was based upon an analysis by Streets and described in reference 6. Since November 1954 the method utilized by WADC to predict thermal inputs is

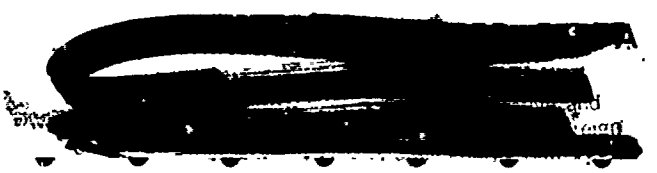

that derived by Chapman and Seavey and presented in reference 7.

2.2.3 Thermal Effects

The thermal effects on an aircraft can be classed as structural or nonstructural. An example of a structural effect is the reaction of a skin-stiffener-type panel when the outside skin surface is irradiated. Temperature gradients exist between the skin and the stiffener, and the resulting restrained expansion produces compressive stresses in the skin and tensile stresses in the stiffener. If the effect is severe, material failure will result, and/or permanent buckling of the skin will destroy its aerodynamic properties.

Nonstructural effects include the burning, melting, or deforming of such components as electrical wiring insulation, paint, and articles made of Fiberglas, rubber, or fabric. The effects of radiant exposure upon occupants of the aircraft may also be placed in this category. While these effects in themselves are usually not serious, they might bring about serious situations. However, as a general rule, such relatively simple steps as insulating, increasing the reflectance, or shielding can be taken to minimize the thermal effects on nonstructural items.

The relationship between the temperature rise of thin skin and radiant exposure is given by the equation

$$\Delta T \quad \frac{Q \alpha L \cos i}{\rho C_p t} \tag{2.3}$$

where ΔT = change in temperature, degrees F,

α = absorptivity coefficient,

i = incidence angle, i.e., the angle between the source-target line and a line normal to the skin surface,

L = heat loss factor,

ρ = density, lb/cu ft,

C_p = specific heat, BTU/lb/°F,

t = skin thickness, ft.

The absorptivity coefficient, that fraction of the total incident thermal energy that is not reflected (or transmitted), is dependent upon the color and degree of irregularity of the metal surface, and the color, thickness, adhesiveness, and heat-transfer properties of the paint or protective covering or of any coating, such as an oil film, resulting from engine operation.

The heat-loss factor represents that part of the absorbed energy lost by radiation, convection, and conduction, which is, therefore, ineffective in raising the temperature of the skin. In reference 8, UCLA reports that radiation losses are small compared to convection losses. For CASTLE, therefore, convection was considered to have the most significance in the heat-loss factor. The technique of correcting for convection losses is based upon the procedure utilized by UCLA in references 8 and 9. This procedure considers convection losses as influenced by air-flow rate or velocity of the aircraft, air density, effec-

tive length of the thermal phase as defined by the time to peak intensity, chordwise position of the area in question, and thermal properties of the material. Conduction losses are those resulting from the transfer of energy from the irradiated sheet to the supporting structure through the area of physical contact. Conduction losses are intimately associated with the stresses set up in the entire assembly, since the temperature gradients result in uneven thermal expansion.

Although the equations stating the temperature gradients and the thermal stresses in a theoretical structure are well known, the solution of a practical problem is made difficult and laborious by many variables and computations. Extensive analyses by UCLA, with consideration of addition of flight loads to those induced by the restrained expansion and of the decrease of allowable material stress with an increase in temperature, have shown that the sheet-stringer type of construction, as used on the wing, stabilizer, and fuselage of the B-36, is less critical than permanent skin buckling of the "hat" and "waffle" panels used on the elevator and wing trailing edges. The effects on these bonded-metal panels were determined by experimental furnace testing after a theoretical solution appeared impractical; in particular, it was determined that a maximum skin temperature rise of 400°F caused definite, visible, permanent buckling of such magnitude as to be considered marginal. By calculations, it was shown that the irradiant exposure required to achieve a 400°F rise in bonded-metal panels was less than that required to induce critical stresses in sheet-stringer panels. Therefore, the limiting thermal response factor for the B-36D for CASTLE was a 400°F rise of skin temperature of the 0.020-in. magnesium "hat" panels of the elevator.

2.2.4 Blast Wave

Rapid expansion of the fireball produced by a nuclear explosion initiates a pressure wave in the surrounding atmosphere that is propagated outward through space at a speed somewhat greater than the speed of sound. Characteristics of this wave (in free air) include a sharp rise to its peak positive pressure (the shock front), followed by a relatively slow decrease of pressure through the initial or ambient value to a negative (below ambient) minimum of approximately a third of the peak positive value, and finally a slow return to ambient conditions. The difference between the transient pressure values of the blast wave and ambient pressure is called overpressure. For CASTLE, peak overpressures were predicted by means of the following empirical equation, derived primarily from data obtained during Operation UPSHOT-KNOTHOLE:

$$\Delta P = 31.3 \frac{W^{1/3}}{R} \left[\log_{10}\left(\frac{R}{W^{1/3}} \right) - 0.88 \right]^{-\frac{1}{2}} \qquad (2.4)$$

where ΔP = peak overpressure, psi,
W = yield, lb TNT equivalent,

$$R = \frac{\text{Slant range, ft}}{\left(\frac{\rho_h a_h}{\rho_b a_b}\right)^{\frac{1}{2}}}$$

ρ = air density

a = speed of sound, fps,

subscript h = altitude of the measurement,

subscript b = burst altitude.

This equation is used only for overpressures less than 2 psi and is based upon an equation developed by Hirschfelder, Littler, and Sheard (see reference 10) for TNT charges and modified by MIT and ARA to fit a data analysis by Lampson (see reference 11).

A second important property of the blast wave is the material or gust velocity, the wind or air movement behind the shock front. The magnitude of the material velocity is a function of the ratio of overpressure to ambient pressure, and its direction is assumed to be the same as the direction of propagation of the shock front for positive overpressures but the opposite for negative overpressures.

Based on the Rankine-Hugoniot relation, the equation used to predict material velocity was

$$w = 1.89\, a_h \frac{\Delta p}{p_h} \left(6 - 7\frac{\Delta p}{p_h}\right)^{-\frac{1}{2}}, \qquad (2.5)$$

where w = material velocity, fps,

a_h = speed of sound, fps, at measurement altitude,

Δp = peak overpressure, psi,

p_h = ambient atmospheric pressure, psi, at measurement altitude.

2.2.5 Blast Effects

The main consequences of the blast wave are the crushing effect associated with a difference in pressure and the change in lift resulting from the sharp-edged gust (material velocity). Consider an aircraft enveloped by the blast wave. The overpressure imposes a crushing load on the external covering, or secondary structure, of the entire aircraft, especially on those surfaces facing the shock front (where the pressures are higher due to wave reflections). At the same time, the moving air, or material velocity, upsets the steady-state aerodynamic conditions by changing the direction and magnitude of the airstream. The resulting variations of the lift and drag forces cause considerable bending of the wing, stabilizer, and aft fuselage as the loads are transmitted to the center of gravity of the aircraft. In this manner, the primary aircraft structure is affected by the blast wave.

Knowledge of the effects of overpressure loading was obtained from small-scale TNT explosions and from the parked-aircraft program of Operation TUMBLER-SNAPPER. Consolidated Vultee Aircraft Company performed a detailed analytical study on the overpressure effects on a B-36 and supplemented the analysis with data obtained from exposure of

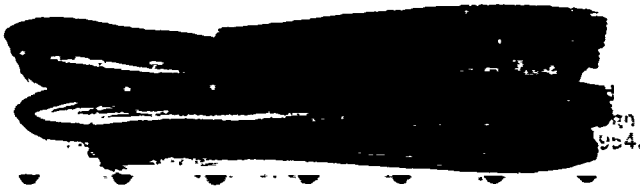

a B-36 stabilizer and elevator assembly during Operation UPSHOT-KNOTHOLE. As a result of these investigations, a critical overpressure criteria of 0.8 psi was established for the B-36. This value was considered to be the maximum overpressure that could be absorbed by a B-36 with a negligible amount of sheet-metal damage.

The effects of the material velocity on an aircraft are similar to its response to the sharp-edged gusts studied during the original design of an aircraft. Because of the material velocity, the changes in the angle of attack or the relative airspeed of the lifting surfaces alter the aerodynamic loads and disturb the equilibrium conditions. As the aircraft "rolls with the punch," the loads imposed by the material velocity are alleviated to a certain extent by the bending of the aircraft structure and the displacement of the entire aircraft; however, additional stresses are created due to the inertial properties of the wings, empennage, and fuselage. The study of the aircraft behavior under conditions such as these involves a rather thorough dynamic analysis. Although the method of analysis is well known due to the sharp-edged gust investigations, the calculations are laborious and time-consuming. Simplification is feasible for a study of wing deflection only, but more thorough analyses must be made for the stabilizer and the fuselage. Some of the factors that must be considered during an analysis of the stabilizer or fuselage are the effects of the wing responses on the tail, unsteady wing downwash, and fuselage flexibility. The problem is treated in detail in references 2 and 12; a summary is given in reference 1.

Operation IVY results indicate that for the B-36 in a "tail-to" attitude at shock arrival, the horizontal stabilizer and aft fuselage reactions to the material velocity are far more critical than wing bending, thus limiting the delivery capabilities of the bomber.

For CASTLE, the material velocity that produced limit bending (two thirds of ultimate bending) on the horizontal stabilizer was defined as the critical material velocity. The actual value of material velocity in ft/sec required to load the stabilizer to limit cannot be determined unless the aircraft altitude, horizontal range from ground zero, airspeed, gross weight, and center-of-gravity location are specified. A typical value of critical material velocity for the conditions that existed during Shot 5 of the CASTLE series is 138 ft/sec, which corresponds to 0.60 psi overpressure.

2.2.6 Danger Region Diagrams

When planning the participation of an aircraft in an atomic test, it is convenient to depict the limiting parameters pertaining to any one set of test conditions in a graphical form. In this way the critical effect is readily apparent, and changes in flight parameters which might be made in order to realize various combinations of all the effects can be studied and determined. Such a graph is called a Danger Region Diagram and is constructed with ground range and altitude as the abscissa and ordinate, respectively. It shows the boundaries of regions within which critical damage will result from the various effects of a nuclear explosion under a given set of conditions which include type of

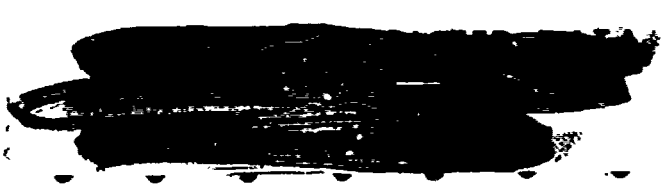

aircraft, weapon yield, and aircraft flight configuration.

Figure 2.1 is a Danger Region Diagram for a B-36D aircraft exposed to an explosion of 12-MT yield with flight parameters as indicated. In viewing the figure, two facts should be recalled: (1) thermal energy is propagated at the speed of light and (2) the blast wave is propagated at a speed approximately that of the speed of sound. As a result of this difference in propagation speeds, the thermal and blast effects on a B-36 at near-limiting ranges are well separated in time. For the conditions of Fig. 2.1, the length of time between burst and shock arrival is approximately 55 sec, during which time the aircraft has traveled, horizontally, on the order of 30,000 ft. With this time difference in mind, it is apparent that Fig. 2.1 indicates that the temperature rise due to thermal radiation is the limiting factor for the conditions stated. Many parameters and their results can be studied by means of Danger Region Diagrams. For example, for the three flight paths shown on the figure, it can be observed that (1) increasing the flight altitude allows the aircraft to be farther from the critical peak overpressure boundary, thus minimizing the overpressure effect, and (2) increasing the flight altitude shows little change with regard to the limit allowable tail load boundary (material velocity effect).

The decisions of aircraft participation and flight path positioning for the B-36D in CASTLE were based on studies of Danger Region Diagrams constructed for the appropriate set of conditions.

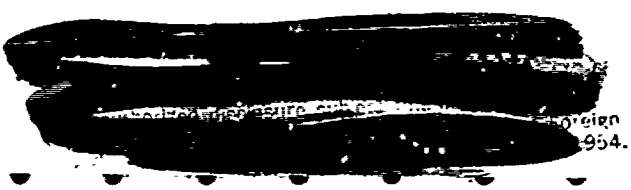

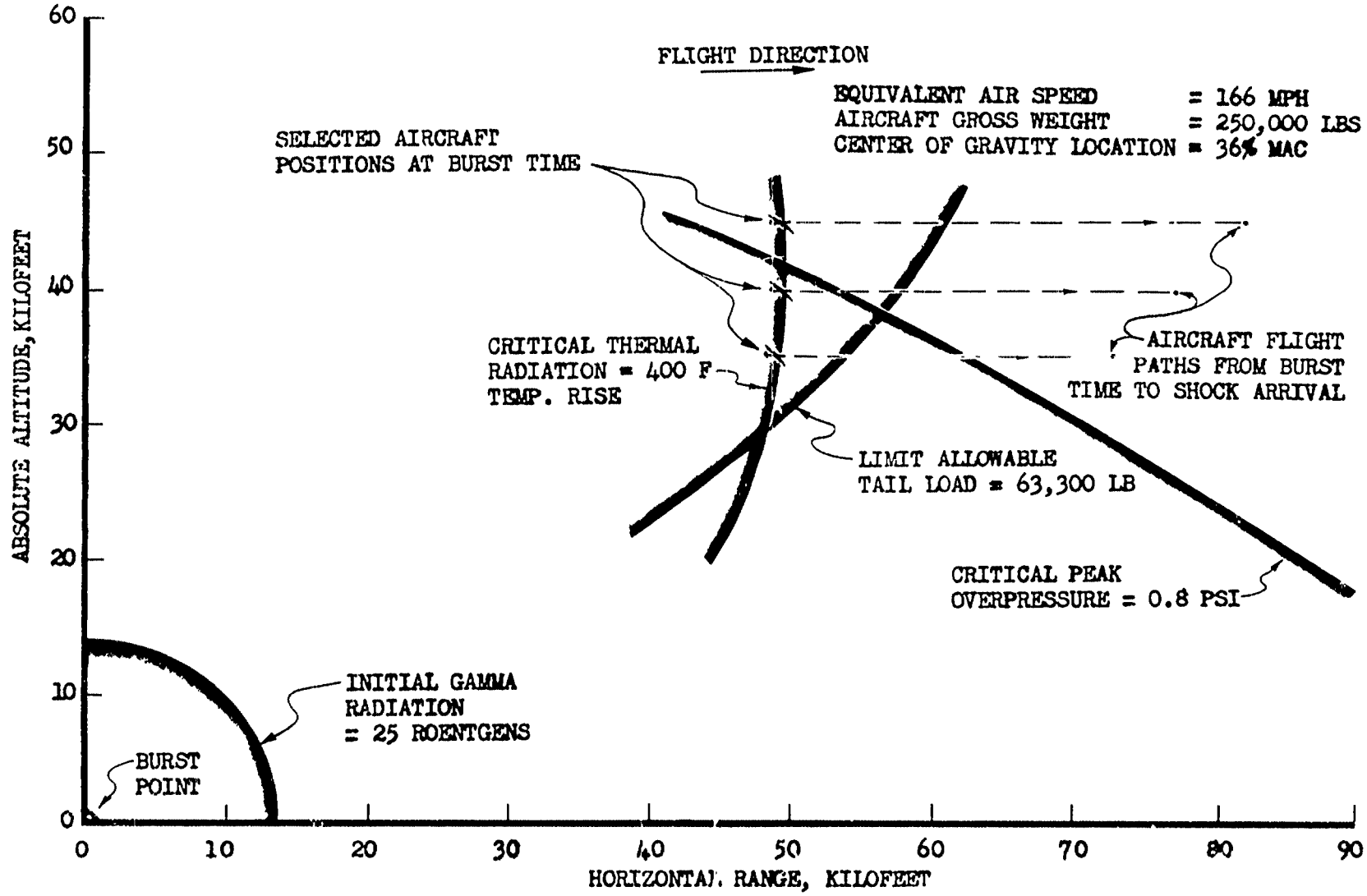

Fig. 2.1 B-36D Danger Region Diagram for 12 MT Yield

CHAPTER 3

PROCEDURE

3.1 GENERAL

The participation of the B-36 "effects" aircraft in CASTLE was the responsibility of WADC who solicited the assistance of two civilian organizations, Allied Research Associates (ARA) and the University of Dayton, and the support of the Strategic Air Command (SAC) and the Air Materiel Command (AMC). ARA analyzed data and performed the calculations required to supply predicted effects information. The University of Dayton Division of Research provided aircraft instrumentation, as well as collection, reduction, and reporting of data. SAC supplied the flight and ground crews and provided light maintenance. AMC performed heavy maintenance and overhaul services.

The aircraft used was the B-36D, serial number 49-2653, used previously in Operations IVY and UPSHOT-KNOTHOLE. The instrumentation system installed and used for the previous tests was reused wherever possible. However, program changes and experience dictated a number of additions and revisions. In addition, time and weather had seriously affected the strain gage installation, necessitating replacement of all gages.

The instrumentation work was started in September 1953 at San Antonio, Texas while the San Antonio Air Materiel Area (SAAMA) was performing a major overhaul on the aircraft. In October, the aircraft was delivered to SAC at Carswell AFB for purposes of flight crew training and further instrument installation. In conjunction with flight crew practice missions, two instrumentation shake-down flights were made. Early in January 1954, the aircraft was returned to SAAMA for a 100-hr inspection, additional Technical Order compliance, painting of the entire underside of the aircraft with white enamel, and preparation for overseas movement.

On 4 February 1954, the aircraft landed at Eniwetok Island, Headquarters of the Air Force Task Group at the Pacific Proving Grounds (PPG) during the 1954 nuclear tests. Before the first shot, two test flights were made as rehearsals not only for the benefit of the B-36D crew, but also for coordination of all participating groups.

To achieve the project objective, the B-36D was instrumented to

measure thermal inputs, thermal responses, blast inputs, and blast responses. Thermal inputs consisted of radiant exposure and irradiance which defined the radiant energy received by the aircraft. Recorded thermal responses included temperature rises of the aircraft skin on the wing, fuselage, stabilizer, and elevator. The measured blast inputs were free-stream overpressure, and pressures on the underside of various surfaces of the aircraft. Blast responses included structural loads imposed on the wing, fuselage, and stabilizer, and accelerations, elevator deflection, and wing deflection. Figure 3.1 shows the general location of the instruments on the aircraft. Additional instrumentation included peak temperature measurements by temp-tapes, as well as still and motion-picture photography. Consolidated Engineering Corporation oscillographs and Gun Sight Aiming Point (GSAP) cameras were used as the time-history recorders. A five-man instrumentation crew prepared and operated the recording system during each flight.

Two basic problems were involved in operation of the aircraft: the flying of the aircraft to a point in space at a given time, and the accurate determination of the actual aircraft flight path during the thermal and blast phases of the detonation. The first problem was solved by the flight crew who executed a modified radar-navigation exercise with equipment standard to a B-36. This involves flying the aircraft, by radar, to a point in space from which a bomb might be released. Normally this exercise does not require the aircraft to be at the release point at a predetermined time. This correlation with time was the major modification to the standard exercise. The second problem, position determination, was attempted by the Raydist Radio Navigation System. Tracking data for the B-36D were obtained during only one test. The aircraft positions during the other tests were obtained by an analysis of radar oscilloscope photos, data recorded by the navigator, and computations based on the time of arrival of the shock front.

3.2 THERMAL MEASUREMENTS

One of the serious effects of a nuclear explosion upon aircraft structures is the temperature rise resulting from the exposure to radiant energy of the fireball. To determine experimentally the relationship between the radiant energy and the temperature changes, the B-36D was instrumented for thermal measurements, both input and response. Input measurements were time-histories of the radiant exposure of the aircraft (cal/sq cm), and irradiance or time rate of radiant exposure. Response measurements consisted of both time-history and peak temperatures of various sections of the aircraft external covering or "skin."

3.2.1 Input Measurements

Calorimeters and radiometers designed, manufactured, and calibrated by the U.S. Naval Radiological Defense Laboratory of San Francisco (NRDL) were used to measure radiant exposure and irradiance, respectively. Details of the construction and operation of these instruments can be found in reference 13. Both instruments utilized copper-constantan thermocouples in the sensing elements. Voltage outputs were of

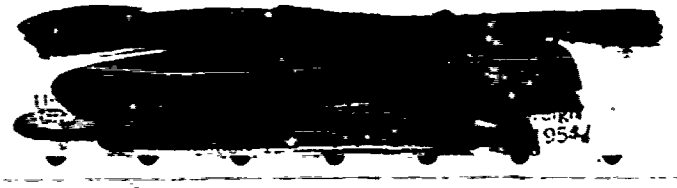

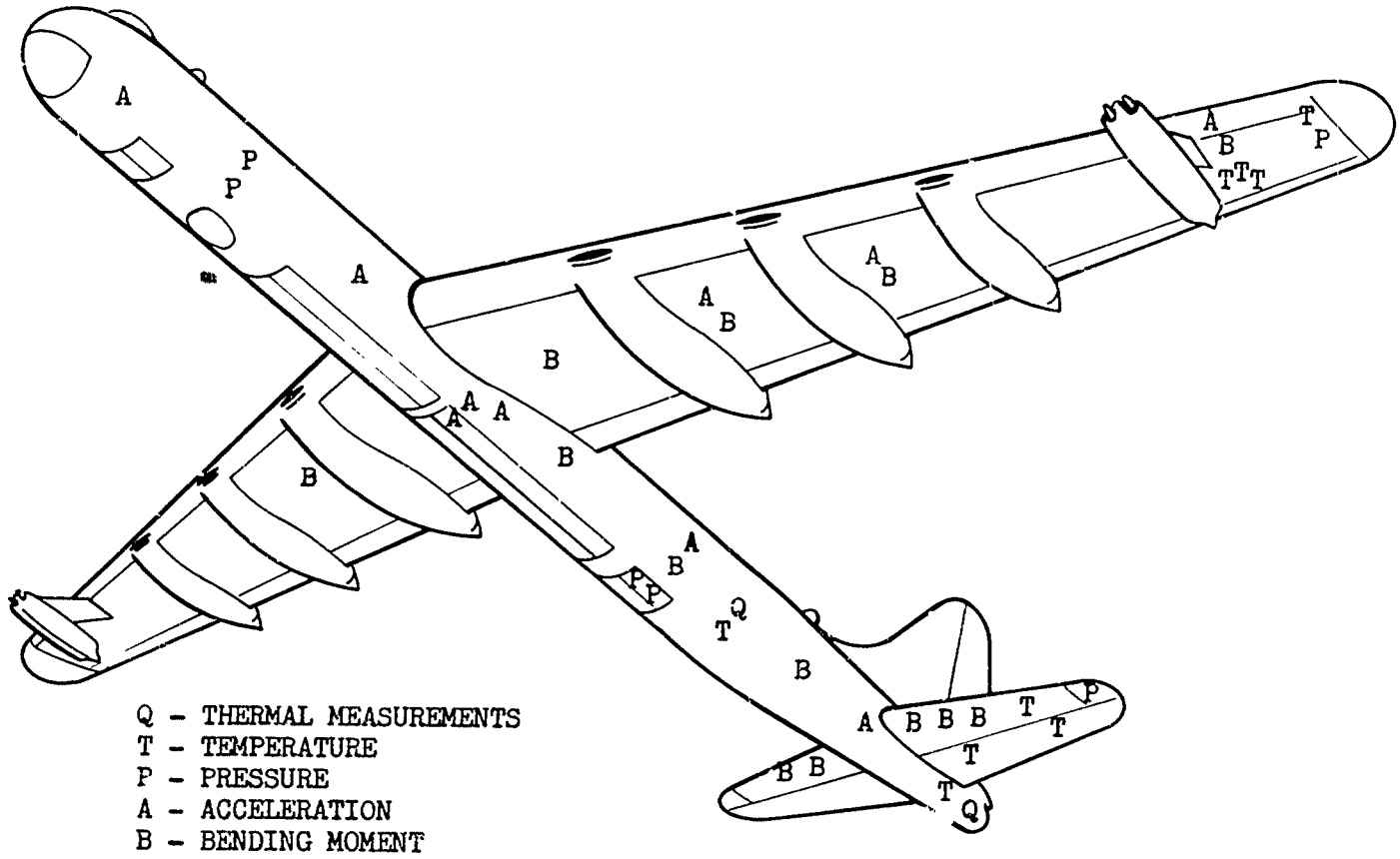

Fig. 3.1 General Location of the Instruments on the B-36D for Operation CASTLE

sufficient magnitude to permit direct coupling to d'Arsonval type recording galvanometers. Resistance networks were used to control galvanometer deflections and to insure optimum damping characteristics.

Four calorimeters and two radiometers were mounted in a special box and installed on the tail turret frame of the B-36D (Fig. 3.2).

Fig. 3.2 Thermal Instruments Installation in Tail Turret

Since the thermal instruments had a 90° conical field of view, care had to be exercised to prevent indirect energy, reflected from the surface of the aircraft, from entering the instruments. The choice, originally made for IVY, of the tail turret for location of the instruments for tail-to exposures was best.

Angular adjustments of the box orientation with respect to the aircraft provided an opportunity to aim the instruments at the intended burst point for various combinations of altitude and ground range. Two GSAP cameras, also mounted in the instrument box, exposed motion picture films which defined the field of view of the instruments at time zero. These films were used to determine the error in aircraft orientation, which affected the amount of thermal energy normal to the various surfaces of the aircraft.

Between Shots 3 and 4, a fifth calorimeter was installed in the aft lower left blister to obtain the energy received inside the Plexiglas blister (Fig. 3.3).

Individual circuit sensitivities for all thermal instruments were established and checked periodically by recording the galvanometer deflection caused by the introduction of a known voltage into the circuit.

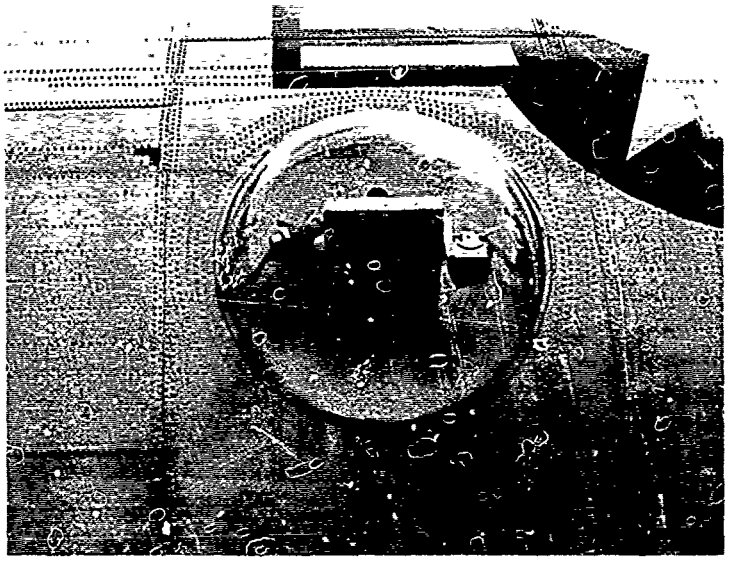

Fig. 3.3 Calorimeter Installation Inside Blister

Table 3.1 presents information concerning the location and instrument range of the thermal input instruments.

TABLE 3.1 Thermal Input Installations

Instrument No.	Location in Aircraft	Instrument Range
	Radiant Exposure	
1	Tail Turret	0-50 cal/sq cm
2	Tail Turret	0-50 cal/sq cm
3	Tail Turret	0-20 cal/sq cm
4	Tail Turret	0-10 cal/sq cm
5	Lower Left Blister (Shots 4 and 5 only)	0-20 cal/sq cm
	Irradiance	
1	Tail Turret, Shot 1 only	0-50 cal/sq cm/sec
2	Tail Turret, Shots 2, 3, 4, 5	0-10 cal/sq cm/sec
3	Tail Turret	0-10 cal/sq cm/sec

In addition to the thermal input measurements mentioned above, Project 6.2a personnel performed the service of installing and operating a Bhangmeter for the Aircraft Radiation Laboratory (ARL) of WADC. The Bhangmeter is a yield-measuring device developed by Edgerton, Germeshausen, and Greer, Inc. (EG&G). The Mark IV instrument installed in the B-36D represented the latest experimental model for measurement

of yields between 80 KT and 10 MT. By means of a Polaroid-Land camera, the instrument recorded the time-history of the fireball light intensity as sensed by a photo-electric element and indicated on the face of an oscilloscope. The yield was calculated from a formula, the only variable of which was the period of time between the instant of detonation and the first minimum of light intensity. The Bhangmeter operated successfully on all six shots; the film was delivered to ARL for reduction and analysis.

3.2.2 Response Measurements

The responses of various parts of the aircraft to the thermal energy were measured by copper-constantan thermocouples and by temptapes. For the first shot, some of the thermocouples that had been installed for IVY were reused. These measurements included two sets of skin, stringer, and skin-under-stringer installations, one additional skin installation, and a special plate inside the aft lower left blister. These thermocouples had been attached by inserting the wire into a small drilled hole and peening the wire to establish mechanical fit and electrical contact. Shot 1 data indicated that several of these installations were unsatisfactory because of intermittent electrical contact. Also, a brief data analysis indicated that a better representation of the thermal response of the aircraft might be obtained by measurements at other locations. Accordingly, all thermocouple installations after Shot 1 consisted of 5-mil wire welded by a capacitance-discharge technique. Installations were made on the elevator, stabilizer, and fuselage skins, as well as on the skin, flange, and stiffener of a wing waffle panel, and the special plate inside the aft lower left blister.

The entire underside of the aircraft had been painted with white enamel to improve the reflecting characteristics of the skin. The standard procedure for painting B-36's involves spraying all magnesium surfaces with aluminized lacquer and leaving all aluminum surfaces bare. To determine the degree of effectiveness of this new procedure, a portion of the wing undersurface was cleaned of the white enamel and refinished with the normal aluminized lacquer. This part of the wing was of waffle panel construction using 0.025-in. magnesium skin. With a skin thermocouple installation, this panel was identical in all respects, except the paint, to a nearby waffle panel.

The welding procedure, in which the thermocouple wire is attached to the back or non-irradiated side of the instrumented component, is described in detail in reference 14.

The air temperature inside of the aft compartment of the aircraft was measured during Shots 1, 2, and 3. Although it was predicted that the inside air temperature rise would be negligible, the measurement was made primarily to relieve the apprehension of those personnel unfamiliar with such shots. The thermocouple for the air temperature measurement was located near the bridge connecting the aft upper blisters. No appreciable rise in air temperature was detected; consequently, the measurement was discontinued in favor of a more meaningful response measurement.

The d-c thermocouple signals were recorded directly by oscillographs. Resistance networks were used as required to control galvanometer deflection and to insure optimum damping characteristics. Individual circuit sensitivities were established and checked by the same method used with the input instruments. Thermos bottles, partially filled with ice water, were used to maintain a constant temperature at the reference junction. Table 3.2 gives the location, the material, and the surface conditions of the thermocouple installations.

Peak temperature measurements were made by temp-tapes, temperature sensitive devices consisting of a combination of 20 sensing elements, each of which melts at a particular temperature in the range from 116°F to 545°F. A detailed description of temp-tapes is contained in reference 15. Installations of temp-tapes were made on the elevator, wing, fuselage, tail turret lower fairing, two propeller spinners, and the special plate in the blister.

Fifty temp-tapes were applied for Shot 1, 69 for Shot 2, and 68 each for Shots 4 and 5. About half of the tapes were installed in the elevator at ten spanwise locations, all on 0.020-in. magnesium skin (hat panels). The tapes on the wing, fuselage, and blister plate were located adjacent to the thermocouple installations of those components. The tapes on the tail turret lower fairing were placed on that part of the fairing that was approximately normal to the thermal radiation. The propeller spinners were instrumented after Shot 1 when the spinner paint was blistered severely.

3.3 BLAST MEASUREMENTS

Time-history measurements of various pressures existing on or about the aircraft during the passage of the shock wave comprised the blast input measurements. Response measurements consisted of bending moments, shear loads, accelerations, and deflections of the elevator, wing, and fuselage. All measurements were recorded on oscillograms, except for wing and fuselage deflections, which were recorded by 16-mm motion picture cameras.

3.3.1 Pressure Measurements

The primary pressure measurement was that of free stream overpressure. Of secondary interest were three surface pressure measurements and one differential pressure measurement. The surface pressure measurements represent the variation of the pressures existing on certain surfaces of the aircraft structure from the pre-shock ambient pressure. The differential pressure is the difference in pressure between the inside and outside of the fuselage midsection.

An accurate measurement of free stream overpressure on an aircraft in flight is largely dependent upon the location of the transducers. It is necessary to exclude, by means of proper location, the pressure variations produced by turbulent air flow over the aircraft structure during normal flight and during the passage of the shock wave. Furthermore, it is necessary that the surface containing the orifice or diaphragm of the transducer be in a plane perpendicular to the shock

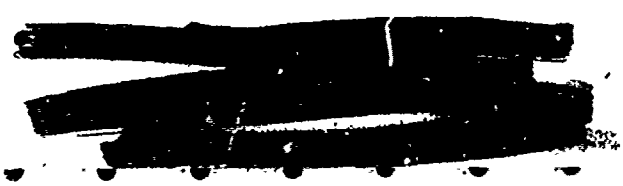

TABLE 3.2 - Thermocouple Installations

Install. No.	Location	Material	Surface Conditions
	Shot 1 Installations		
1	Left stab. Sta. 310 in.	0.020-in. aluminum skin	White enamel w/film of oil
2	Left stab. Sta. 310 in.	0.020-in. aluminum skin under stringer	White enamel w/film of oil
3	Left stab. Sta. 310 in.	0.020-in. aluminum skin on stringer	White enamel w/film of oil
4	Left wing Sta. 1270 in.	0.040-in. aluminum skin	White enamel
5	Left wing Sta. 1270 in.	0.040-in. aluminum skin under stringer	White enamel
6	Left wing Sta. 1270 in.	0.040-in. aluminum skin on stringer	White enamel
7	Left wing Sta. 1095 in.	0.025-in. mag. waffle panel skin	White enamel
8	Aft lower left blister	0.032-in. aluminum sheet (Shots 1 & 2)	White enamel
	Installations for Shots 2, 3, 4, 5, and 6		
9	Left elev. Sta. 144.5 in.	0.020-in. mag. hat panel skin	White enamel
10	Left elev. Sta. 312 in.	0.020-in. mag. hat panel skin	White enamel w/film of oil
11	Left stab. Sta. 313 in.	0.020-in. aluminum skin	White enamel w/film of oil
12	Fuselage Sta. 1898.5 in.	0.025-in. aluminum skin	White enamel
13	Left wing Sta. 1106 in.	0.025-in. mag. waffle panel skin	Aluminized lacquer
14	Left wing Sta. 1068 in.	0.025-in. mag. waffle panel skin	White enamel
15	Left wing Sta. 1068 in.	Mag. waffle panel flange	
16	Left wing Sta. 1068 in.	Mag. waffle panel stiffener	
17	Aft lower left blister	0.020-in. mag. hat panel skin (Shots 3, 4, 5, and 6)	White enamel

front, so that pressure increases produced by shock reflections and the dynamic pressure effects of the material velocity will be minimized. Theoretically, if a surface is passed by a blast wave at any incidence angle other than 90° (parallel flow), the surface will receive, besides the static pressure, an additional pressure component caused by the reflection of the pressure wave from the surface and by the mass flow or material velocity. On the B-36D aircraft, the location chosen for the measurement of free stream overpressure was the side of the fuselage at Station 391 in. (from the nose reference line), adjacent to the aircraft instrument static ports.

Because of the importance of the overpressure measurements, four independent transducers were installed at fuselage Station 391 in., two instruments on each side. For pressures other than overpressure, the installations were as follows: one pressure transducer on the undersurface of the left wing near the tip at Station 1270 in. (from the fuselage centerline), one on the undersurface of the left stabilizer at Station 359 in., and two located at the aft lower gun turret door.

All pressure measurements were made with differential type gages, with the reference side of all transducers, except one, connected to airtight systems containing pressures at the ambient pre-shock level for the particular flight altitude. This was accomplished by venting the referencing system to the atmosphere until shortly before detonation times, when the vent was closed by means of a solenoid valve, thus sealing the system. By this method, the pressures sensed by the gages represented changes from the ambient pre-shock pressure at flight altitude. The one exception to this referencing system was one of the two gages installed on the aft lower gun turret door. The reference side of this transducer was left open to the interior of the gun-turret enclosure, thereby measuring the difference in pressure between the inside and outside of the aircraft, which represents the crushing force exerted upon the structure.

Two different excitation systems were employed for these pressure measurements. The majority of the transducers was excited by a simple d-c system utilizing batteries and Consolidated Engineering Corporation bridge balance units. The use of a sensitive recording galvanometer limited the flat frequency response of the d-c systems to 0-60 cps. In order to reproduce some of the higher frequency components of the shock wave, a galvanometer capable of responding to signals of these frequencies was used, thus sacrificing the electrical sensitivity. For this reason, electronic amplification of the signal was required. Three pressure transducers were installed to reproduce frequencies from 0 to 500 cps by the use of a 3-kc carrier excitation and amplification system (Consolidated Engineering Corporation's System "D"). The pressure transducers used for these installations were also capable of the desired frequency response. Detailed information concerning all pressure measurement installations, including locations of the transducers, is presented in Fig. 3.4.

A static calibration of all pressure gages, for both positive and negative pressures, was performed with the transducers mounted in place in the aircraft, by using a special air pump and a fluid manometer

Location	Type Gage	Exciting Systems	Flat Freq. Resp. (cps)
Fuselage Sta 391 in. left side	Statham P-69	d-c	0-60
Fuselage Sta 391 in. right side	Statham P-96	d-c	0-60
Fuselage Sta 391 in. left side	Consolidated 3-310	3-kc	0-500
Fuselage Sta 391 in. right side	Wiancko 3 PAD 10	3-kc	0-500
Fuselage Sta 1287.5 in. aft lower gun turret door	Statham P-69	d-c	0-60
Fuselage Sta 1294.5 in. aft lower gun turret door	Statham P-69	d-c	0-60
Left Wing Sta 1270 in. under surface	Wiancko 3 PAD 10	3-kc	0-500
Left Stabilizer Sta 359 in. under surface	Statham P-69	d-c	0-60

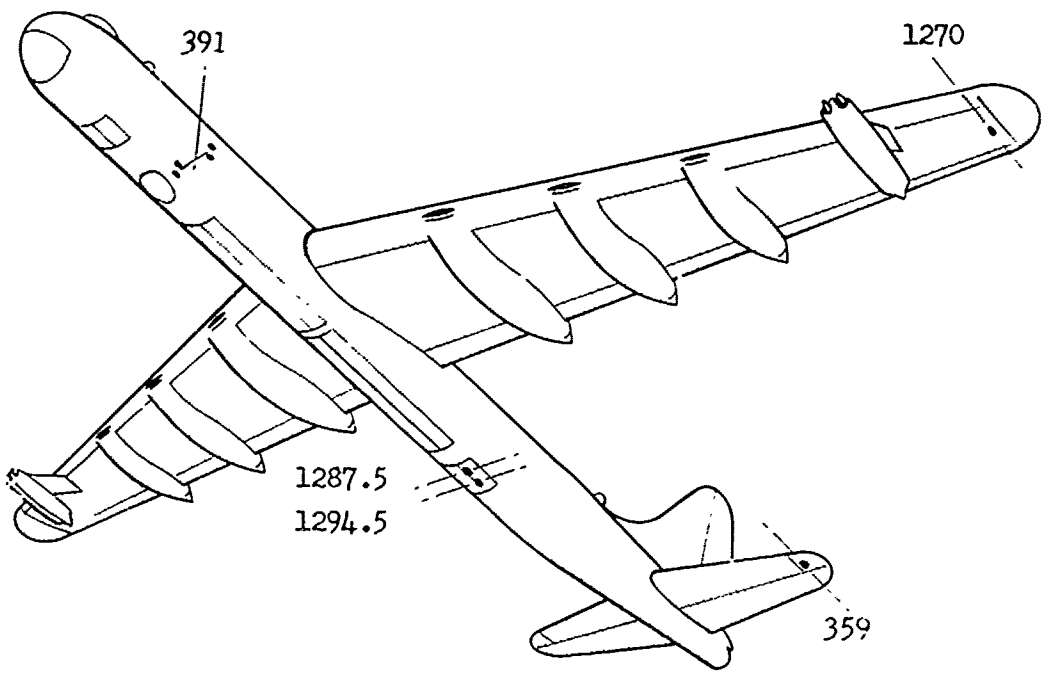

Fig. 3.4 Locations of Pressure Transducers, B-36D Aircraft

Sensitivity of the installations was established, with relation to variables such as excitation voltage and circuit resistances changes, by means of a resistance calibration; that is, the shunting of one arm of the bridge with a precision resistance and the recording of the resulting signal. The details of this procedure are described on page 73 of reference 16. The initial calibrations of the pressure gages were checked by periodic application of calibration pressures and resistance calibrations signals.

3.3.2 Bending Moment and Shear Load Measurements

All bending moment and shear load measurements utilized bonded wire strain gages as the sensing elements. Because of difficulties encountered by previous projects with strain gage installations subjected to the rigors of overseas flight operations, brief laboratory tests were conducted to select a process as well as process materials for the strain gage installations. Baldwin EBDF-13D temperature-compensated, bakelite gages were bonded to the appropriate structural components with Armstrong's type A-6 Epoxy resin cement, and moisture-proofed with Minnesota Mining Company EC-847 compound and Dow Corning silicone grease.

All strain bridge measurements were recorded on oscillographs, with electrical circuits completed through d-c bridge balances as shown in Fig. 3.5. The flat frequency response of all strain bridge

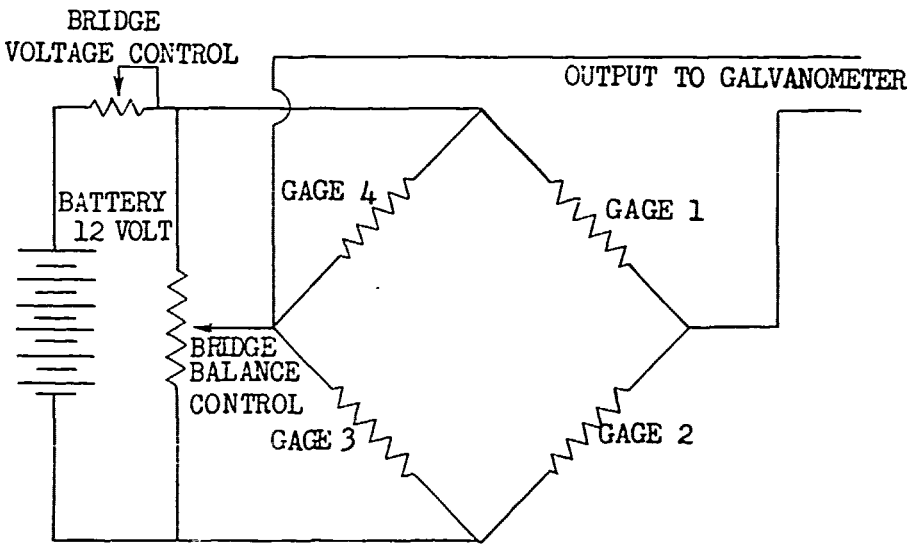

Fig. 3.5 Strain Bridge Electrical Circuit Diagram

channels was 0-60 cps. Bending moment measurements were divided into two general categories determined by the type of strain bridge installation. One type of strain bridge was arranged and located to respond to the bending of an entire structure, such as a wing, stabilizer, or fuselage. Hereafter, this type of bridge will be referred to as a

total bending bridge. Other strain bridges were arranged so as to respond to the bending moment of one main structural member of the aircraft, such as one of the spars of the stabilizer, so that the total bending of the structure would be obtained from the mathematical combination of the outputs of several of these bridges. This type of bridge is defined as a point load bridge. All shear measurements were accomplished using point load bridges.

Total bending bridges were installed in the left wing at Stations 1067, 604, 390, and 110 in., and in the right wing at Station 390 in. The station dimensions, measured from the fuselage centerline, represent the intersection of the station chord line and the elastic axis of the structure. The strain gages were located so that a line extended in a chordwise direction from front to rear spar gage installations would intersect the elastic axis at right angles. Total bending bridges were installed in the fuselage at Stations 1037, 1293, and 1597 in., measured from the nose reference line. The horizontal stabilizer was instrumented with total bending bridges at Stations 224, 153, and 62 in. on the left side, and at Station 62 in. on the right. Gages were located in the same manner as those in the wing with reference to a line intersecting the elastic axis at right angles. Typical total bending installations are shown in Fig. 3.6.

Point load bridges were installed in the horizontal stabilizer structure at Station 62 in. on the left and at Stations 62 and 144 in. on the right. The installation at each of these locations consisted of two bending and two shear bridges, one of each on the front spar and rear spar, respectively; a typical installation is shown in Fig. 3.7. Because of the critical nature of the horizontal stabilizer structure, the additional instrumentation using point load bridges was installed in order to provide a more complete picture of the behavior of this component when struck by the blast wave. Figure 3.8 presents a view of the entire aircraft with the locations of all strain bridge measurements shown.

Because of time limitations, a calibration of the strain bridge installations in terms of bending moment and shear was not accomplished prior to the field operation; however, the results of a simple loading procedure, used primarily to check strain bridge relative sensitivity at intervals throughout the test program, were established as a preliminary type of calibration. This was necessary in order to evaluate the results obtained from the tests between each shot of the series, so that correlation with predicted effects and, if necessary, revision of the desired position of the aircraft for the next shot could be accomplished. Although these check loadings were performed under conditions considered adverse to obtaining calibration data, the actual calibration constants, determined after the test series had been completed, differed from the preliminary constants by less than 5 per cent with one exception, in which the difference was 8 per cent.

The calibration of the strain bridge installations in the horizontal stabilizer was performed at the Consolidated Vultee Aircraft Corporation (Convair) at Fort Worth, Texas, during the months of July and August 1954, and consisted of two independent procedures, a distributed load type of calibration for the total bending bridges, and a

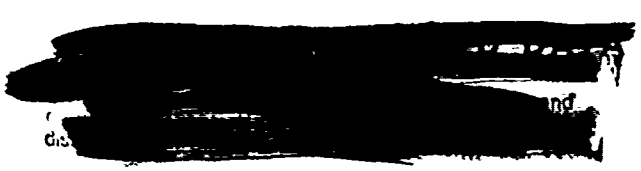

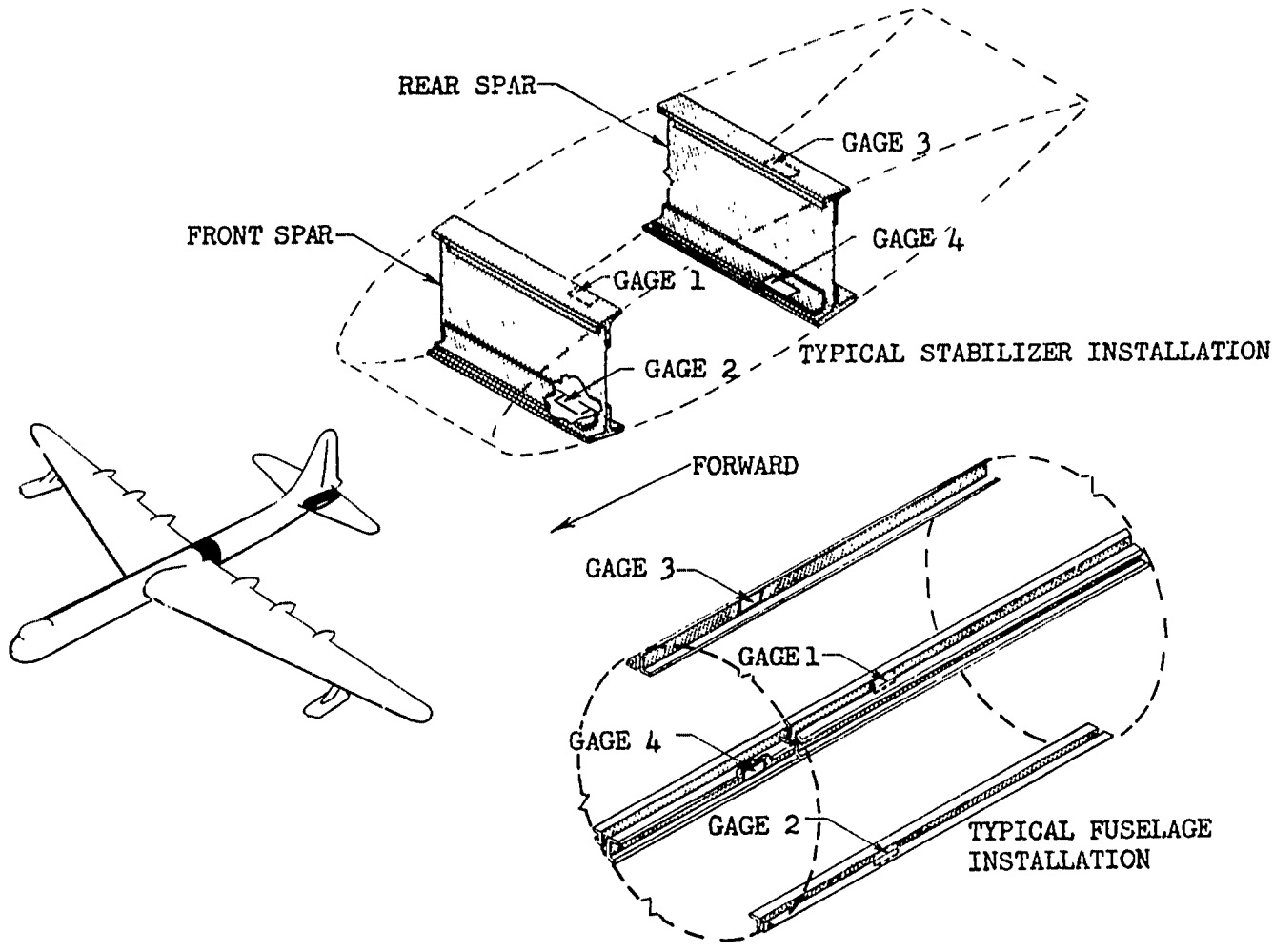

Fig. 3.6 Typical Total Bending Strain Bridge Installations

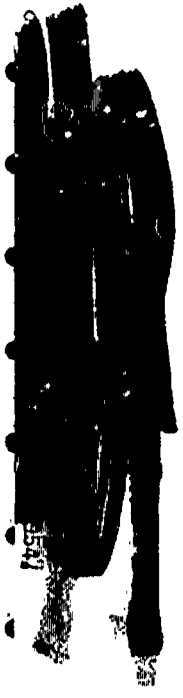

HORIZONTAL STABILIZER
REAR SPAR

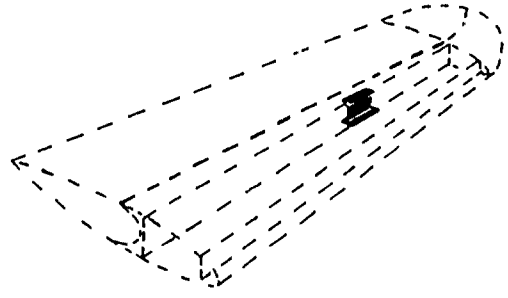

B- BENDING GAGE
S- SHEAR GAGE

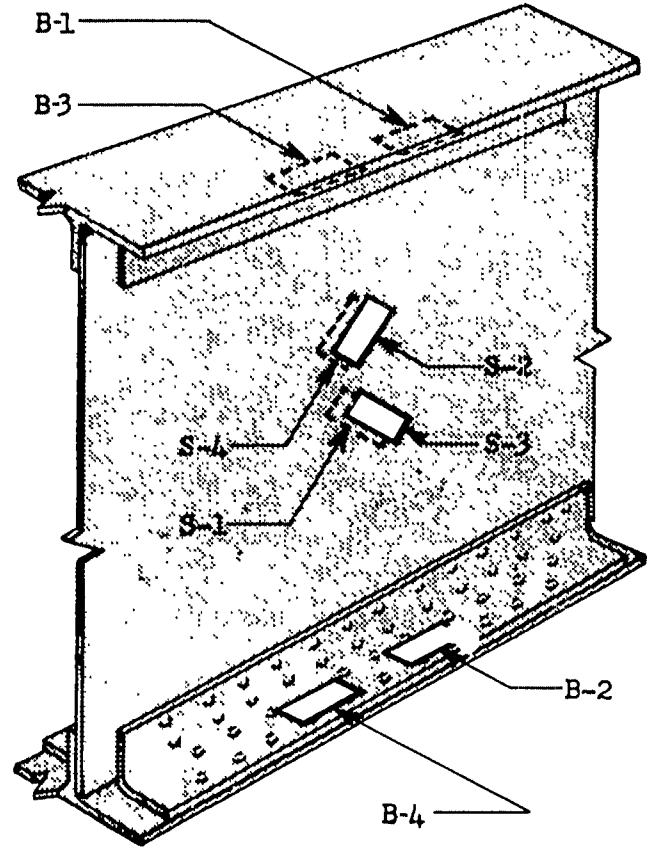

Fig. 3.7 Typical Point Load Strain Bridge Installations

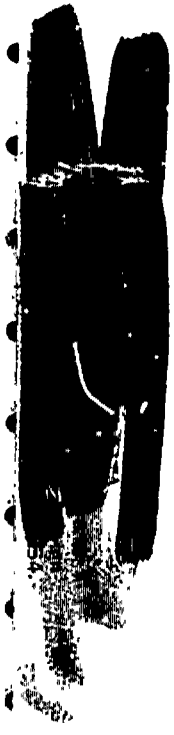

Wing Strain Bridges	
Location	Type of Measurement
1062", Left	Total Bending
604", Left	Total Bending
390", Left	Total Bending
110", Left	Total Bending
390", Right	Total Bending

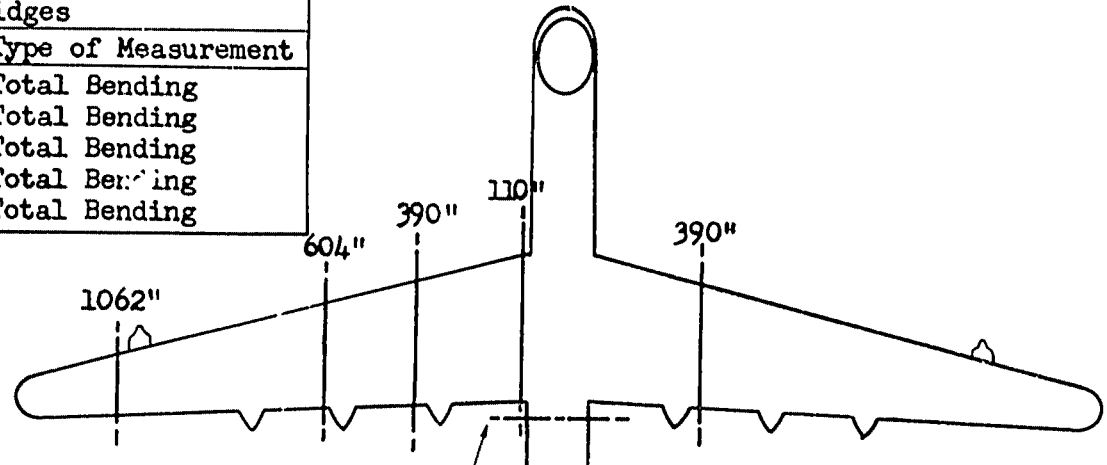

Stabilizer Strain Bridges	
Location	Type of Measurement
224", Left *	Total Bending
153", Left *	Total Bending
62", Left	1) Total Bending 2) Point Load Bending 3) Point Load Shear
62", Right	1) Total Bending 2) Point Load Bending 3) Point Load Shear
144", Right	1) Point Load Bending 2) Point Load Shear

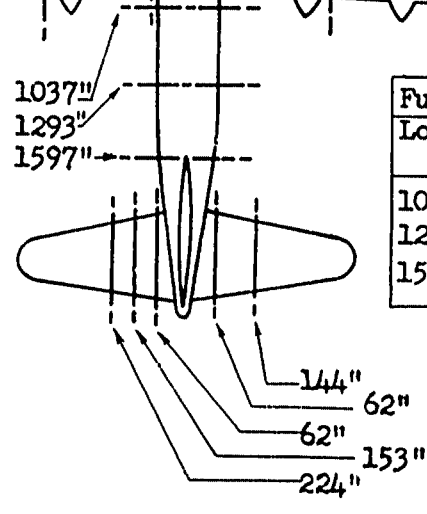

Fuselage Strain Bridges	
Location	Type of Measurement
1037"	Total Bending
1293"	Total Bending
1597"	Total Bending

* Bridges installed after Shot 2 (ROMEO)

Note: Locations are Station numbers (in.)

Fig. 3.8 Locations of Strain Bridges, B-36D Aircraft

point load calibration of the point load bridge installations. The distributed load calibration consisted of the simultaneous application of many loads to the stabilizer structure, their locations and magnitudes being chosen such that pure bending about the elastic axis was experienced by the structure. The stabilizer was stressed to 90 per cent of limit load during the calibration process, limit load being defined as two-thirds of the allowable load that the structures may safely experience. A calibration of the fuselage strain bridge was obtained during the stabilizer calibration loadings. The point load bridges of the horizontal stabilizer were calibrated by the point load method: that is, the application of single loads to the structure at a number of points for several conditions of loading. The separation of shear, bending moment, and torsion was achieved by a mathematical combination of bridge outputs. This method is described in a technical note published by the NACA, reference 17 of this report. The results from total bending bridges located in the wing were considered of secondary interest only, and, because of the expense involved, a static wing calibration was not performed. Instead, a less accurate method was used. This consisted of obtaining the sensitivity relationship between bridge output and wing bending moment by use of calculated theoretical flight loads for appropriate aircraft configurations and maneuvers.

The electrical sensitivity of all strain bridge channels was established during the calibration by means of a resistance calibrate signal. The use of this system related the electrical sensitivity of each channel for every recording, to the electrical sensitivity at the time of actual mechanical calibration of the structure. This operation is described on page 73 of reference 16. The sensitivities of the strain bridge transducers located in the stabilizer and fuselage were checked periodically by the application of check loads to the tips of the horizontal stabilizer. One of these check loadings was accomplished just after the strain bridge installations had been completed, two more were performed at the overseas base of operations, and a final loading preceded the static calibration by a few weeks. From an examination of the bridge outputs obtained from these loadings, any significant change of transducer sensitivity would have been detected.

3.3.3 Acceleration Measurements

Two general types of acceleration measurements were made on the B-36D aircraft. These were vertical linear acceleration at various stations of the wing and fuselage and angular acceleration about the center of gravity. Statham type A-18 instruments were located at Stations 1052, 576.5, and 375.5 in. in the left wing structure at the rear spar and in the fuselage at Stations 208.5, 661.5, 907, 1319.5, and 1772 in. The angular accelerometer was located on the left side of the fuselage at Station 904 in., this location approximating the center of gravity of the aircraft. This transducer was a Statham type AA7 liquid rotor instrument.

The linear accelerometers incorporated a self-contained thermostatically-controlled heating system for maintaining correct viscosity

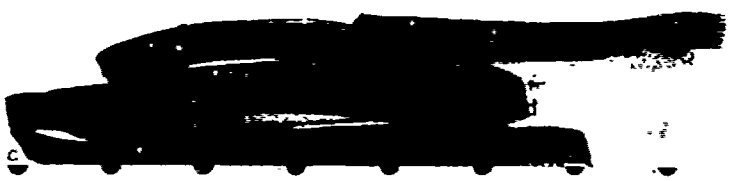

Location	Direction of Sensitivity	Statham Type
Fuselage Sta 208.5 in.	Vertical	A18-6-350
Fuselage Sta 661.5 in.	Vertical	A18-6-350
Fuselage Sta 904 in.	Angular	AA7-3-350
Fuselage left side Sta 907 in.	Vertical	A18-6-350
Fuselage right side Sta 907 in.	Vertical	A18-6-350
Fuselage Sta 1319.5 in.	Vertical	A18-6-350
Fuselage Sta 1772 in.	Vertical	A18-6-350
Left Wing Sta 1052 in.	Vertical	A18-12-350
Left Wing Sta 575.5 in.	Vertical	A18-12-350
Left Wing Sta 375.5 in.	Vertical	A18-12-350

Note: The frequency response of all acceleration channels was flat from 0 to 10 cps.

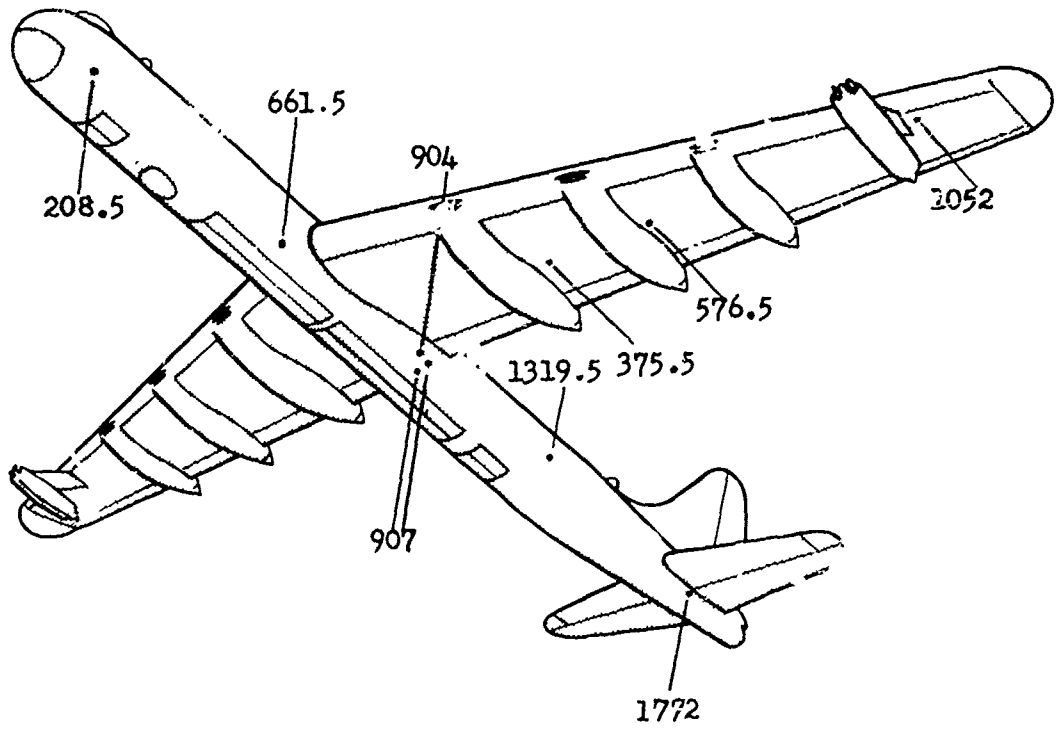

Fig. 3.9 Locations of Accelerometers, B-36D Aircraft

of the silicone damping fluid. The angular instrument, lacking a self-contained heater, was enclosed in a special box containing heating elements and a thermostatic control. Fig. 3.9 shows the locations of accelerometer transducers in the B-36D aircraft. A typical linear accelerometer installation is shown in Fig. 3.10, and the angular accelerometer with the special temperature-controlled enclosure is shown in Fig. 3.11. Heater elements of the enclosure are attached to the cover which is shown removed.

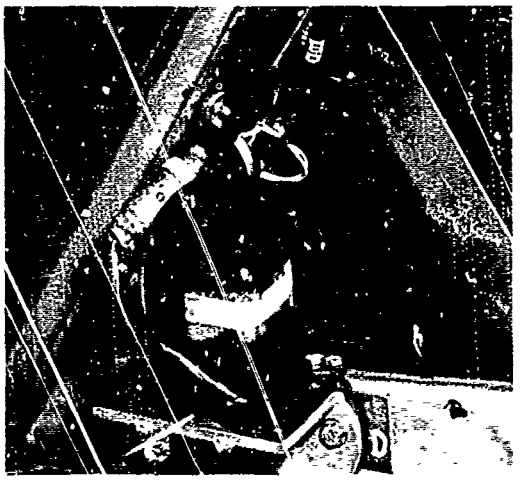

Fig. 3.10 Typical Linear Accelerometer Installation

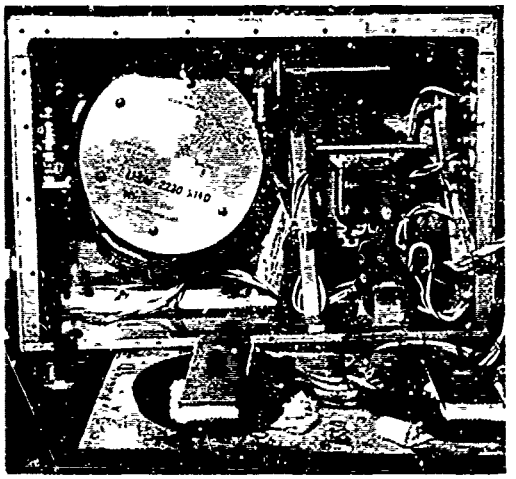

Fig. 3.11 Angular Accelerometer Installation

The linear accelerometers were calibrated in terms of units of gravity by subjecting them to known accelerations by means of a device known as a linear accelerator or "shake table." This device produces equal forces of positive and negative accelerations for a given frequency setting. The angular accelerometer was calibrated on a pendulum where known angular accelerations produced by the pendulum's oscillations were related to the electrical output of the instrument. As with the pressure and strain bridge transducers, electrical sensitivity of the accelerometer circuits was established by means of a resistance calibration signal.

Galvanometers were selected to restrict the flat frequency response of all acceleration measurement channels to 0 to 10.5 cps.

3.3.4 Elevator Deflection Measurements

Elevator deflection, the movement of the elevator about its normal pivot axis, was measured by means of a special bridge type of circuit, using a precision potentiometer mechanically coupled to the elevator torque tube as the variable resistance of the bridge. This system was excited by direct current and recorded as a regular oscillograph channel. The resulting curve was a time-history description of elevator deflection referenced to the normal in-flight position of the elevator just prior to time zero.

The elevator deflection system was calibrated by moving the

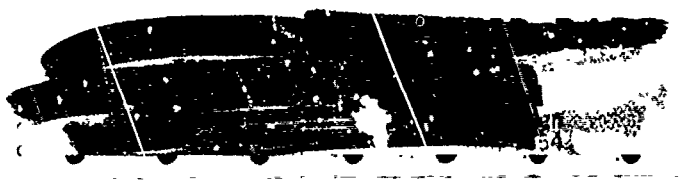

elevator to a position which had been accurately established and recording the output from the bridge circuit. This was accomplished for a number of these positions in both directions from the streamlined position of the elevator. As with other oscillographic channels, a resistance calibration signal was used to establish the electrical sensitivity of the circuit.

3.3.5 Wing and Fuselage Deflection Measurements

Five GSAP motion picture cameras were installed in a special housing on top of the fuselage at the wing intersection in order to photograph deflection of the wing and fuselage. Small stub antennas were used as reference pylons so that movements of the structures relative to the cameras could be measured accurately from the projected film. The camera housing is shown in Fig. 3.12, and the four wing pylons are shown in Fig. 3.13.

Since detonation times for all shots occurred before sunrise, it was necessary to illuminate the camera subjects in order to obtain satisfactory pictures. This was accomplished by using standard Air Force retractable landing lights, one of which, in the retracted position, is visible in the foreground of Fig. 3.13. One camera was

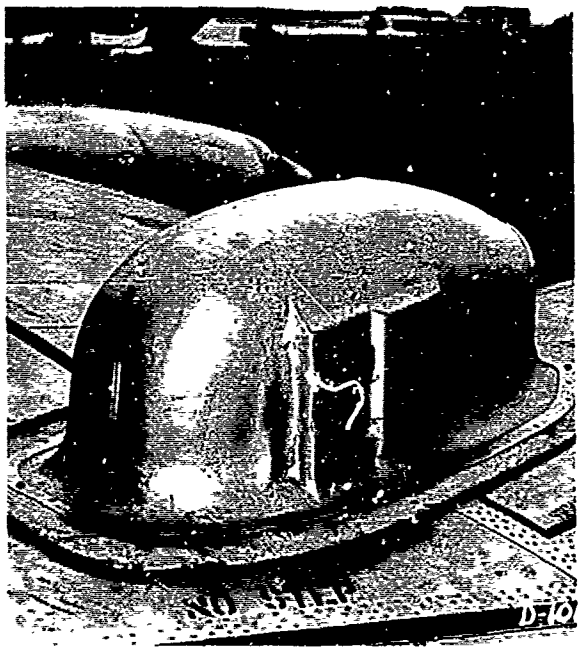

Fig. 3.12 Camera Housing on Top of Fuselage at Wing Intersection

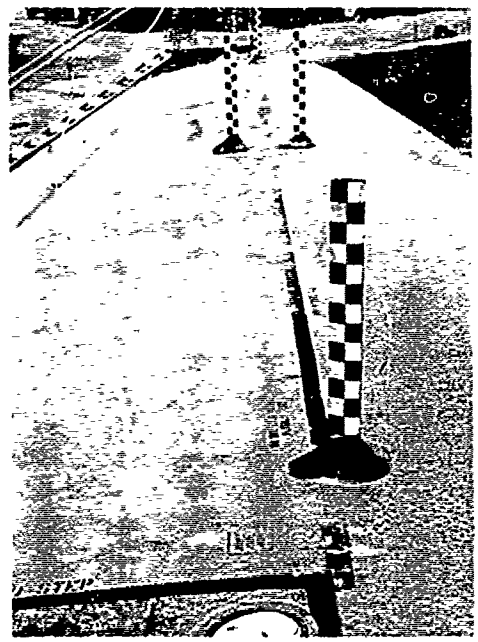

Fig. 3.13 Camera Target Pylons, Left Wing

oriented to photograph the forward fuselage using the navigator's astrodome as a reference point, and two cameras were oriented to include the vertical fin and a small portion of the horizontal stabilizer in their

fields of view. The remaining two cameras were focused on the pylons on the left wing. All cameras were set for a film speed of 64 frames sec, and the lenses used were of 76- or 35-mm focal length, dependent upon the field of view required. Cameras were calibrated for deflection by an accurate determination of the field of view and distance to the subject.

3.4 RECORDING SYSTEM

Permanent records of the time-history data were made by means of oscillographs and motion picture cameras. Four Consolidated Engineering Corp. 18-channel oscillographs were used: one oscillograph each for distributed-load strains, thermal inputs and temperatures, pressures and accelerations, and the stabilizer point-load strains. Exceptions to this distribution were made as a compensative measure in the event of an operational failure of one oscillograph. Two oscillograph speeds were used: the slower speed of the thermal and point-load oscillographs permitted continuous recording from a few seconds before detonation until the subsidence of the blast effects; the higher speed of the distributed load and pressure-acceleration oscillographs resulted in better record definition during the blast phase at the expense of no records during the thermal phase. The exact channel distribution in each of the four oscillographs is presented in tabular form in the Appendix.

Timing signals recorded on each oscillograph consisted of the 100 lines/sec generated within each recorder, a 100-cps sine wave of an electronic oscillator, a periodic pulse that occurred every 4 in. of record length, time zero indication from a photoelectric cell "blue box," and various special signals initiated by the control panel operator.

The EG&G "blue box" consisted of an electronic circuit triggered by a photocell. A high rate of change of light intensity, as well as a high intensity, is required to energize the device. The installation was located in the non-pressurized aft fuselage, with light admitted through a plexiglas window. To avoid large reflection losses, the light was directed normal to the window by an adjustable stainless-steel mirror protected from the airstream by a sheet-metal fairing. The mirror-fairing installation is shown in Fig. 3.14, the photocell enclosure appearing on the other side of the window.

Supplementary equipment required in conjunction with the oscillographs included bridge batteries, bridge balances, 3-kc carrier equipment, a thermocouple calibration instrument, spare parts, and a complete spare oscillograph.

Four 12v storage batteries were used to excite all the d-c Wheatstone-bridge-type instruments through the bridge balances. The voltages of the batteries were monitored by meters on the bridge balances and, during the recording period, by one channel on each of the four oscillographs.

All the oscillographs and supplementary equipment were located in the aft pressurized crew compartment on or near a special table constructed in the space normally occupied by crew bunks. Figure 3.15

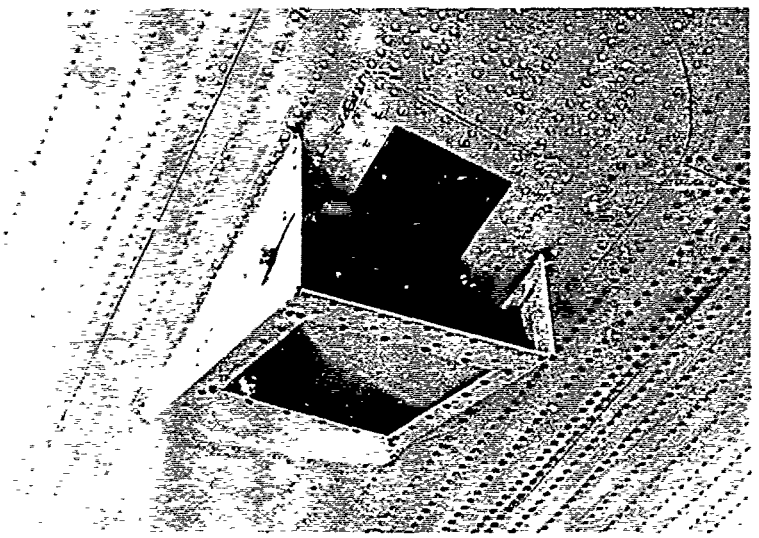

Fig. 3.14 Blue Box Mirror and Fairing Installation

presents the general arrangement of the instrumentation equipment in a plan view sketch of the aft crew compartment. Only the major items of equipment are shown; details of some of the equipment on the table can be seen in the four close-up photographs presented in Fig. 3.16. The directions from which the photos were taken are shown by arrows on Fig. 3.15. Views A, C, and D illustrate the arrangement of the oscillographs and supplementary equipment and the desk space used to work on check lists and forms for recording pertinent information. View B shows the control panel station with the main control panel ir the foreground, the camera control panel above and to the left of the main panel, two time-delay intervalometers above and to the right of the main panel, and the flight instrument panel in the upper right corner of the photograph. This flight instrument panel was a special installation in the aft crew compartment and will be described in detail later in this chapter. The installation at the extreme left of the photo is the oxygen station for the control panel operator; at the lower right hand corner of the photo is the back side of the 3-kc carrier amplifier system with an oscillograph magazine strapped to the top.

The flight instrumentation crew consisted of five members: an operator for each of the four oscillographs and a control panel operator. The oscillograph operators performed the function of checking, balancing, adjusting, and calibrating each channel of instrumentation and of taking emergency measures, if necessary, to provide an optimum instrumentation coverage. The control panel operator provided liaison between the instrumentation and the aircraft crews and, by means of the control panel, controlled the oscillograph and camera recording, bridge batteries, pressure gage solenoids, blue box, timing signals, and angular accelerometer heater.

The motion-picture photographic effort consisted of 50-ft reels of 16-mm film in eight GSAP cameras. In addition to the camera installations previously described, one camera was mounted inside the aft crew

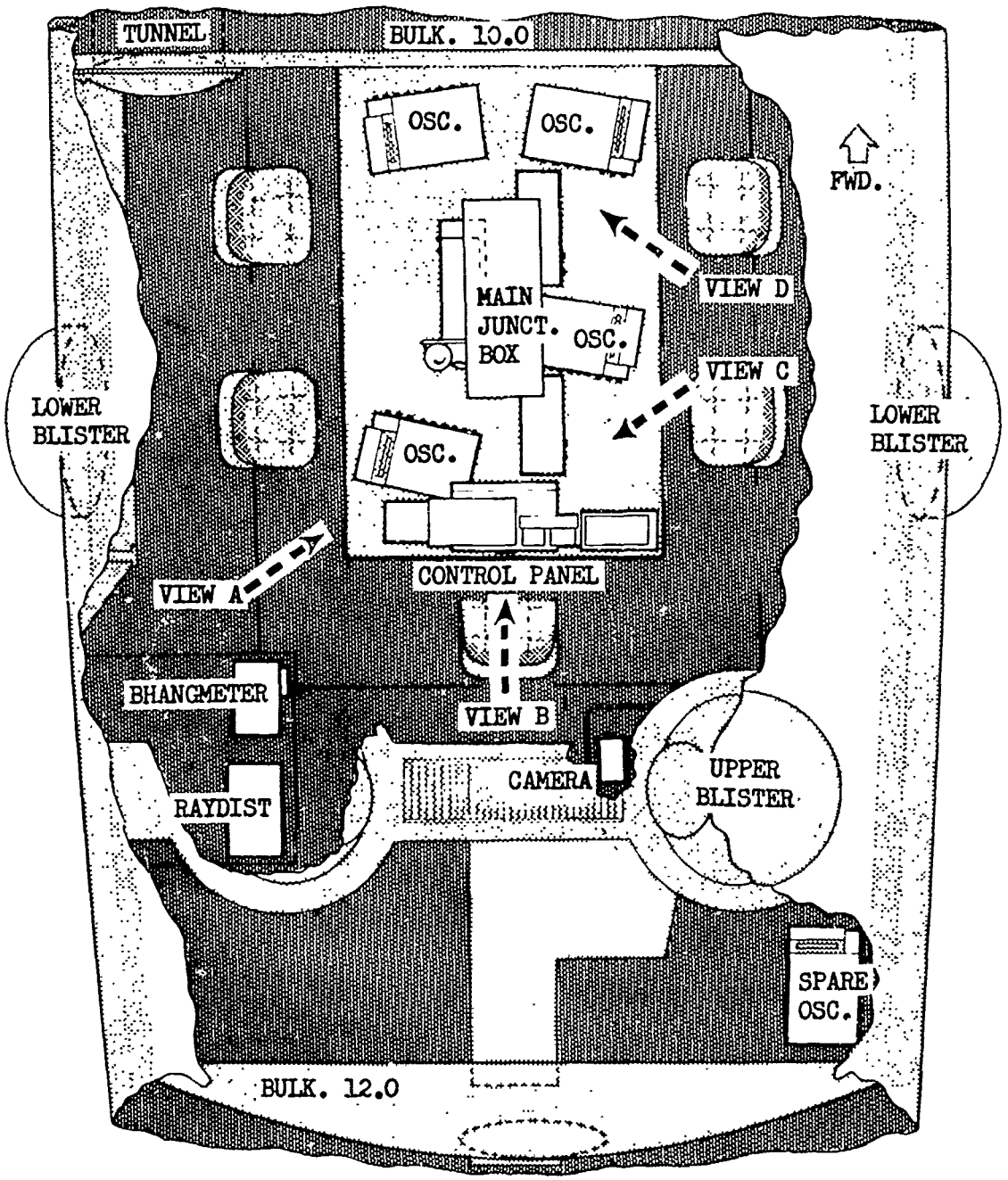

Fig. 3.15 General Arrangement of Instrumentation Equipment in Aft Crew Compartment

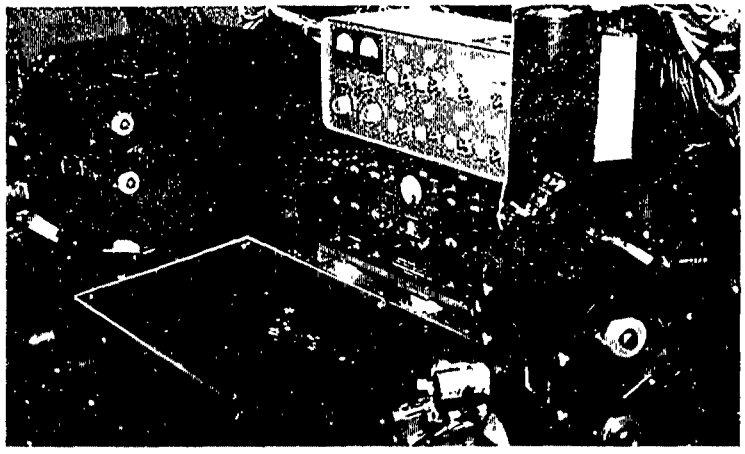

View A

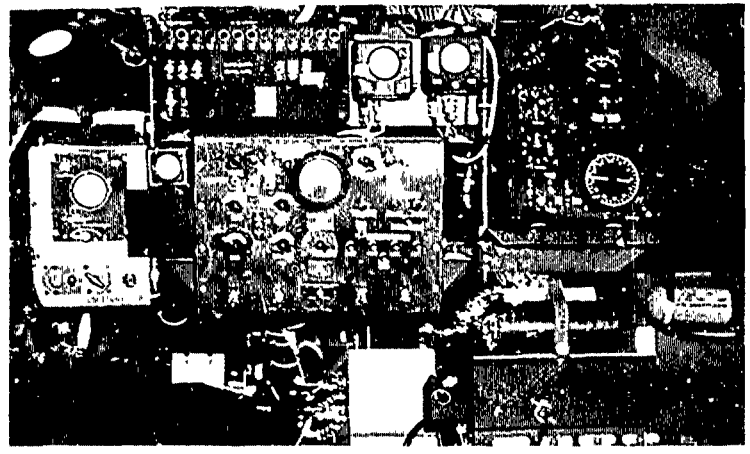

View B

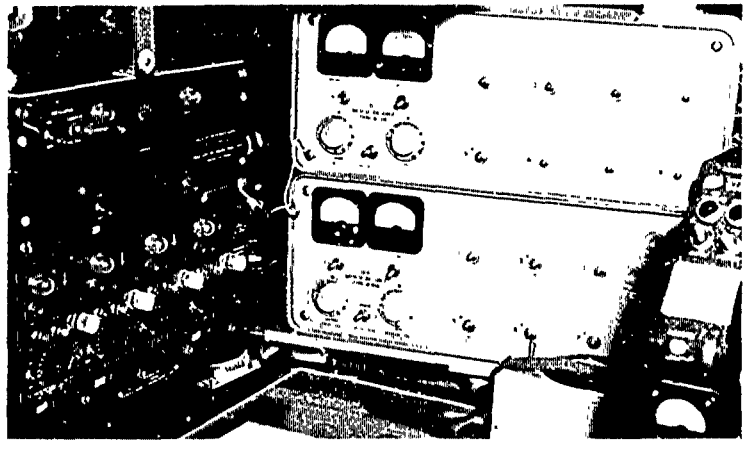

View C

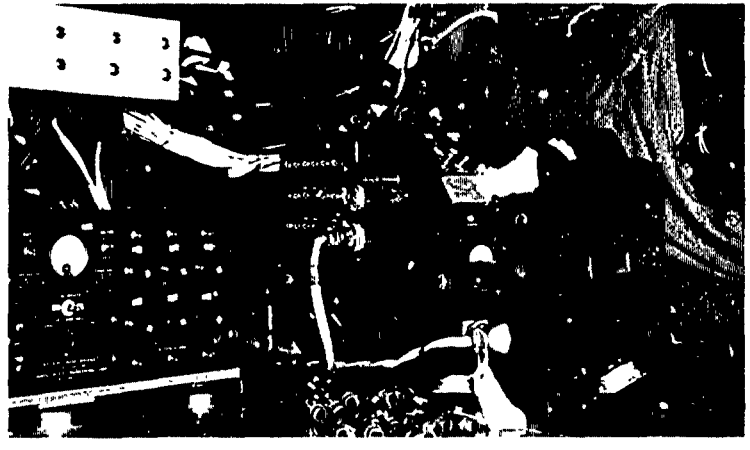

View D

Fig. 3.16 Close-up Views of Instrumentation Equipment In Aft Crew Compartment

compartment and viewed the panel of flight instruments.

3.5 FLIGHT AND POSITIONING PROCEDURES

The following sections describe the operational procedures involved in the preparation and flight of the aircraft, the method of positioning the aircraft at a point in space, and the accumulation of general flight data.

3.5.1 Preparatory Phase

Planning for a given shot participation began with the announcement of the probable and maximum expected yields of the forthcoming shot. Decisions as to aircraft flight altitude, airspeed, and gross weight were made, and followed by the calculation of the nearest safe position for the aircraft. Depending upon whether or not good data could be expected at this position, the decisions as to aircraft participation and position were made. These plans were submitted to the Task Group 7.1 Commander for final approval and for coordination with other participating units. Calculations were made to determine the time delays used to start the two higher-speed oscillographs and the blast-phase cameras, orientation angles of the thermal instrument box, blue box mirror, Bhangmeter photo head, and an attenuation figure for each channel of instrumentation.

Actual preparation of the aircraft and instrumentation system was accomplished during the four days preceding the shot. This work included an operational check of each channel of instrumentation, oscillographs, cameras, and all associated equipment. Final preparations consisted of loading the cameras, applying temp-tapes, and inserting ice into thermocouple cold junction bottles.

Assembly of the flight crew occurred approximately 7 hr before shot time. After an inspection of personal equipment by the aircraft commander, each crew member pre-flighted those parts of the aircraft and equipment for which he was responsible. Discrepancies, if any, were reported at a second crew assembly, final flight briefing was given, and radiation film badges were distributed before boarding the aircraft.

3.5.2 Flight Phase

Take-off was performed 4 hr and 40 min before shot time. During the climb to the test altitude, the instrumentation system was warmed up and preliminary checks and adjustments were made. Upon reaching the test altitude, the aircraft was stabilized in straight-and-level, constant speed flight while each strain bridge channel was balanced, each thermocouple resistance was measured, and circuit sensitivities were recorded. After this instrumentation work was finished, the aircraft was flown over a predetermined path for purposes of checking and calibrating the Raydist tracking system.

At approximately 2 hr before shot time, the radar navigation pattern was entered. A typical pattern, positioned for a tail-to

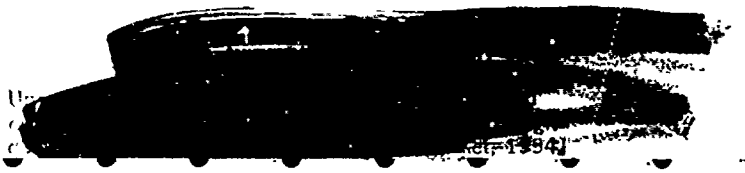

exposure, is shown in Fig. 3.17. Working backwards, the extreme western end of the pattern was located by the point 1 naut mi. (ground range) from the intended time-zero position toward ground zero. From this point, designated B on Fig. 3.17, the pattern was constructed on an east-west axis.

The path was entered at any point and at any time, and the pilot flew the aircraft as closely as possible to the prescribed path under the guidance of the radar operator, who obtained aircraft position information from the K-3 radar system. Since wind conditions varied between shots, the proper aircraft headings on the straight legs had to be calculated, and the optimum bank angle for the turns had to be determined experimentally during the first few cycles around the pattern. As the six points (A through F) of the path were crossed, the times of crossing were noted and recorded. In this manner, the average lengths of time to travel the straight legs and to execute the turns were obtained, and were used to predict the time required for the last (90°) turn and for the 1 naut mi. straight leg immediately preceding time zero.

After the pattern had been traversed several times, the period, or time to complete one cycle, was calculated. By computing ahead to time zero, the number of complete cycles and, in general, the fraction of a cycle remaining, were computed. The partial cycle was eliminated by lengthening or shortening the straight legs of the pattern to lose or gain the required time. The time to fly one normal cycle was on the order of 10 min. As a rule, after five or six cycles, the timing of the pattern flight was accurate to a few seconds; thus about one hour remained to achieve further proficiency and accuracy. The autopilot was used during pattern flying in the interests of maximum consistency and for the maintenance of constant altitude and, indirectly, constant airspeed. During the straight legs of the pattern, the instrumentation crew checked and adjusted, if necessary, the balance of the strain bridge channels. During the last two cycles, each crew member executed final precautionary measures, which included covering all windows with aluminized asbestos shields, the fastening of safety belts, and the switching of his oxygen regulator to 100 per cent oxygen.

On the last cycle, when point B was crossed, the aircraft was rolled out of the turn and flown on a south heading. Shot detonation occurred after 1 naut mi. of straight and level flight. The heading was held through the thermal and blast phases and until all oscillograph recording had ceased. The autopilot was disengaged shortly before expected blast arrival to preclude the possibility of elevator deflections due to autopilot corrections, and to allow the aircraft to ride out the blast disturbance rather than to attempt to hold the aircraft attitude constant. Post-shot circuit sensitivity check procedure was undertaken with the aircraft still at test altitude.

The pattern shown in Fig. 3.17 is representative of the paths used on Shots 1 through 5, the only differences being relocation of the pattern with respect to the earth's surface to accommodate the three different ground zero locations and the various exposure ranges and altitudes. Fig. 3.18 presents the pattern used on Shot 6; in this instance the path consisted of turns to the right and, at detonation,

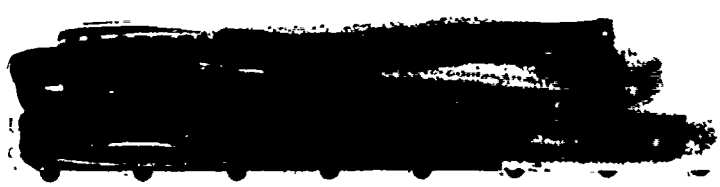

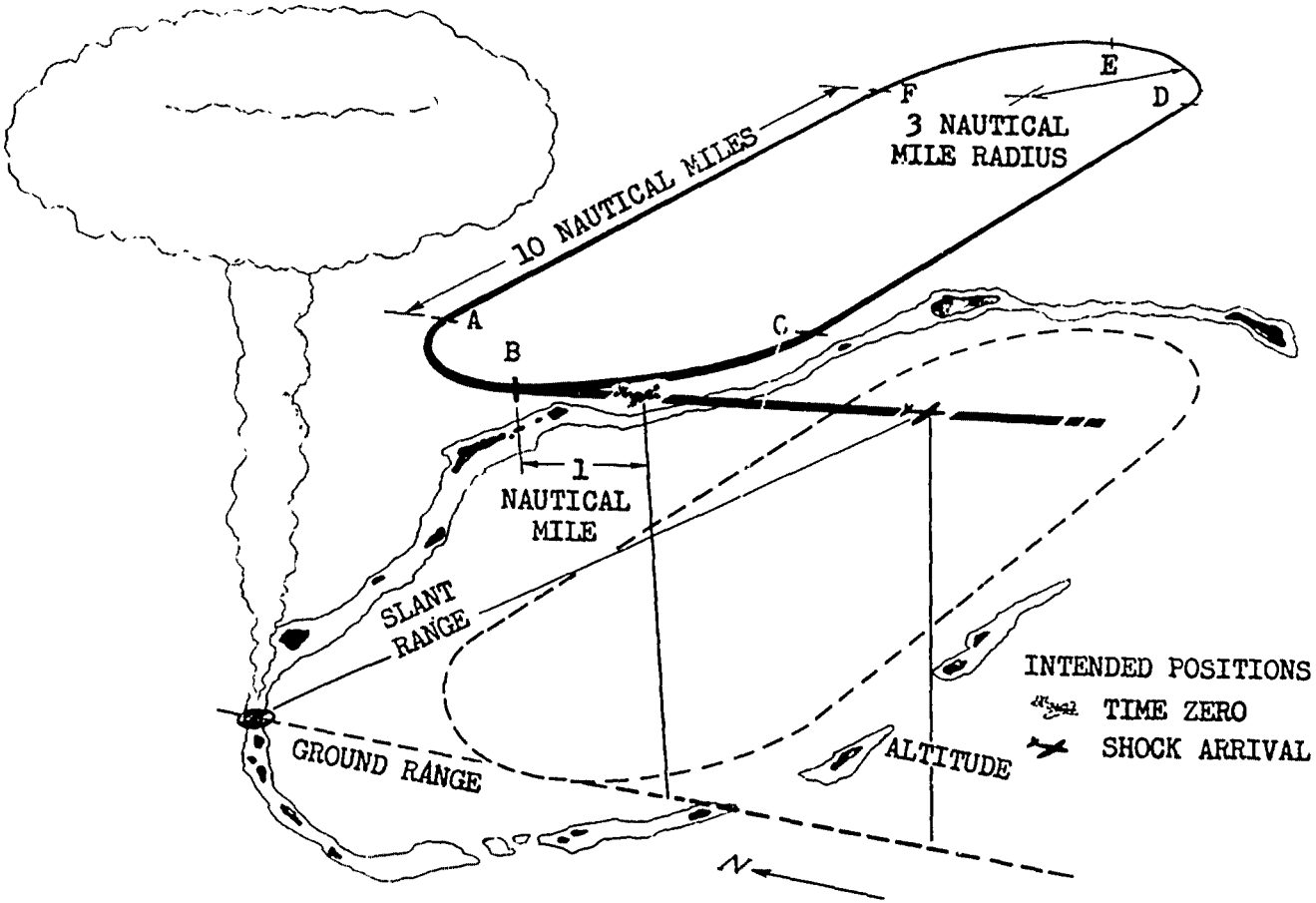

Fig. 3.17 Typical Flight Path For Tail-to Exposure

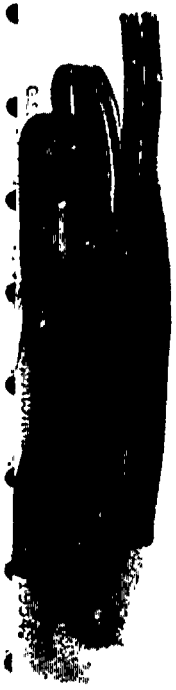

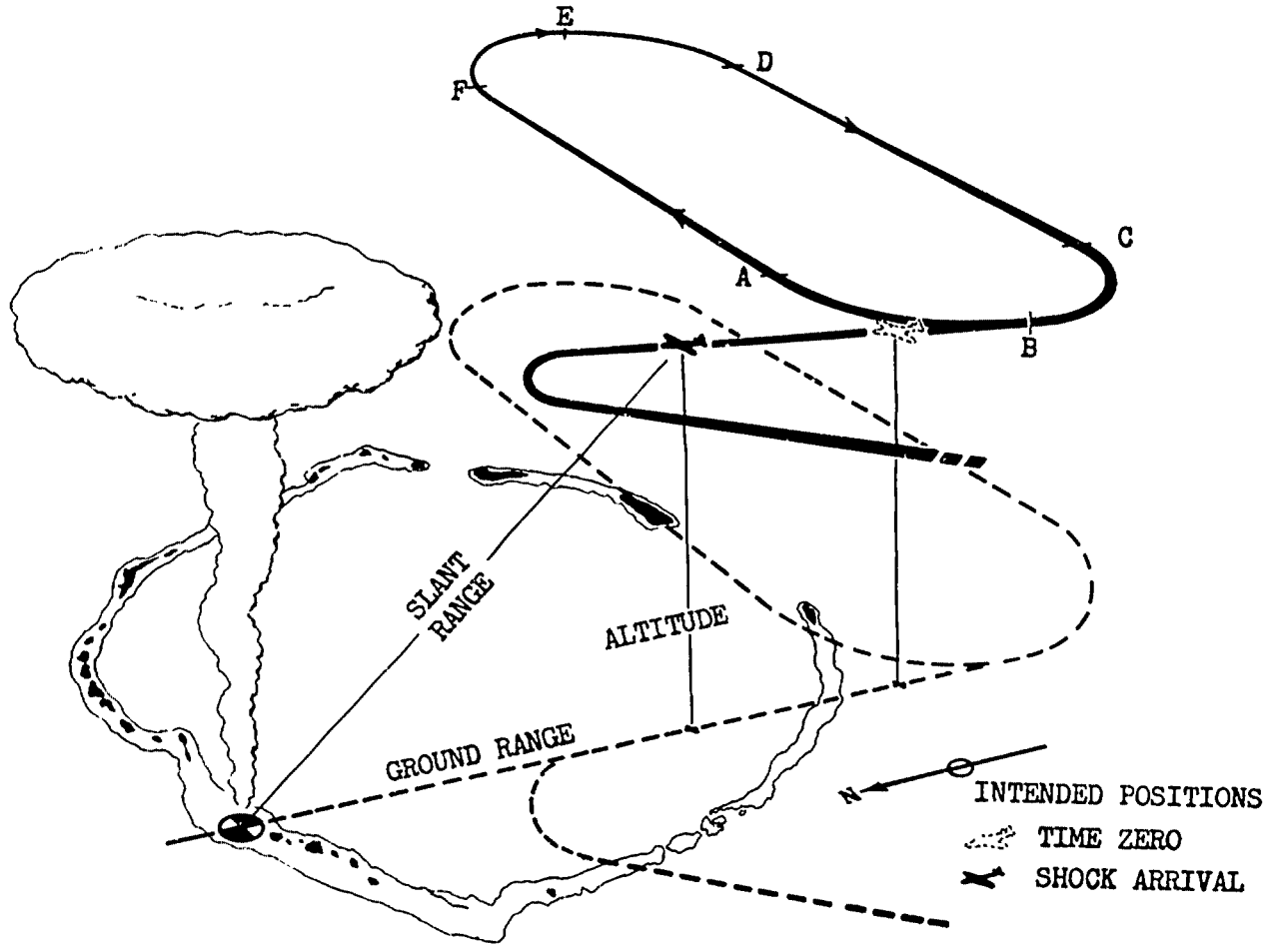

Fig. 3.18 Shot 6 Flight Path, Head-on Exposure

the aircraft was headed north and toward ground zero. This heading was held until 15 sec after the shock arrival, at which time a sharp left turn was executed to avoid the radioactive cloud.

3.5.3 General Flight Data

Very accurate determination of the actual aircraft flight path during the detonation was to have been accomplished by the Raydist radio navigation system, which is explained in detail in reference 18. The system used with the B-36D consisted of a single 100-watt transmitter carried aboard the aircraft and a network of three ground stations, one master and two slave stations. The ground stations received signals from the moving transmitter and also from a fixed transmitter at the master station and, by a technique of phase comparison, the two-dimensional hyperbolic coordinates of the aircraft path were determined. Using simplified mathematical procedures, the hyperbolic coordinates were converted to rectangular coordinates. Due to operational difficulties associated with the unmanned ground stations, Raydist tracking of the B-36D was successful only on Shot 6.

In lieu of Raydist data, the actual aircraft flight paths for Shots 1, 2, 4, and 5 were determined by an analysis of position information obtained from three different sources, namely, the film of the radar system camera, the aircraft navigator, and the time of arrival of the shock front.

The first source mentioned, the radar film, is considered the most accurate of the three: it consists of 35-mm sequenced photographs of the radar return signals as they appeared on the face of the oscilloscope. From shortly before time zero until after the passage of the blast wave, the camera shutter was open for about 355° of each circular radar sweep which required approximately 3 sec for one cycle. During the remaining 5° of sweep, the camera shutter was closed, the film transported, and the shutter reopened. The radar antenna was directed at the area of the detonation so that almost all of the islands of the atoll, as well as the shock front, were visible. Since the aircraft was represented by the point at the center of the sweep, it was possible to determine the aircraft position by comparison of the radar photographs to charts of the area. Accuracy of these position measurements was limited by distortion in the radar "map" and by the effect of the forward motion of the aircraft.

The aircraft navigator, the second source of position information, was requested to record the aircraft positions at time zero and at shock arrival, along with other information, on a special form. The navigator obtained the position information from the radar "dials," two indicators that showed the distances in miles along north-south and east-west lines from the aircraft to a given point of strong radar return such as a barge or a point of an island, the location of which was well known and had been set into the radar system by the radar operator. It was this method that the flight crew employed to fly the aircraft through the racetrack pattern. However, during pattern flying, the radar set was adjusted to operate in "sector scan" which differed from the full circular sweep in that only a small part, perhaps 30°, of

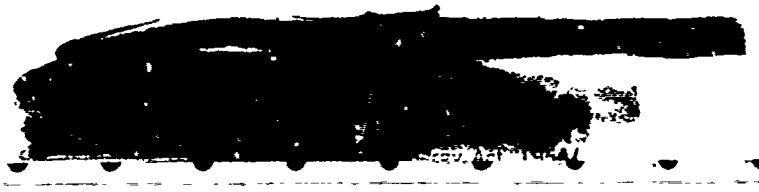

the complete 360° area was searched, and this was accomplished in a reciprocating fashion at a much higher cyclic rate. Improved accuracy is the advantage of the sector scan; but, if used during the detonation to obtain oscilloscope photos, only a few islands of the atoll and a small part of the shock front would be visible. Therefore, the radar operator switched from sector scan to full sweep shortly before time zero.

The third source of position information, the time of arrival of the shock front, involved the calculation of the range from a formula relating range to yield, and the time between the instant of detonation and arrival of the shock front at a given receiver. This interval of time was obtained by counting, on the oscillograph record, the number of cycles of the 100-cps timer between time zero, as indicated by the blue box, and the deflection of that oscillograph channel first affected by the shock front.

Additional data and information of a general nature concerning each shot and flight were obtained from check lists completed by crew members, from the photographs of a special instrument panel and from the measurement of the fuselage incidence angle.

The aircraft commander wrote, after each flight, a short report containing his observations, impressions, and reactions, as well as those of the other crew members. The navigator completed a special form which contained the above mentioned position information, as well as flight times, airspeed, wind, ground speed, heading, track, and absolute and pressure altitudes, all for both time zero and shock arrival. The flight engineer's form contained gross weight, center-of-gravity location, and fuel distribution information for both pre-takeoff and time zero, engine speeds, cabin temperature and pressure altitude at time zero, engine operating periods, and comments about the operation of the engines and propellers during the thermal and blast phases. In addition to the general interest value of these reports, some of these data were required to define the test conditions and, in this way, to assist in the analysis of the time-history oscillograph data.

The absolute altitude obtained by the navigator was read from one of the aircraft barometric altimeters which was adjusted and calibrated by means of the K-3 radar system to indicate absolute altitude. The radar accuracy was checked, in turn, at least once during each flight by the radio altimeter.

A special instrument panel and camera were provided in the aft crew compartment for the purpose of obtaining, automatically, a permanent record of certain flight variables in the event that unusual or emergency measures on the part of the crew might result in the loss of important flight information. The instruments on the panel were a clock, altimeter, airspeed meter, directional gyro, turn-and-bank indicator, and free-air temperature gage. With necessary lighting provided by floodlamps, the panel was photographed by a GSAP motion-picture camera for a period of about 2 min., starting approximately 5 sec before detonation.

To define the orientation of the aircraft in the vertical plane, the incidence angle of the fuselage was measured during each flight shortly before time zero. This angle varied with altitude, airspeed,

gross weight, and the thrust of jet engines in operation. Since the relationships between the surface angle of each thermal response measurement location and the fuselage centerline had been established by measurements while on the ground, it was important that the angle between the fuselage centerline and the horizontal be determined for each shot. This angle, plus those resulting from ground ranges and altitude, defined the thermal radiation incidence angle at time zero and the blast incidence angle at shock arrival. Changes in the angles due to structural elasticity of the aircraft are not included. A Watts Clinometer, Mark VA, was used to measure the angle from horizontal to the top of the instrumentation table in the aft crew compartment, the table being referenced to the fuselage centerline by a ground calibration.

3.6 PARTICIPATION AND PREDICTED INPUTS AND RESPONSES

For safety reasons, positioning of the B-36D was based on the predicted maximum possible yields. If a large difference existed between maximum and probable yields, the possibility of obtaining data approaching the aircraft limitations was remote; nevertheless, participation in every shot was considered valuable, provided it did not compromise the participation in a later shot that was expected to produce more conclusive results.

For Shots 1 through 5, the aircraft was flown in a tail-to orientation with respect to the burst point during both thermal and blast phases, and for all five shots the exposure positions were determined by the critical thermal response. It was predicted that, if the aircraft were in proper position and the yield were equal to the predicted maximum, the elevator skin temperature would rise 400°F (the critical thermal response) and the stabilizer, at shock arrival would be stressed to some value less than 100 per cent of limit allowable bending moment (the critical blast response).

For Shot 6, the aircraft aspect was head-on or toward ground zero. Since this was the first attempt at experimental verification of theoretically predicted responses for this orientation, positioning was based on obtaining conservative but useful values of wing, stabilizer and fuselage moments during the blast phase. To achieve the selected position at shock arrival with head-on aspect, the aircraft position during the thermal phase was at such a distance from the fireball as to make the thermal response insignificant.

Table 3.3 presents positioning and predicted inputs and response information for each of the six shots.

TABLE 3.3 - Positioning Information

Shot	1	2	3	4	5	6
Predicted Yields						
Maximum (MT)	12	15	6	15	12	5
Probable (MT)	5	8	2.5	4	12	2
Aircraft Position and Configuration						
Absolute Altitude (ft)	33,000	37,000	40,000	37,000	40,000	32,000
Horizontal Range at Time Zero (ft)	50,000	50,000	40,000	50,000	39,500	121,400
Horizontal Range at Shock Arrival (ft)	75,700	78,500	67,800	78,500	65,450	90,350
Equivalent Airspeed (mph)	166	166	166	166	176	166
Gross Weight at Time Zero (lb)	250,000	250,000	250,000	250,000	230,000	250,000
Predicted Inputs, Based on Maximum Yield						
Radiant Exposure (cal/sq cm)	42	46	25	46	47	2.5
Overpressure (psi)	0.68	0.62	0.44	0.62	0.60	0.39
Predicted Responses Based on Maximum Yield						
Temperature Rise of Critical Skin (°F)	400	400	400	400	400	----
Stabilizer Bending (Percent of Design Limit)	57	59	60	59	83	44

CHAPTER 4

RESULTS

4.1 GENERAL

Project 6.2a participated in all six shots of the CASTLE sequence. On four of the shots, data pertaining to tail-to exposures were obtained. It appears that sufficient data were obtained on these four shots to permit a correlation between predicted and measured effects within the ranges of 37 to 64 per cent of the aircraft safe thermal limit and of 37 to 76 per cent of the safe blast limit. During Shot 6, the head-on aspect was explored and blast loads up to 27 per cent of the aircraft safe limit were measured. During Shot 3, no useful data were recorded because of the unexpected low yield.

The Shot 1 yield of about 15 MT, approximately 25 per cent greater than the positioning yield, provided interesting results, including the highest peak overpressure, 0.81 psi, recorded at the B-36D during the entire sequence. The damage to the aircraft from this relatively high overpressure necessitated the replacement of the bomb bay doors, the aft lower plexiglas blisters, and the radar antenna radome. The replacement of these items, plus the repair of other damaged components on the aircraft, required approximately 818 man-hours of labor.

The yields of Shots 2 and 4 were less than the predicted values on which the aircraft positioning was based; as a result, the B-36D was stressed to less than half of its safe limits during these two shots, but the data were valuable in confirming the relationships between lower-level inputs and responses.

The conditions of Shot 5 were most conducive to the attainment of responses approaching the safe limits of the aircraft. The yield was predicted (12 MT) with less conservatism compared to previous shot estimates, since the Shot 5 device was similar to the one previously detonated as Shot 2. This realistic yield prediction, with consequent close-in positioning, and the fact that the actual yield was about 13.5 MT, resulted in the largest temperature rise and stabilizer bending moment recorded, 322°F and 76 per cent of limit, respectively. The radiant exposure at the aircraft during Shot 5, 45.9 cal/sq cm, was less than that for Shot 1, 47.5 cal/sq cm, but the incidence angle was smaller, resulting in more thermal energy absorbed by the underside of

the aircraft during Shot 5. This was apparent from the extent of the thermal damage after Shot 5. The elevator skin was permanently buckled at four places, and a large percentage of the paint on the stabilizer and elevator was blistered and peeled.

Although radiation monitors were carried aboard the aircraft on all shots, only on Shot 5 was a reading observed. The maximum value was 20 mr, with radiation detected over a period of about 20 sec. After the completion of the overseas phase of the experiment, and upon the arrival of the aircraft in the continental U.S., residual radiation, eminating from microscopic particles imbedded in the paint and lodged in the joints of the aircraft skin, was detected. The problems produced by this contamination are discussed in detail in Chapter 5 of this report.

General flight information; that is, the data necessary to define the position, orientation, and configuration of the aircraft, and also certain atmospheric data for each shot, is presented in Table 4.1. Absolute altitude was read from the aircraft barometric altimeter which had been calibrated and checked periodically during each flight by the K-system radar.

A comparison of the actual range figures, as given in Table 4.1, with the intended ranges of Table 3.3 shows that the crew flew the aircraft to the intended position at time zero with errors ranging between 600 to 1700 ft. In percentage of the horizontal range to ground zero, these distance errors vary from 0.5 to 3.3 per cent.

Table 4.2 is a summary of the maximum values of the principal items of instrumentation, which include the thermal and pressure inputs and the temperature and strain responses.

For Shot 6, the only head-on exposure, the aircraft was at so great a range at time zero that the data recorded during the thermal phase was of no useful value.

Time-history input and response curves, photographs of the damage to the aircraft, and observations of the flight crew, with all items divided into the two principal phases of the detonation, thermal and blast, are presented in the following sections of this chapter. The time-history curves represent the bulk of the data obtained by Project 6.2a; they are presented here primarily to convey general variations of the functions rather than to emphasize detailed or minute variations. All channels of time-history instrumentation, plotted on graph paper from which fine details of the curve can be read, are available in reference 19.

The observations of the flight crew, although excluded from the collection of scientific data, are presented in this report in the belief that they may be beneficial to participants in future tests of this nature and to Air Force personnel being trained for strategic missions. It should be realized that the observations of human beings are tempered by experience and emotion and, in some instances, may not be true representations of the actual conditions; however, valuable information may be obtained from data of this nature.

4.2 THERMAL RESULTS

Significant thermal data were obtained during Shots 1, 2, 4, and

TABLE 4.1 - General Flight Data

SHOT	1	2	4	5	6
CODE NAME	BRAVO	ROMEO	UNION	YANKEE	NECTAR
YIELD, M.T.	15.0±0.5	11.0±0.5	7.0±0.3	13.5±1.0	1.7±0.3
Altitude, absolute, ft	33,000	37,000	37,100	40,000	33,000
Ambient pressure at a/c altitude, psi*	4.14	3.52	3.46	3.00	4.14
Equivalent airspeed, mph	166	166	166	176	166
Free air temperature, °F	-16	-45	-37	-53	-22
True airspeed, fps	426	450	457	508	423
Wind at test altitude					
Speed, knots	35	24	38	60	17
Direction	238°	187°	263°	265°	184°
Ground Speed, fps	399	409	444	509	452
Gross weight, lb	245,679	246,039	249,879	230,068	250,079
C.G. location, % M.A.C.	36.0	36.5	36.0	36.0	36.0
True heading	180°	180°	188°	180°	360°
Incidence angle of fuselage centerline	3° 15'	4° 2'	3° 0'	2° 5'	3° 20'
At Time Zero					
Horizontal range, ft	50,800	51,700	50,500	40,600	122,000
Slant range, ft	60,580	63,580	62,700	56,990	126,380
Angle to horizontal	33° 1'	35° 35'	36° 18'	44° 35'	15° 8'
At Shock Arrival					
Time, seconds after zero	53.87	62.45	69.49	57.245	79.588
Horizontal range, ft	71,500	77,900	81,600	69,700	86,000
Slant range, ft	78,750	86,240	89,600	80,360	92,111
Angle to horizontal	24° 46'	25° 24'	24° 27'	29° 51'	20° 59'

NOTE: All data concerning ranges are calculated from radar scope photos except for Shot 6, which is Raydist data.

*Weather Balloon Readings Taken From U.S.S. Curtiss

TABLE 4.2 - Data Summary

SHOT	1	2	4	5	6
Code Name	BRAVO	ROMEO	UNION	YANKEE	NECTAR
Time	0645	0630	0610	0610	0620
Date	1 March	27 March	26 April	5 May	14 May
Yield	15.0±0.5	11.0±0.5	7.0 ± 0.5	13.5±1.0	1.7±0.3
Radiant Exposure, cal/sq cm	47.5	35.2	17.4	45.9	—
Max. Irradiance, cal/sq cm/sec	6.2	5.2	3.7	7.2	—
Max. Temperature rise of elevator skin at Sta. 144.5 in., per cent of 400°F limit	52*	45	37	64	—
Max. Overpressure, psi	0.81	0.56	0.42	0.60	0.22
Max. Pressure on underside of					
Wing, psi	0.90	0.62	0.48	0.68	0.27
Fuselage, psi	0.92	0.64	0.48	0.67	0.23
Stabilizer, psi	1.20	0.83	0.60	0.85	0.25
Max. Positive Bending Moments,** per cent of limit***					
Stabilizer, Station 62 in.	59	60	37	76	27
Fuselage, Station 1476 in.	50 to 70	47 to 67	22 to 42	67 to 87	4 to 20
Wing, Station 1062 in.	50	50	44	53	49

*Temp-tape data

**Max. positive bending moments are the peak incremental bending moments plus dead weight and in-flight conditions.

***Bending moment limits are defined in Section 5.3

5. These results include time-history input and response curves, peak temperature data, damage photographs, and flight crew observations.

4.2.1 Thermal Input Results

The radiant exposure and irradiance for Shots 1, 2, 4, and 5 are shown in Fig. 4.1 and 4.2, respectively. The curves represent the average of the data available from the multiple instrumentation. All known instrument corrections have been applied. The photographs taken by the GSAP cameras mounted in the box along with the thermal instruments indicated angular misalignments of approximately 1°, 1°, 4°, and 2° for Shots 1, 2, 4, and 5, respectively; corrections for these misalignments are negligible. Fireball photographs taken at approximately one-half second after detonation and used in this determination of the aircraft orientation are shown in Fig. 4.3.

In Fig. 4.1, on which radiant exposure data are graphically presented, the curves for Shots 1, 2, and 4 are the average of the data from calorimeters No. 1, 2, and 3 (see Table 3.1). The calibrated recording range of calorimeters No. 1 and 2 was never exceeded, but the range of calorimeter No. 3 was exceeded during Shots 1 and 2; however, the values of radiant exposure read from calorimeter No. 3, with an extended calibration, agreed well with the readings of instruments No. 1 and 2. Therefore, the data from all three instruments were considered in the final curves. For Shot 5, the range of calorimeter No. 3 was exceeded and the data were about 9 per cent less than the readings of calorimeters No. 1 and 2, which agreed with each other to within ± 2 per cent; therefore, the curve for Shot 5 is the average for instruments No. 1 and 2, only. The range of calorimeter No. 4 was exceeded to such an extent on Shots 1, 2, 4, and 5 that the data from this instrument were not usable.

The irradiance curves are the average of the data from the two radiometers, which agreed relatively well with each other for all shots.

4.2.2 Thermal Response Results

The time-history temperature data are shown in Figs. 4.4, 4.6, 4.7, 4.8, 4.10, 4.11, 4.12, and 4.13.

Figure 4.4 presents the skin temperatures for the two instrumented stations of the left elevator. One should note that the ambient temperature of the installation at Station 312 in., for a given shot, is higher than the ambient temperature for the same shot at Station 144.5 in. The reason for this is that Station 312 in. was directly behind the left inboard engine and was heated somewhat by the exhaust gases and particles of oil from that engine.

That Shot 5 caused a greater thermal response than either Shot 2 or 4 is obvious from the curves, not only because the peak temperatures of Shot 5 are the highest, but also because the time-zero temperatures of Shot 5 are the lowest. A close examination of the Shot 5 curves in Fig. 4.4 reveals that the temperature rise at Station 144.5 in. was 322°F, and the rise at Station 312 in. was 247°F. A preliminary investigation indicates that the 247°F figure is in line with the other thermal response data, and that the 322°F value is much too high. An

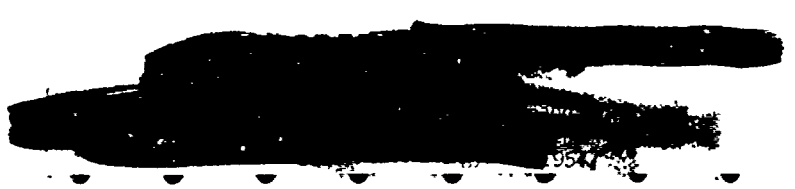

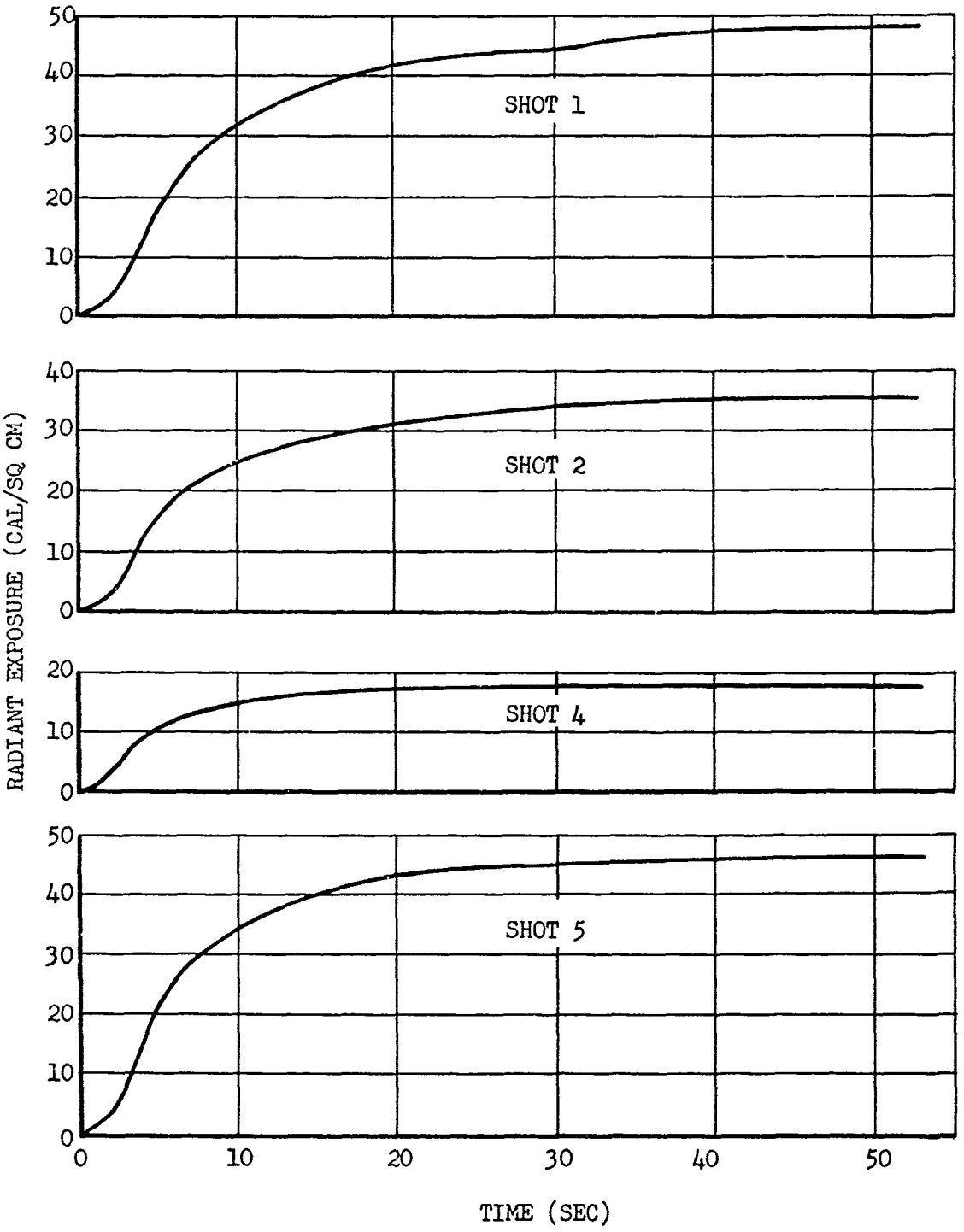

Fig. 4.1 Radiant Exposure vs Time

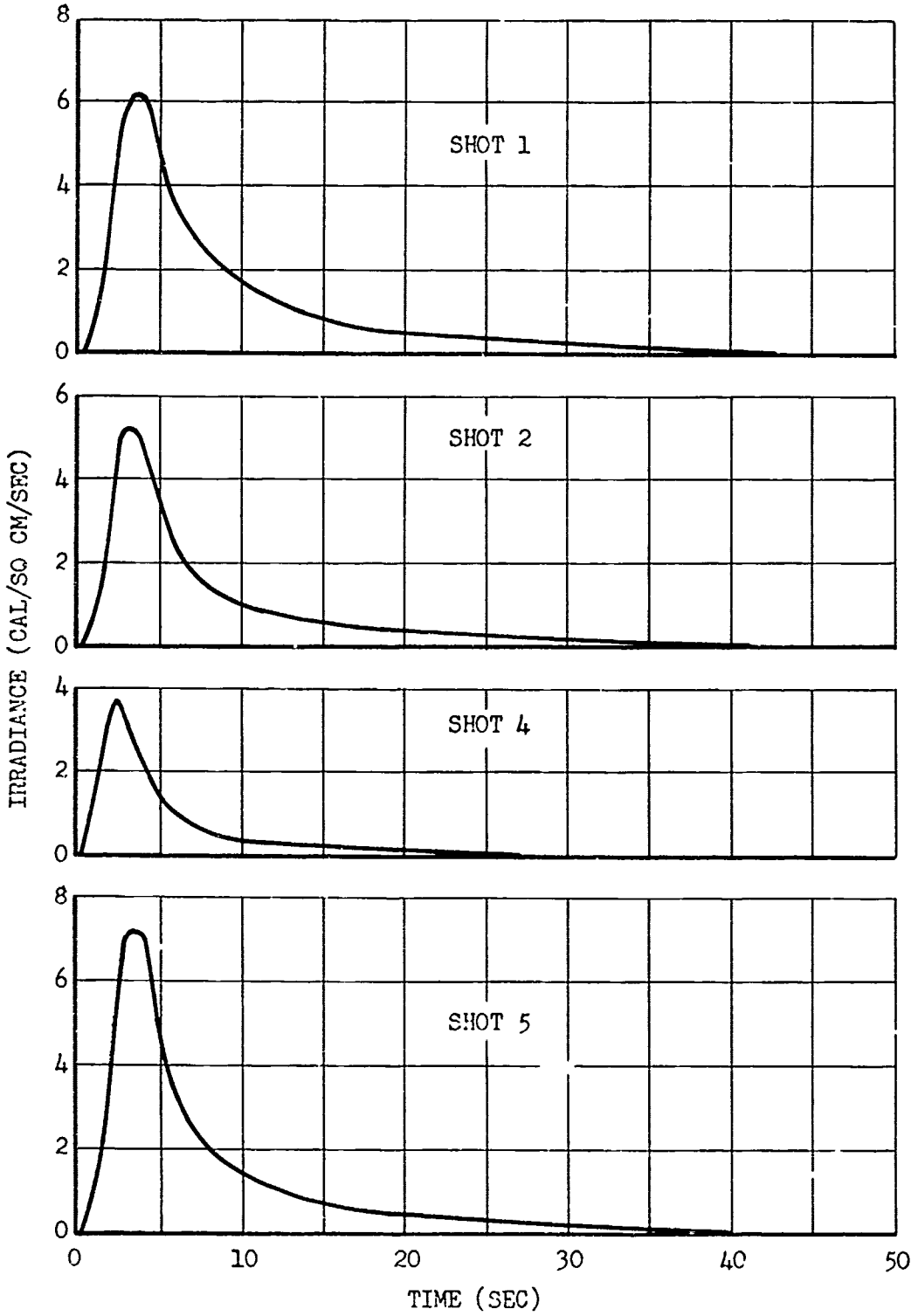

Fig. 4.2 Irradiance vs Time

Shot 1

Shot 2

Shot 4

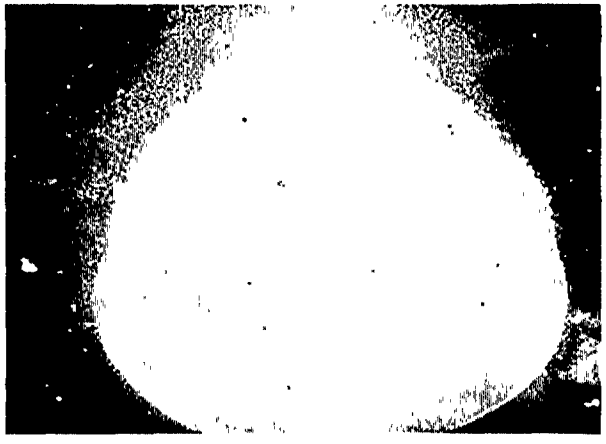

Shot 5

Fig. 4.3 Fireball Photographs Taken From the B-36D Tail Turret

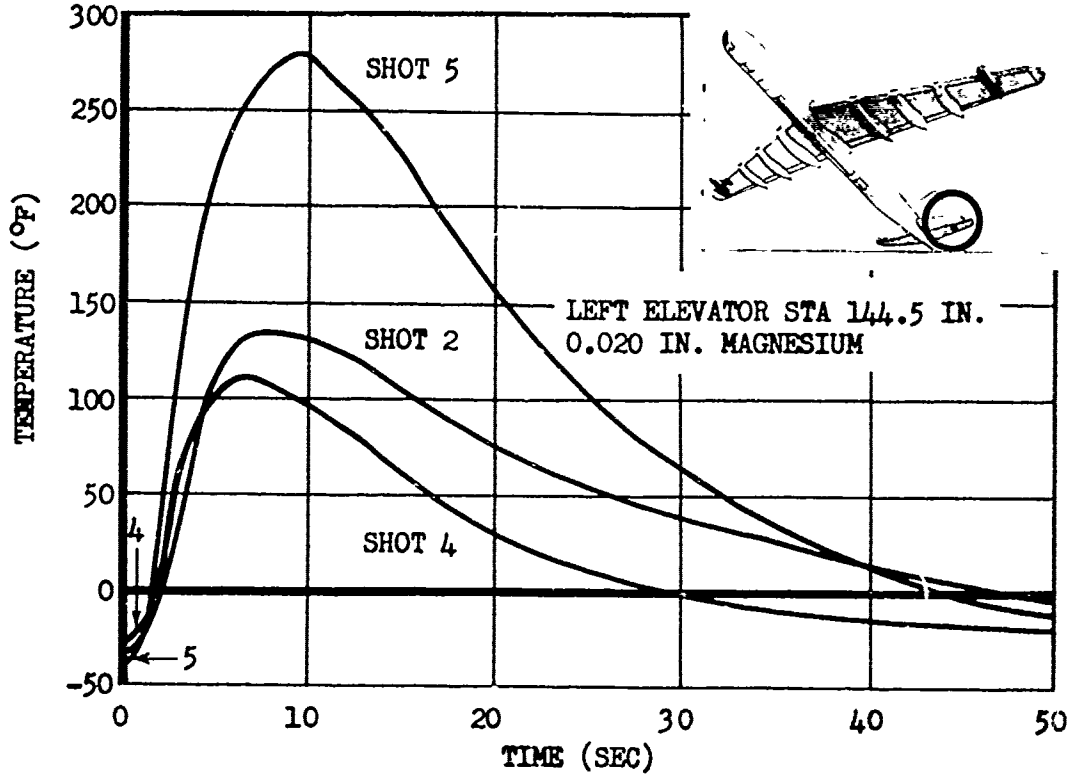

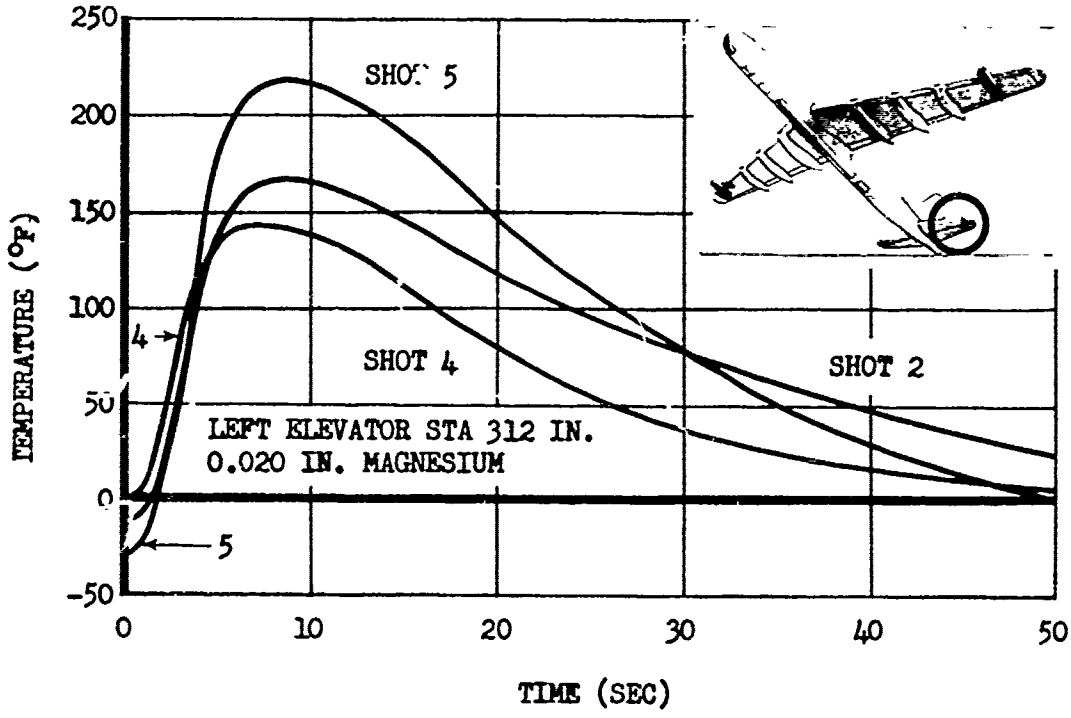

Fig. 4.4 Elevator Skin Temperature vs Time

explanation of this high temperature rise is given in the following paragraph.

The installations at the two elevator stations, 144.5 and 312 in., were similar in all respects except one - Station 312 in., being behind the inboard reciprocating engine, was usually dark in color because of black oil thrown out by the engine and carried back to the elevator by the slipstream. Station 144.5 in., however, was outside of the contaminated zone and the surface remained relatively clean. As a result of this difference in color, one would expect the temperature rise at 312 to be higher than at 144.5. A check of the curves for Shots 2 and 4 (see Table 4.3) bears this out; however, the Shot 5 results

TABLE 4.3 - Temperature Rises of Elevator Skin

	Shot 2	Shot 4	Shot 5
STATION 144.5 in.	167°F	139°F	322°F
STATION 312 in.	178°F	147°F	247°F

appear to be contradictory. An examination of the installations after the shot revealed that the white paint was missing in spots over the entire elevator, and one of the larger spots was found around the thermocouple at Station 144.5 in., as shown in Fig. 4.5; however, the

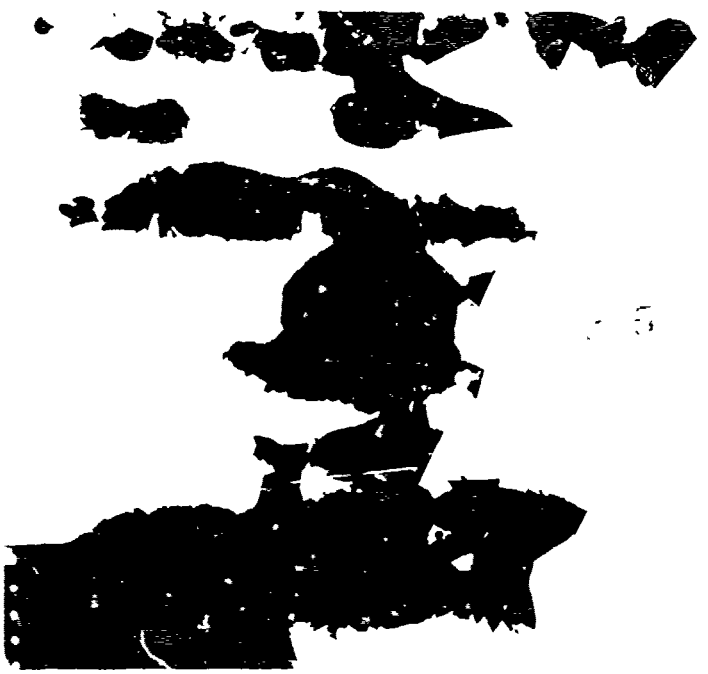

Fig. 4.5 Undersurface of Left Elevator at Thermocouple Location, Sta. 144.5 in., After Shot 5

white paint in the immediate area around the thermocouple at Station

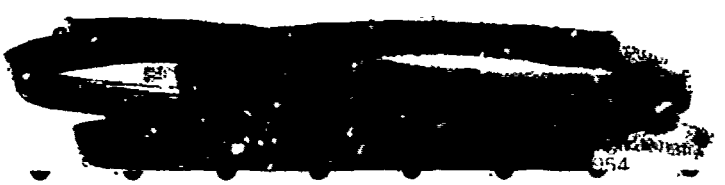

312 in. was intact. Therefore, the paint around Station 144.5 in. was blistered during the first few seconds of the thermal phase and blown away by the slipstream, thus presenting during the remainder of the thermal phase the dark and bare magnesium surface which then absorbed a greater percentage of the thermal energy, causing it to rise to a higher temperature than its white-painted counterpart.

TABLE 4.4 - Temperature Rises of Stabilizer Skin

	Shot 1	Shot 2	Shot 4	Shot 5
STATION 313 in.	227°F	174°F	82°F	206°F

Figure 4.6 presents the temperature response curves for skin of the left stabilizer at Station 313 in. for Shots 1, 2, 4, and 5; maximum temperature rises are summarized in Table 4.4. This was the only Shot 1 thermocouple installation that was reinstrumented for subsequent shots. The curves show that the temperature rise for Shot 1 was 21°F greater than that for Shot 5. Calculations of the effective radiant exposure, that is, the total radiant exposure as indicated by the calorimeters multiplied by the cosine of the incidence angle, indicate that the temperature rise of the stabilizer skin should have been greater for Shot 5 than for Shot 1. No reason or explanation for this reversal has been proposed, but the effect might have been caused by

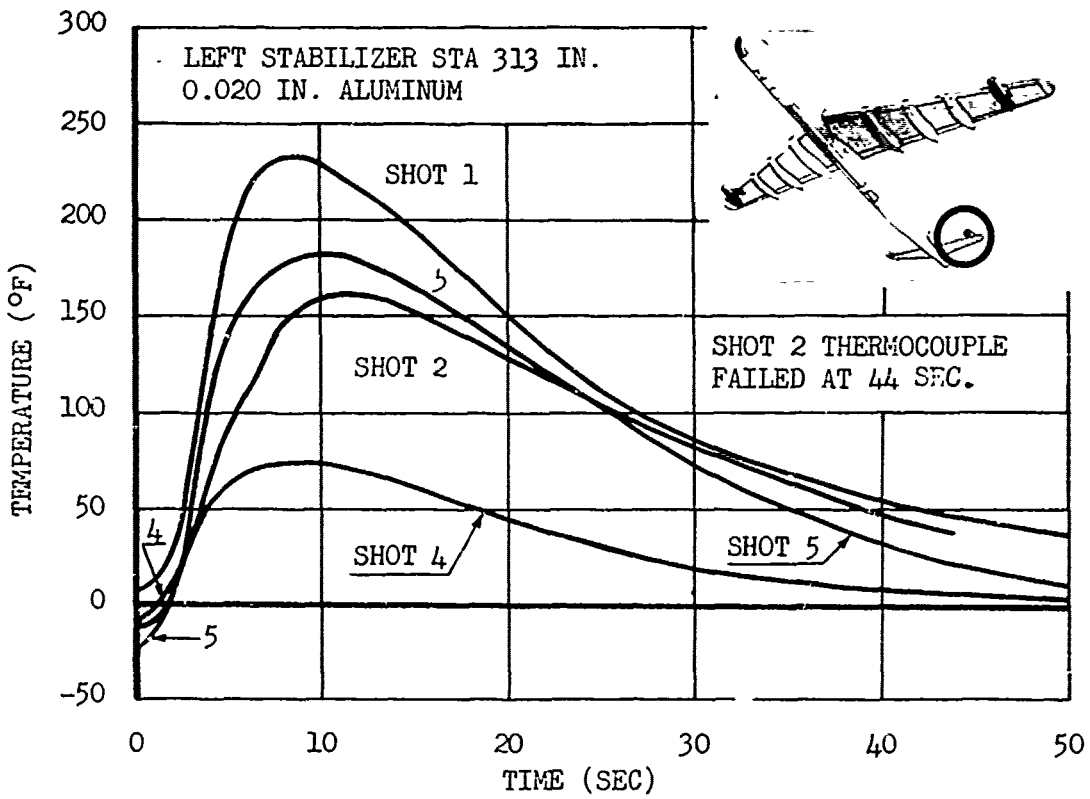

Fig. 4.6 Stabilizer Skin Temperature vs Time

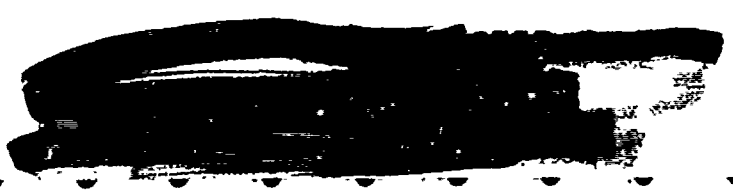

many factors, such as different conditions in the deposit of oil from the engine, a possible difference in response between the peened-wire installation of Shot 1 and the welded-wire installations used on all other shots, or the higher equivalent airspeed and the lower time-zero temperature during Shot 5 as compared to Shot 1.

Shown in Fig. 4.7 are the temperature response curves for the fuselage skin at Station 1898 in. for Shots 2, 4, and 5, where the fuselage construction was 0.025-in. aluminum skin riveted to stringers. This location and construction might explain why the temperature curves appear to have more rounded peaks and a lower rate of cooling than the curves for the Metlbonded hat panels of the elevator (Fig. 4.4).

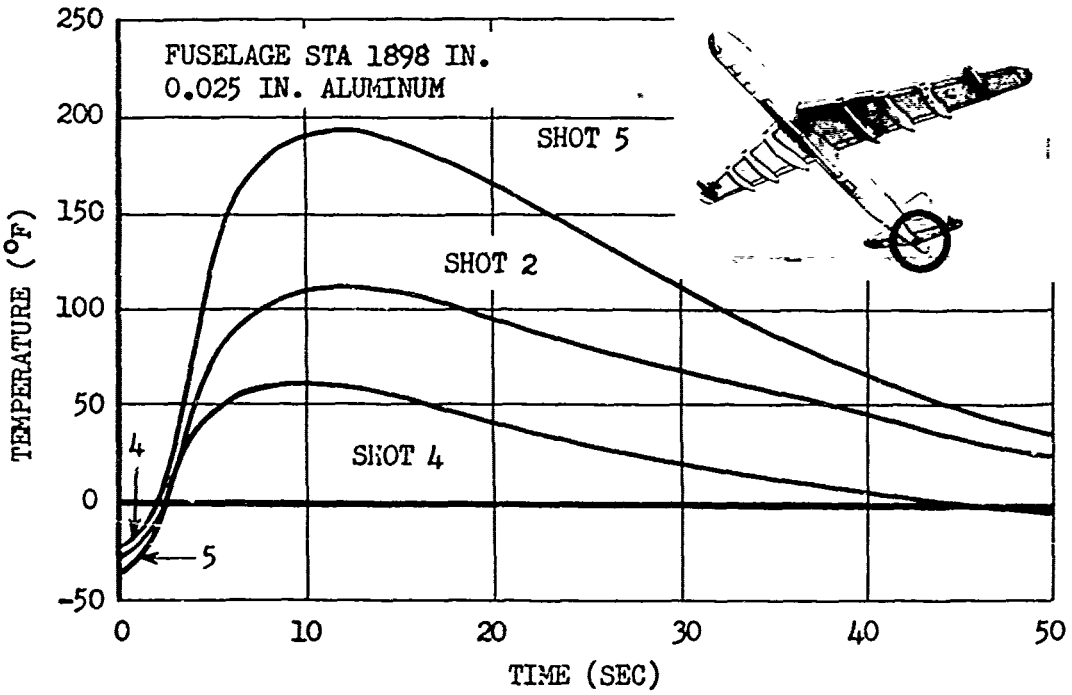

Fig. 4.7 Fuselage Skin Temperature vs Time

Figures 4.8, 4.10, 4.11, and 4.12 present the temperature curves for installations on Waffle panels of the left wing. Figure 4.9 shows the thermocouple arrangement that was utilized during Shots 2, 4, and 5 for wing waffle panel temperature measurements. The difference between the use of white enamel and aluminized lacquer can be studied by comparing the temperature rises of the skins at Stations 1068 and 1106 in. The data presented in Table 4.5, indicate that the absorptivity of the aluminized lacquer surface was slightly higher than the white enamel surface for Shots 2 and 5 and essentially equal for Shot 4.

The waffle panel temperature distribution curves are interesting in that they show graphically the time lags of the temperature rises of the three points of the waffle panel which bring about uneven expansion of the panel as a unit and result in thermal stresses.

Figure 4.13 presents the data obtained from the special instal-

TABLE 4.5 - Temperature Rises of Wing Waffle Panel Skin

	Shot 2	Shot 4	Shot 5
STATION 1106 in. (aluminized lacquer)	178°F	111°F	297°F
STATION 1068 in. (white enamel)	160°F	112°F	286°F

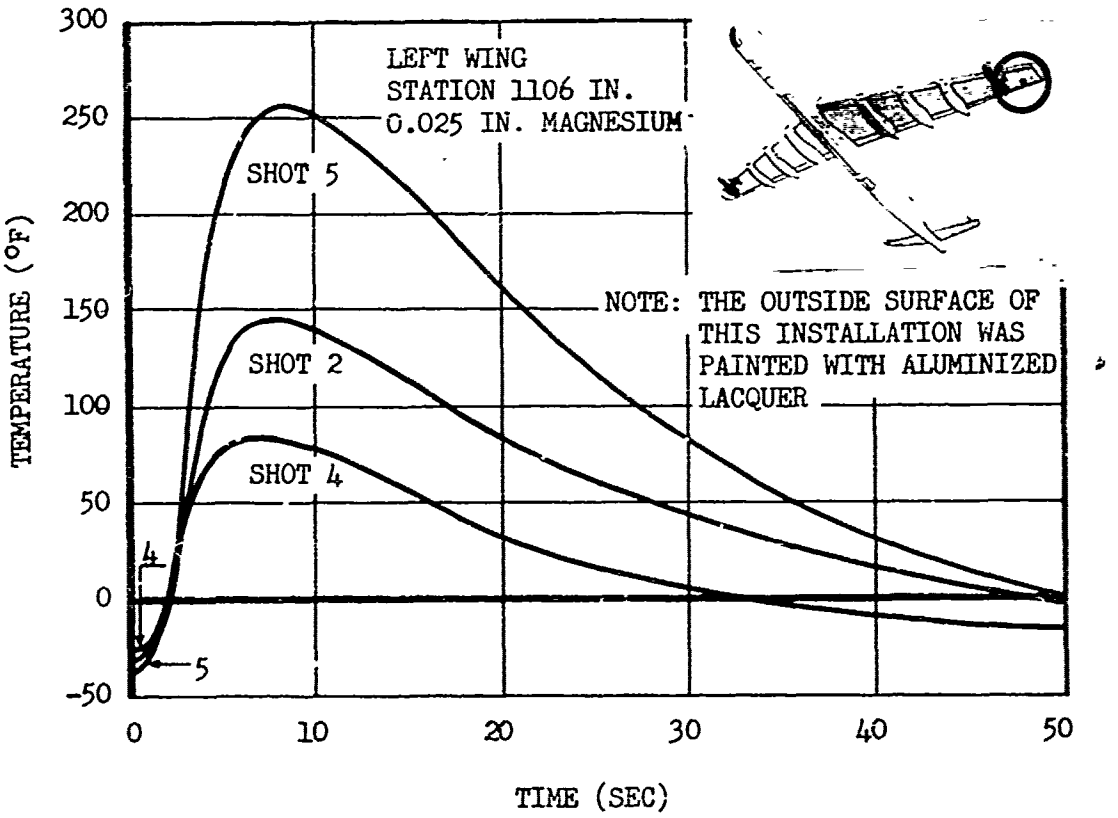

Fig. 4.8 Wing Skin Temperature vs Time

lation located inside the aft lower left blister for shots 4 and 5. A comparison of the energies received inside the blister with those received outside (Fig. 4.1) for corresponding shots indicates that 76 and 71 per cents of the energies were received inside the blister for Shots 4 and 5, respectively. With this attenuation of the Plexiglas blister in mind, the hat panel skin temperature data can be analyzed to determine the cooling effect of the airstream over the external skin of the aircraft, in particular, that of the elevator since the installation was constructed from a section of an elevator hat panel and oriented so that the thermal energy would be received at approximately the same angle as that of the elevator.

The peak temperature data, as obtained from temp-tapes positioned

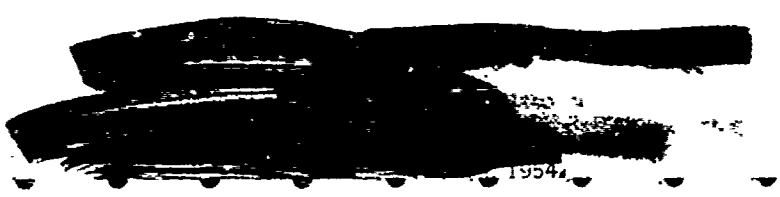

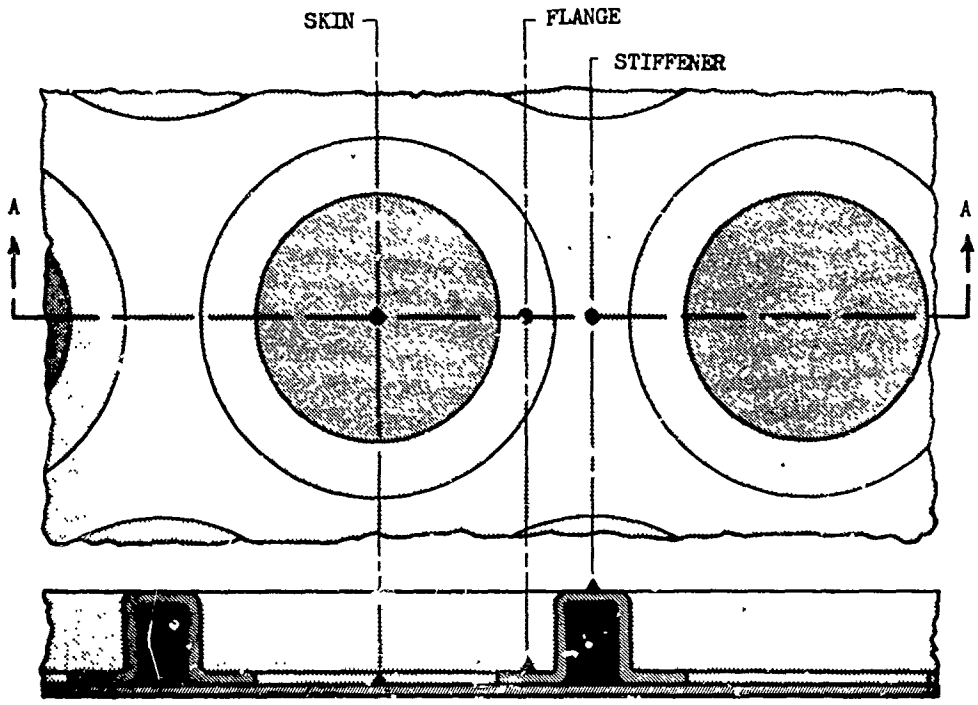

Fig. 4.9 Wing Waffle Panel Thermocouple Installations

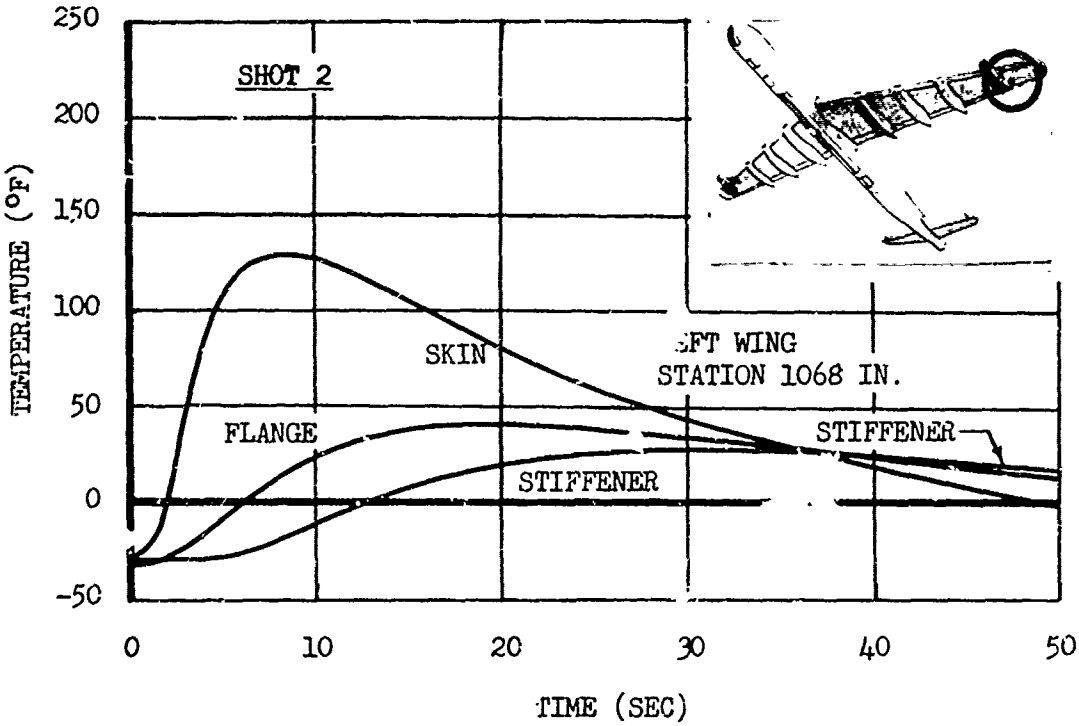

Fig. 4.10 Shot 2 Waffle Panel Temperature Distribution vs Time

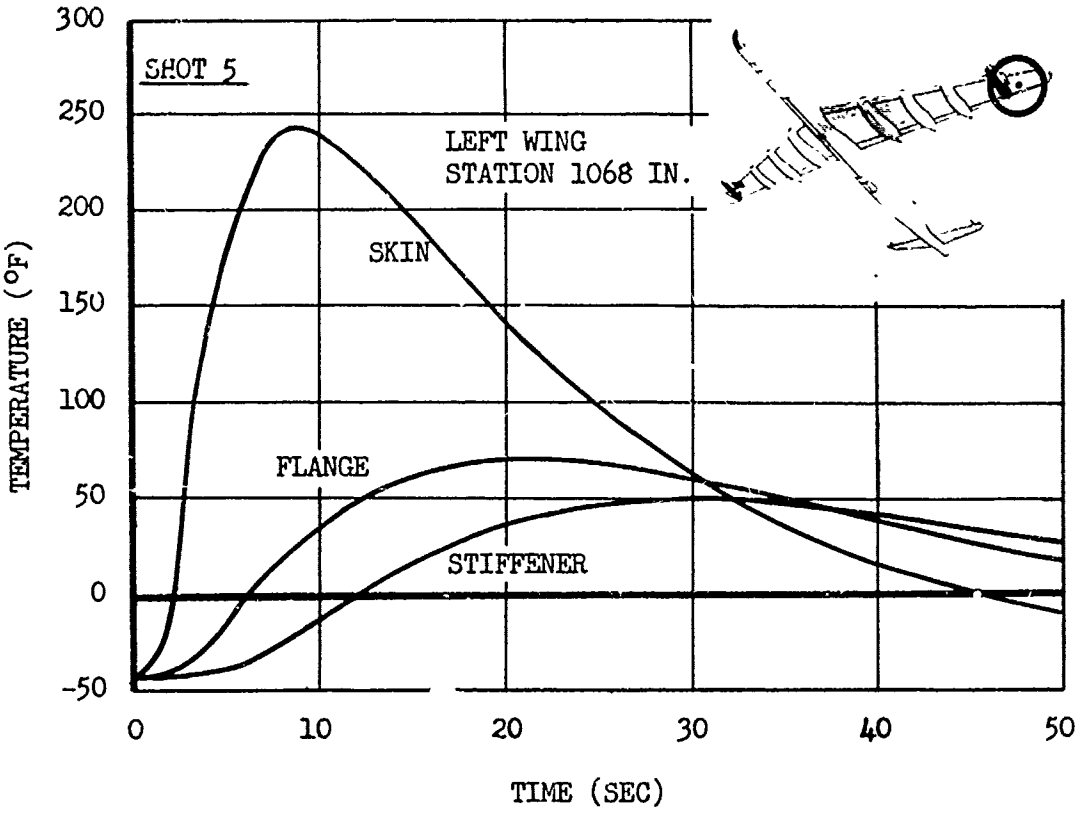

Fig. 4.11 Shot 4 Waffle Panel Temperature Distribution vs Time

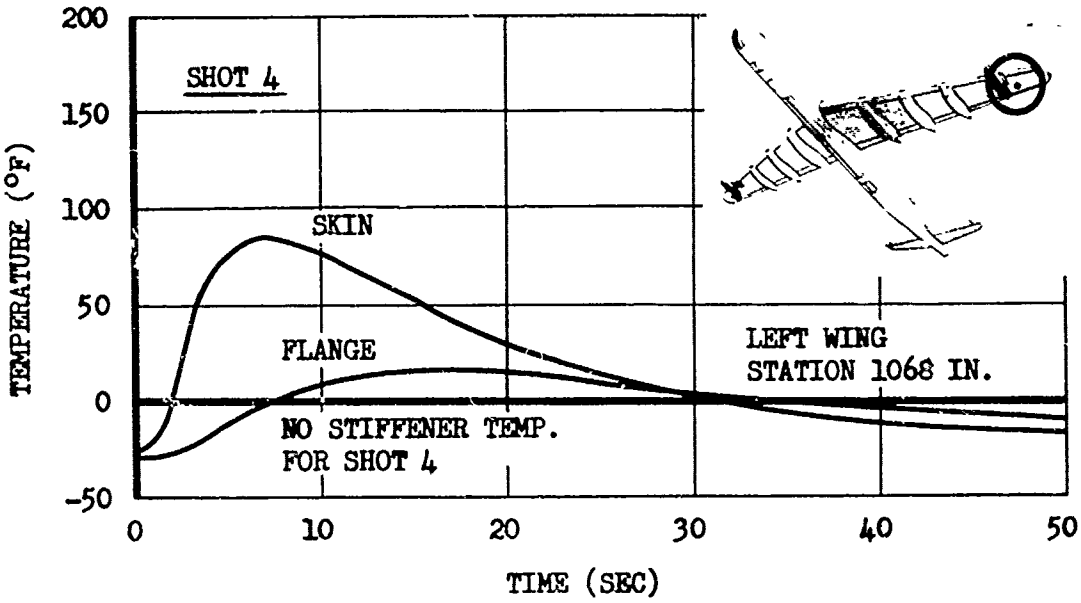

Fig. 4.12 Shot 5 Waffle Panel Temperature Distribution vs Time

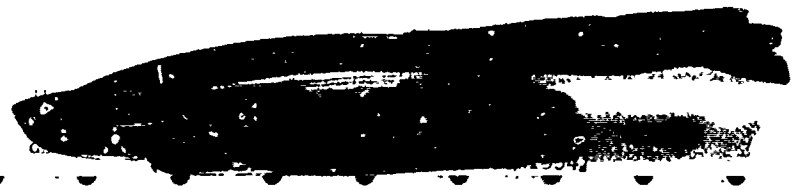

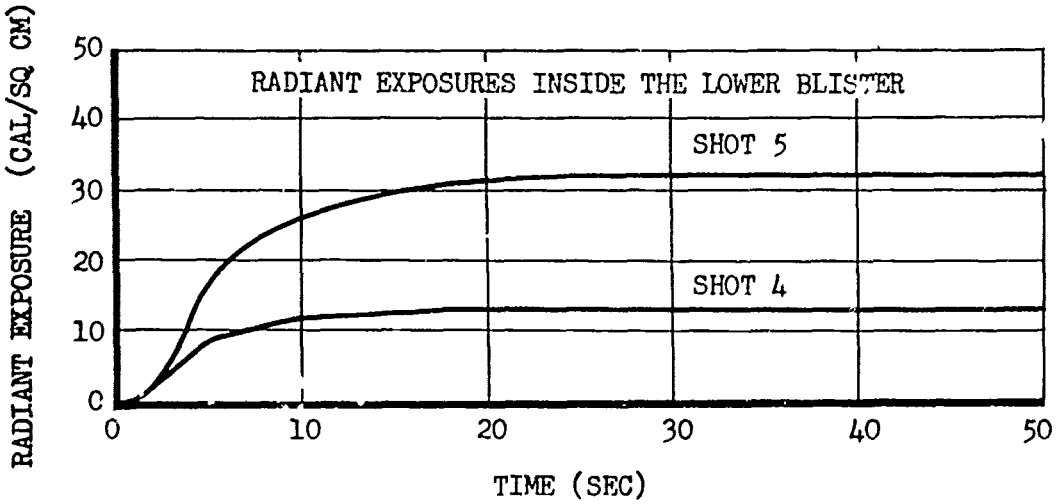

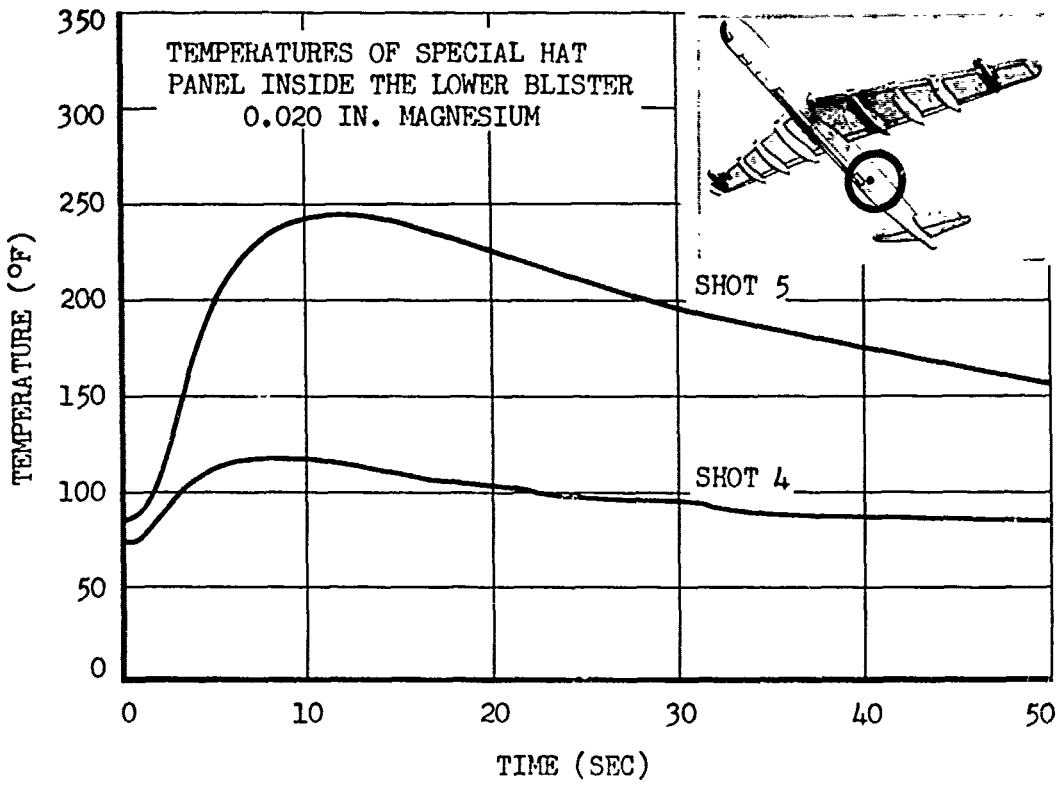

Fig. 4.13 Radiant Exposures and Skin Temperatures Inside the Lower Blister

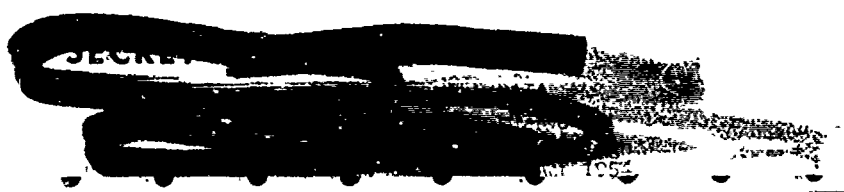

at various locations on the aircraft, are given in Table 4.6.

4.2.3 Thermal Damage

Thermal damage to the aircraft was visible on various parts of the aircraft skin, on certain rubber-covered components, and on one asbeston shield. Photographs showing typical thermal damage are presented in Fig. 4.14 through Fig. 4.26.

Before Shot 1, the entire underside of the aircraft was painted with white enamel over a protective coat of clear lacquer. After Shot 1, it was obvious that two vulnerable parts of the aircraft had been overlooked; these were the stabilizer trailing edge fairing and two small parts of the main landing gear doors. These parts had been treated in the usual manner, with aluminized lacquer. The stabilizer trailing edge fairing was made of 0.016-in. magnesium and was curved to allow clearance for the rotational movement of the elevator. As shown in Fig. 4.14, the lower half of the fairing was buckled and the paint blistered and peeled; the undamaged upper half was shielded from direct radiation by the elevator. Similar damage occurred to the parts of the landing gear doors (Fig. 4.15). Also during Shot 1, the black rubber pads around the rims of the aft lower blisters were scorched by thermal radiation (Fig. 4.16). Flat metal plates with reinforced circumferences had been fitted to the blister rims for protection of the interior of the crew compartment, but they did not shield the rubber pads. After Shot 1, the rubber was removed and all exposed parts of the blister rims were painted with white enamel.

Paint damage of varying degrees was incurred during Shots 1, 2, 4, and 5. The nature of the damage appeared to be a blistering or separation of the paint from the lacquer undercoat or metal, followed by tearing and peeling by the airflow over the surface or by the blast wave. One complicating factor was the oil film deposited on those portions of the stabilizer and elevator directly behind the inboard reciprocating engines. The amount of deposited oil varied from one flight to another; one of the heaviest contaminations occurred during Shot 2 and is shown in Fig. 4.17. The relatively light damage to the paint on the elevator tab during Shot 2 can also be seen in Fig. 4.17; one should note that some of the paint blisters have been broken while others remained intact. The most severe paint damage occurred during Shot 5. Figure 4.18 shows the left and right stabilizer and elevator assemblies; one should note here the light deposit of oil as compared to that for Shot 2. A close-up of the elevator tab after Shot 5, Fig. 4.19, shows the typical paint damage. After Shot 5, at four places on the elevator, two left and two right, where almost all of the white paint was missing, there was evidence of permanent skin buckling. The most severe buckling occurred at a hat panel section about halfway out the right elevator; a close-up of this area is shown in Fig. 4.20. Coincidentally, one of the two paint-stripped areas of the left elevator was instrumented by thermocouples, the time-history curve of which was presented in Fig. 4.4, and represented the largest temperature rise measured on the B-36D during CASTLE (322°F).

A small area of white paint damage on the wing flap adjacent to a reciprocating engine is shown in Fig. 4.21. Damage to the aluminized

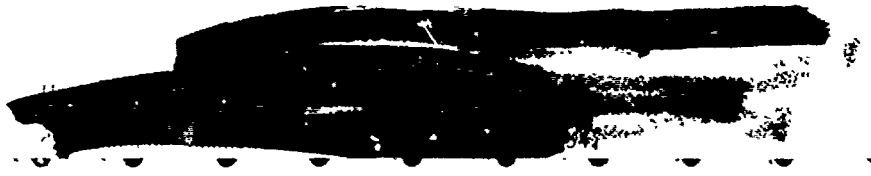

TABLE 4.6 - Temp-Tape Data

Component	Station In.	Material	Thickness	Remarks	Peak Temperature °F		
					Shot 1	Shot 2	Shot 5
Right Elevator	136	Mag.	0.020 in.	Hat Panel Skin, White Enamel	190	*	210
Right Elevator	156	Mag.	0.020 in.	Hat Panel Skin, White Enamel	140	*	190
Right Elevator	268	Mag.	0.020 in.	Hat Panel Skin, White Enamel	190	180	220
Right Elevator	287	Mag.	0.020 in.	Hat Panel Skin, White Enamel	190	190	220
Right Elevator	332	Mag.	0.020 in.	Hat Panel Skin, White Enamel	215	150	200
Left Elevator	136	Mag.	0.020 in.	Hat Panel Skin, White Enamel	190	150	210
Left Elevator	156	Mag.	0.020 in.	Hat Panel Skin, White Enamel	190	*	190
Left Elevator	268	Mag.	0.020 in.	Hat Panel Skin, White Enamel	190	*	200
Left Elevator	287	Mag.	0.020 in.	Hat Panel Skin, White Enamel	190	*	190
Left Elevator	312	Mag.	0.020 in.	Hat Panel Skin, White Enamel	---	190	200
Left Elevator	332	Mag.	0.020 in.	Hat Panel Skin, White Enamel	210	190	220
Left Wing	1068	Mag.	0.025 in.	Waffle Panel Skin, White Enamel (Shots 2 thru 5)	---	*	200
Left Wing	1095	Mag.	0.025 in.	Waffle Panel Skin, White Enamel (Shot 1 only)	150	---	---
Left Wing	1106	Mag.	0.025 in.	Waffle Panel Skin, Aluminized Lacquer (Shots 2 thru 5)	---	165	220
Fuselage	1826	Alum.	0.025 in.	Sheet-Stringer, White Enamel	160	*	200
Fuselage	1893	Alum.	0.025 in.	Sheet-Stringer, White Enamel	190	150	210
Tail Turret Fairing		Alum.	0.032 in.	Sheet Metal, White Enamel	160	*	175
Special Plate in Blister		Alum.	0.032 in.	Sheet Metal, White Enamel (Shots 1 and 2)	170	145	---
Special Plate in Blister		Mag.	0.020 in.	Section of Hat Panel, White Enamel (Shots 4 and 5)	---	---	220

*Temperatures below minimum required to indicate on Temp-Tape (140°F). All Shot 4 temperatures were below this minimum.

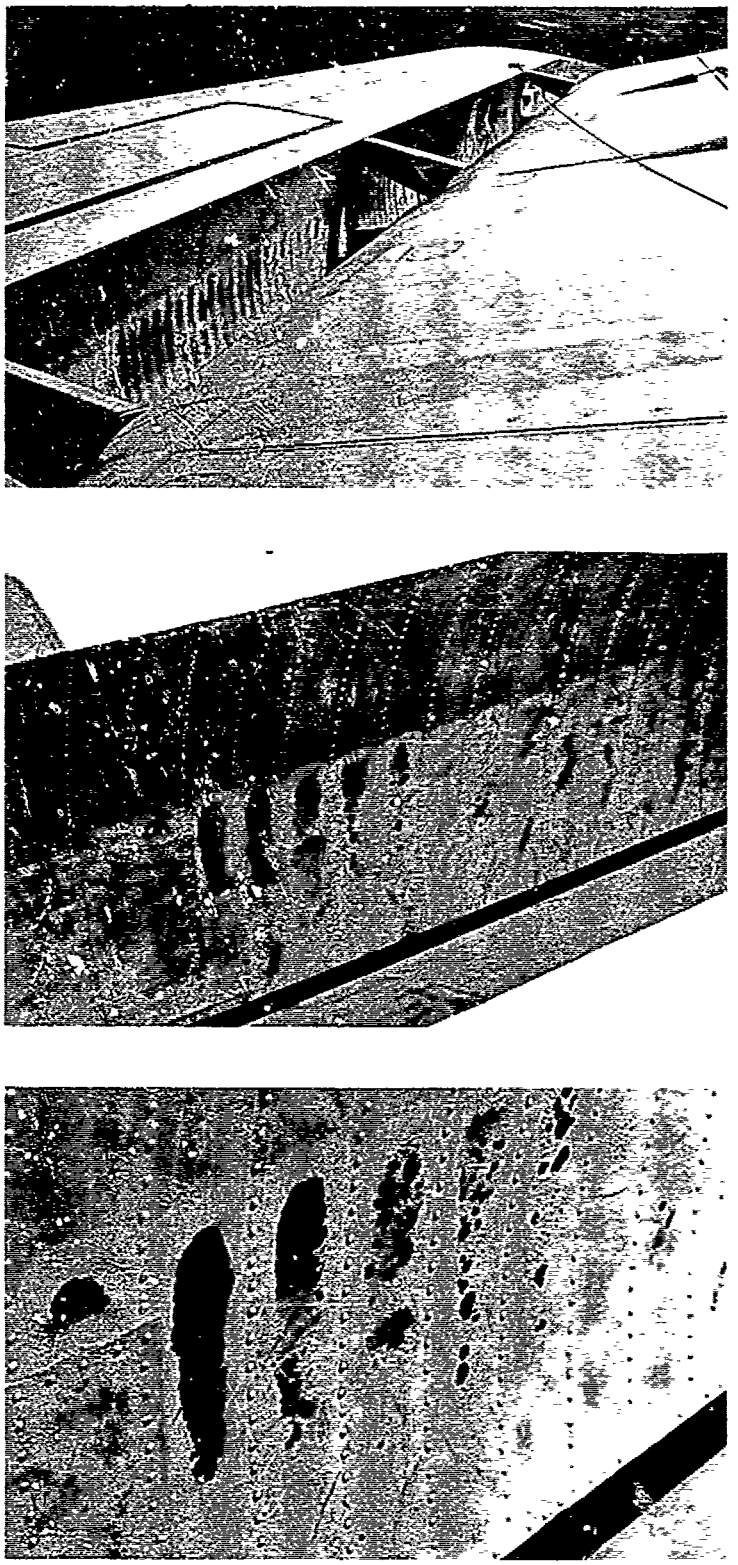

Figure 4.14 Shot 1 Thermal Damage to Trailing Edge Fairing of Right Stabilizer

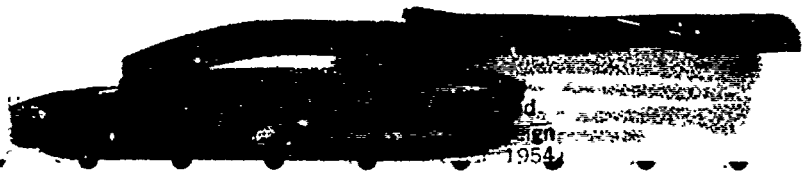

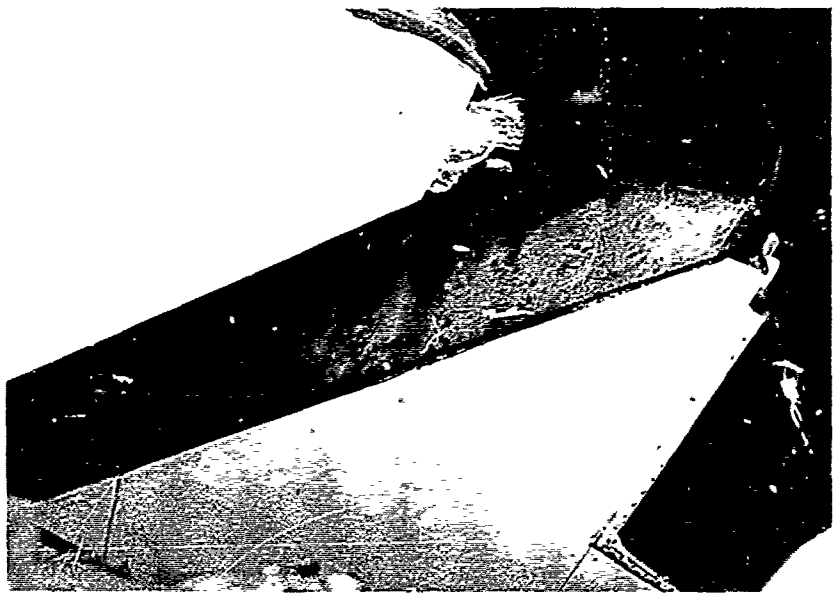

Figure 4.15 Shot 1 Thermal Damage to Small Section of Main Landing Gear Door

Figure 4.16 Shot 1 Thermal Damage to Rubber Pad on Rim of Aft Lower Right Blister

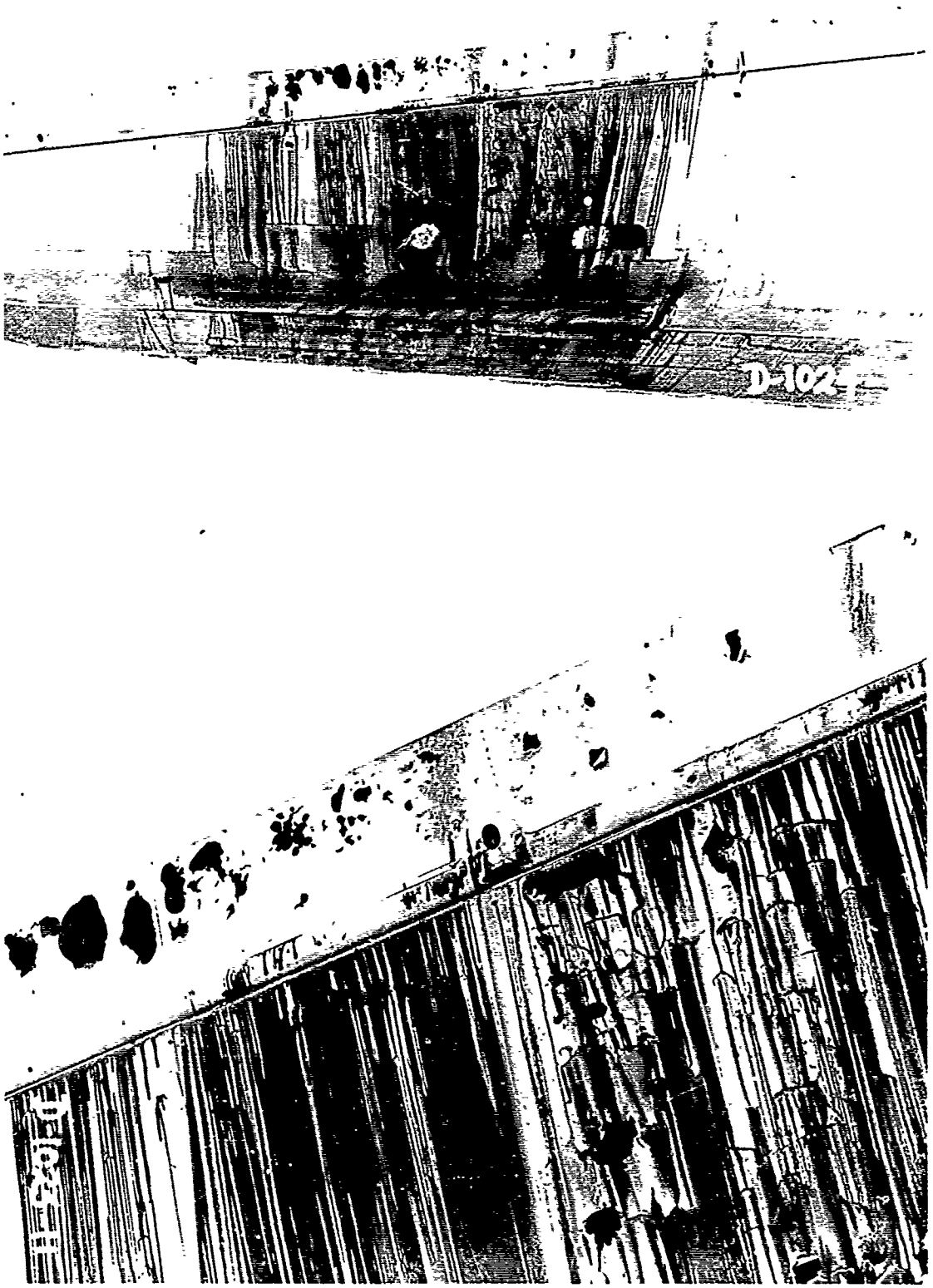

Fig. 4.17 Oil Deposit And Damaged Paint On Left Elevator After Shot 2

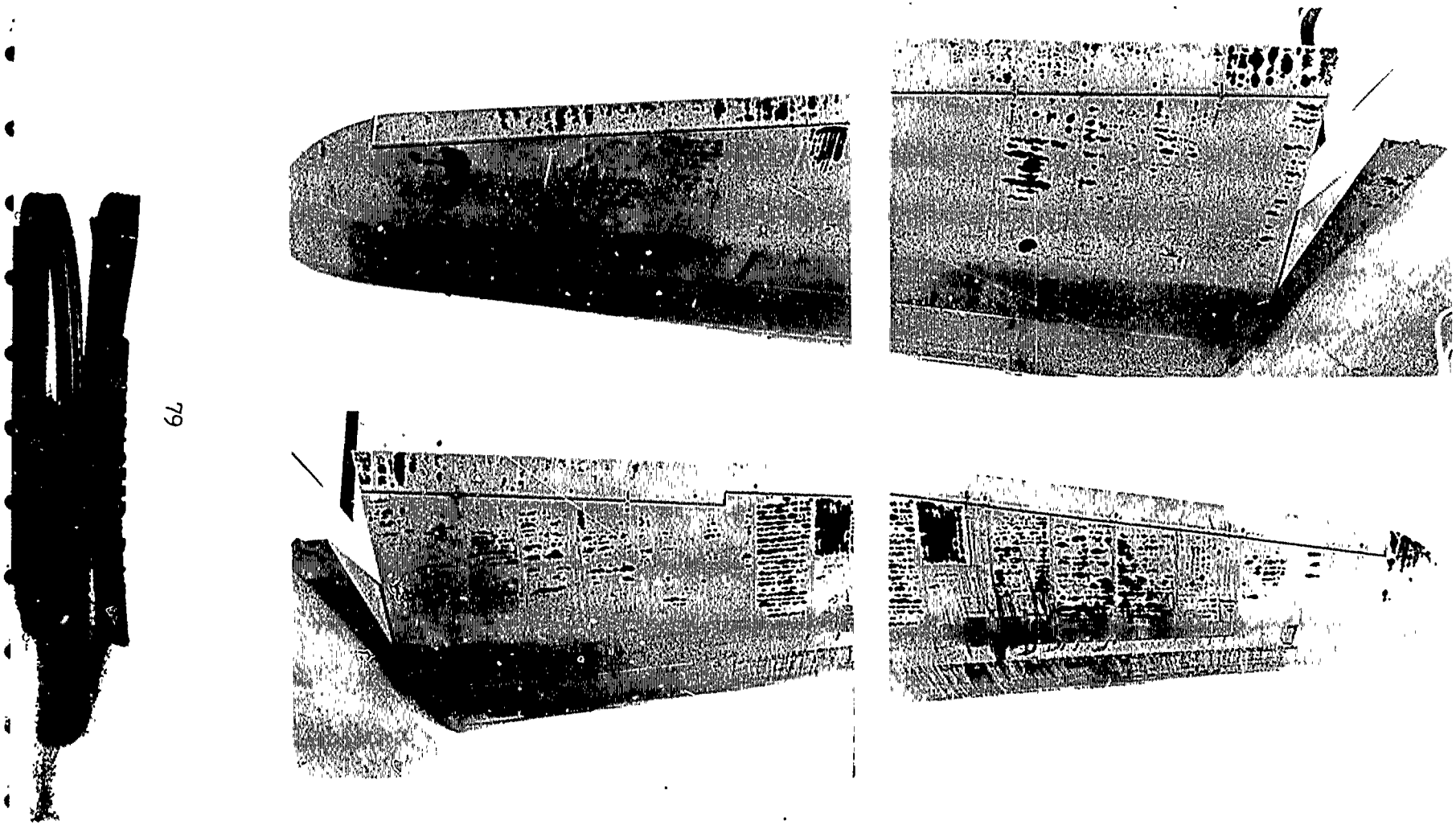

Fig. 4.18 Left and Right Elevators After Shot 5

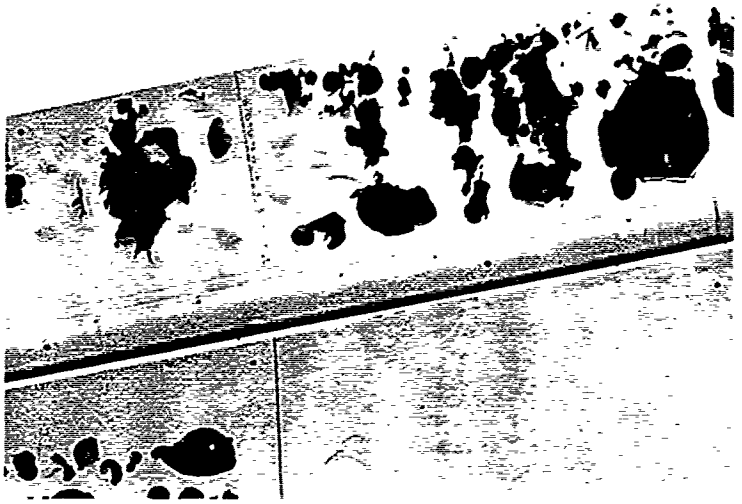

Fig. 4.19 Damaged Paint Of Left Elevator Tab After Shot 5

Fig. 4.20 Permanently Buckled Skin Of Ha Panel Section On Right Elevator After Shot 5

lacquer on one propeller spinner after Shot 1 is shown in Fig. 4.22, and similar damage after Shot 5 is given in Fig. 4.23.

Rubber-covered components adversely affected by the thermal energy were the radio antenna cover and the radome. Damage to the radio antenna cover after Shot 2 is shown in Fig. 4.24. An overall and a close-up view of the radome after Shot 5 are presented in Fig. 4.25. Only the forward portion of the Fiberglas radome was covered with rubber.

During Shot 5, an asbeston shield with an aluminized outside surface was located in the aft lower right blister. That portion of the shield which received direct or near-direct thermal radiation was scorched and the thread that held the pieces of the shield together was burned; photographs of both the outside (exposed) and the inside surfaces are presented in Fig. 4.26.

4.2.4 Flight Crew Observations of the Thermal Phase

During each thermal phase, a bright red glow was seen through the asbeston shields; the intensity was higher for Shots 1 and 5 than for Shots 2 and 4 and was relatively low during Shot 6. Two distinct light pulses were noted near the start of the thermal phases.

Considerable smoke was generated in the aft crew compartment during Shots 1 and 5. The smoke came through holes and gaps in the metal guards over the lower blisters and through openings in the compartment floor. No flame was seen and the smoke generation stopped at or near the end of the thermal phase.

During Shot 5, the flight engineer saw the fire warning lights for four of the reciprocating engines lit for about 4 sec. The fire warning devices are thermocouple bulbs located on the lower skin panels of the engine nacelles and are connected to energize a warning light if the rate of temperature rise exceeds a critical value.

4.3 BLAST RESULTS

For the relatively slow-speed, propeller-driven aircraft such as the B-36, the effects of the blast wave resulting from the detonation of a nuclear weapon may very well limit the operational capabilities of the aircraft during a strategic mission; therefore, a large portion of the data obtained by Project 6.2a was concerned with the blast phenomena. The results, as presented in this chapter, were obtained from five of the six CASTLE detonations; Shot 3, being of unexpectedly low yield, produced no usable blast results.

During some nuclear weapon effects investigations, the interaction or coupling between the thermal effects and the blast effects is an important consideration because the specimens may still be hot, and therefore under thermal stresses, at the time of the shock arrival. For this experiment, the coupling effect appears to be negligible. This was indicated by some of the bending moment and shear measurements, which were recorded throughout the thermal phase, and returned to ambient conditions, for each detonation, before the arrival of the shock wave.

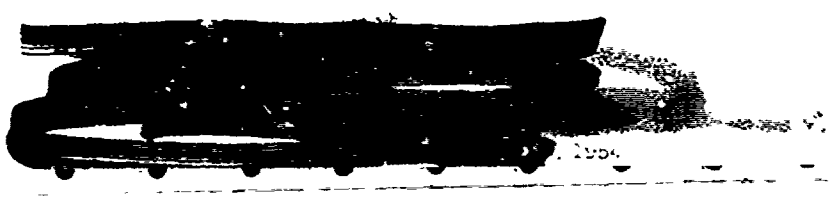

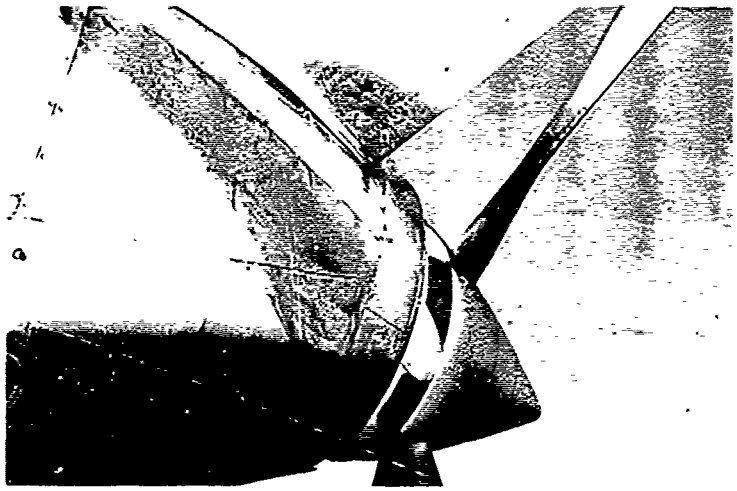

Fig. 4.21 Shot 5 Thermal Damage to Wing Flap Paint

Fig. 4.22 Shot 1 Thermal Damage to Aluminized Lacquer on Propeller Spinner

Fig. 4.23 Shot 5 Thermal Damage to Aluminized Lacquer on Propeller Spinner

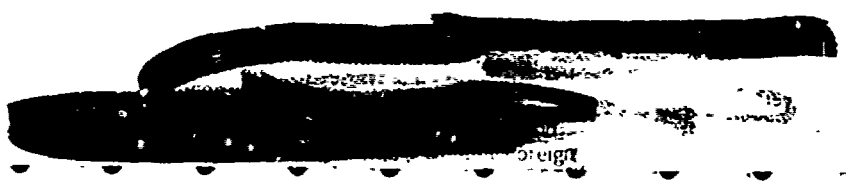

Figure 4.24 Shot 2 Thermal Damage to the Radic Antenna Cover

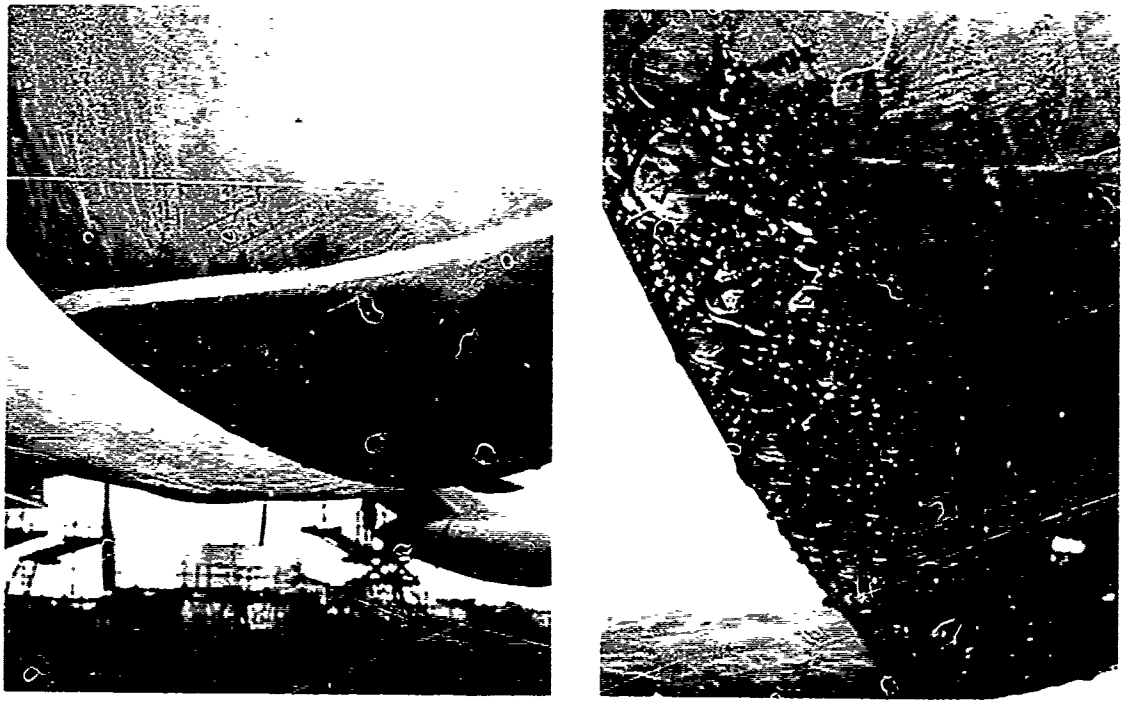

Figure 4.25 Shot 5 Thermal Damage to the Rubberized Coating of the Radome

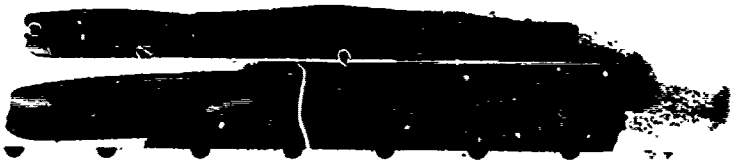

Outside (Exposed) Surface

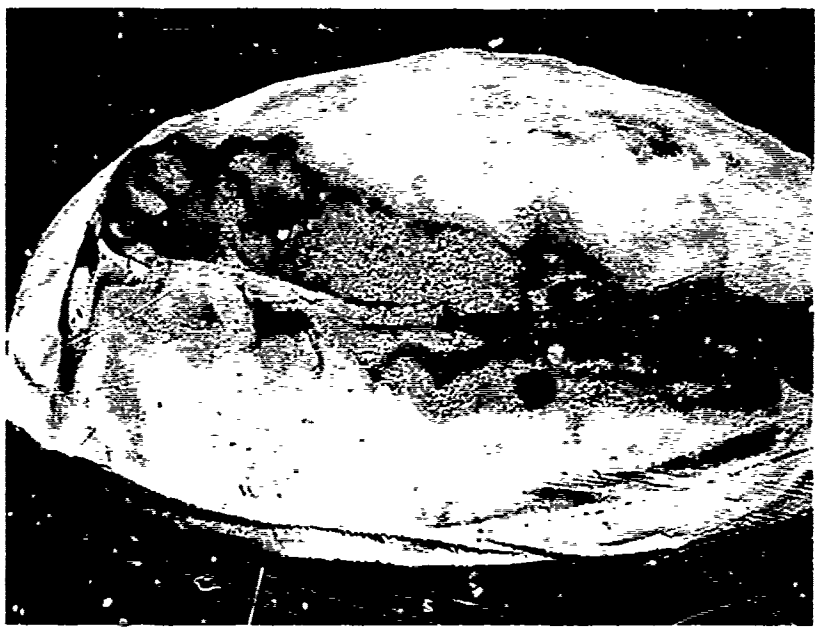

Inside Surface

Fig. 4.26 Shot 5 Thermal Damage To Asbeston Shield Located In Aft Lower Right Blister

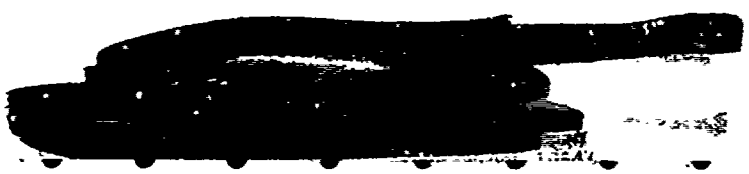

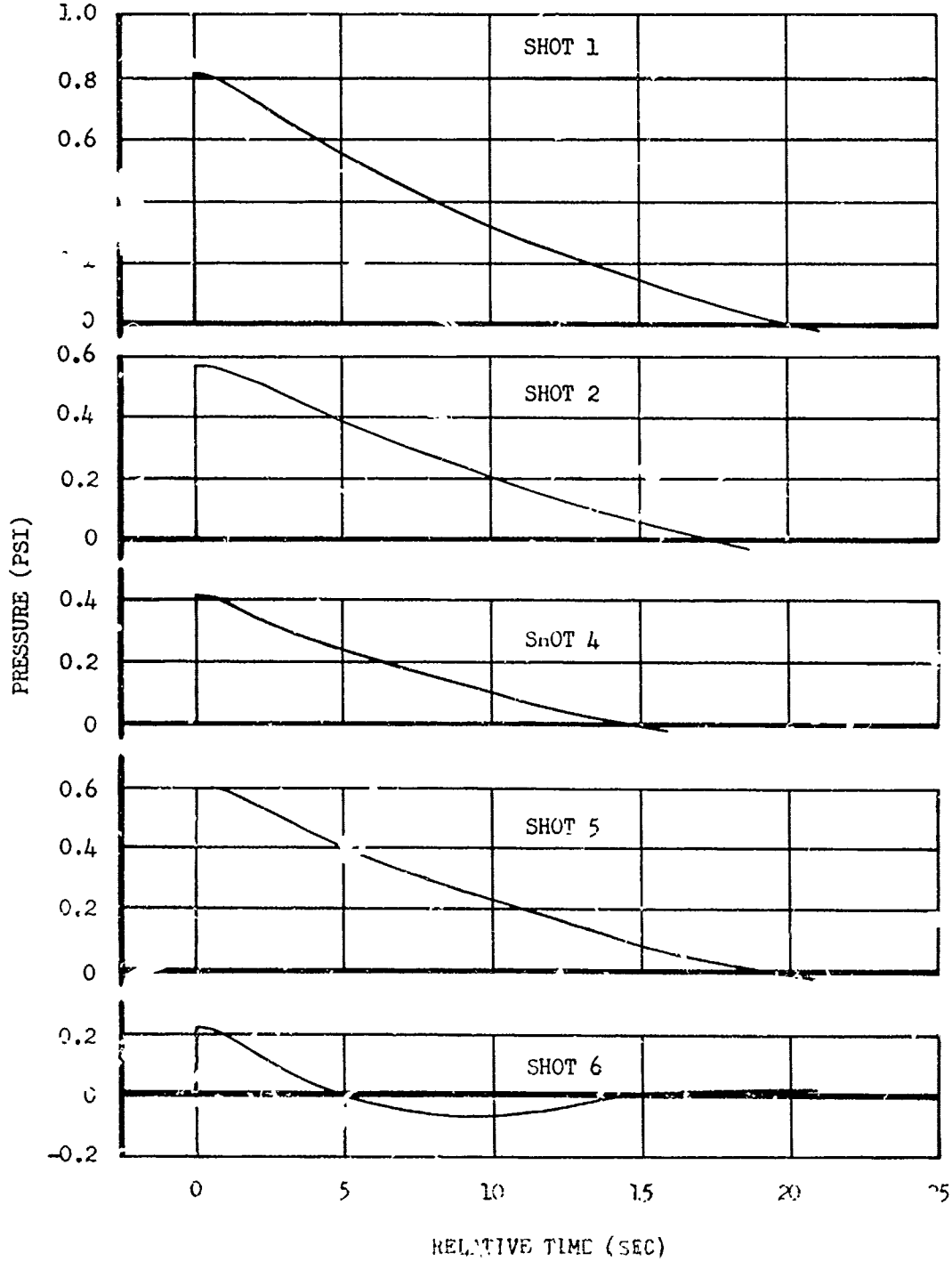

Fig. 4.2" Free-Stream Overpressure vs Time

The following subdivisions of this section contain the oscillographic data, damage photographs, and general observations of the flight crew and other participating personnel with respect to the results of the aircraft being subjected to the blast wave for the CASTLE detonations.

4.3.1 Blast Input Results

Blast input results include the time-history curves for the free-stream overpressure and for the pressure on the underside of various parts of the aircraft. Since blast effects theory makes direct use of free-stream overpressure for effects predictions, the main effort of the blast input instrumentation was centered on the overpressure measurement. The overpressure results are presented here as a composite curve for each shot; this curve was obtained by averaging the output values obtained from several independent transducers described in Chapter 3. The actual value of overpressure obtained from any one of the transducers did not vary from the corresponding average value by more than five per cent. Overpressure measurements are presented in Table 4.7.

TABLE 4.7 - Overpressure Measurement Information

Shot No.	Ambient Air Press. at Flight Altitude	Shock Arrival From Zero Time	Peak Free Stream Overpressure	Duration of the Positive Phase
1	4.14 psi	54.01 sec	0.81 psi	20.08 sec
2	3.52 psi	62.61 sec	0.56 psi	17.42 sec
4	3.46 psi	68.64 sec	0.42 psi	14.68 sec
5	3.00 psi	57.40 sec	0.60 psi	19.13 sec
6	4.14 psi	79.03 sec	0.22 psi	4.84 sec

Shock arrival time, referenced to detonation time, was measured at Fuselage Station 391 in. The objective of the overpressure measurements by this project was to obtain an accurate value of peak overpressure, rather than to define the exact shape of the pressure curve, and instrumentation components were selected on this basis. The ideal shock wave pressure is represented as a sharp saw-tooth form; however, in practice, the sharp peak of this pressure is not well defined when measured by instrumentation such as utilized by Project 6.2a. For purposes of this presentation, the peak overpressure shall be defined as the highest average overpressure shown by the response curve after the first high frequency oscillations have subsided. This peak usually occurs about 0.5 sec after the blast arrival.

The free-stream overpressure curves are presented in Fig. 4.27. The important features of the overpressure measurement so far as Project

6.2a was concerned are contained in the positive phase portion of the curve. For this reason, no attempt was made to obtain a complete time-history of the pressure variation which would have included the negative phase. A direct comparison of the initial portion of the pressure curve as recorded by four different types of transducers is presented in Fig. 4.28. These curves are typical of all shots and are presented without fairing or smoothing in order to show actual transducer response to the input received.

The variation of pressures on the undersurface of the left stabilizer and left wing are presented in Figs. 4.29 and 4.30, respectively. For convenience, the time scales of the curves have been started at zero. The corresponding time from detonation is shown in Table 4.8.

TABLE 4.8 - Shock Arrival Times

Shot No.	1	2	4	5	6
Shock arrival at Left Stab., Sec after zero	53.875	62.465	68.498	57.250	79.100
Shock arrival at Left Wing, Sec after zero	53.940	62.537	68.580	57.323	79.067

The reversal of times of arrival for Shot 6 occurred because of the head-on orientation of the aircraft.

As expected, the surface pressures are higher than the overpressures because of reflections and dynamic effects of the shock wave. This is also true of the surface and differential pressures of the aft lower fuselage, as shown in Fig. 4.31. From these curves it can be observed that the differential pressure decreased rapidly compared to the surface pressure; thus, the crushing force of the overpressure upon the unpressurized fuselage section is of short duration. Shock arrival times for the fuselage surface and differential pressure installations are: Shot 1, 53.918 sec; Shot 2, 62.510 sec; Shot 4, 68.540 sec; Shot 5, 57.300 sec; and Shot 6, 79.070 sec.

As an example, the rise characteristics of the four different surface pressure curves are presented with an expanded time scale in Fig. 4.32. These curves are typical of all shots.

4.3.2 Blast Response Results

Prior to Operation CASTLE, the horizontal stabilizer structure was defined as the critical structure for a tail-to configuration of the aircraft when exposed to the air blast effects of an atomic detonation. For this reason, an extensive instrumentation system was installed in this structure in order to define its response to the blast wave. The bending moments at Station 62 in., left and right stabilizers, were employed as a measure of the total tail load for purposes of establishing the safe limits of the aircraft. The term shear as used in

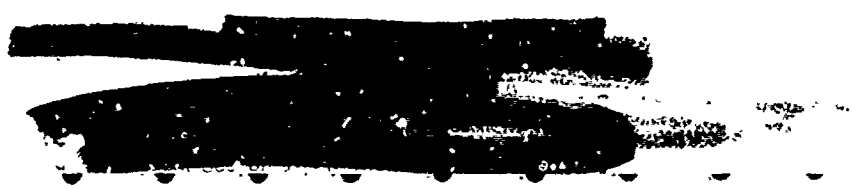

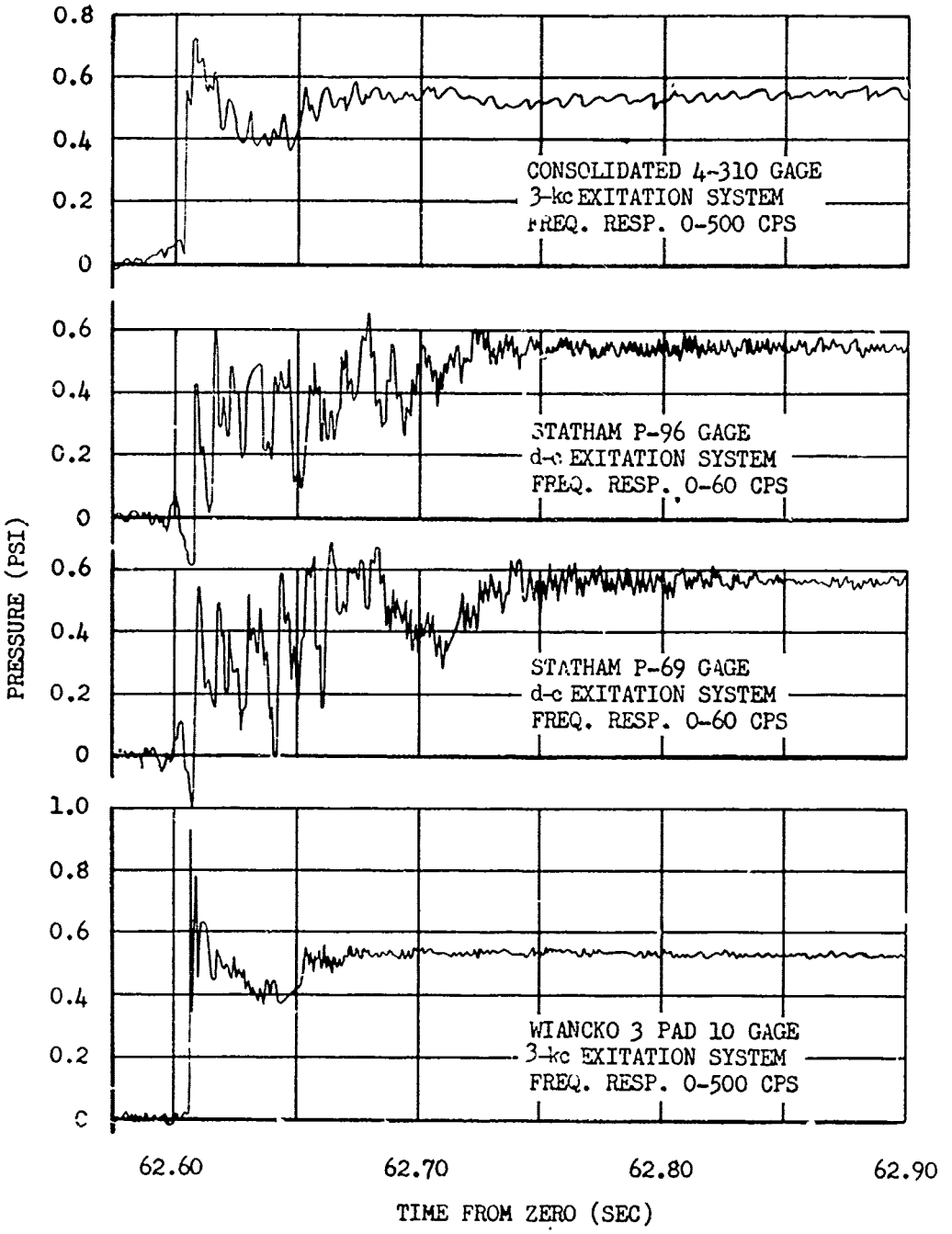

Fig. 4.28 Typical Responses of Free-Stream Overpressure Gages to the Shock Front

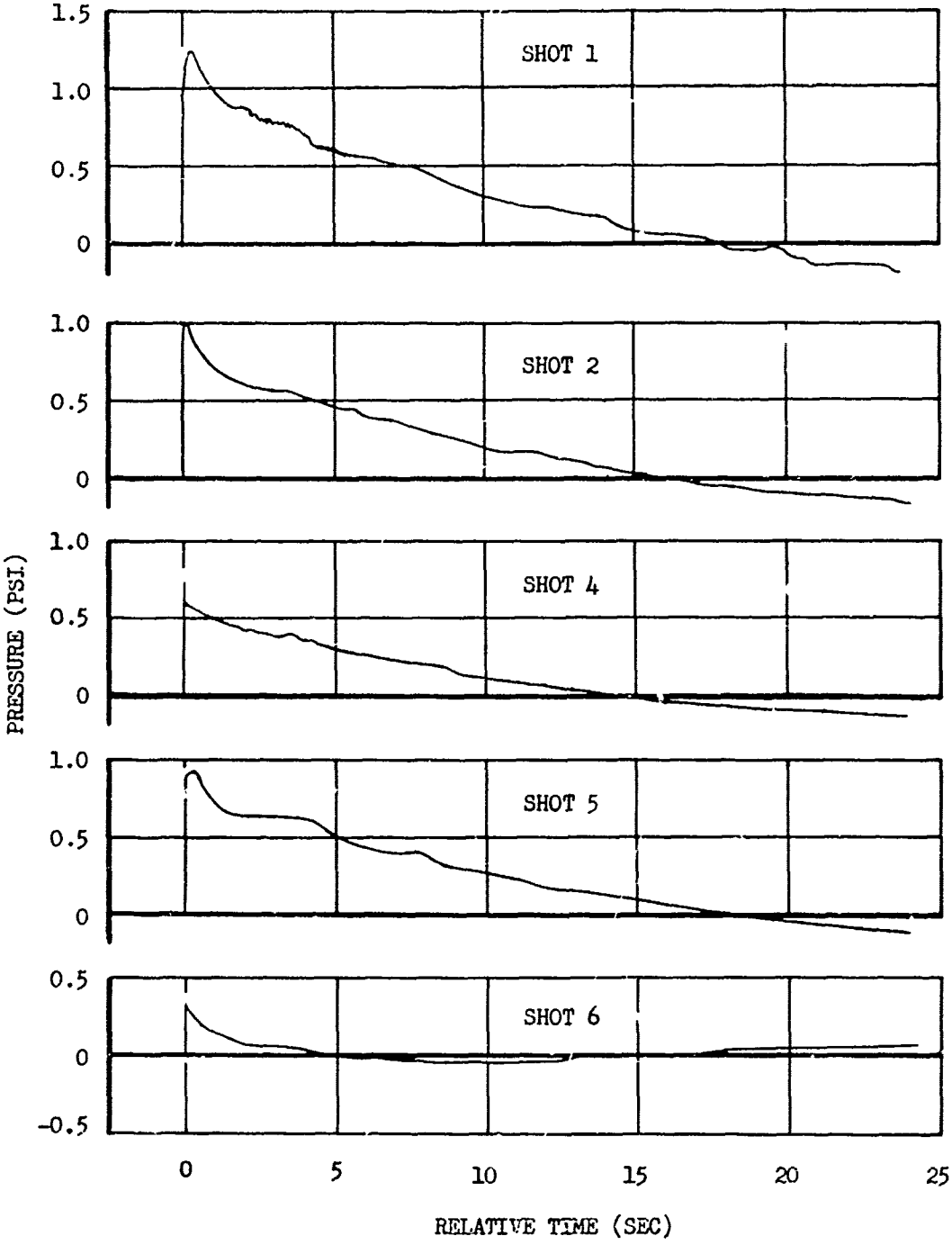

Fig. 4.29 Stabilizer Surface Pressure vs Time

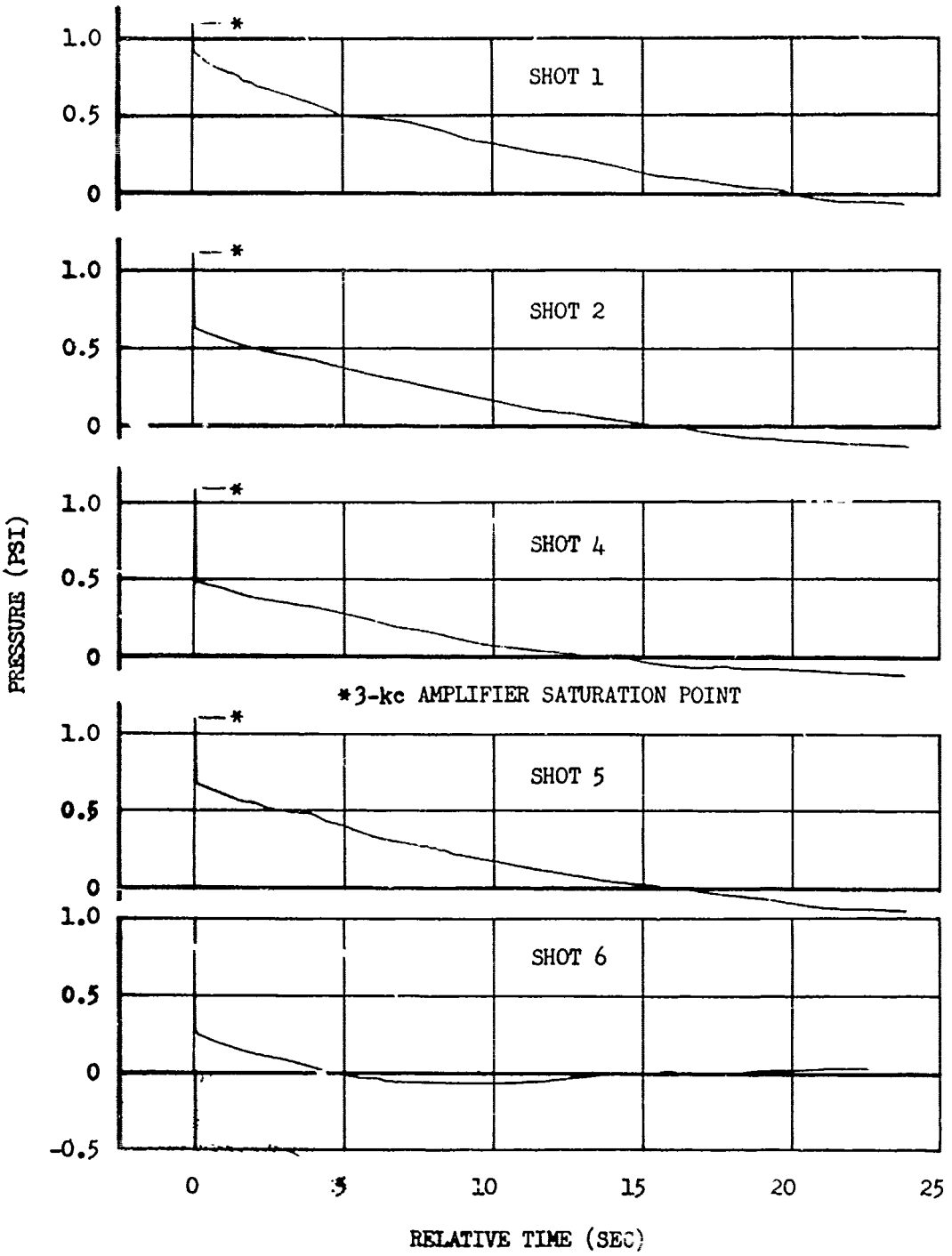

Fig. 4.30 Wing Surface Pressure vs Time

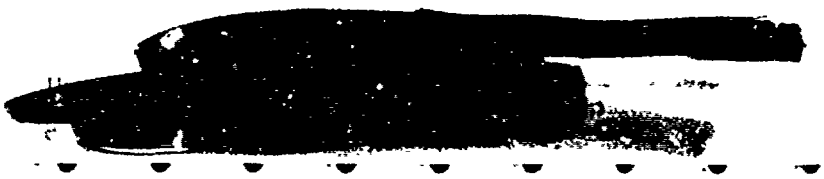

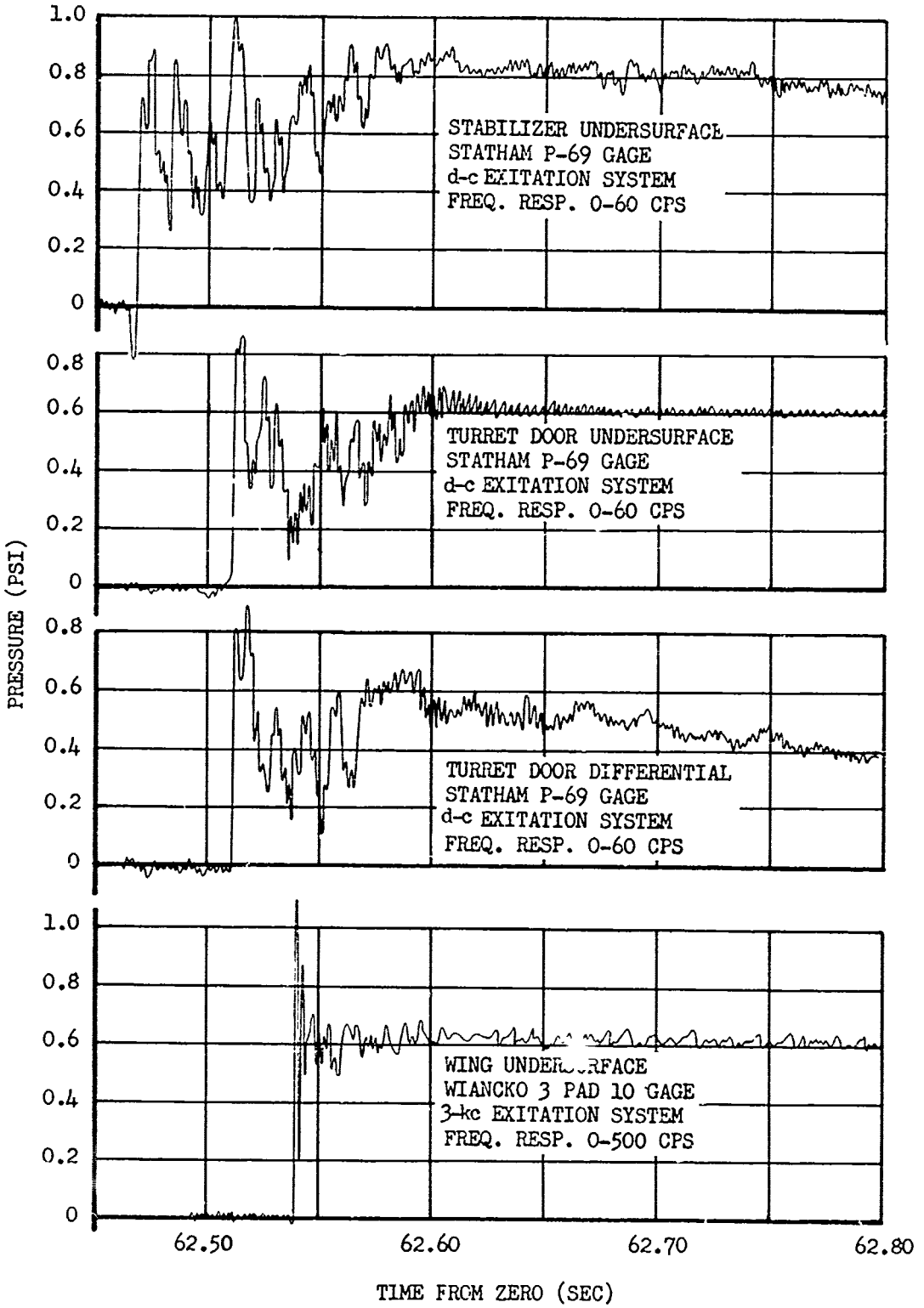

Fig. 4.32 Typical Responses of Surface Pressure Gages to the Shock Front

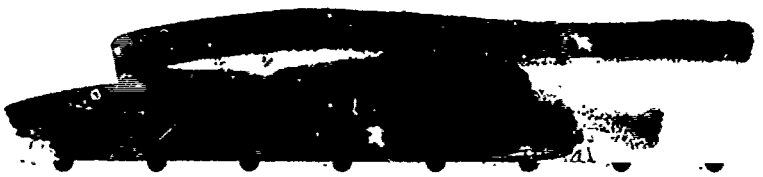

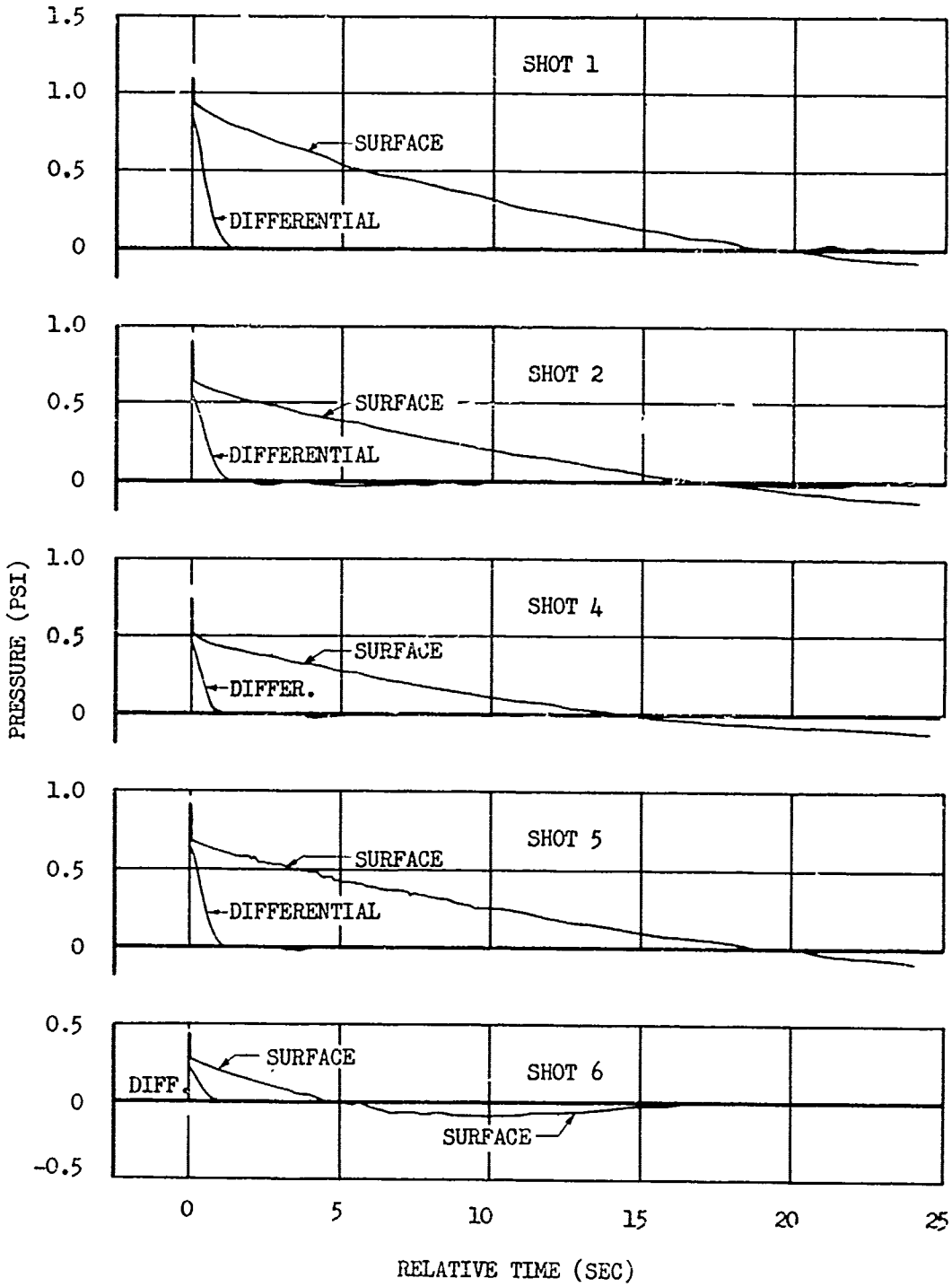

Fig. 4.31 Fuselage Surface and Differential Pressures vs Time

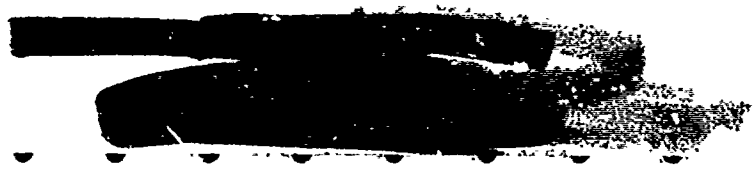

this report means shear load, which represents the summation of all vertical loads acting upon the stabilizer outboard of the gage location. The terms bending moment and shear actually mean a variation of the bending moment or shear from conditions which existed just prior to shock arrival. Positive bending moment is defined as a bending moment producing compression in the upper stringers or longerons, and positive shear is the shear producing a positive bending moment. The values given in tables and by graphs do not represent absolute bending moments or shears unless so noted. The bending moments of Station 62 in. are the results of the point load measurements. Although good results were obtained from both point load and total bending installations, the point load measurements are generally considered to be more accurate and they are used, where available, in preference to total bending. Figure 4.33 is a comparison of the point load and total bending measurements, and is typical for all shots.

Stabilizer bending moment and shear response curves for the five CASTLE detonations are presented in Figs. 4.34 to 4.43, inclusive. The yield of the Shot 1 device was considerably higher than expected. Because of the resulting unexpected increase in the magnitude of the aircraft response, several of the fast moving galvanometer traces used for recording point load installation outputs became indistinguishable at the peak loads, due to excessive writing speeds. These curves have been shown as discontinuous wherever there was any doubt as to the actual value. Maximum values of shear and bending moment have been noted on the curves. The highest stabilizer loads were obtained on Shot 5, and the lowest on Shot 6. The general shapes of the bending moment and shear curves were similar for all tail-to shots with some differences noticeable for the head-on configuration.

Fuselage bending moments are presented in Figs. 4.44, 4.45, and 4.46. The aft fuselage is thought to be the second most critical structure with respect to blast response. An unusual feature of the fuselage bending curves is the appearance of a negative spike at the beginning of the curves for Station 1597 in., starting with Shot 4. The relative magnitude of this spike increases with each succeeding detonation. It should be noted that at Station 1597 in. the construction of the fuselage is different from the other two stations where bending moments were measured.

Wing bending moments are presented in Figs. 4.47 through 4.51. Shot 1 appeared to be unusual as compared to the other shots. The typical bending moment response curve at Station 110 in. for tail-to exposures, as evidenced by Shots 2, 4, and 5, had a negative peak followed by a larger positive peak and then an oscillation of much lesser amplitude centered about the zero moment line. For Shot 1, however, the first negative peak was greater than the following positive peak, and the oscillation centered about a curve which decreased rather slowly to a negative peak of greater amplitude than the positive maximum. This confirmed the sensation of falling as felt and reported by some of the flight personnel. These data appear to indicate that the aircraft wing was stalled at this time. Additional discussion of this phenomenon appears in the next chapter.

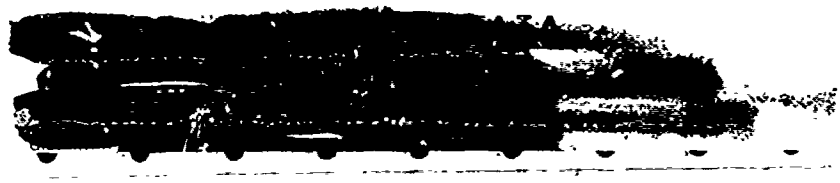

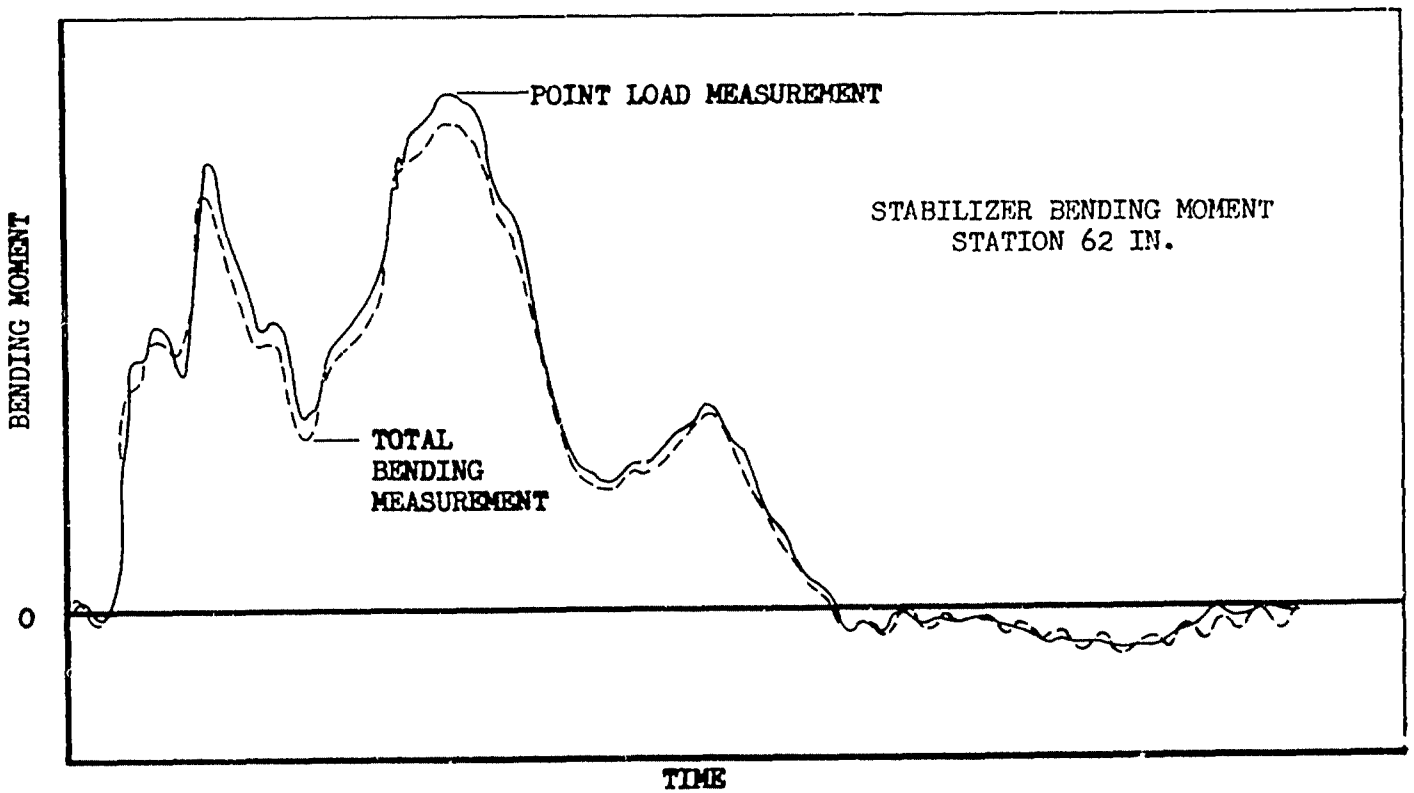

Fig. 4.33 Comparison of the Total Bending and Point Load Bending Response Curves

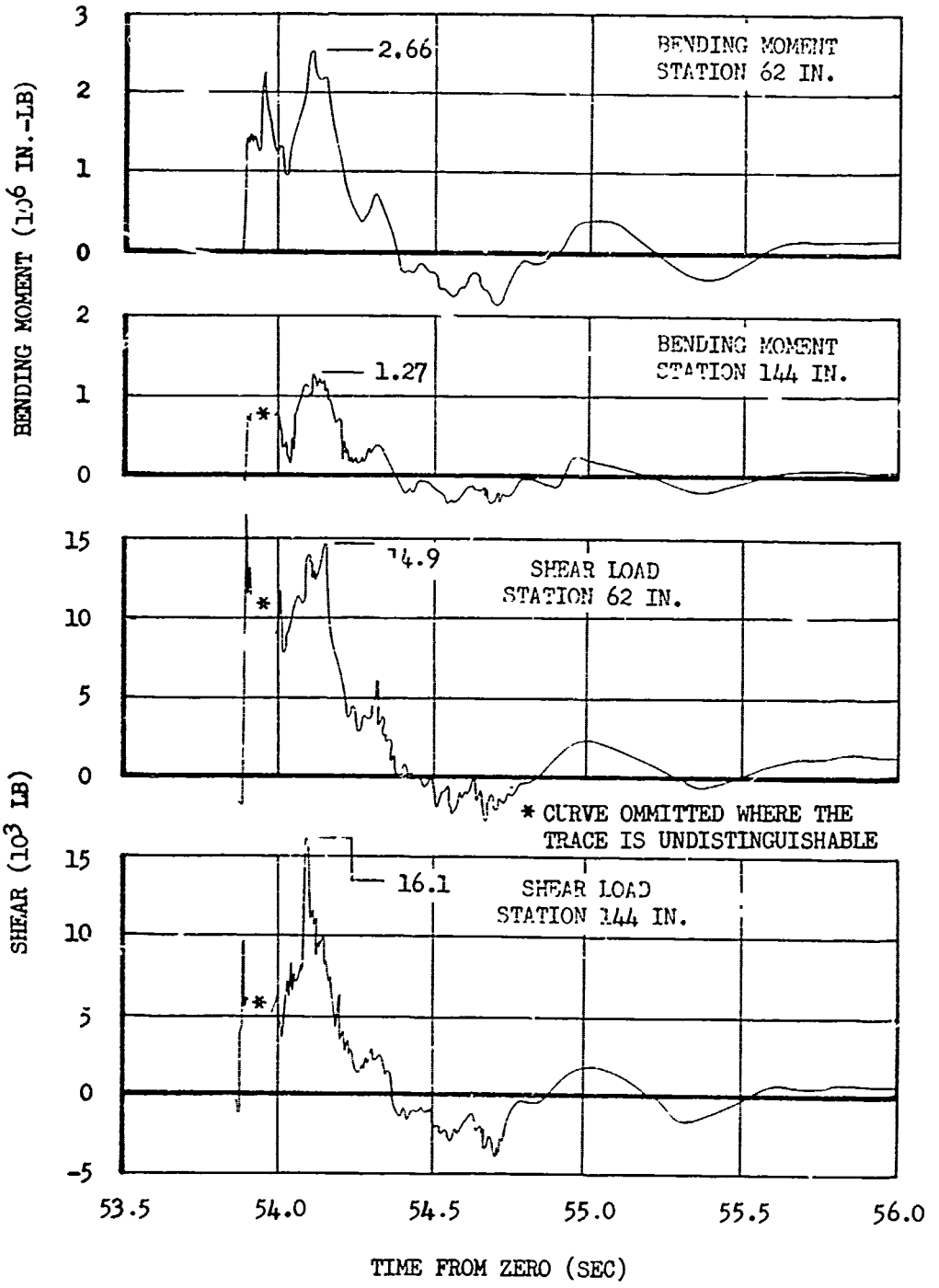

Fig. 4.35 Bending Moments and Shear Loads of Right Stabilizer vs Time, Shot 1

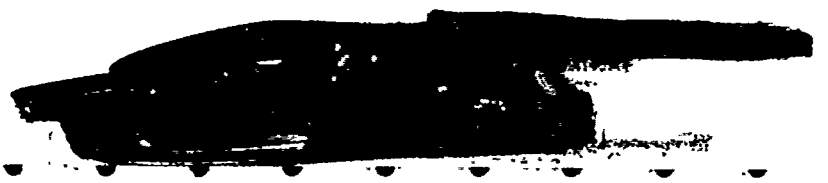

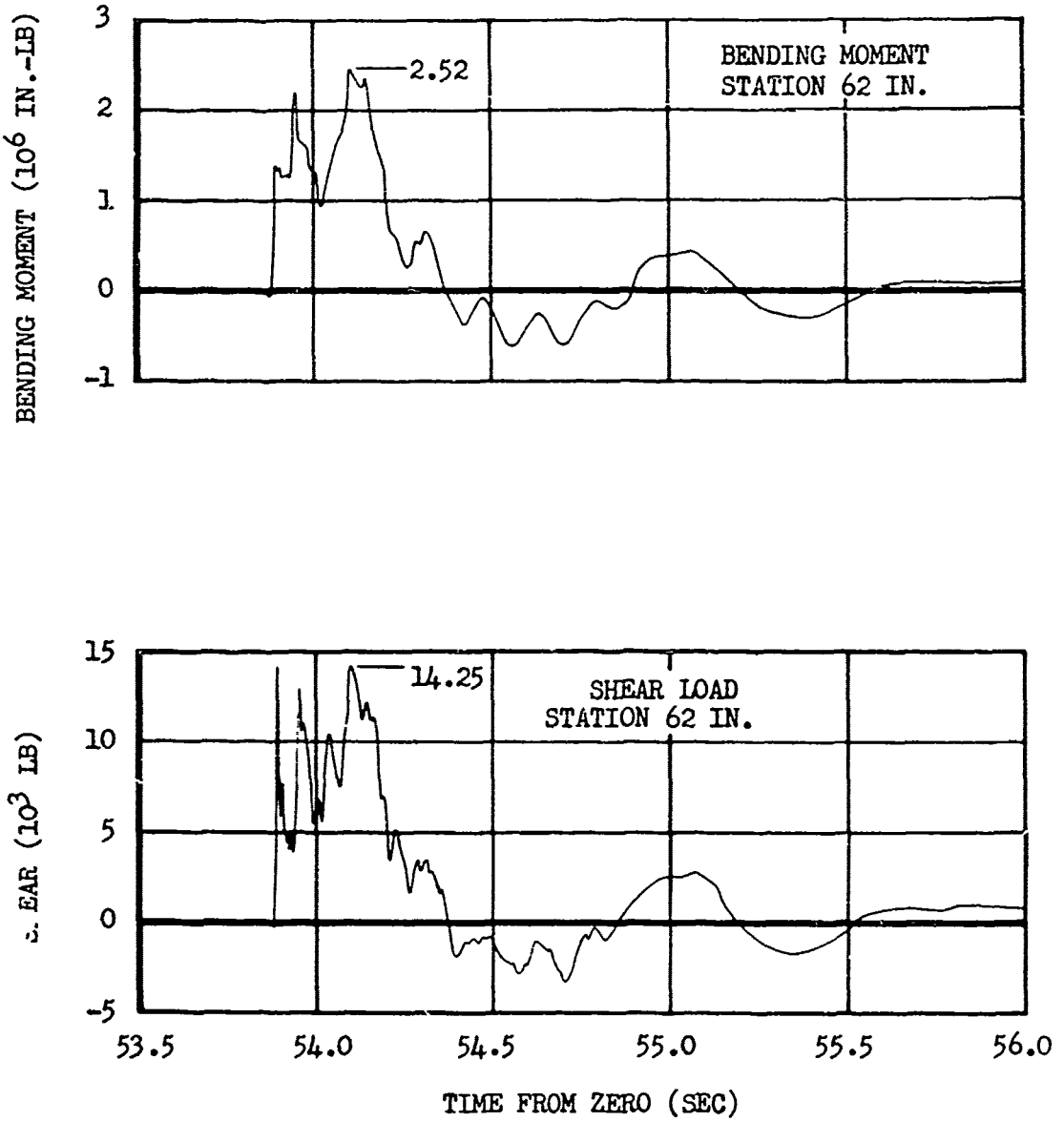

Fig. 4.34 Bending Moments and Shear Loads of Left Stabilizer vs Time, Shot 1

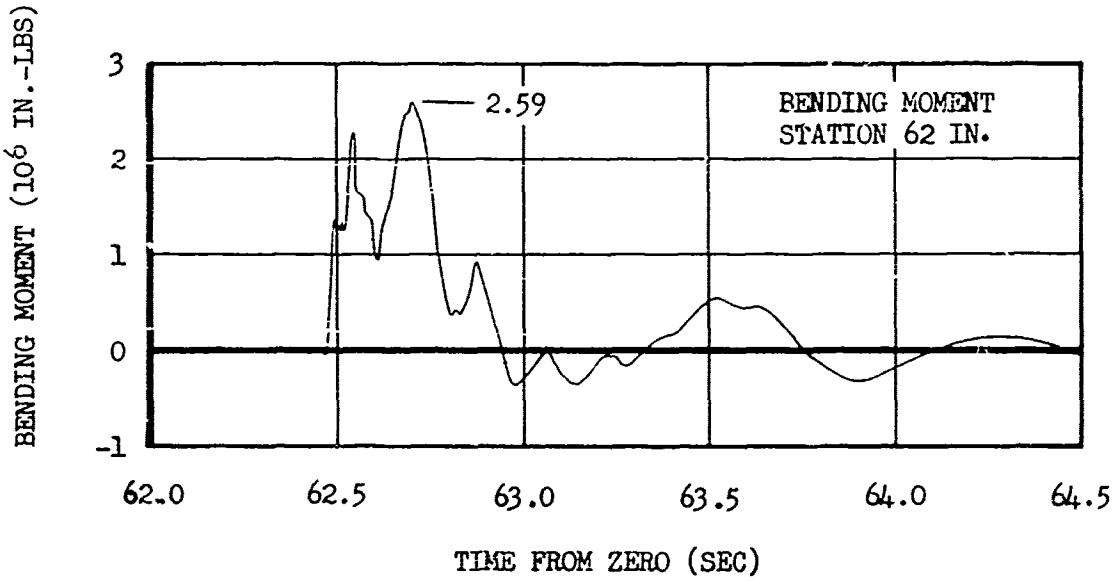

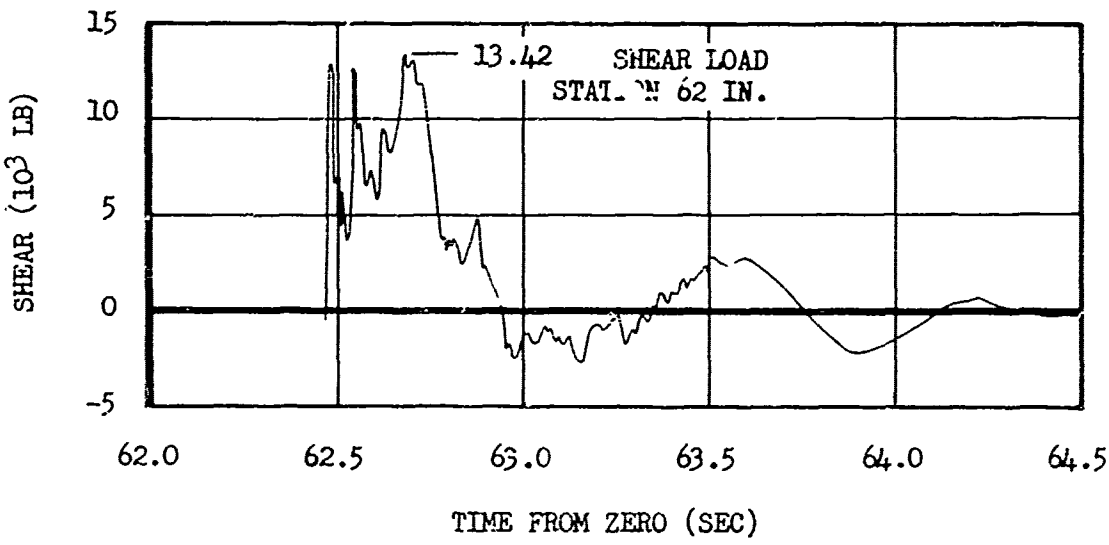

Fig. 4.36 Bending Moments and Shear Loads of Left Stabilizer vs Time, Shot 2

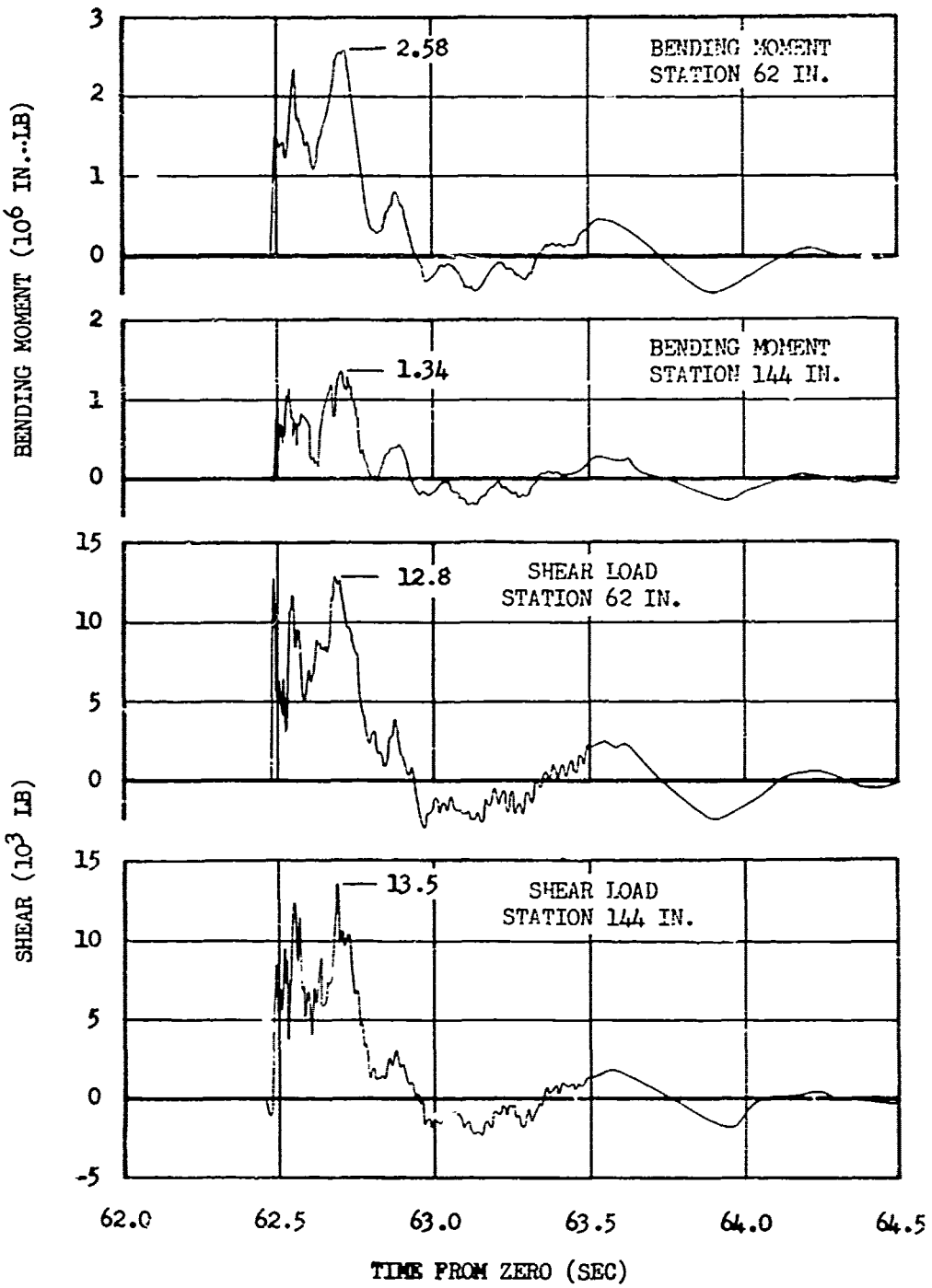

Fig. 4.37 Bending Moments and Shear Loads of Right Stabilizer vs Time, Shot 2

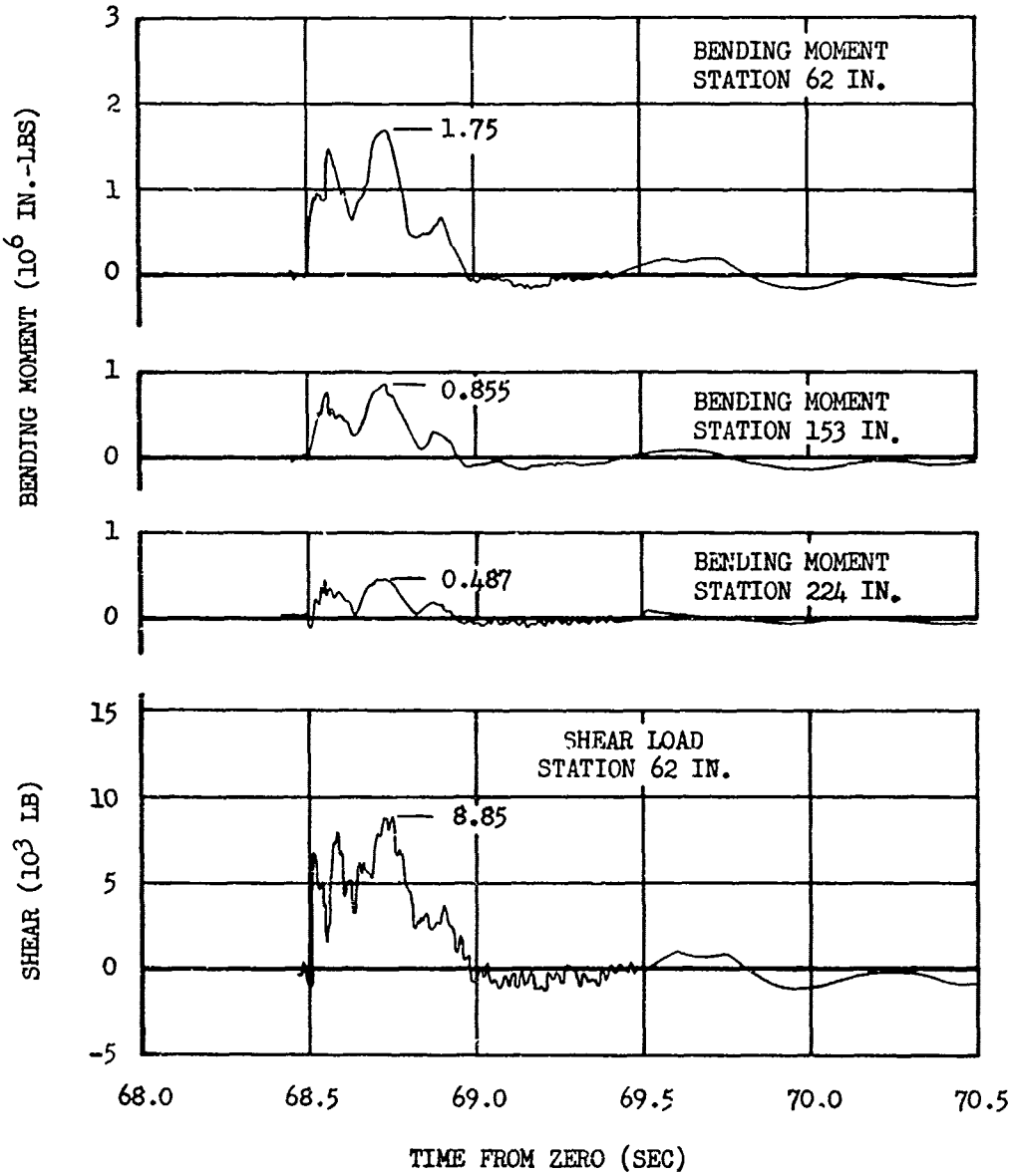

Fig. 4.38 Bending Moments and Shear Loads of Left Stabilizer vs Time, Shot 4

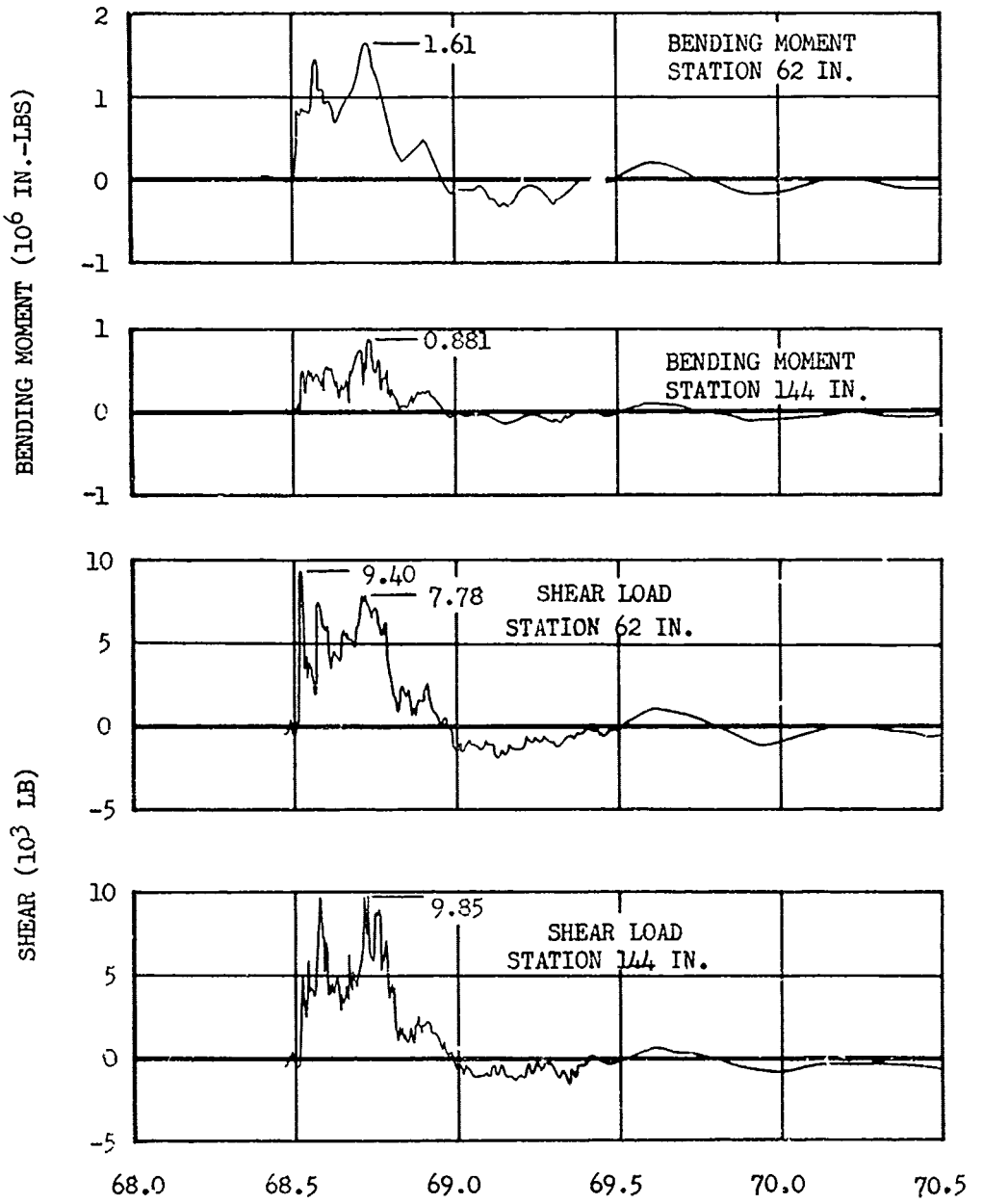

Fig. 4.39 Bending Moments and Shear Loads of Right Stabilizer vs Time, Shot 4

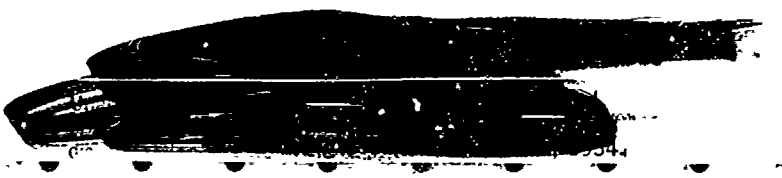

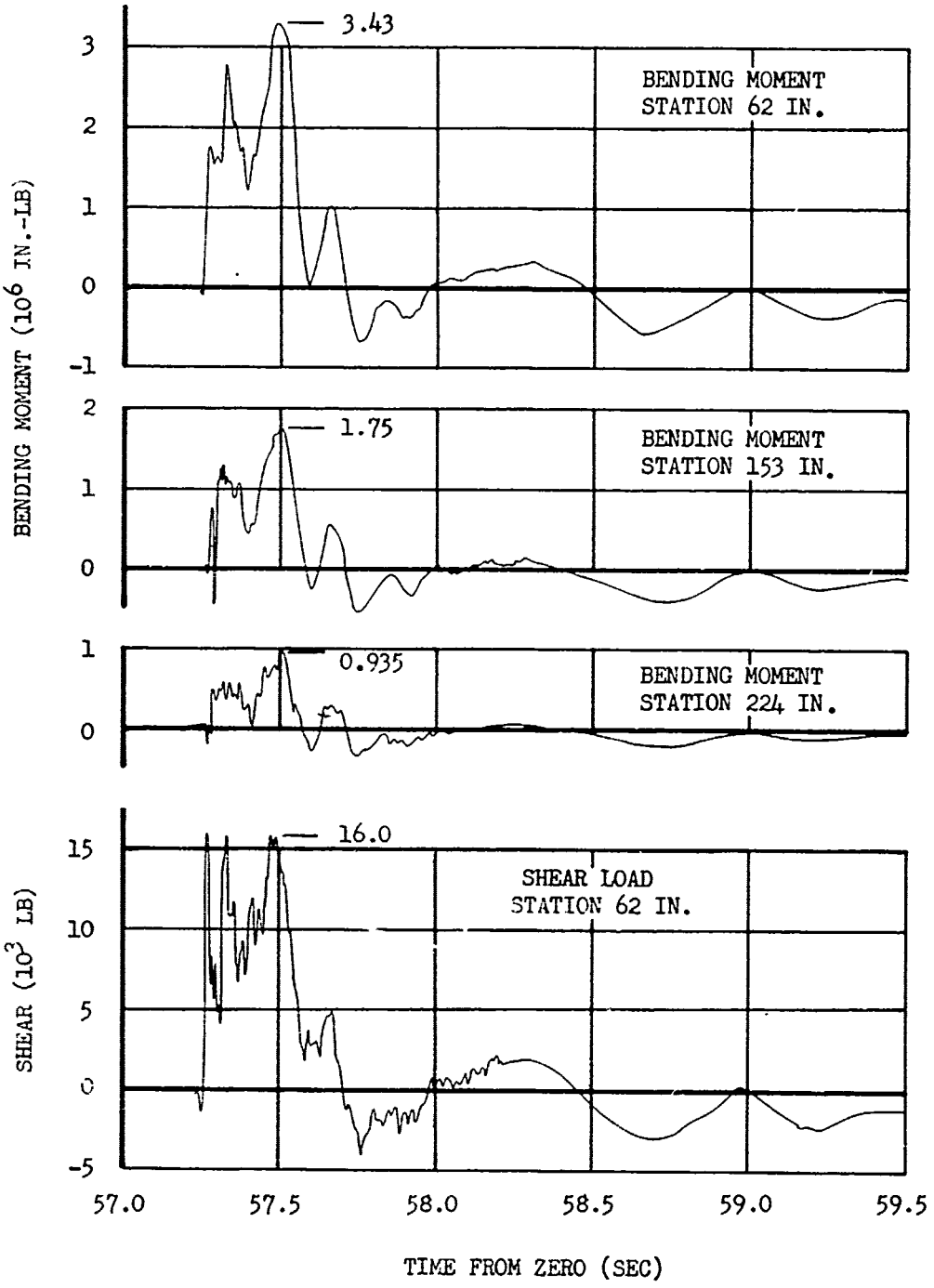

Fig. 4.40 Bending Moments and Shear Loads of Left Stabilizer vs Time, Shot 5

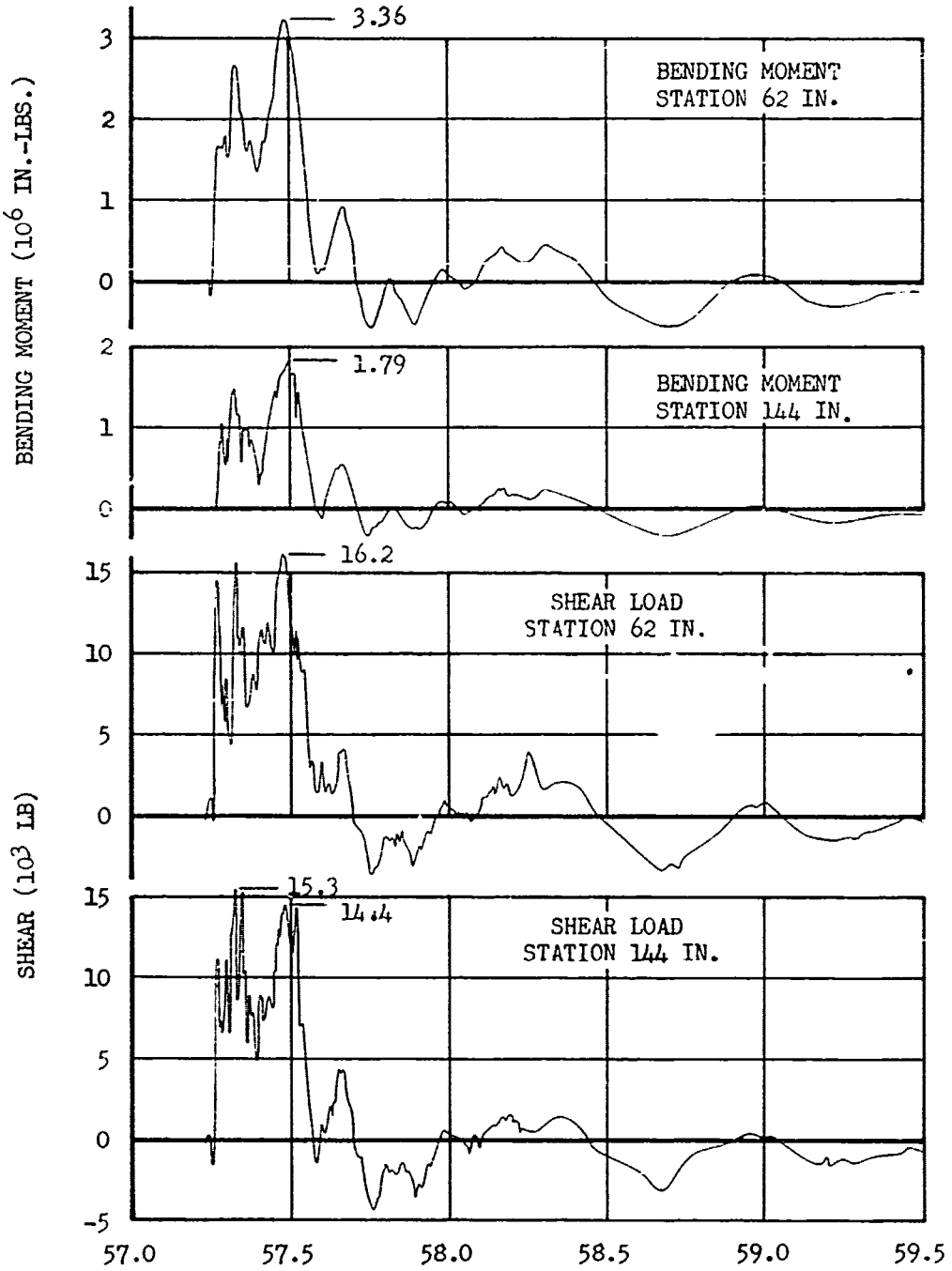

Fig. 4.41 Bending Moments and Shear Loads of Right Stabilizer vs Time, Shot 5

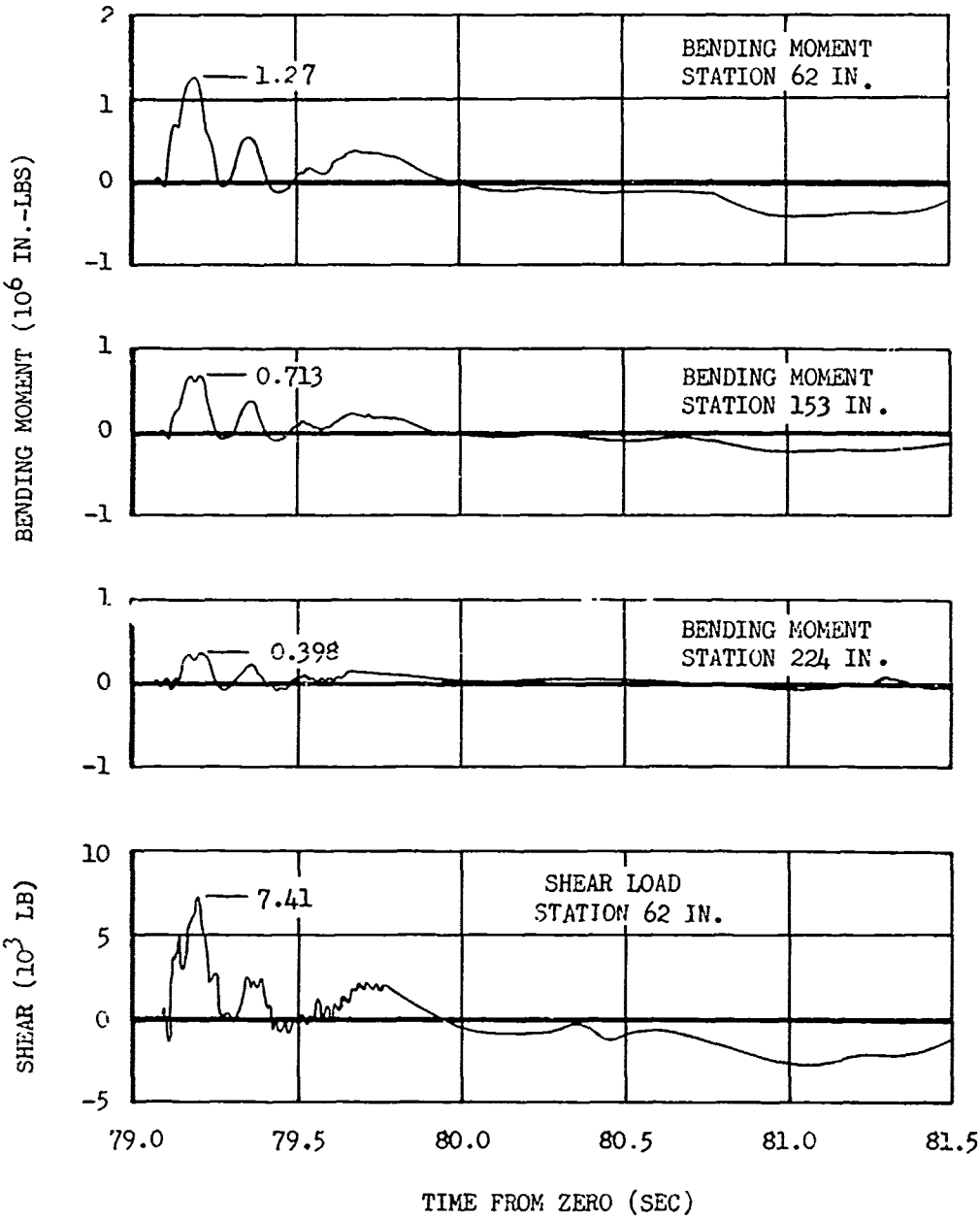

Fig. 4.42 Bending Moments and Shear Loads of Left Stabilizer vs Time, Shot 6

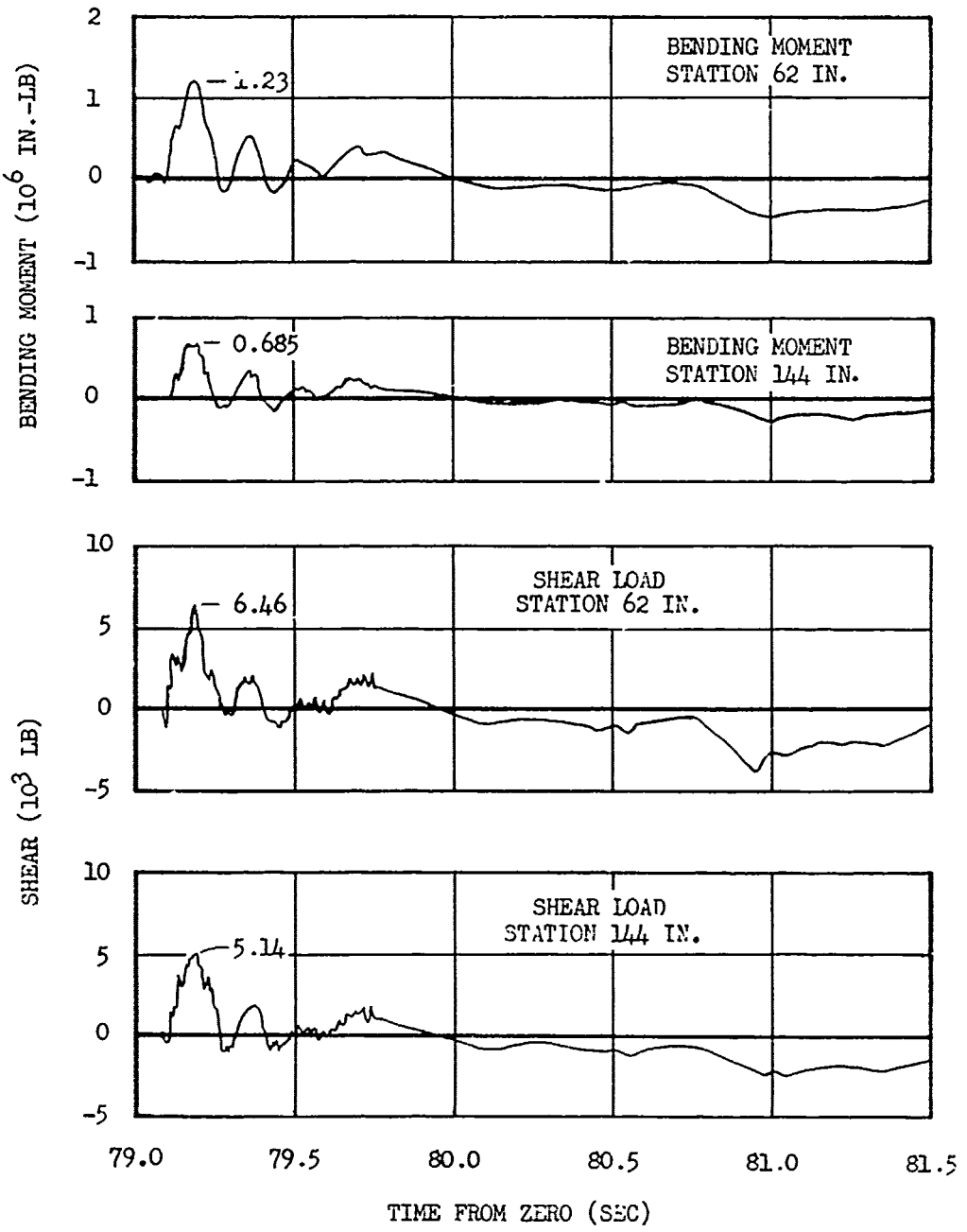

Fig. 4.43 Bending Moments and Shear Loads of Right Stabilizer vs Time, Shot 6

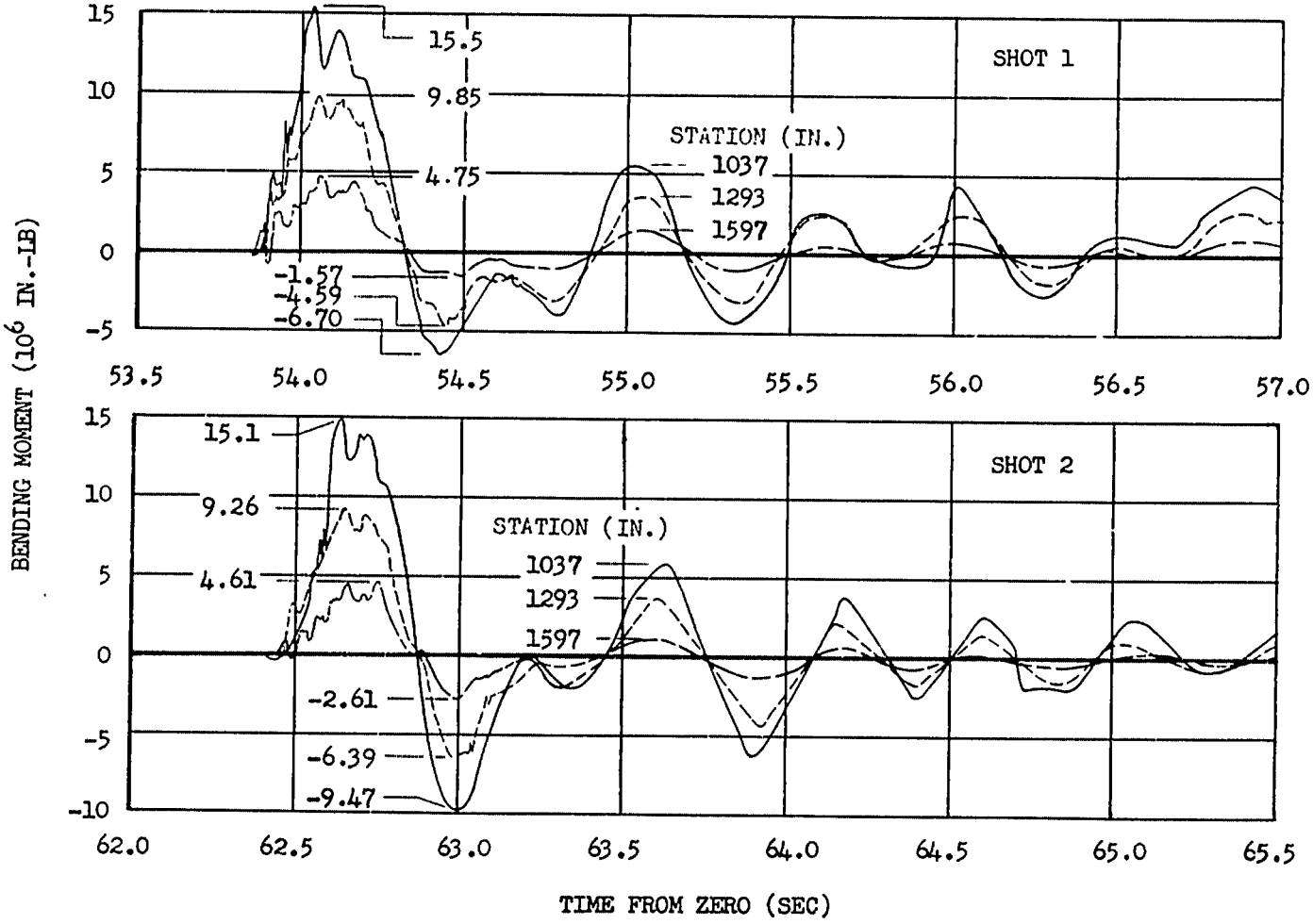

Fig. 4.44 Fuselage Bending Moments vs Time, Shots 1 and 2

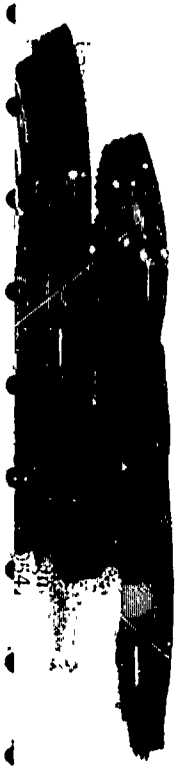

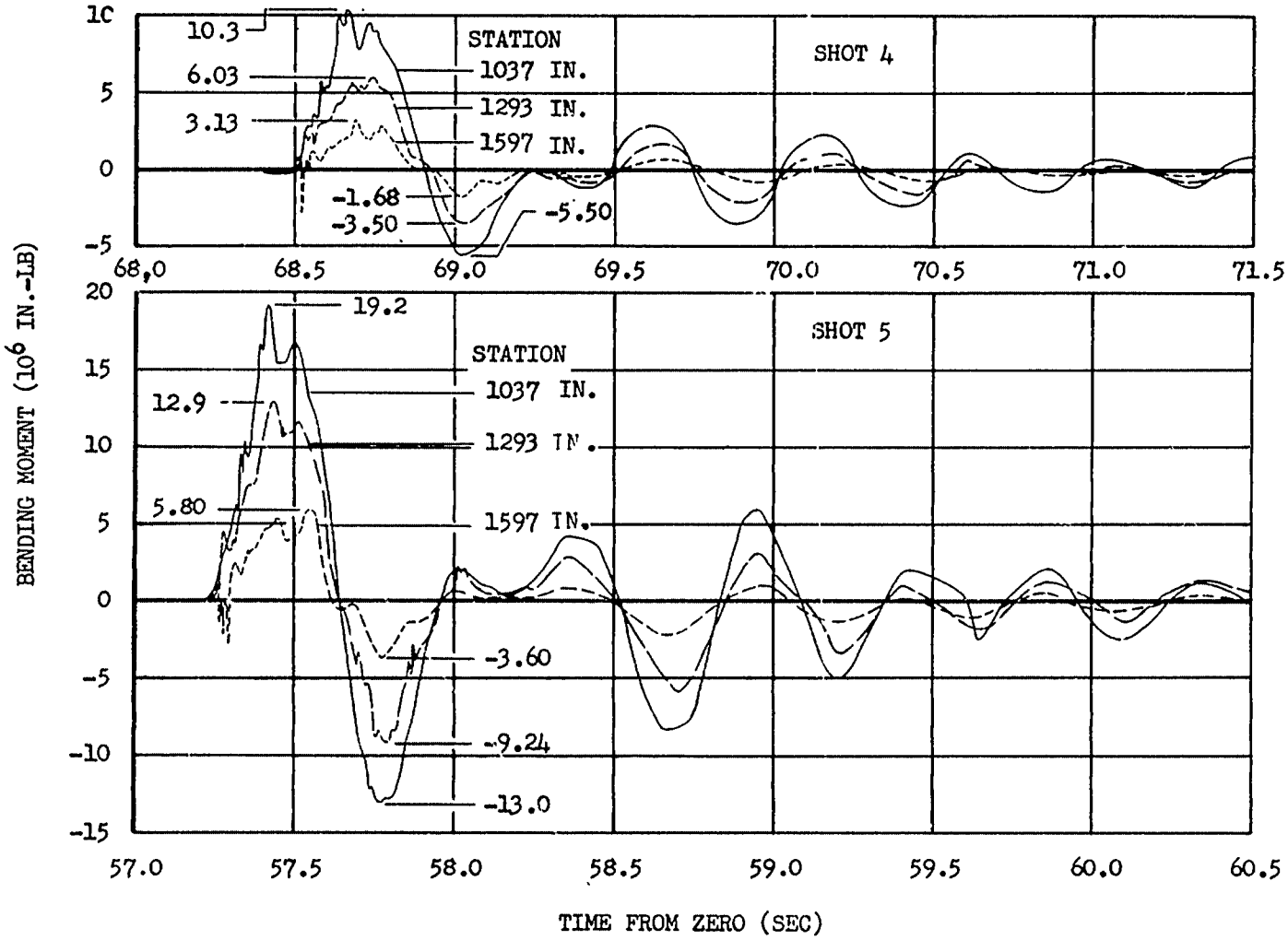

Fig. 4.45 Fuselage Bending Moments vs Time, Shots 4 and 5

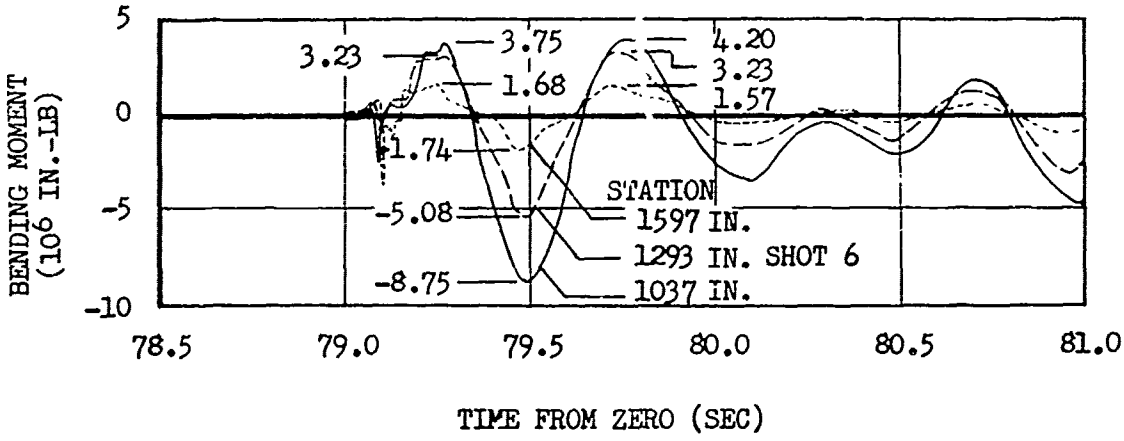

Fig. 4.46 Fuselage Bending Moments vs Time, Shot 6

Acceleration data are presented in Figs. 4.52 through 4.58. Zero G's on the curves corresponds to straight and level flight where the absolute value would be one G, thus the ordinate scales of these curves represent changes from the straight and level flight condition. Positive acceleration is the result of forces acting in the direction of positive lift. Wing and fuselage data for Shots 5 and 6 only are presented here; similar data for Shots 1, 2, and 4 are contained in reference 19.

Angular accelerations, measured at the center of gravity and in the plane of the pitching motion of the aircraft, are presented in Fig. 4.58. Positive angular acceleration is that caused by a nose-up motion.

The deflection of the elevator with respect to time is represented by the curves of Fig. 4.59. The term elevator deflection represents the deflection of the control surface in rotating about its normal pivot axis. Curve variations during the first second are believed to be caused by the blast alone, but variations after 1 sec could be the result of the blast and/or the movement of the controls by the pilot. Zero deflection of the elevator represents the in-flight position just before shock arrival, and the positive direction is that of up elevator.

Deflections (vertical displacements caused by bending) of the left wing relative to the fuselage at three separate locations are presented in Figs. 4.60 and 4.61. These deflections were obtained directly from motion picture film. There is no direct time correlation between the motion picture film and the actual time or the oscillograms; therefore, the time scale on the wing deflection curves is in terms of film frame number. The zero position of the wing represents the in-flight condition just before blast arrival.

4.3.3 Blast Damage

Blast damage to the B-36D aircraft was experienced as a result of the exposure of the aircraft to these three phenomena accompanying the blast wave(s):

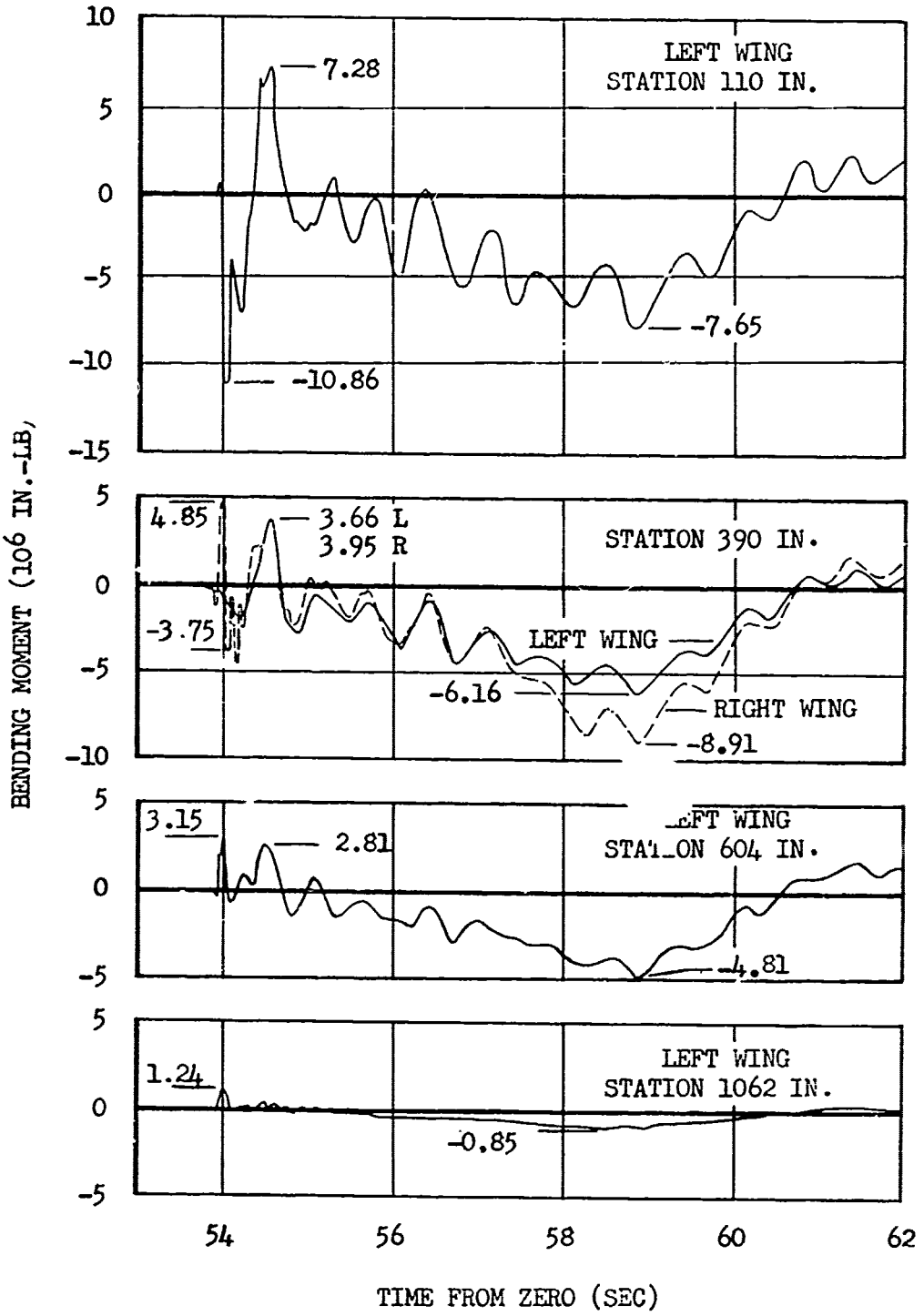

Fig. 4.47 Wing Bending Moments vs Time, Shot 1

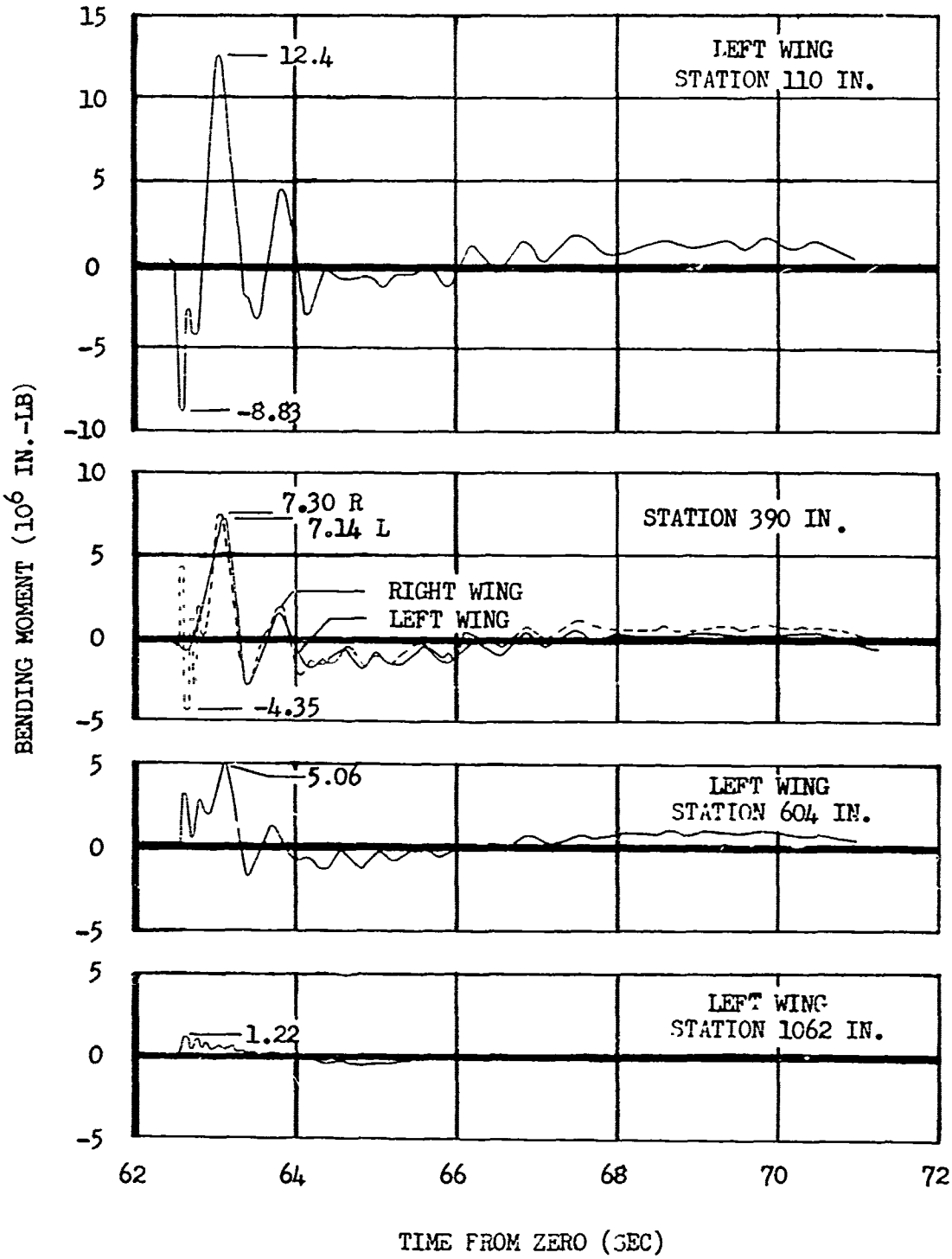

Fig. 4.48 Wing Bending Moments vs Time, Shot 2

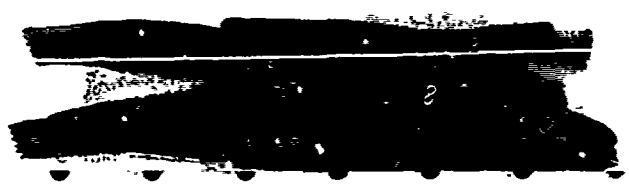

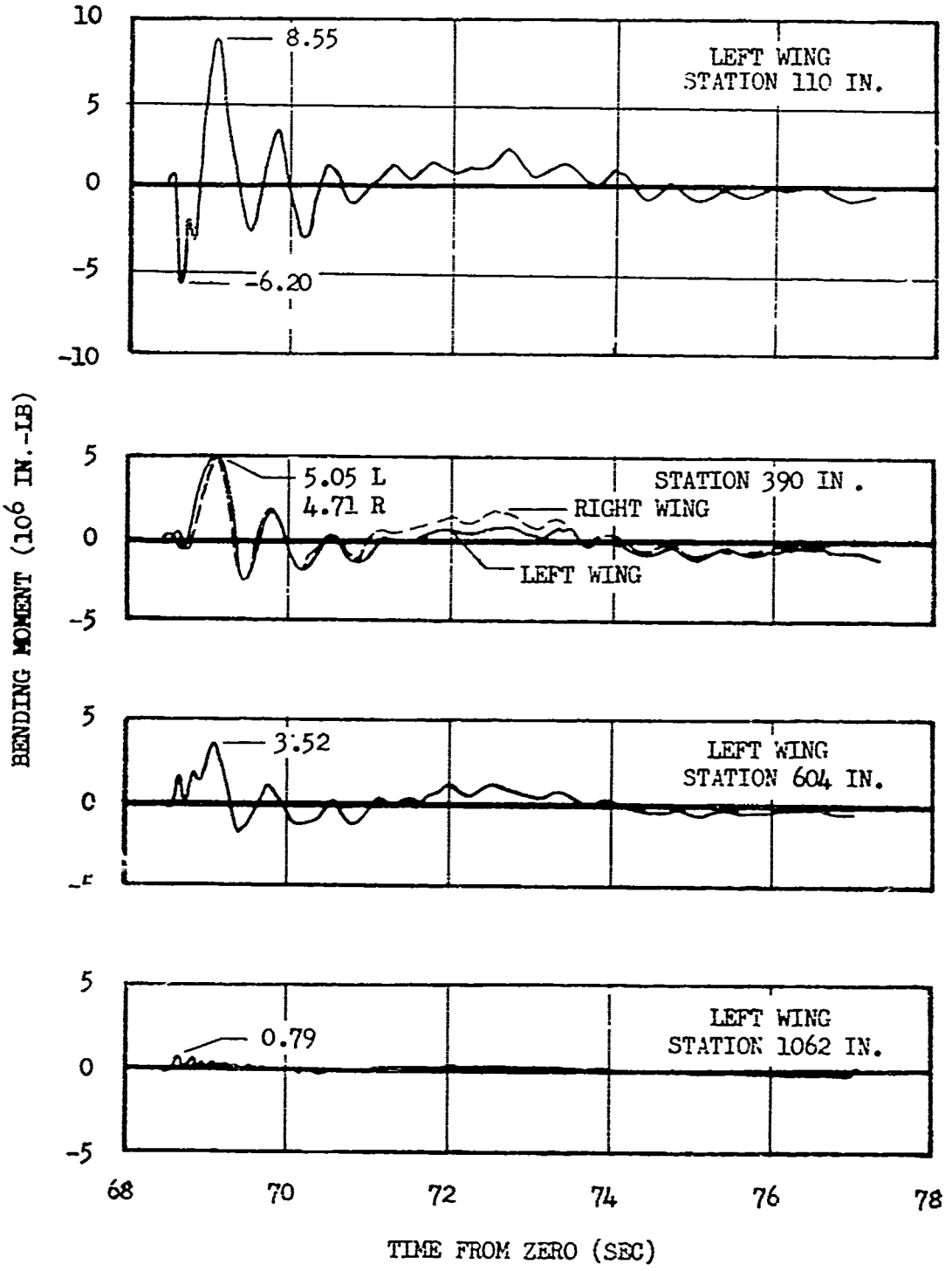

Fig. 4.49 Wing Bending Moments vs Time, Shot 4

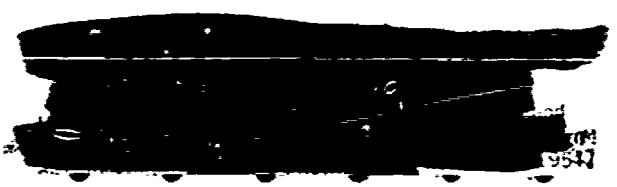

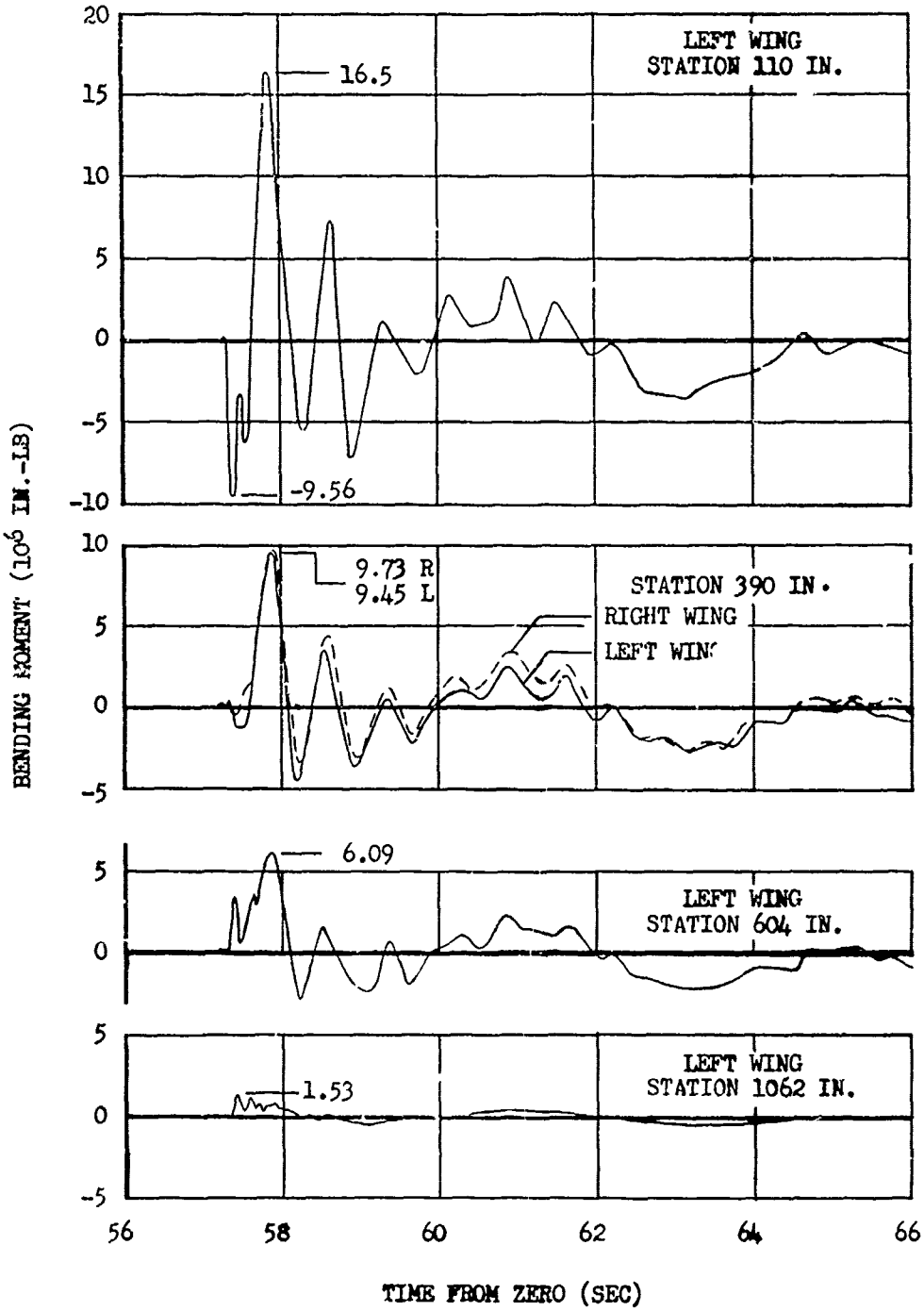

Fig. 4.50 Wing Bending Moments vs Time, Shot 5

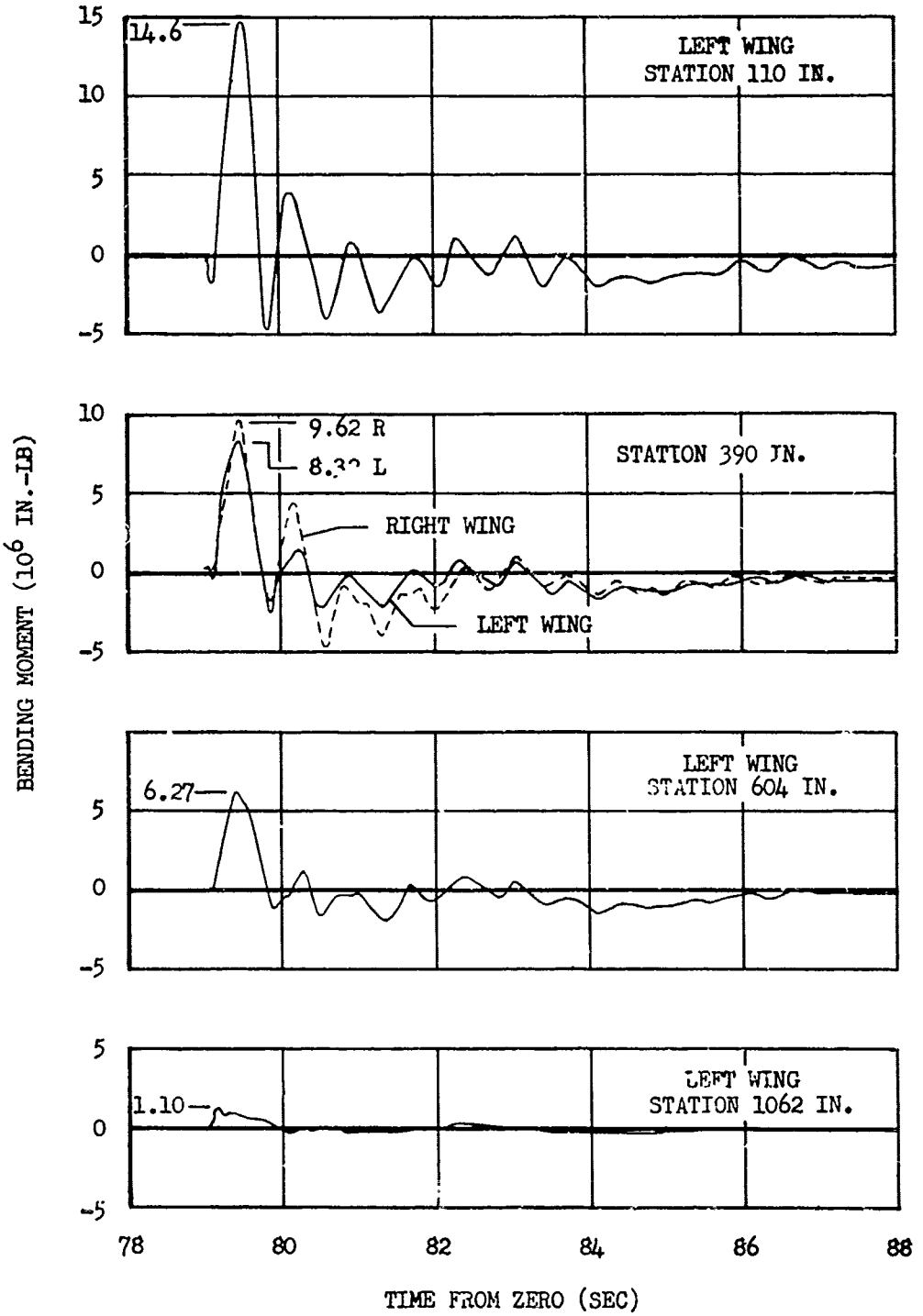

Fig. 4.51 Wing Bending Moments vs Time, Shot 6

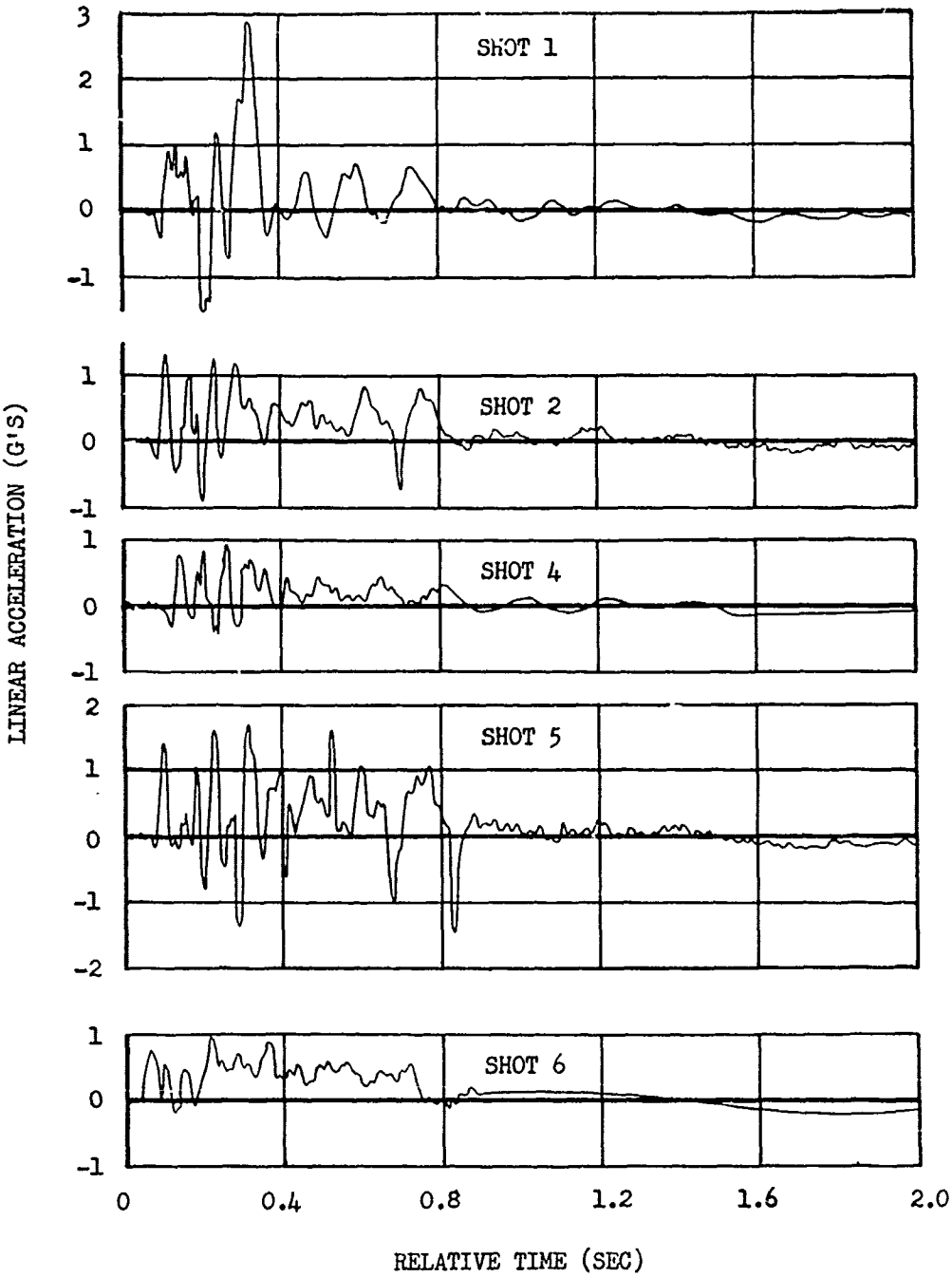

Fig. 4.52 Vertical Acceleration of Aircraft Center of Gravity vs Time

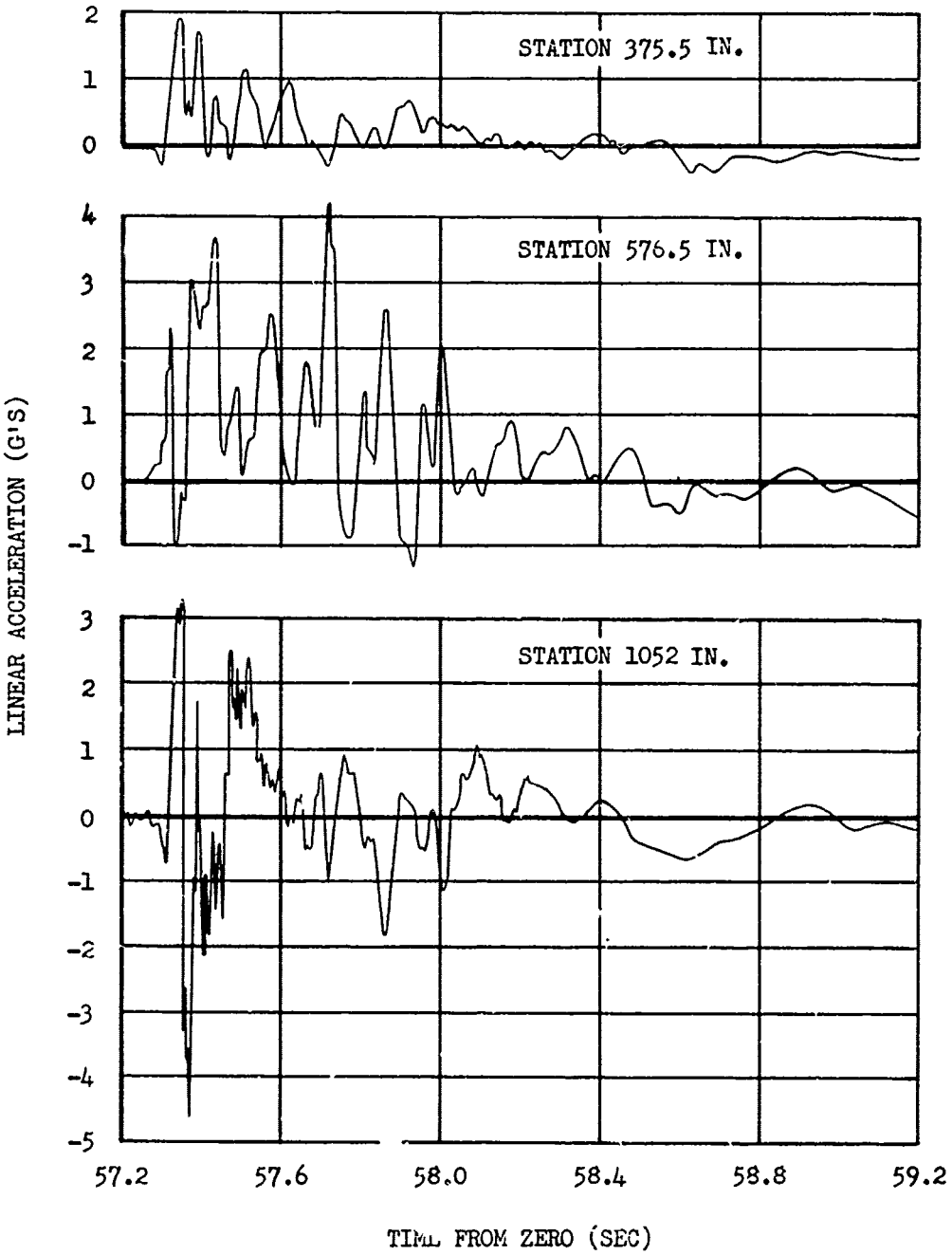

Fig. 4.53 Vertical Acceleration Distribution Along Left Wing vs Time, Shot 5

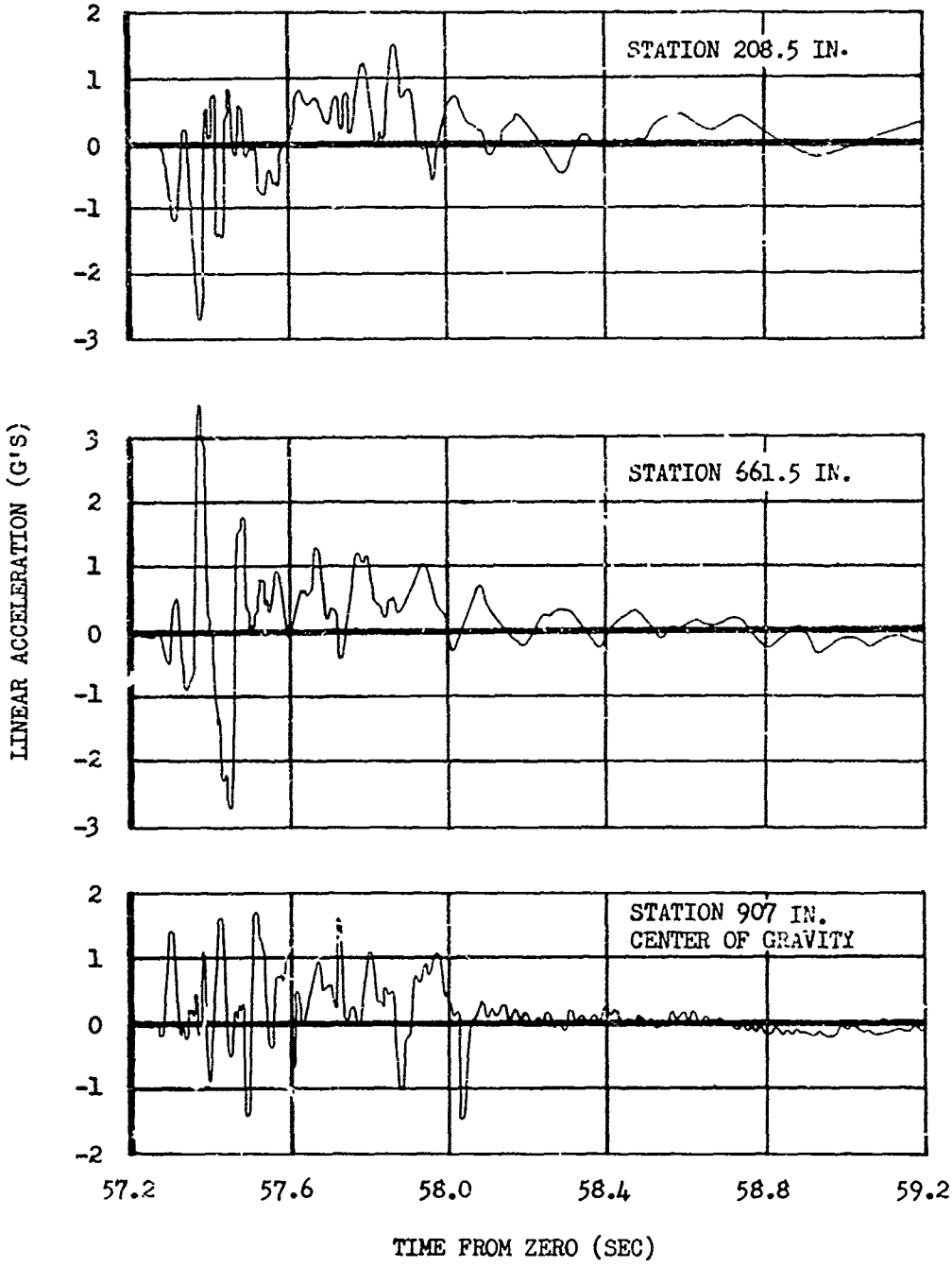

Fig. 4.54 Vertical Acceleration Distribution Along Forward Fuselage Section vs Time, Shot 5

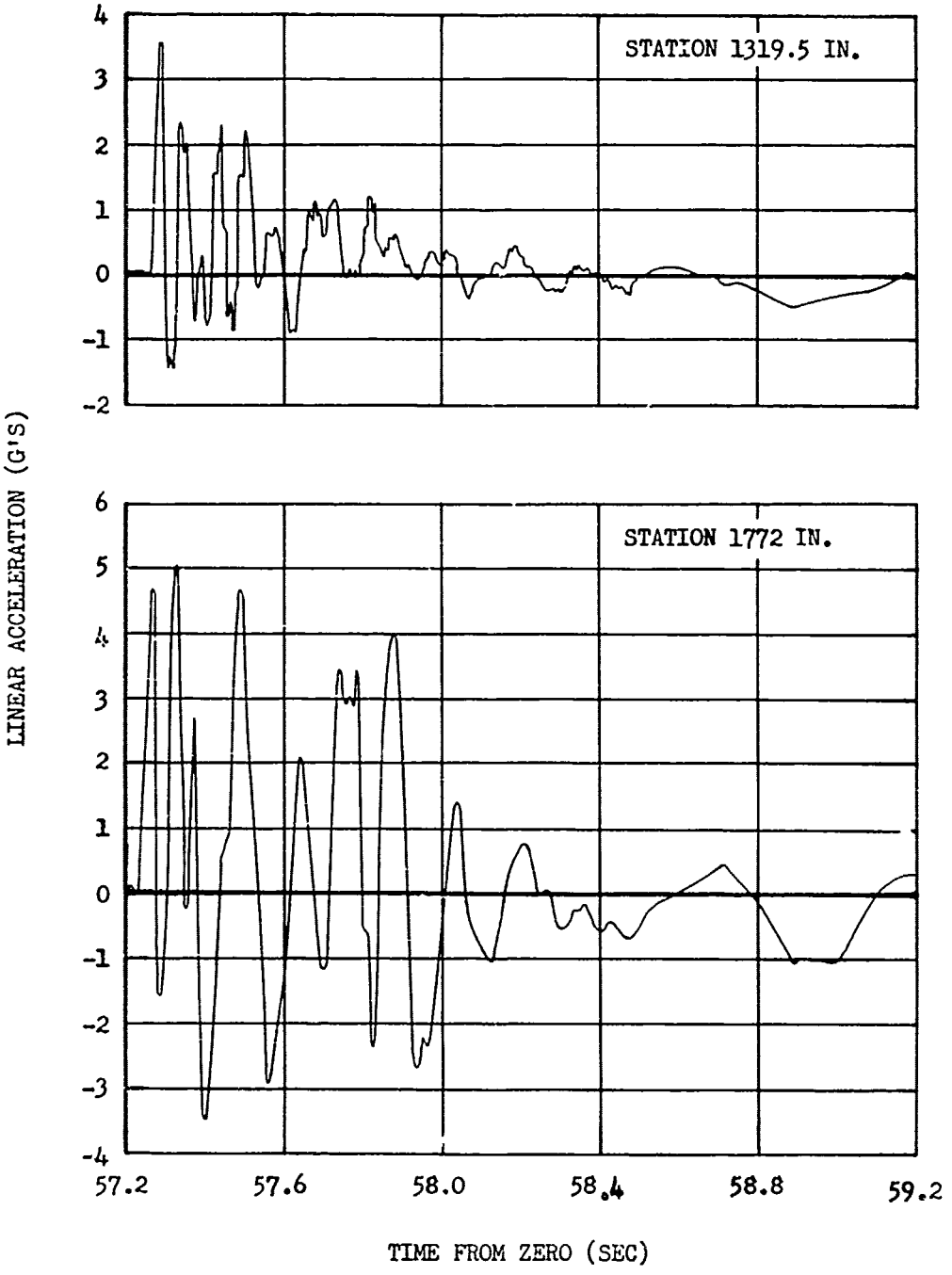

Fig. 4.55 Vertical Acceleration Distribution Along Aft Fuselage Section vs Time, Shot 5

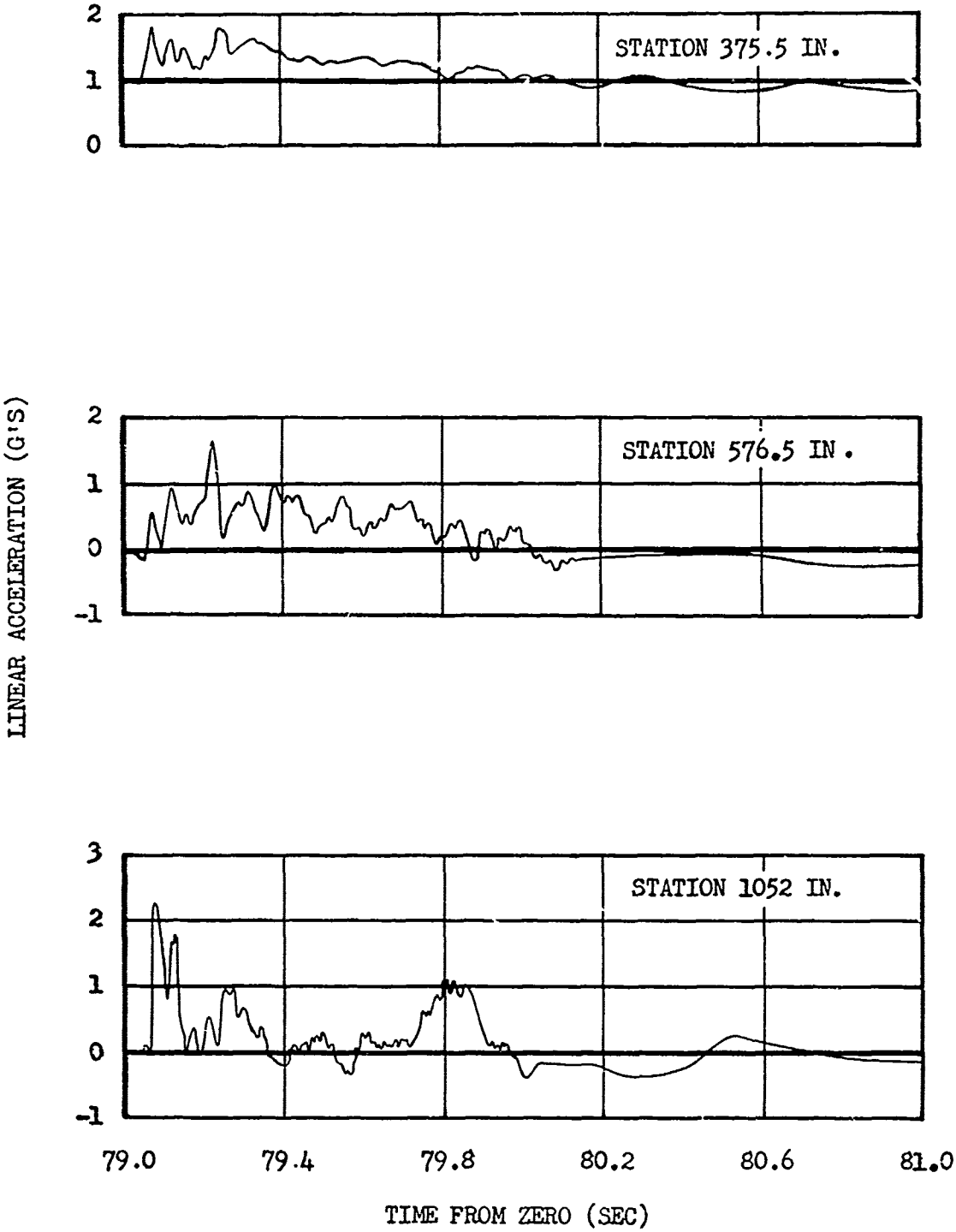

Fig. 4.56 Vertical Acceleration Distribution Along Left Wing vs Time, Shot 6

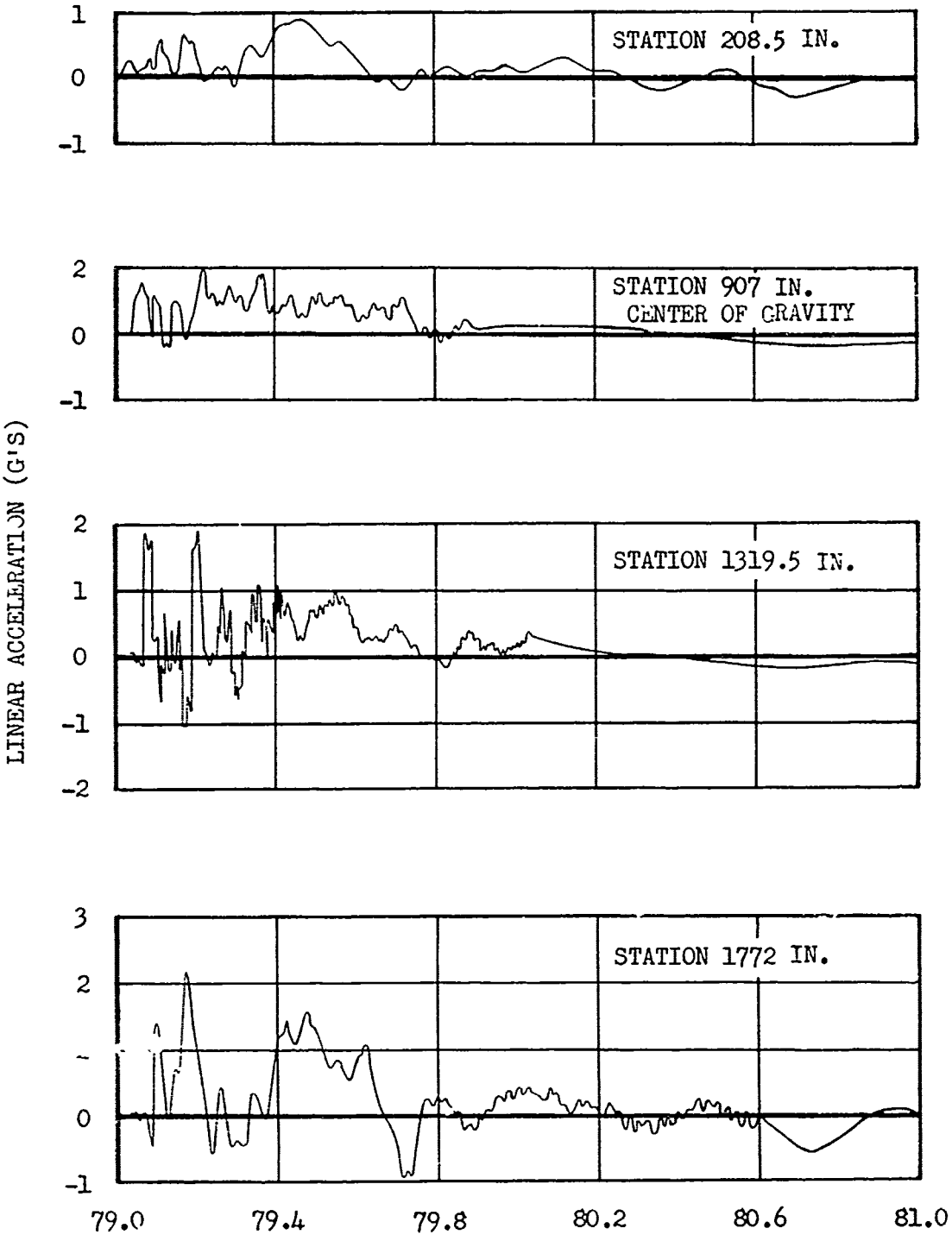

Fig. 4.57 Vertical Acceleration Distribution Along Fuselage vs Time, Shot 6

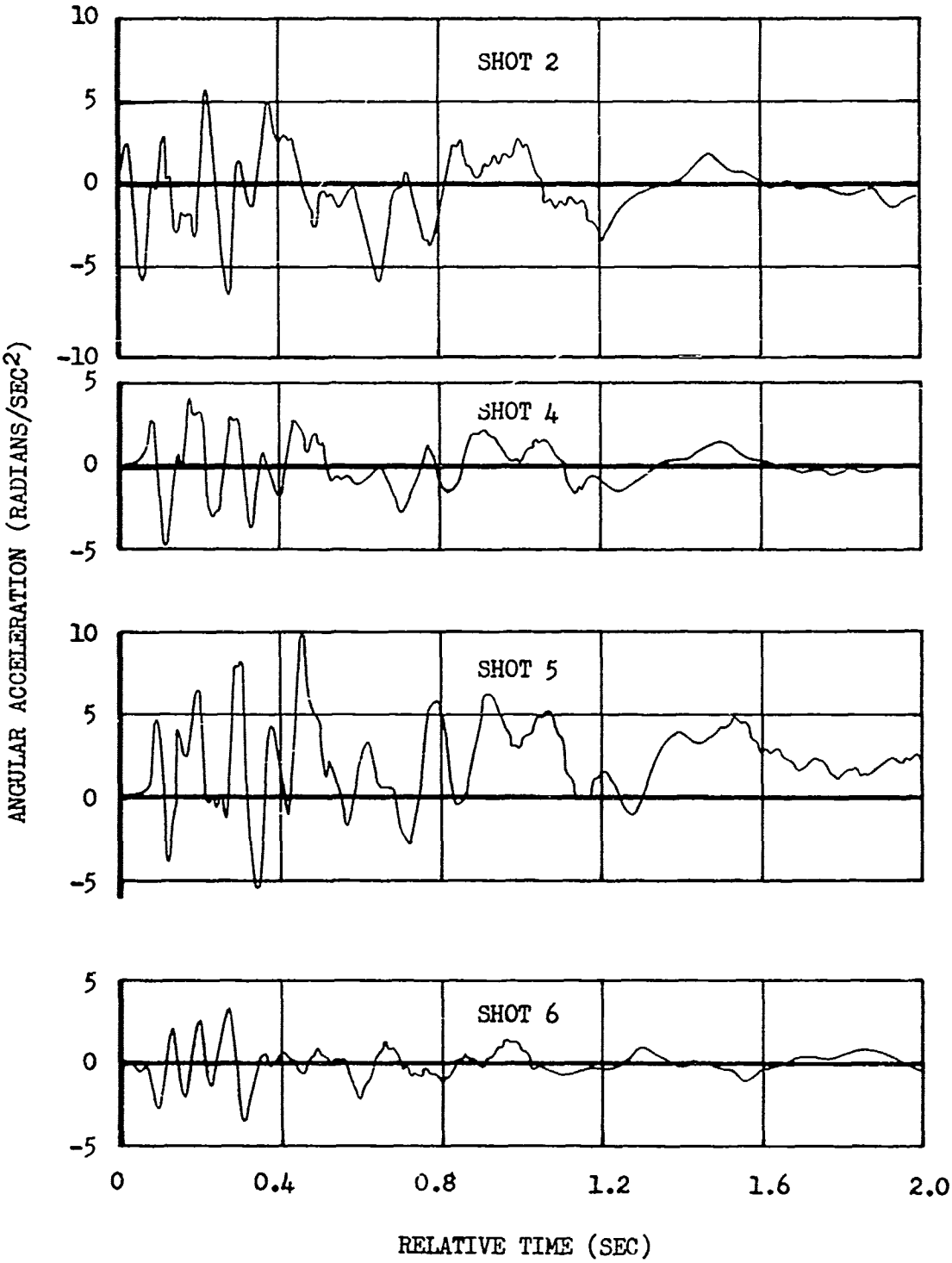

Fig. 4.58 Angular Acceleration of Aircraft Center of Gravity vs Time

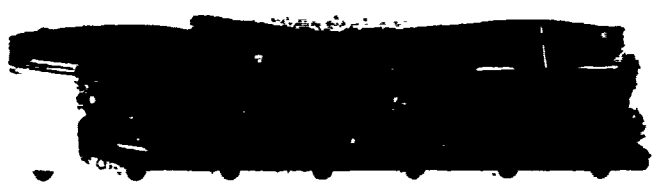

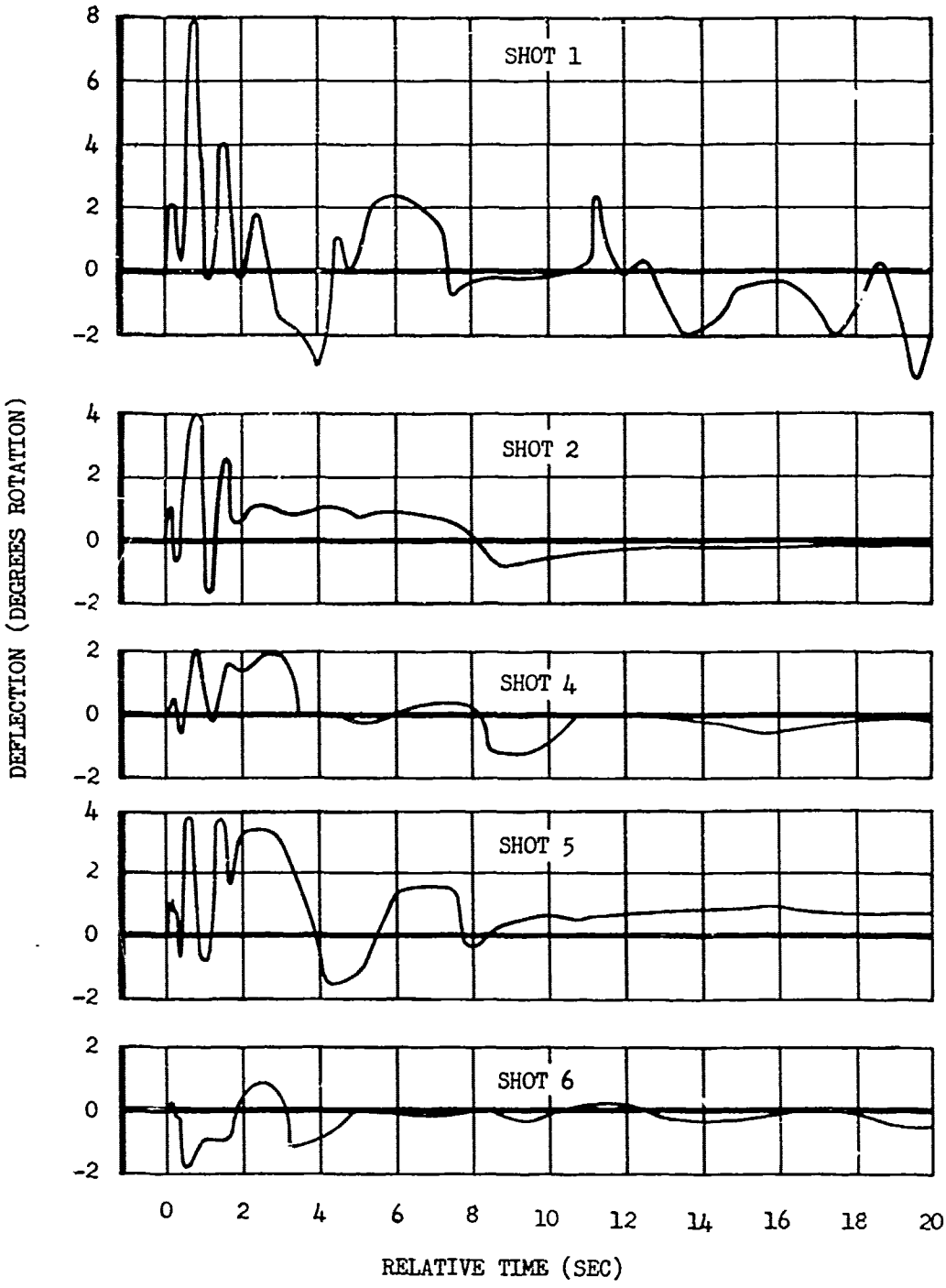

Fig. 4.59 Elevator Deflection vs Time

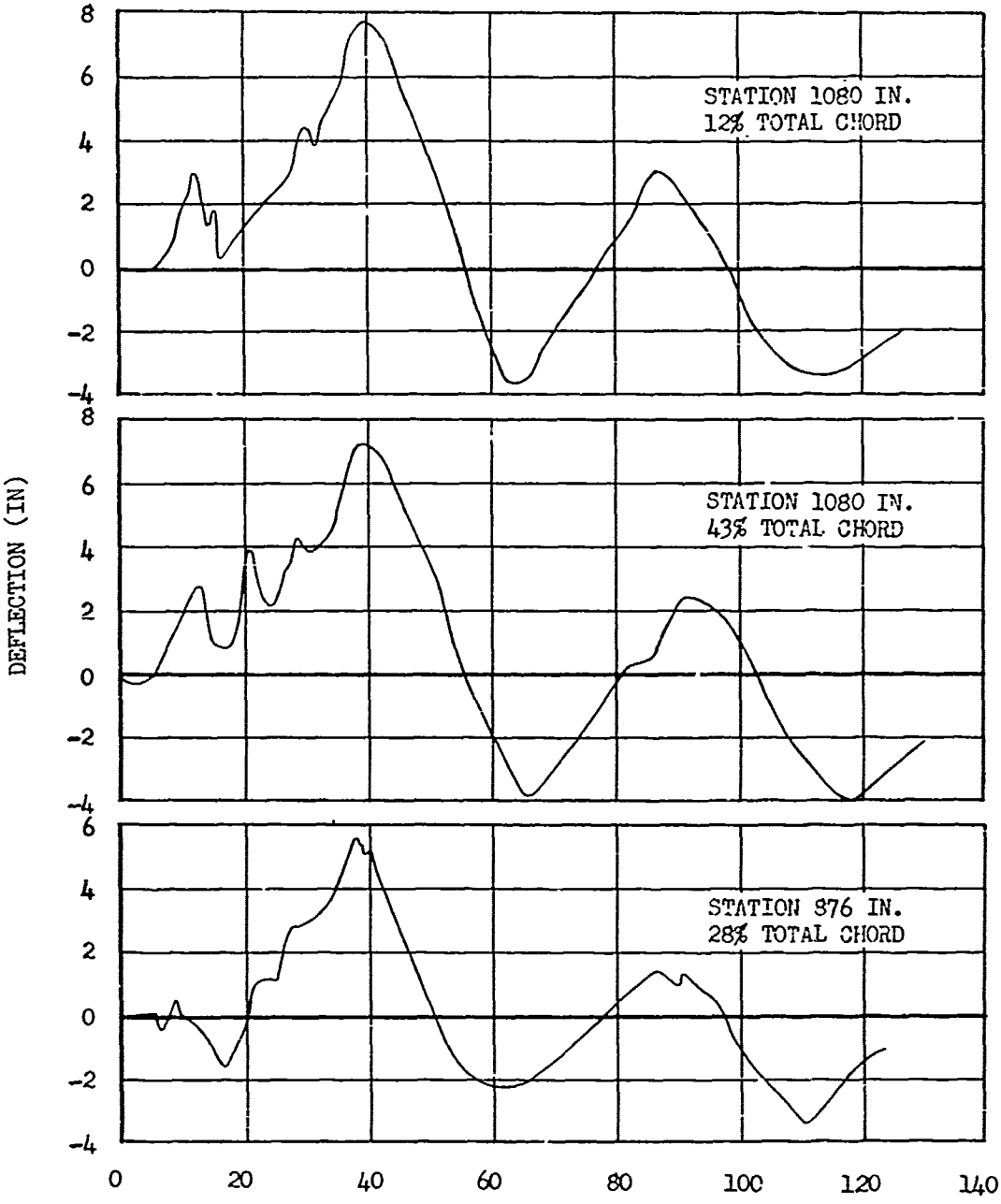

Fig. 4.60 Wing Deflection vs Time, Shot 5

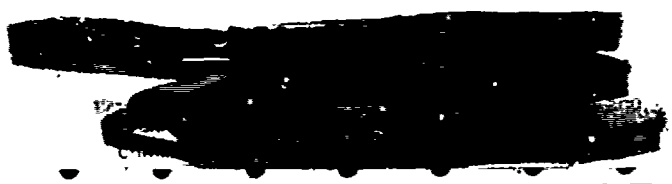

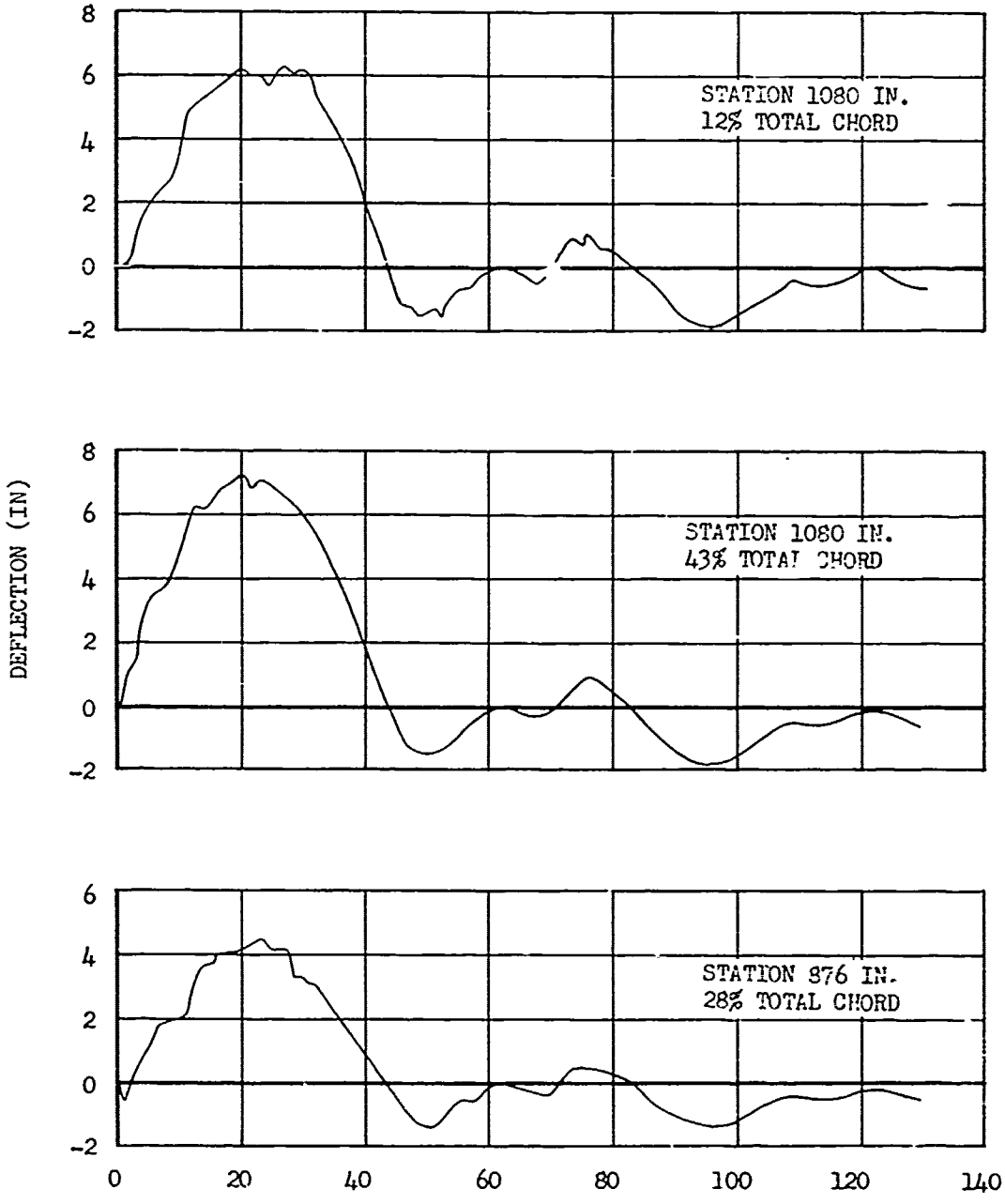

Fig. 4.61 Wing Deflection vs Time, Shot 6

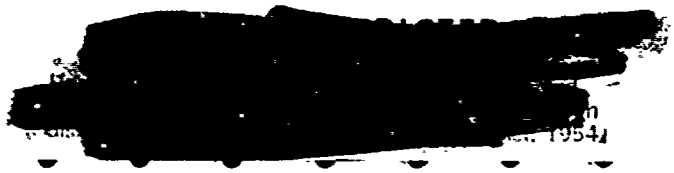

a. Free stream overpressure,
b. Pressure reflection from the surfaces,
c. Material velocity of the shock wave.

It is difficult to say that any one of these phenomena was primarily responsible for the blast damage, because the effects of each are not easily separated; therefore, in this presentation, the term blast damage shall refer to the effects of any or all of these phenomena.

The major portion of the blast damage inflicted upon the aircraft was confined to secondary structure or sheet metal components. The damage, as experienced in Operation CASTLE, had little or no effect upon the performance of the aircraft; however, the possibility of more serious effects existed. Had the damage level been slightly higher or the performance requirements of the aircraft been greater, such as might be experienced during a wartime mission, an undesirable degradation of the capabilities of aircraft could be realized. The general areas of blast damage to the B-36D aircraft are shown in Fig. 4.62.

From visual damage assessments conducted after each shot, the component most susceptible to blast damage appears to be the bomb bay door assembly. The bomb bay doors were damaged by all shots of the CASTLE series except for Shot 3, which produced no significant inputs. The most severe damage was obtained on Shot 1 (0.81 psi overpressure). Figure 4.63 is a three-quarter front view of the forward bomb bay doors, showing the damage received from Shot 1.

The rear doors were damaged to the same extent. The type of buckling shown is typical of all shots but of different magnitude, the extent of damage being roughly proportional to the overpressure encountered.

Other typical types of damage experienced by the bomb bay doors are shown in Fig. 4.64. The damaged fuselage bomb bay door seal in the photograph on the left should be noted. It is believed that the doors were actually deflected up into the bomb bay, catching this seal and bending it out on their return to normal position. A view of damage to the edge of an upper door, where it joins the lower door, is presented in the right photograph of Fig. 4.64.

Sheet metal damage, other than that to the bomb bay doors, consisted of buckling of the skin of the aft lower turret door, the main landing gear canoe doors, the nose landing gear door, and the engine nacelles. In addition to the skin buckling, small failures at corners of the doors and some rivet failures were observed. Typical damage of this type is shown in Fig. 4.65, and ranged from the order of magnitude shown (Shot 1) to near insignificance (Shot 6).

Severe dishing in of the forward radome (bombing and search radar) occurred on Shot 1. This damage is shown in Fig. 4.66. The normal operation of the radar antenna was not affected. Blast damage to the radome occurred on Shot 1 only. The aft radome (tail turret radar) suffered delamination, but it is not known when the damage was inflicted, as this was not discovered until the aircraft returned to the continent for overhaul after the test series.

Several of the elevator and aileron inspection panels which were held in place by Messerschmidt fasteners were lost on Shot 1. This situation did not occur again as the fasteners were safety-wired for

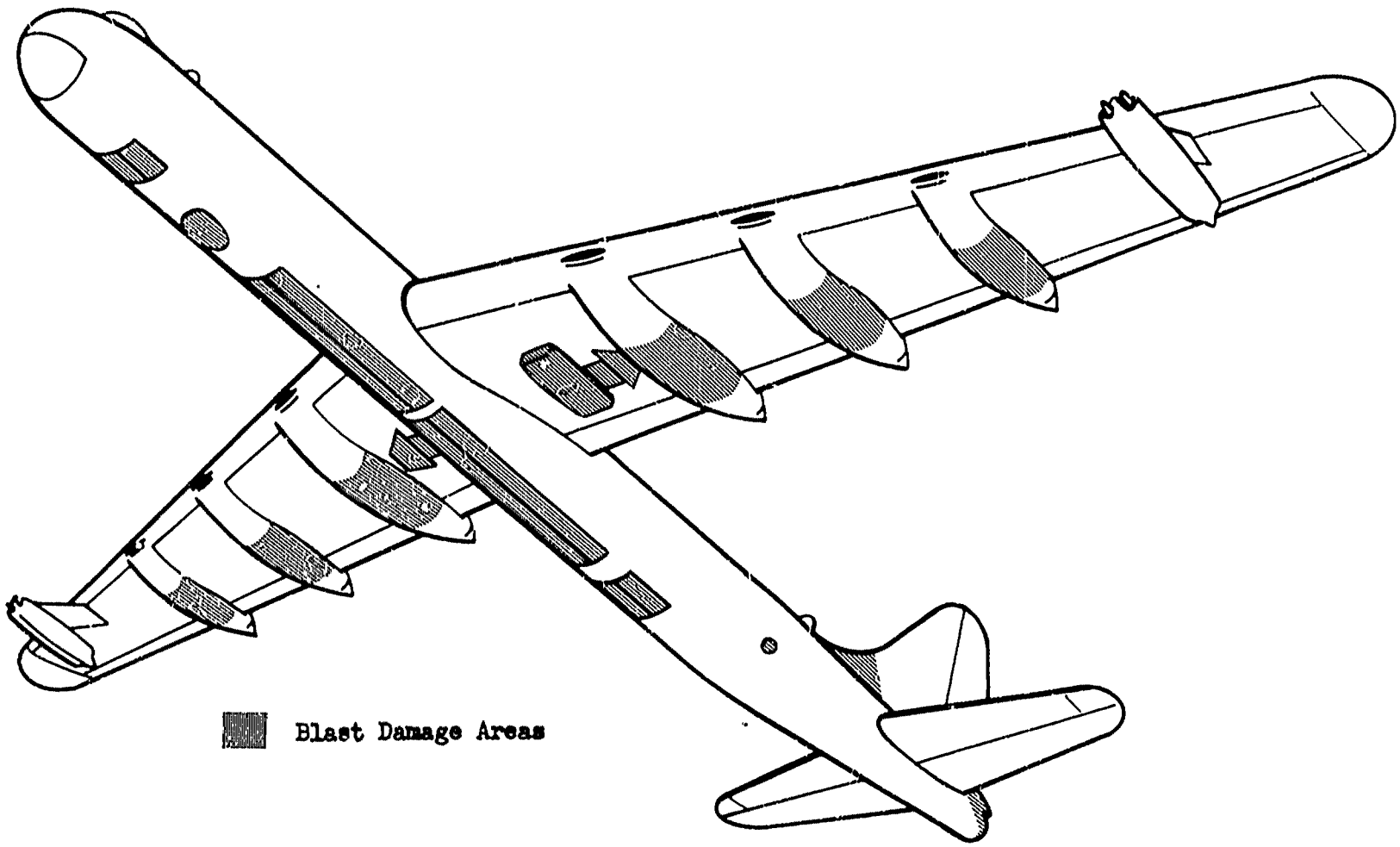

Fig. 4.62 General Areas of Blast Damage To The B-36D

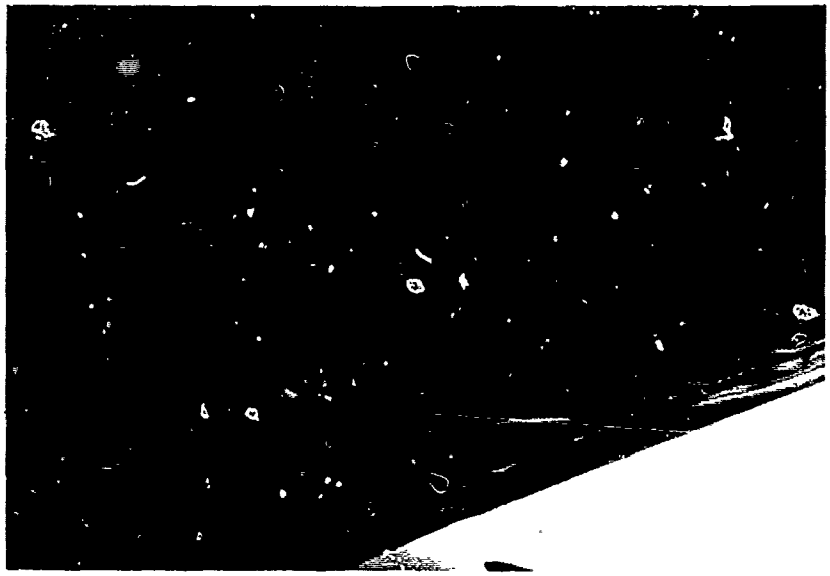

Fig. 4.63 Blast Damage to Forward Bomb Bay Doors, Shot 1

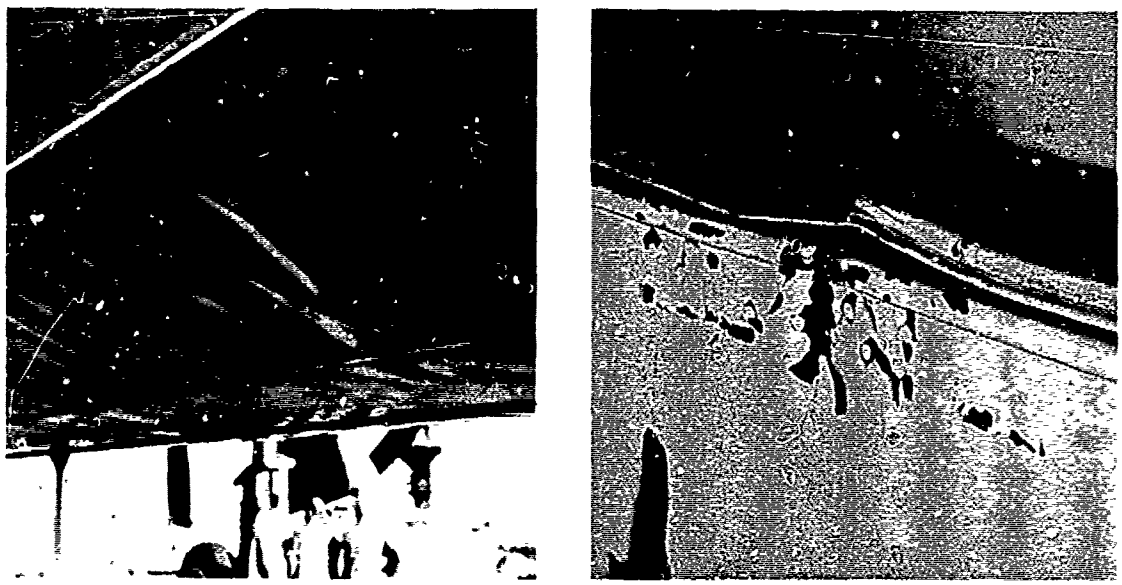

Fig. 4.64 Typical Bomb Bay Door Damage

subsequent shots.

Failure of one bomb bay door limit switch link occurred on Shot 1. This failure is shown in Fig. 4.67. Also, several failures of the rivets used to fasten the brackets to the door and the fuselage structure occurred.

Additional blast damages incurred on Shot 1 only, were cracks about 1½ in. long in the aft lower blisters (Plexiglas), and a sheet metal crack in the crew access tunnel between Bulkheads 5 and 6.

Although it is believed that all of the damage to the aircraft

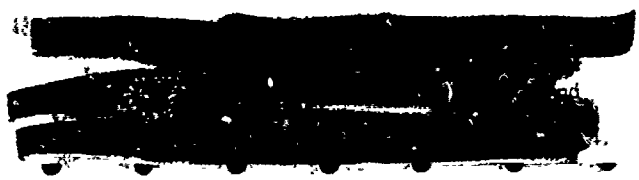

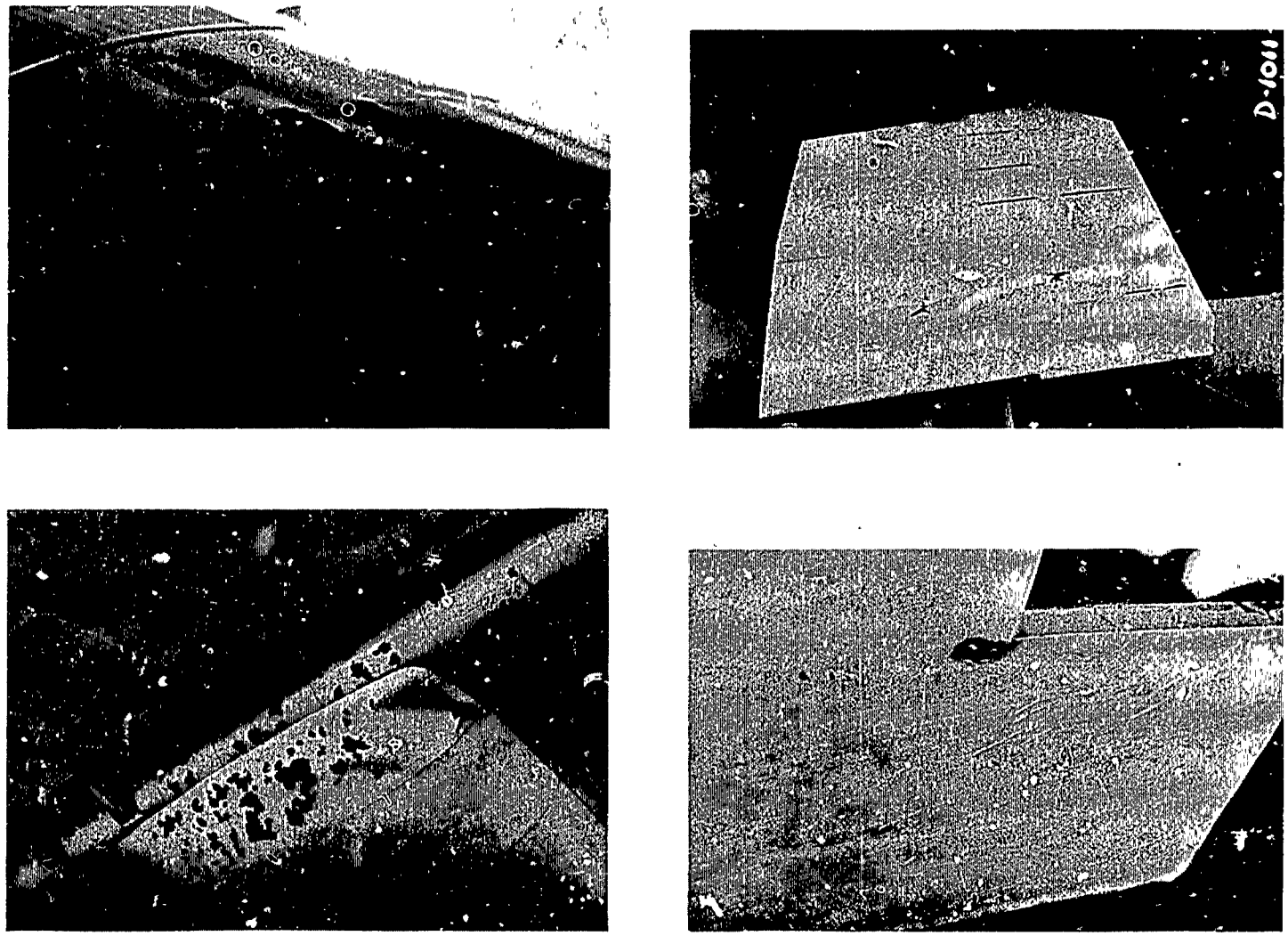

Fig. 4.65 Blast Damage to Turret and Landing Gear Doors

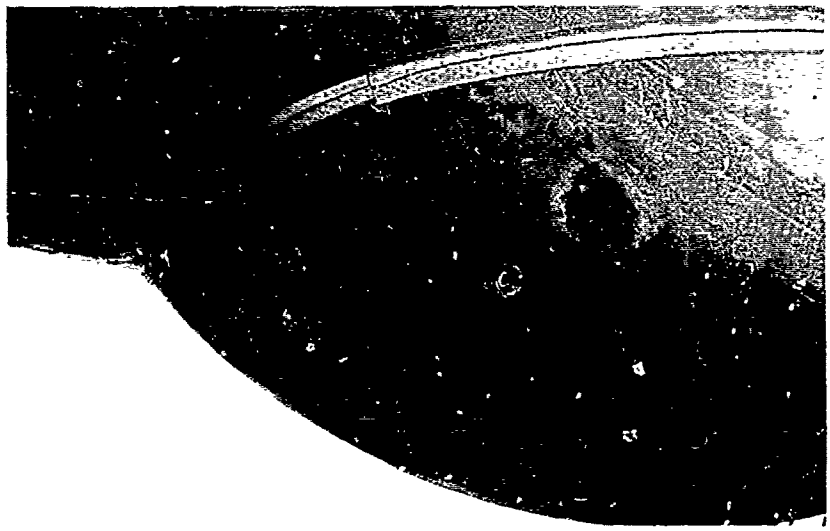

Fig. 4.66 Damage to Forward Radome, Shot 1

was detected by visual inspection, there is always the possibility that some of the internal components were damaged or that some damage was not detected.

4.3.4 Flight Crew Observations of the Blast Phase

Shot 1 was described as a very sudden, but not sharp, bump, not unlike a thunderstorm bump of short duration. The reaction of the aircraft did not appear to be localized; rather, the structure was affected as a whole. Subsequent to the initial shock, a sensation of falling was observed by some of the crew members. Relative to Shot 1, the blast phase of Shot 2 was described as more rapid but less violent, and Shot 4 as moderate and short. The observations during Shot 5 indicated structural flexibility, as the reaction to the shock wave was described as similar to "one shake of a rag doll." Shot 6 produced a very small and fast jolt.

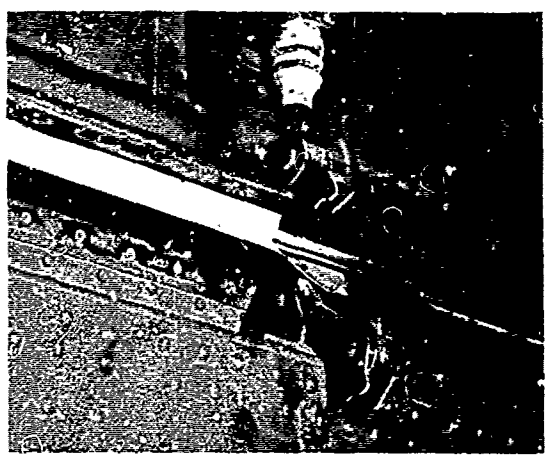

Fig. 4.67 Bomb Bay Limit Switch

During the blast phase of all shots, the aircraft was controlled manually rather than by the autopilot. The feel of the controls was described as free-floating during the passage of the shock wave for Shot 1. No other comments were made for subsequent shots.

The static and pitot-static flight instruments were affected by the overpressure during all shots, the magnitude and duration of the effect being proportional to the overpressure encountered. After the

shock wave of Shot 4 had passed, it was noted that the barometric altimeter indicated an altitude 200 feet above the pre-shock altitude. The gyroscopic instruments were not affected by the blast.

The aircraft engines, both jet and reciprocating, were affected by the shock wave. The jet engine tail-pipe temperature, normally about 500°C, was observed to be about 750°C just after shock arrival, Shot 1. At this time, the temperature was returning to the normal reading and the peak was not obtained. For subsequent shots, the tailpipe temperature indicating instruments were watched and the results are as follows:

Shot 2 - instruments reached their limit of 1000°C during blast phase. Engine J-1 appeared to flame out and was shut down, but a broken thermocouple wire was found after landing. Whether or not the engine did flame out is uncertain.

Shots 4, 5, and 6 - no change in temperature observed.

The reciprocating engines experienced a change in speed (rpm) during the passage of the shock wave. Normally the engine speed is governed automatically by a propeller pitch control device. Observations during Shot 1 indicated that the reciprocating engines, governed at a speed of 2080 rpm, first experienced a reduction in speed to 1600 rpm, then an increase to 2500 rpm, and finally a return to the normal governed speed. For Shot 2, the speeds of the engines were controlled manually and the maximum variation was 250 rpm, high to low. In order to obtain additional information, the normal automatic control was allowed to operate for Shot 5. The variations observed were:

normal speed - 2150 rpm
low - 1800 rpm
high - 2400 rpm

Shots 4 and 6 produced no significant changes in rpm.

Shock phenomena were observed on the radar scope during the blast phase and appeared very similar to the description by Project 6.1 (reference 20). The cloud itself presented a small return on the radar scope.

Visual observations of the atomic cloud were possible after the thermal radiation had subsided and the protective curtains were removed from the Plexiglas windows. The appearance of the cloud was reported as being very impressive, and there was a powerful illusion that it would overtake the aircraft. This was especially true for Shot 5, because of the close range, and for Shot 6, because the aircraft was heading toward the cloud.

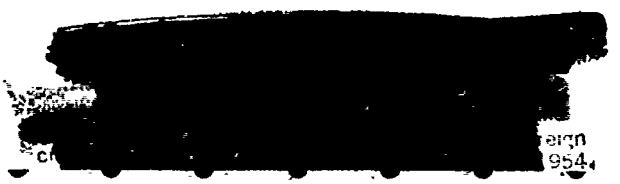

CHAPTER 5

DISCUSSION

5.1 GENERAL

The data obtained by Project 6.2a can be used to evaluate at least three related studies. The first is the verification of predicted effects of a nuclear detonation upon a B-36D aircraft. In pursuing this correlation, the various measured responses of the B-36D are compared to responses predicted by theoretical equations and empirical relationships developed from the laws of physics and improved according to a limited amount of experimental data. This investigation assumes inputs or forcing functions of given magnitude and shape.

The second study is the correlation of the inputs measured at the position of the B-36D with those inputs predicted by theory for such given parameters as yield, slant range, and altitude. In this study, the B-36D aircraft, as such, is of little concern since it is no more than a platform upon which the instruments are mounted. The aircraft would be considered only if the readings of the instruments were affected by their installation in the aircraft.

The third study is the prediction of the largest yield weapon that might be dropped by a B-36D aircraft without serious damage to the aircraft or the determination of the minimum safe distances from explosions of less than limiting yield. The main problem in this investigation is the determination of the relationship between the yield of an explosion and the degree to which the aircraft structure is stressed as a result of the effects of the explosion. Since the entire aircraft could be destroyed if the effects were of sufficient magnitude, it remains to be determined what component part of the aircraft is the weak "link" and the degree of the effects required to stress that part to its limit.

The attainment of responses of the B-36D to nuclear detonations at levels of from 27 to 76 per cent of the aircraft safe limits demonstrated that the theory and procedures for predicting effects are essentially correct. That differences exist between predicted effects and experimental results, and that the theory can be improved, cannot be denied. As a direct result of the data obtained by Project 6.2a with the B-36D, refinements in the empirical formulas used to predict effects have been made and one more step has been taken toward the

TABLE 5.1 - Post Shot Comparison Between the Maximum Values of Theoretical and Measured Inputs and Responses

		Shot 1	Shot 2	Shot 4	Shot 5	Shot 6
Radiant Exposure, cal/sq cm	Post Shot Theoretical	50.8	33.4	22.8	53.8	---
	Measured	47.5	35.2	17.4	45.9	---
Overpressure, psi	Post Shot Theoretical	0.78	0.56	0.44	0.61	0.26
	Measured	0.81	0.56	0.42	0.60	0.22
Temperature Rise, per cent of critical rise of elevator skin, 0.020 in. mag.	Post Shot Theoretical	98	76	58	119	---
	Measured	52*	45	37	64**	---
Bending Moment, per cent of critical moment of stabilizer at Station 62 in.	Post Shot Theoretical	60	49	40	69	27
	Measured	59	60	37	76	27

*Temp-tape data

**For Sta. 144.5 in. At Sta. 312 in. where the paint was missing, the per cent of critical temperature rise was 81.

complete understanding of the overall problem.

Table 5.1 presents a comparison between the maximum values of theoretical and measured inputs and responses. The theoretical figures were calculated using the actual yield and aircraft range for each shot; therefore, differences between the theoretical and measured quantities reflect directly the state of the art of predicting and measuring the phenomena. It should be remembered that many sources of error and inaccuracy are involved in work of this nature. Some of these are:

1. The assumption that the partition of energy was a constant for CASTLE shots
2. The empirical formulas used to predict inputs and responses
3. The determination of the yield of the detonation
4. The determination of the actual path of the aircraft in space during shot time
5. The instrumentation system as a whole.

A clearer appreciation of the discrepancies between the theoretically predicted and the measured values of any one of the four basic measurements can be obtained by expressing the arithmetic difference as a percentage of the theoretical figure. The results of this effort appear in Table 5.2; positive and negative figures indicate that the measured values were, respectively, greater and less than the theoretical values. Table 5.2 points out that by far the largest differences are present between the theoretical and measured values for temperature and radiant exposure.

TABLE 5.2 - Difference Between Theoretical and Measured Values in Per Cent of the Theoretical Figure

	Shot 1	Shot 2	Shot 4	Shot 5	Shot 6
Radiant Exposure	-6.4	5.7	-24	-15	---
Overpressure	3.9	0	-4.5	-1.6	-15
Temperature Rise	-47	-41	-36	-46	---
Bending Moment	-1.7	22.5	-7.5	10	0

Considering the instrumentation system as a whole, including the type of measurement, the instruments or sensing elements used, the recording and the reduction of the data, it is the opinion of the writers that the probable errors in the data as presented, are less than $\pm$ 5 per cent for temperatures, pressures, and bending moment measurements of the fuselage and stabilizer, less than $\pm$ 10 per cent for the shear load measurements of the stabilizer, and less than $\pm$ 15 per cent for the bending moment measurements of the wing.

In addition to the data measurements, a number of observations were made that might be of use to future projects of similar nature. These topics include flight crew psychology, the flying of the aircraft to a specific position in space at a prescribed time, the determination of the actual aircraft position, the desirability of automatic

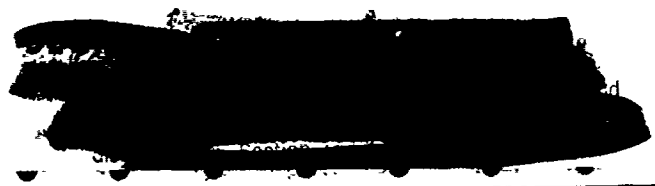

instrumentation, the corrosion problem, and the difficulty associated with working on a radioactive aircraft in the continental United States.

Before Shot 1, no member of the aircraft flight crew had been associated with the testing of aircraft for nuclear weapon effects. Since it was obvious that the complete confidence and cooperation of the flight crew in flying and positioning the aircraft were essential for the success of the project, every effort was made to acquaint the crew before each flight with the phenomena and effects. Although the crew briefings were as complete as humanly possible, the crew did undergo effects never before experienced by human beings. That recovery from the resulting "little emergencies" was effected properly and quickly is a tribute to the training and mental attitude of the crew members.

With regard to the positioning of the aircraft in space, the problem with the B-36D was not so much the accurate flying of the aircraft to within a few feet of the designated position, but rather was the accurate determination of the actual path of the aircraft. The value of any data obtained is directly dependent on accurate knowledge of the position where the data were measured. The most desirable situation would be one in which the equipment and procedures used to fly the aircraft to position were sufficiently accurate for the determination of the position. For the B-36D in CASTLE, the positioning accuracy was dependent upon the readings from a set of radar dials, the smallest division of which was 0.1 mi. With the possibility of human error existing, not only in reading the dials but also in controlling the aircraft, the decision was made to use the Raydist equipment for position determination. Since the position information from Raydist was not immediately available but depended upon the reduction of time-history records after the detonation, the system could not be used to position the aircraft. As mentioned in Chapter 3, Raydist operated properly only on Shot 6; therefore, the actual position for Shots 1, 2, 4, and 5 had to be determined from the information available, which included the navigator's check list, the radar oscilloscope photos, and the time of arrival of the shock wave. These data were reduced to range figures and it appeared that the most accurate and most consistent results were obtained from the radar scope photos; the greatest disagreement between the ranges determined from the various methods was 2000 ft for the horizontal range at shock arrival which was on the order of 80,000 ft, or approximately 2½ per cent error. During the radar scope photo reduction, considerable time was expended in attempting to correct for distortion of the radar map. If the radar-oscilloscope-camera system could be improved in definition, accuracy, and presentation, this method could serve the purpose of position determination.

The method of instrumentation recording as used on the B-36D was satisfactory in that no data were lost; however, from the experience gained during the operation, it is obvious that, due to the tension and emotional strain that exists at shot time, it is quite possible for the instrumentation crew to commit errors which might result in improper recording and consequent loss of data. Much can be said in favor of having engineers and technicians aboard the aircraft to adjust, balance, and check the channels of instrumentation well before the detonation.

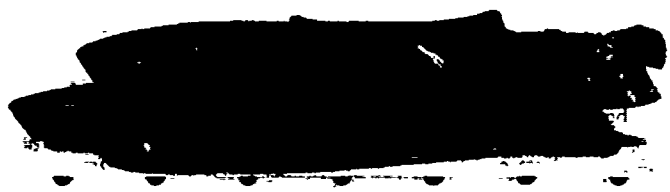

In order to eliminate the human element, the very important functions that must be accomplished a few seconds before or during the shot, such as switching on the recording equipment, should be done by reliable timing equipment.

The problem of salt-atmosphere corrosion at the Pacific Proving Grounds cannot be overemphasized. On Project 6.2a, for the first four or five weeks, few corrosion difficulties were apparent, but thereafter, the number increased rapidly. There were several instances of 5-mil thermocouple wire corroding to the point of failure. A second problem was the corrosion of electrical parts such as terminals, plugs, switches, and connectors. Also the precision-made parts of cameras and recording equipment appeared to be most susceptible to rusting. Prevention is, of course, the best policy. For electronic gear, a procedure of switching on and warming up the equipment once a day appeared to work well. The battle is half won if the problem is recognized and given sufficient importance.

A disturbing and costly problem arose when the aircraft was flown to Convair for the post-shot strain gage calibration. The aircraft was radioactive in general to an extent of about 1 mr with parts of the aircraft, notably the landing gear, at levels as high as 10 mr. Normally, at atomic proving grounds, a level of 1 mr might be less than the average background radioactivity for that area; personnel are permitted to work without protective clothing, film badges, or monitors at levels up to 10 mr. At Convair, however, the plant safety office was under orders to prohibit general work without certain precautions in areas of radiation levels greater than twice the value of background radiation which was on the order of 0.1 mr. The radioactivity was a result primarily of the accumulation of fission products on and within the paint, oil, and dirt on the aircraft, and not induced radiation. It was possible, therefore, to remove the radioactive particles by proper washing and paint-removal techniques. However, the used water and cleaning solutions could not be allowed in the normal sewer system for fear of polluting the nearby cities. The delay of the calibration as well as the decontamination of the aircraft were costly. It is not known exactly how the aircraft became contaminated. One theory is that the contamination was probably effected by having operated off the same runway and by proximity to sampling aircraft which flew through the atomic cloud as part of their mission. It can be expected that other aircraft in future tests of this nature will be contaminated in like manner, and suitable decontamination procedures and schedules should be planned.

5.2 THERMAL MEASUREMENTS

This section contains a discussion of the data obtained during the thermal phase of the CASTLE detonations. Included are several observations which were made in the act of processing the data in preparation for presentation.

5.2.1 Thermal Inputs

In the calculation of the radiant exposure expected at the air-

craft position for any given shot, the only factors that were considered as variables from one shot to another were the expected yield and the slant range of the aircraft from ground zero. During the CASTLE series, the figure of 0.008 per kilofoot for the atmospheric attenuation coefficient was used throughout, since it represented the best available data. To determine the reasons for the differences between the theoretical and measured values of radiant exposure, two factors appear to be important. These are the constant motion of the aircraft away from ground zero and the rise of the fireball.

For the tail-to exposures of the B-36D, the aircraft was headed away from ground zero and flying at a speed on the order of 450 fps. Since the release of the thermal energy occurs over a period of 30 sec or more, the aircraft was considerably farther from ground zero at the end of the thermal phase than at the beginning. Since the radiant exposure incident to a point in space is inversely proportional to the square of the slant range, one would expect that a prediction of radiant exposure based on the slant range at time zero would be conservative for an aircraft moving away from the point of detonation. However, the rise of the fireball tends to offset and might actually override the effect of the aircraft motion away from ground zero. Although the nuclear device is detonated at ground zero, the fireball rises rapidly; the center of the fireball might be as high as 2500 ft above the ground within 1 sec after detonation and then continue to rise at a rate of about 600 fps. Calculations using these figures show that, at 1 sec after detonation, the distance between the aircraft and the fireball can be as much as 2 per cent less than the slant range to ground zero and that this distance to the fireball remains essentially constant over a period of about 8 sec, increasing gradually thereafter.

Admittedly, the figures given above on fireball rise may vary, but the effect appears to be of sufficient importance that it should be considered in future tests of this nature.

5.2.2 Thermal Response

The measured thermal responses (temperature rises) of the various parts of the aircraft were, in general, much lower than the predicted values. For Operation CASTLE, temperature rises of the various aircraft components were predicted from the formula that relates the change of temperature of a given material to the radiant exposure, the density, and the specific heat of the material. Allowances were made for the cooling effect of the airstream and for the fact that, because of the color of the surface, only part of the incident thermal energy was absorbed. Where the surface was covered with a film of black engine oil, the reflectivity meter indicated a higher value of surface absorptivity than for the clean white-painted surfaces. Accordingly, it was predicted that the temperature rise of the oily surface would be about 50 per cent greater than a similar clean surface. The data results indicate that, in general, the temperature rises of the oily surfaces were greater than those of the clean surfaces, but only by about 6 per cent.

One proposed theory for the lower-than-predicted temperature

rises is that part of the thermal energy absorbed at the surface of the paint was dissipated by airstream cooling during the time required for the transfer of heat through the effective insulator, which consisted of the paint layer, the undercoat layer, and the minute layers of air between the paint and the undercoat and between the undercoat and the metal. Also, although the oily surface may have absorbed much more heat than a similar clean surface, the oil film itself may have absorbed some of the additional energy. A second effect, which does reduce the peak skin temperature to some extent and which was not used in the theoretical calculations, is the conduction of heat away from the skin to the supporting stringers or stiffeners. That the supporting structure temperature does rise has been shown in Figures 4.9, 4.10, and 4.11,

The project 6.2a thermal response data indicate that "absorptivity coefficients," obtained by measurements of the reflectivity of the surface of coated materials, may be considerably in error. In this discussion, the heat absorbed is taken as that heat which affects a temperature rise of the metal. Since future projects will probably be concerned with painted or coated surfaces, it is important that a method be developed to predict with at least fair accuracy that fraction of the radiant exposure that does effect a temperature rise of the metal.

The fact that damage to the white paint, used to improve the reflecting characteristics of the metal surfaces, occurred on all shots indicates that improvements in the heat-resisting qualities of the paint are needed. Whereas the damage after Shots 1, 2, and 4 was not serious with respect to the aircraft, it did require considerable effort on the part of the ground crew to clean and repaint the blistered areas. After Shot 5, several relatively large areas of the elevator were devoid of paint and the metal skin was permanently buckled. It appeared that where the paint remained on the elevator, the paint performed well the function of protecting the metal skin from serious thermal damage. Where the paint was missing, it appeared that the threshold of serious thermal damage had been reached.

The large amounts of smoke in the aft crew compartment and the indications of the fire warning lights of the reciprocating engines are important primarily as psychological factors. The smoke apparently was generated by the heating, through the fuselage lower skin, of oil-soaked insulation between the floor of the compartment and the skin. On several occasions, hydraulic oil was found under the floor, evidently a result of spillage from the reservoir for the manual bomb-bay door controls. Near the end of the thermal phase, the smoke stopped as did the indications of the fire warning lights, and no permanent effects were found.

5.3 BLAST MEASUREMENTS

A discussion of the measured blast data and the combinations of these measured data and calculated preshock conditions is presented in this section. The results of blast loading are compared to the strength of the aircraft in order to establish the stressed conditions encountered on this experiment.

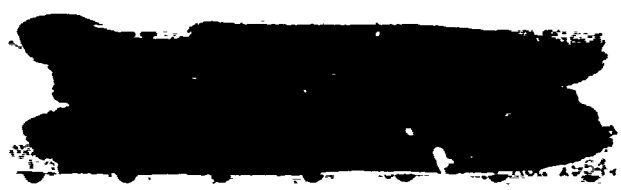

5.3.1 Pressures

The graphical representation of the positive pressure phase, as shown by the curves in this report, does not represent the true positive phase duration such as a stationary receiver would experience. The measured pressure-time curves appear distorted because of the receiver motion away from or toward the burst point during the blast phase. Theoretically, all portions of the curve are affected, including the peak, but since the rate of the pressure rise to the peak is relatively high compared to the rate of pressure decay, the true peak pressure should be essentially the same as the measured peak pressure within the limitations of the instrumentation system utilized. Even so, some of the roundness of the measured overpressure peaks may be attributed to receiver motion away from the burst points for Shots 1, 2, 4, and 5. The length of this apparent or effective positive phase is approximately 50 to 70 per cent greater than the true duration, exact values being dependent upon the yield, airspeed, slant range, and velocity of propagation of the blast wave at the flight altitude for each shot. Moving toward the burst point, such as the flight path for Shot 6, decreases the effective positive phase. For Shot 6, the measured positive phase duration was about 70 per cent of the true duration.

A direct comparison of the overpressure measurements from the three different types of gages utilized may be interesting to future projects of this nature. Of these three, the Statham gage with the d-c excitation is the superior system for requirements such as those of this project. If it is desirable to obtain the high frequency rise characteristics of the shock wave pressure, it is necessary to employ a system capable of higher frequency response. The Wiancko gage and 3-kc system are excellent for this purpose. The diaphragm-type gage was unsatisfactory because the diaphragm was exposed to the thermal energy, thus affecting the elastic response of this sensing element.

All of the pressure curves show a very slight decrease in pressure just after the initial rise and before the peak (neglecting reflection spikes) is reached. This is only apparent on the expanded time scale, Figs. 4.27 and 4.31. A possible explanation is that the thin sheet metal containing the gage orifice buckled away from the shock front creating a small rarefaction, thus decreasing the pressure for a very short period of time.

The crushing effect of the overpressure can be decreased by having enclosures well vented so that the pressure will equalize rapidly. The differential pressure measurement is representative of the net crushing effect upon a vented enclosure. The curves of Fig. 5.1 show how the pressure inside of the bomb bay equalizes with the overpressure, thus reducing the crushing effect upon this enclosure. No extra vents were provided for this test, and the equalization of pressure occurred because of the normal openings in the structure.

The surface pressure measurements on the underside of the wing, fuselage, and horizontal stabilizer show evidence of some of the dynamic components produced by the material velocity, as well as the typical spike formed by the reflected shock. These effects may be seen in Fig.

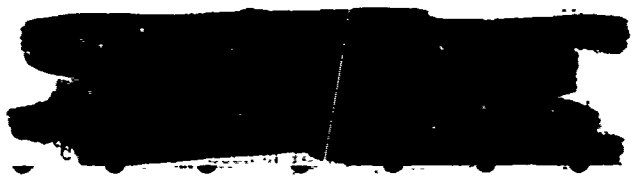

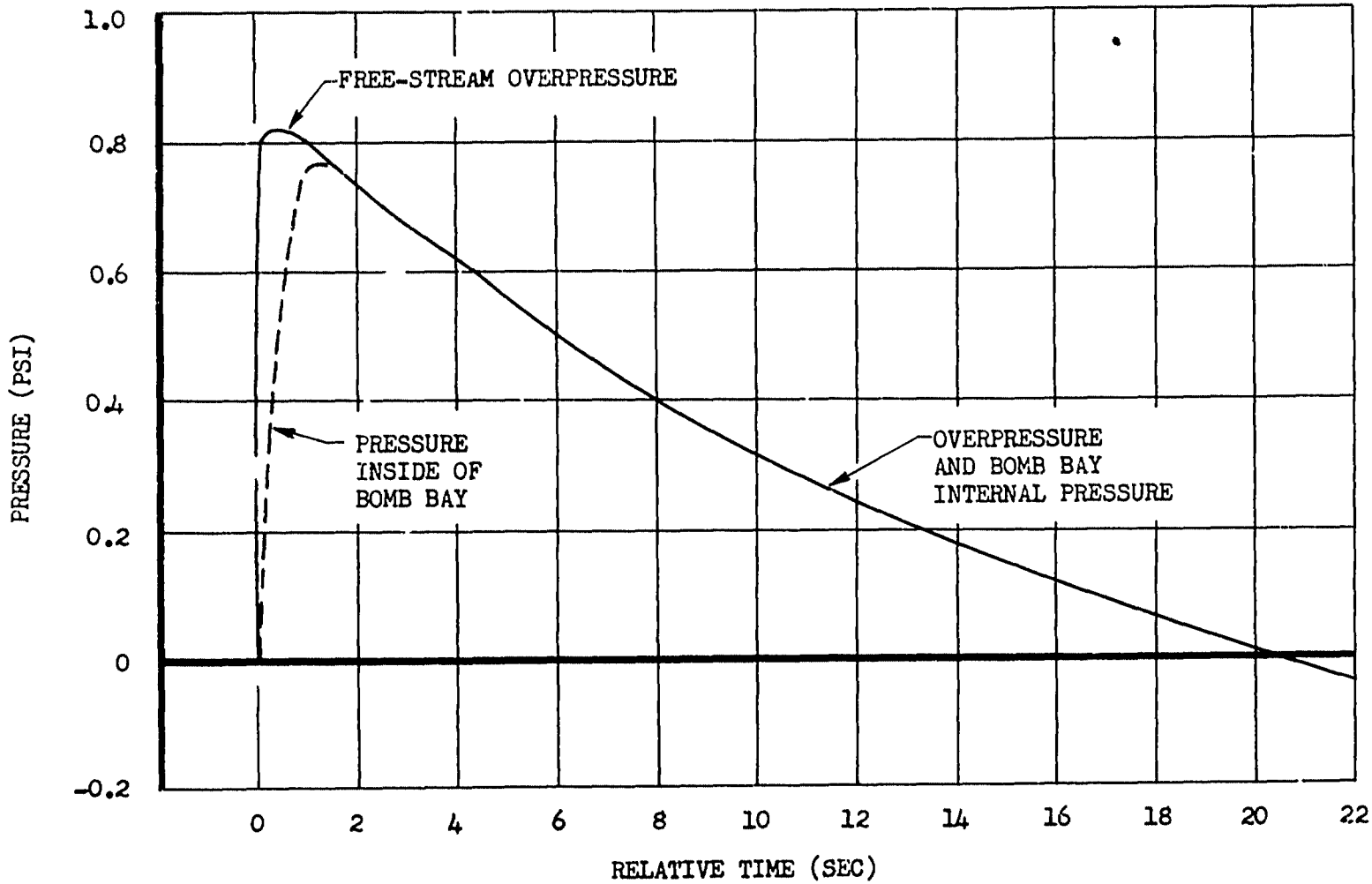

Fig. 5.1 Comparison of Bomb Bay Internal Pressure and Free-Stream Overpressure

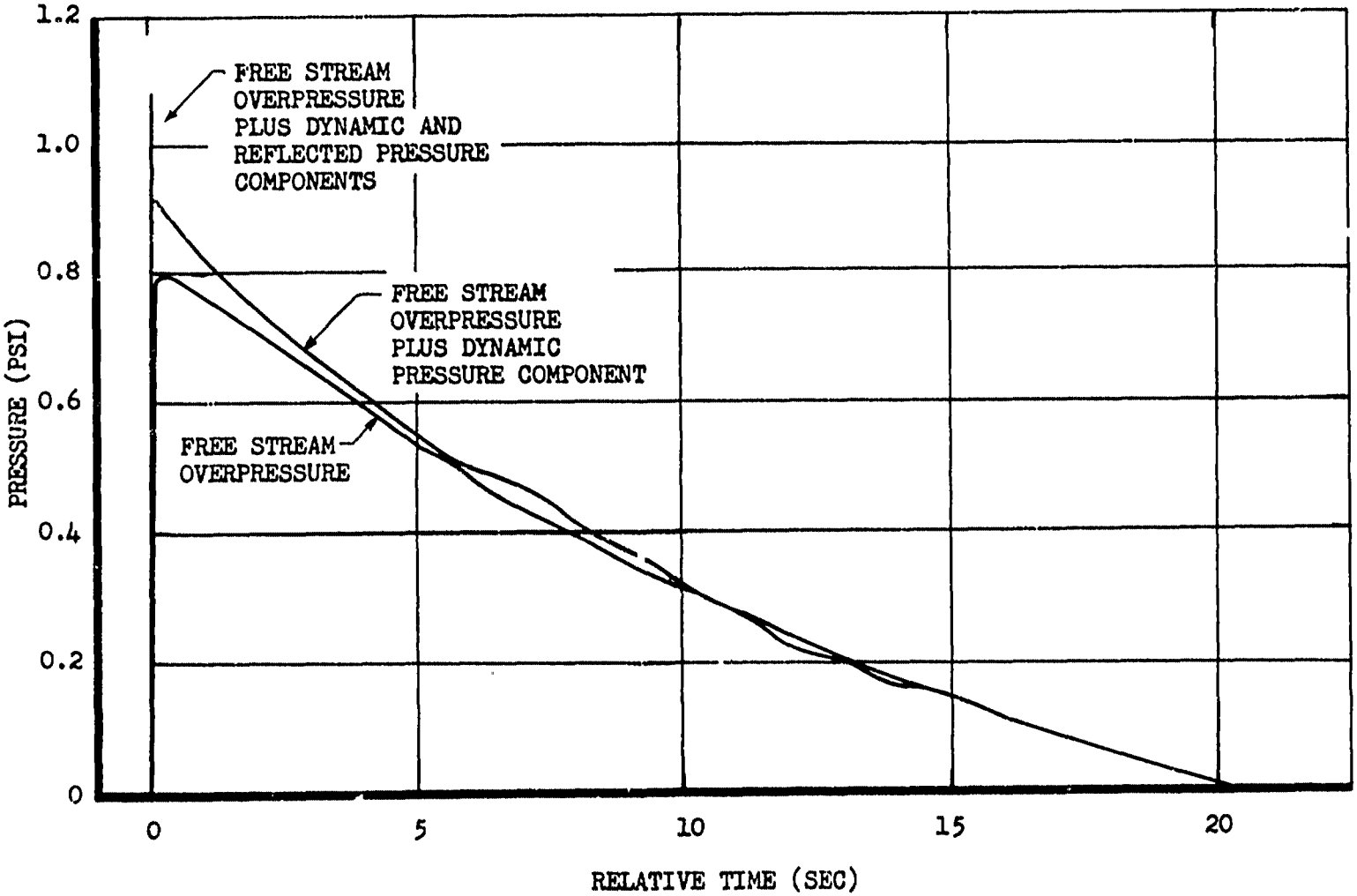

Fig. 5.2 Comparison of Typical Fuselage Surface Pressure and Free-Stream Overpressure

5.2. The reflection spike was not adequately reproduced for correlation of the peak reflected pressure with theory, for several reasons. These are:

1. The Statham gages (fuselage and stabilizer measurements) and their associated instrumentation system were not intended for an accurate reproduction of the higher frequency components of the shock wave, but were designed to define the area under the pressure-time curve which is adequately represented without the reflections spike.

2. The sensitivity of the 3-kc amplification system, utilized for the surface pressure measurement on the left wing, was adjusted for the best representation of the entire curve which resulted in the amplifier being overdriven into non-linear regions by the reflected pressures. Although the amplifier was calibrated into the non-linear region, pressure inputs above 1.1 psi could not be reproduced electrically with an acceptable accuracy.

5.3.2 Bending Moments

In order to evaluate the limiting response of an aircraft component such as the stabilizer, wing, or fuselage to the blast effects of an atomic detonation, it is necessary to determine at least three conditions or properties of the structure. These are:

a. The limit loading condition, or in other words, the critical loading of the structure with regard to the strength of the structure itself which, if exceeded, will produce undesirable effects upon the structure.
b. The initial or in-flight load, if any, on the structure prior to the blast effects.
c. The incremental effects upon the structure by the atomic blast.

Of these three, this report is concerned primarily with the blast effects alone, but unless the total load upon the structure can be evaluated in terms of a limiting condition, the structural blast results of this experiment cannot be used to evaluate the delivery or performance capabilities of the B-36D aircraft.

The limiting conditions of loading for the B-36D stabilizer, wing, and fuselage components presented in this report are derived from conditions designated by the manufacturer of the airframe which will produce a failure of the component or other undesirable results. This is entitled ultimate load and is usually defined in terms of bending moment or shear load. Since it is undesirable to approach the ultimate loading condition, a factor of safety is used. The maximum safe structural load is termed limit load and is defined as being two-thirds of the ultimate load. Ultimate loads are derived from design data, static testing, or a combination of the two. Graphical definitions of these are presented in Fig. 5.3, where the limit bending moment curve is derived from the static test ultimate by use of the safety factor. The in-flight weight configuration of the B-36D was arranged to produce a theoretical zero-strain tail load at detonation time so that the lift of the horizontal stabilizer would be equal to the dead weight of the structure, and a strain zero condition would be in effect; however,

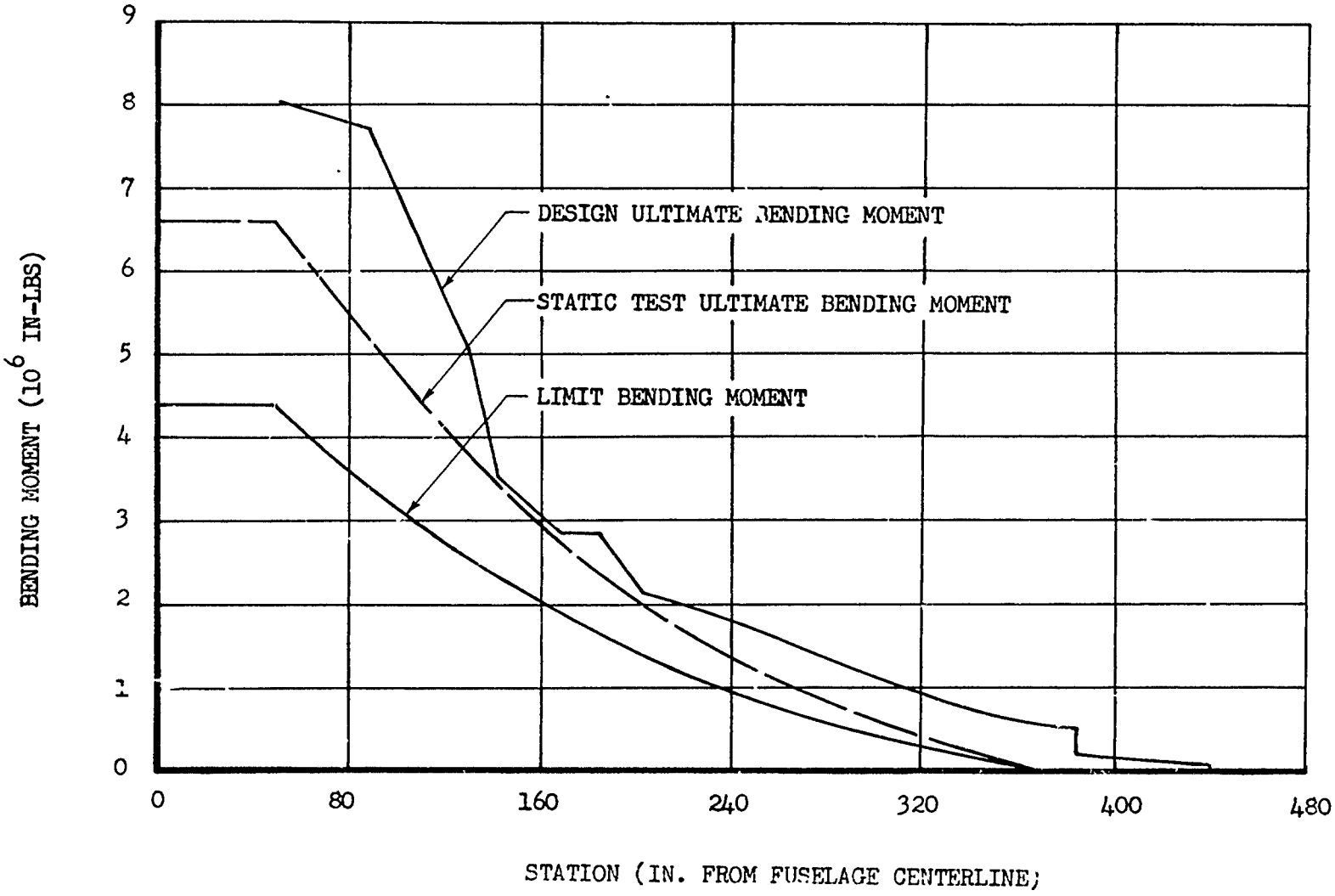

Fig. 5.3 Ultimate and Limit Bending Moments for Horizontal Stabilizer Semi-Span

because of practical operational problems, this condition was never exactly achieved. The in-flight bending moments of the horizontal stabilizer in existence at detonation time were computed from the flight configurations actually attained and are presented in Table 5.3. It can be seen that the largest deviation from the strain zero condition is 0.299 x 10^6 in-lb at Sta. 62 or about 7.3 per cent of the limit bending moment (4.1 x 10^6 in-lb) and in the negative or downward direction. Computations of these values are based on performance data of the aircraft and not on the scientific measurements conducted for this experiment.

TABLE 5.3 - In-flight Condition of Horizontal Stabilizer at Detonation Time

Shot	Bending Moment - 10^6 in-lb (Includes Dead Weight)			
	Station			
	62	144	153	224
1	-0.161	-0.0895	-0.0831	-0.0435
2	-0.117	-0.0650	-0.0605	-0.0316
4	-0.156	-0.0869	-0.0805	-0.0421
5	-0.299	-0.166	-0.154	-0.0807
6	-0.161	-0.0895	-0.0831	-0.0435

When the values from Table 5.3 are combined with the measured bending moments resulting from the blast, the total bending moment referenced to a strain-zero condition is obtained. This value can then be related to the limit bending moment of the structure in order to express a percentage load indicative of the stressed condition of the structure, this load being directly applicable to the performance or delivery capabilities of this particular aircraft.

The total bending moment values expressed in terms of the limit bending moments have been computed for the peak positive values obtained from the experimental data. The values pertaining to the horizontal stabilizer structure are contained in Table 5.4 and Fig. 5.4.

From the preceding discussion, it can be seen that the safety or capability of the aircraft may be increased, insofar as the critical nature of the horizontal stabilizer is concerned, by flying at such a weight and balance configuration so as to produce an initial down-load on the stabilizer. Theoretically, the optimum condition would be to start with sufficient tail down-load so that bending moments produced by the blast wave would reach limit, both in the positive and negative directions. From an examination of the positive and negative peak bending moments measured on Operation CASTLE and their extrapolation to higher values, it appears that the maximum possible blast load could be tolerated if an initial down load of 26,600 lbs (total, both sides) was present at shock arrival time. This condition assumes the same

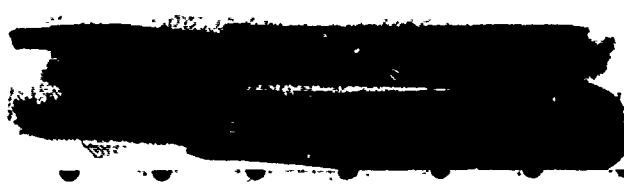

TABLE 5.4 - Horizontal Stabilizer Peak Positive Bending Moments as a Percentage of Limit Bending

Shot No.	Bending Moment (Per Cent Limit)				
	Left Stab.			Right Stab.	
	Sta. 62 in.	Sta. 153 in.	Sta. 224 in.	Sta. 62 in.	Sta. 144 in.
1	57.5	*	*	60.8	51.5
2	60.5	*	*	60.2	55.8
4	38.9	36.9	40.1	35.5	34.8
5	76.5	75.8	76.9	74.2	71.3
6	27.0	30.0	31.9	26.2	26.1

* - not installed

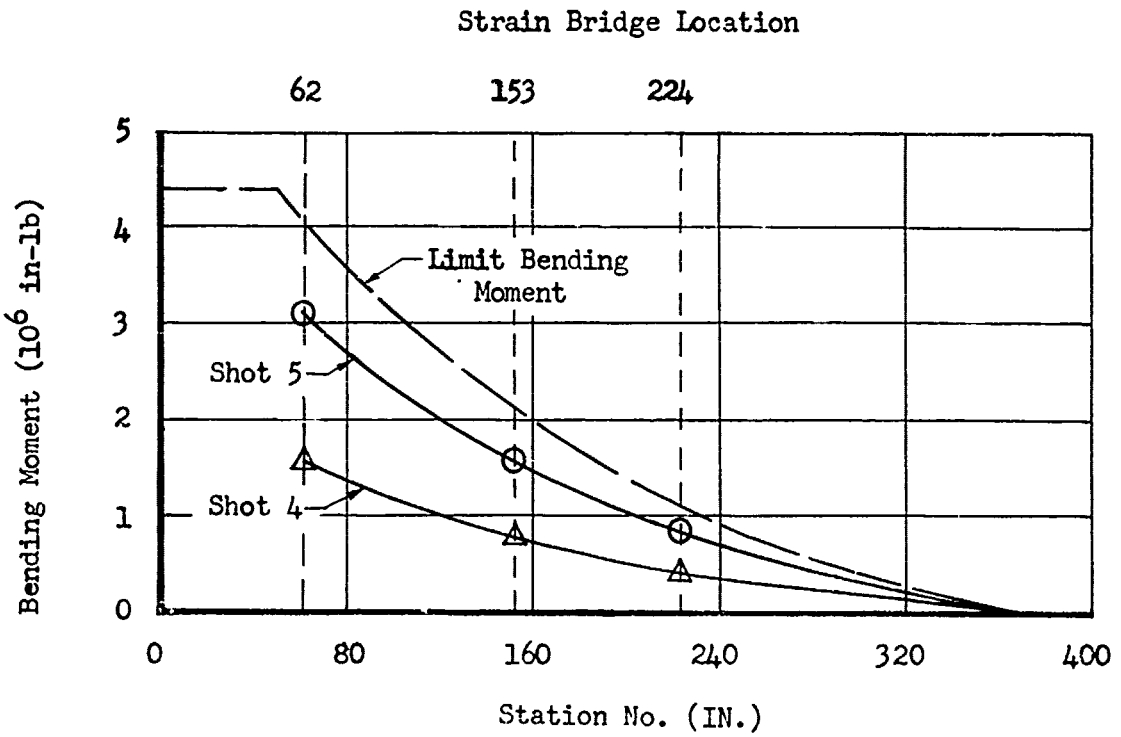

Fig. 5.4 Bending Moment Distribution Left Horizontal Stabilizer

gross weights and flight conditions as Shot 5; however, this theoretical condition places the location of the center of gravity of the aircraft far forward of the limits assigned as noted in the pilots' operating manual. If the forward limit of C.G. location (17 per cent MAC) is assumed to be a possible location and with the same weight conditions as for Shot 5 prevailing, the peak positive bending moment, induced by the blast, could safely be 50 per cent greater than the values experienced on Shot 5. This discussion is not intended to define absolute values, or to change existing flight plans, but merely to point out an order of magnitude relationship between the structural limits and blast induced bending moments for conditions other than those of the experiment.

The expression of fuselage bending moments as a percentage of limit presents difficulties not encountered for the stabilizer structure. The aft fuselage section is constructed to carry, in a cantilever fashion, the dead weight of the crew compartment, equipment, and empennage, plus an air load induced by the horizontal stabilizer. The air load may act in a positive (up) or negative (down) direction, but the weight of the structure and equipment always produces negative bending moments for normal flight configurations. The different magnitudes of the weight increments along the length of the fuselage produces a non-linear dead weight moment distribution in the negative direction. An up tail load, such as produced by the blast wave, is essentially applied at a point, this point being at the intersection of the horizontal stabilizer and the fuselage. For static up-loads at the horizontal stabilizer, the bending moment distribution through the fuselage length would be a linear function of the load and the moment arm; however, because of the concentration of mass at the aft crew compartment and other locations, the dynamic bending moment distribution for transient loads applied to the horizontal stabilizer is a non-linear function of this load and the moment arm.

The non-linear characteristics of both the dead-weight moments and the dynamic moments induced by transient loading of the horizontal stabilizer tend to reduce the net peak positive bending moments, especially at locations forward of the aft crew compartment. A graphical representation of these effects is shown in Fig. 5.5. As an aid to the evaluation of the peak positive moments, the design ultimate bending moment curve for the fuselage section under consideration is reproduced on the same graph. The bending moment ultimate varies somewhat with the shear load; therefore, a particular shear load must exist for the curve shown in Fig. 5.5 to be valid. In addition, this curve assumes that the shear load is static and applied at the tail, thus affecting all cross sections forward of the loading point as a constant shear. The transient tail load obtained from the blast and the dynamic characteristics of the fuselage affect the shear loading in the same manner as the bending moment; therefore, a constant shear such as that static shear which is the basis for the ultimate moment curve of Fig. 5.5 does not exist; however, an effective shear, varying in magnitude along the length of the fuselage, is present. This means that in order to represent a distribution of bending moments in percentages of their limiting values, the ultimate and therefore the limit bending moments

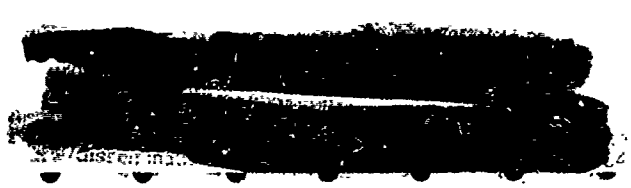

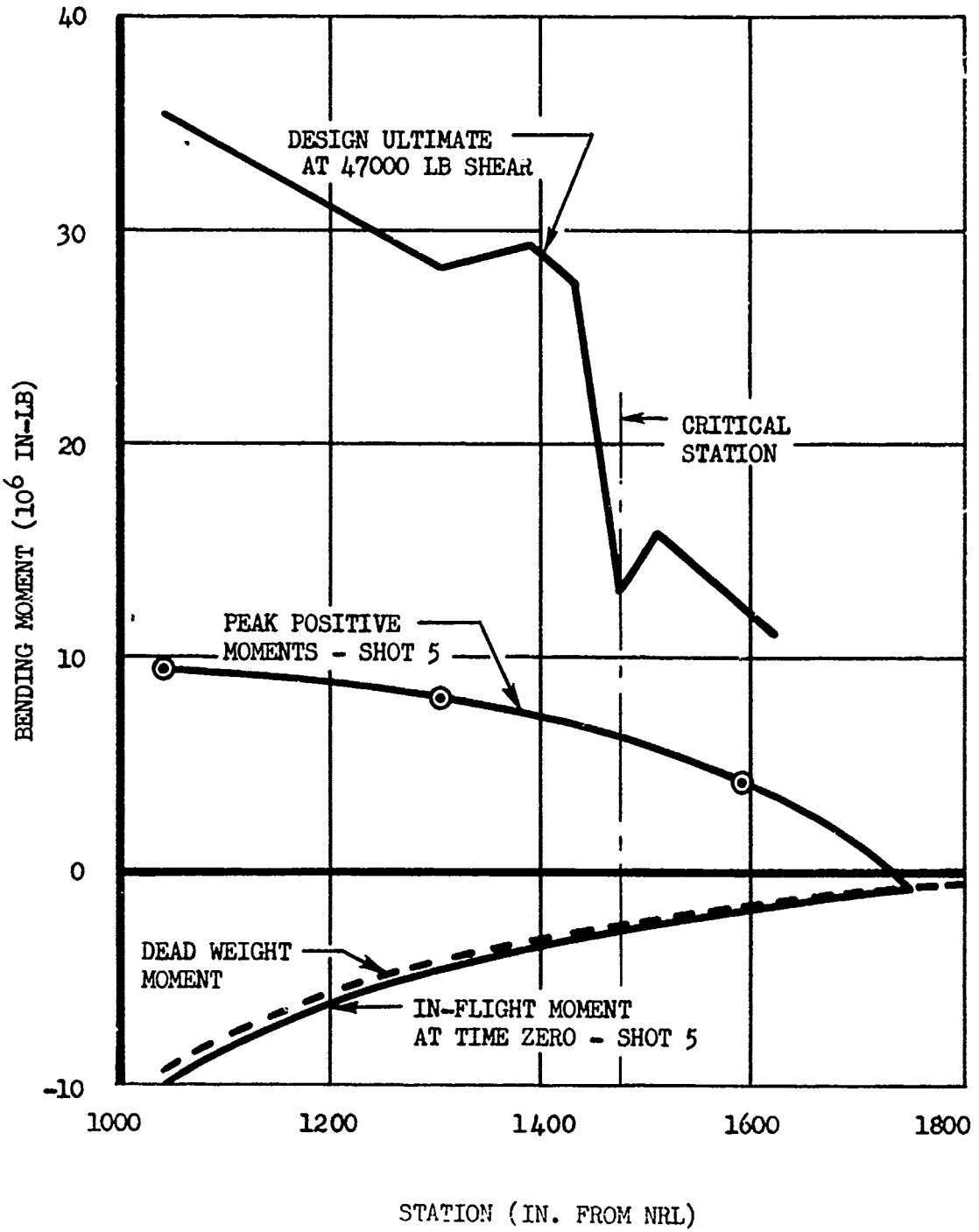

Fig. 5.5 Bending Moment Distribution Aft Fuselage Section, Shot 5

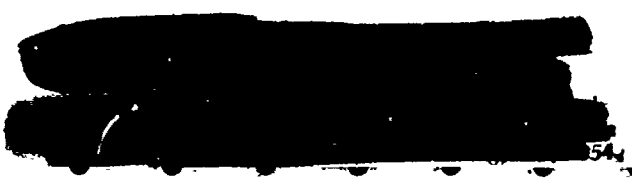

would have to be established according to the effective shear at their respective stations by a dynamic analysis of the structure.

An analysis of this type is beyond the scope of this presentation; however, the change in magnitude of ultimate bending with a change in shear is not so large as to prohibit an approximation utilizing an ultimate curve established for a constant shear value. The curve presented in Fig. 5.5 is the ultimate bending moment distribution for a 47,000-lb. shear load, this load approximating the static load upon the horizontal stabilizer, at 90 per cent of limit bending of the stabilizer. From this curve it appears as if Stat: 1476 in. is the critical station, representing the aft bulkhead (No. 12) of the aft crew compartment. The use of the usual safety factor in order to define a limit moment at this station results in a limit moment of 8.65 x 10^6 in-lb, which is two-thirds of the ultimate value. The peak positive bending moments, that is, the peak moments above the strain-zero condition, define a moment distribution along the fuselage section. These peak positive moment values are the differences between the in-flight bending moments and the measured peak moments obtained from the experiment. In order to define the moment at the critical station, it is necessary to draw a curve through the three points obtained from the measured data. A fourth point may be utilized, the point where there is no change of bending moment due to the blast loading. Theoretically, this point occurs at the location of the effective loading, where the horizontal stabilizer transfers its load to the fuselage. The results may be seen as the smooth curve of Fig. 5.5. It is realized that this smooth curve may not represent the bending moment distribution; however, in order to define the percentages of limit attained during the experiment, it will be used as a first approximation.

It should be noted that the percentages given are in terms of absolute bending moment; therefore, the positive bending moment value is obtained from the experimental value by including the pre-shock, in-flight condition of bending moment. Table 5.5 presents a summation of this effort.

The percentages of limit listed in Table 5.5 apply only for the gross weights and flight conditions of this particular experiment.

Although the wing bending moments were not of a critical nature for this experiment, they are an interesting part of the measured data. The wing, being the principal lifting surface of the aircraft, is designed to accept wide variations in bending moments, whether due to static or dynamic conditions. The major portion of the fuel load of the aircraft is carried within the wing of the aircraft; therefore, the analysis of a dynamic response of the structure is dependent upon the fuel distribution in terms of weight and location. Table 5.6 presents the fuel and oil distribution for all significant test flights of this experiment. For straight and level in-flight conditions, the absolute bending moment about any chordwise section of the wing will be positive because the wing, in addition to its own dead weight and the weight of the fuel contained within the structure, supports the weight of the rest of the aircraft (neglecting fuselage and stabilizer lift). The computed in-flight bending moments for the wing at the instrumented stations are presented in Table 5.7.

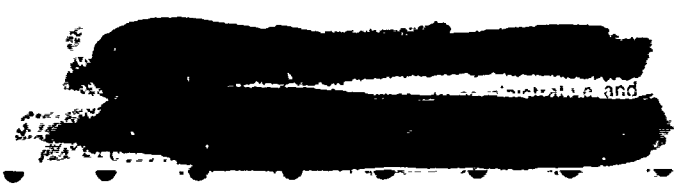

TABLE 5.5 - Aft Fuselage Bending Moments and Per Cent Limit Values

Shot	Pre-shock Bending Moment 10^6 in-lb (Dead wt. Airload)			Peak Bending Moment* in Positive Direction 10^6 in-lb			Approximate Per Cent Limit at Critical Sta. (1476 in.)
	Station (in.)			Station (in.)			
	1037	1293	1597	1037	1293	1597	
1	-8.68	-3.93	-1.49	6.84	5.92	3.26	54
2	-8.26	-3.66	-1.40	6.87	5.60	3.21	53
4	-8.63	-3.90	-1.48	1.67	2.13	1.65	23
5	-9.99	-4.77	-1.79	9.26	8.22	4.01	71
6	-8.68	-3.93	-1.49	-4.93	-0.70	0.19	3.5

* Peak Incremental Bending Moment (Measured Value) plus Pre-shock Bending Moment.

** Limit = 8.65×10^6 in-lb

These bending moments were computed from theoretical lift, which, in turn, was obtained from the coefficient of additional lift, C_{La}. The coefficient of basic lift, C_{Lb}, was neglected in the computations; therefore, the values given in Table 5.7 may be slightly in error but not by more than 5 per cent for the region of flight configurations investigated. The peak positive bending moment at each station is obtained by adding the measured peak change of moment to the appropriate in-flight condition from Table 5.7. This positive moment is then compared to the limiting moment of the structure in the same manner as the horizontal stabilizer and the fuselage moments. Table 5.8 contains the results of this comparison as a tabulation of the percentage of limit attained by each of the instrumented stations for each shot.

The wing bending moment distribution during Shot 5 is graphically represented by Fig. 5.6. The limit curve shown on this figure has been drawn as a smooth curve rather than following the small irregularities in the ultimate bending curve.

From a comparison of the percentages of limit bending attained by the stabilizer, the fuselage, and the wing for the shots of the CASTLE tests, it appears as if the aft fuselage at 1476 in. would be the limiting component for tail-to blast exposure to high yield weapons, however the bending moments of the horizontal stabilizer would be very close to their respective limits. From the data of one head-on exposure, it appears as if the horizontal stabilizer would be limiting for

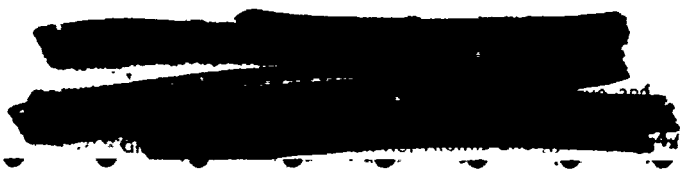

TABLE 5.6 FUEL AND OIL DISTRIBUTION, B-36D AIRCRAFT, ALL EVENTS AT TIME ZERO

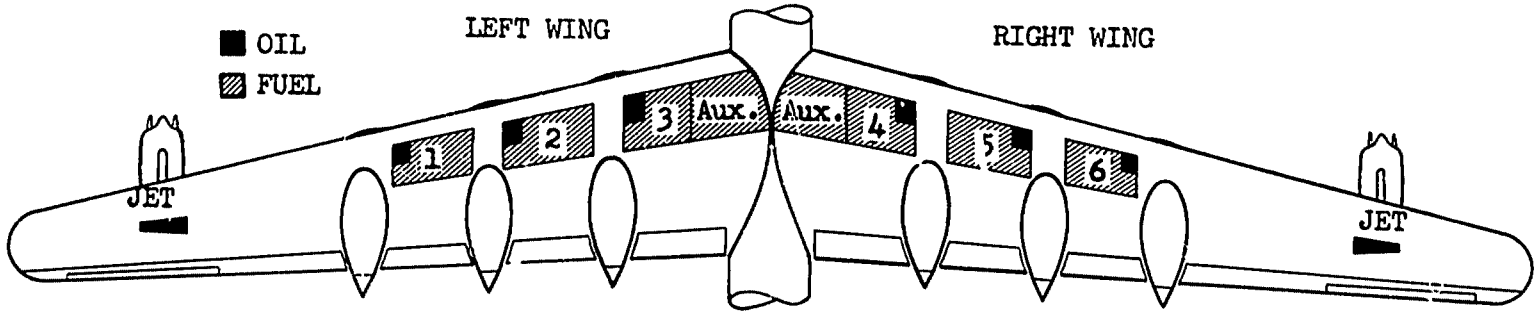

FUEL & OIL DISTRIBUTION, B-36D AIRCRAFT, ALL EVENTS AT TIME ZERO

SHOT	1	2	4	5	6
Gross Weight (lbs)	245,679	246,039	249,879	230,068	250,079
Fuel (lbs)					
Tanks #1 & #6 (each)	11,100	11,700	12,690	10,500	12,800
Tanks #2 & #5 (each)	22,500	22,230	22,800	15,000	22,200
Tanks #3 & #4 (each)	0	0	0	0	0
Aux. Tanks R. & L. (each)	0	0	0	0	0
Oil (lbs)					
Jet Oil Tank R. & L. (each)	150	150	150	150	150
Tank #1	975	975	975	975	975
Tank #2	975	975	975	1050	1050
Tank #3	975	975	975	1050	1050
Tank #4	975	975	975	1050	900
Tank #5	975	975	975	1050	1050
Tank #6	975	937	975	975	975

NOTE: Data obtained from information furnished by the flight engineer.

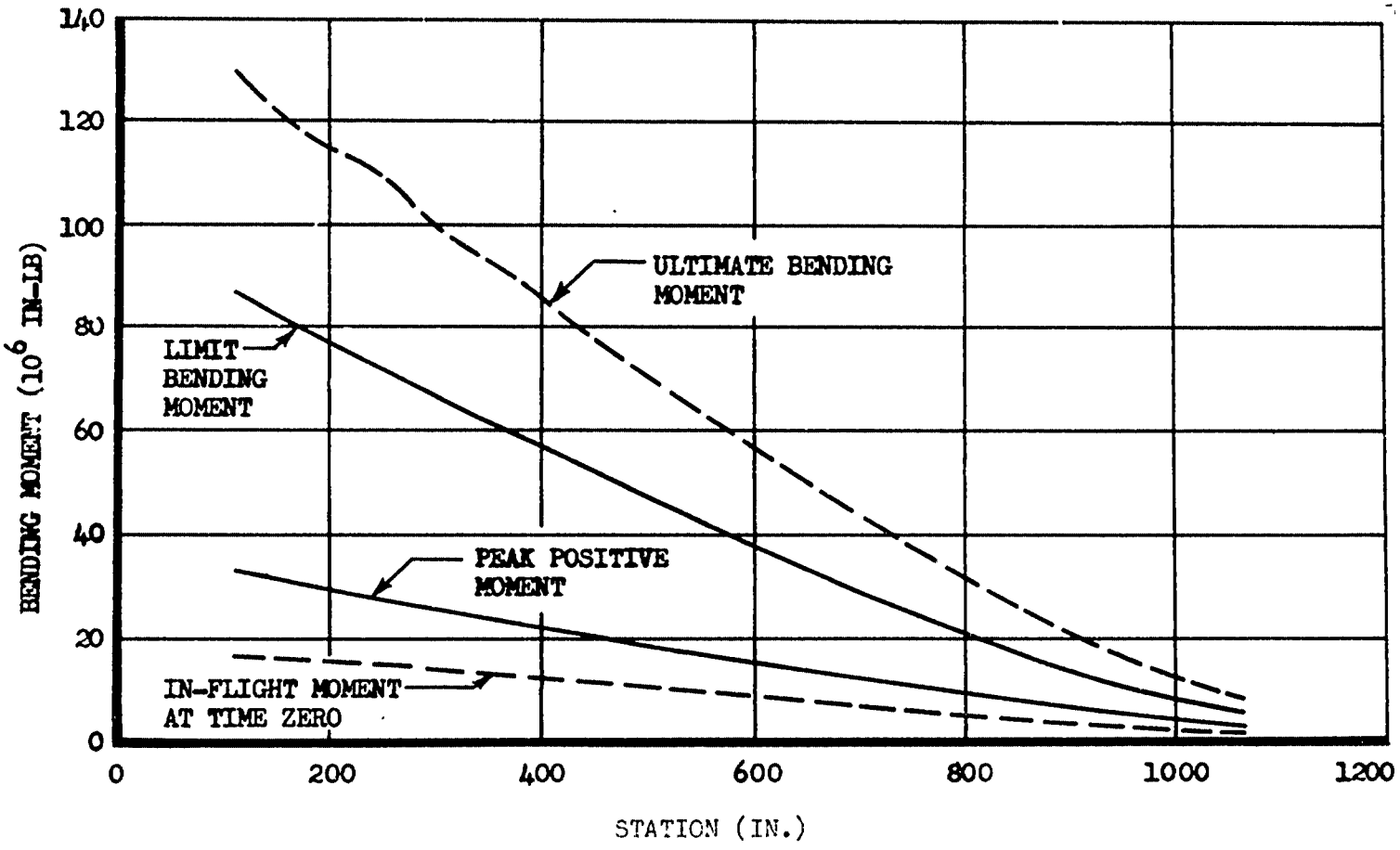

Fig. 5.6 Bending Moment Distribution Left Wing. Shot 5

TABLE 5.7 - Computed In-flight Wing Bending Moments at Detonation Time

Shot	Bending Moments (10^6 in-lb) at Station (in.)			
	110	390	604	1064
1	17.4	14.0	9.4	1.8
2	16.6	13.9	9.9	1.8
4	17.5	14.1	10.2	1.9
5	16.5	12.5	8.9	1.7
6	17.6	14.1	10.2	1.9

TABLE 5.8 - Peak Positive Wing Bending as Per Cent Limit

Shot	Per Cent Limit at Station (in.)				
	Left Wing				Right Wing
	110	390	604	1064	390
1	28.5	30.5	33.6	49.8	32.5
2	33.6	36.3	40.0	49.5	36.6
4	30.1	33.0	36.7	44.1	32.4
5	38.0	37.8	40.1	53.0	38.3
6	37.0	38.7	44.0	49.2	40.9

this exposure condition.

5.3.3 Accelerations

An attempt was made to perform a double integration of the linear acceleration results in order to obtain the displacement of various portions of the aircraft with respect to time, however the accelerometer outputs appear to be the results of local vibrations of the structural members. The net acceleration of the aircraft is overshadowed by the response to local accelerations, thus prohibiting the attainment of an accurate displacement through the process of integration.

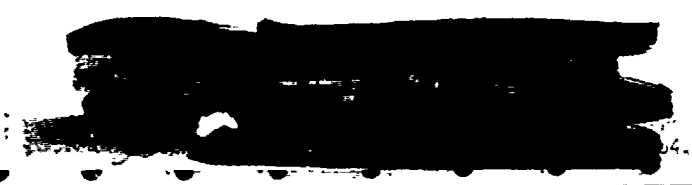

5.3.4 Effects on Engines

The variation of engine speed during the passage of the shock wave was reported by the flight crew after the first shot. For the second shot, the flight engineer attempted to minimize the speed variation by hand-controlling the speed, rather than depending on the governor action; and this effort was reported to have helped considerably. For Shot 5, the governor control was allowed to function automatically in order to obtain additional data on the variation of engine speed under these conditions. The preliminary data were obtained from the flight engineer who reported the observed speed variation after each shot. A study of the oscillograms obtained from various test flights revealed a vibrational response of the horizontal stabilizer, the frequency of which was proportional to propeller and therefore engine speed. From the frequency changes of these vibrations during the passage of the shock waves, the apparent engine speed variations with time were computed, and the results appear on Figs. 5.7 and 5.8 in graphical form. Although the vibrational response of the horizontal stabilizer appears to be proportional to engine speed, there are several limitations to the data obtained in this manner. They are as follows:

a. The two inboard engines (No. 4 and 5) are responsible for the stabilizer vibrations as their propellers are directly ahead of the stabilizer airfoil; therefore, the curves of Figs. 5.7 and 5.8 probably represent the speed variations of these two engines although some effects from the other engines may possibly appear on the record.

b. The response characteristics of the horizontal stabilizer may limit the rate to which it can provide a reliable indication of engine speed for transient input conditions.

c. Resolution of the time axis is limited to 0.2-sec increments by the method of data reduction.

The relative response of engine speed to the shock waves for fully-automatic and hand-governed operation may be seen by comparing the response curves for Shots 1 and 5 with Shot 2. It is apparent that the hand-controlled method minimizes the engine speed fluctuations, but this is then dependent upon the skill of the flight engineer where an error in judgment might produce a more detrimental effect than the blast itself. It appears that the engine speed variation is not of sufficient magnitude to cause damage to the engines or their associated equipment; however, because it would probably occur again under similar circumstances, flight crews of propeller-driven aircraft capable of participating in a nuclear strike should be acquainted with the phenomenon as part of a briefing in order to prevent undesirable crew reactions to an unexpected engine speed change.

The effect of the blast wave upon the jet engines may be of extreme importance to modern all-jet aircraft operating in the vicinity of a nuclear detonation. Unfortunately, a time-history response of this effect was not obtained and the only data available is in the form of the observations made by the flight crew. Significant effects were observed during Shots 1 and 2. These were the apparent increase in tail-pipe temperature, as reported in Chapter 4. Observations on subsequent shots indicated that no detectable change in tail-pipe tempera-

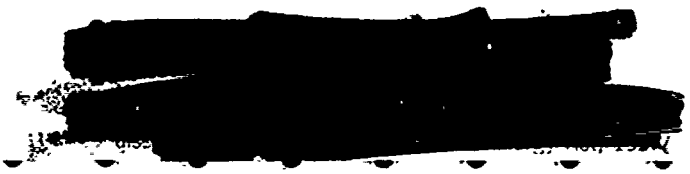

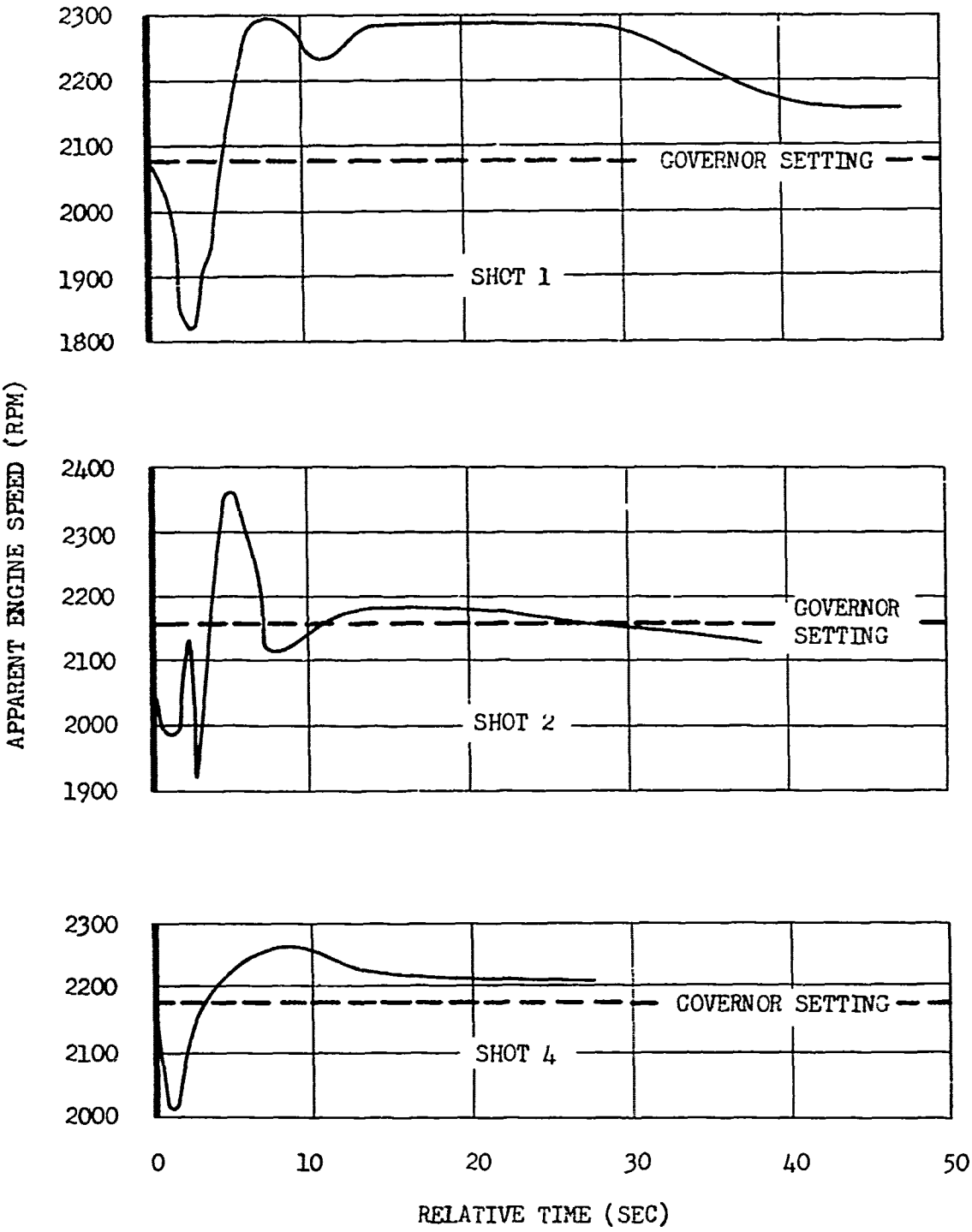

Fig. 5.7 Apparent Engine Speed Change, Shots 1, 2 and 4

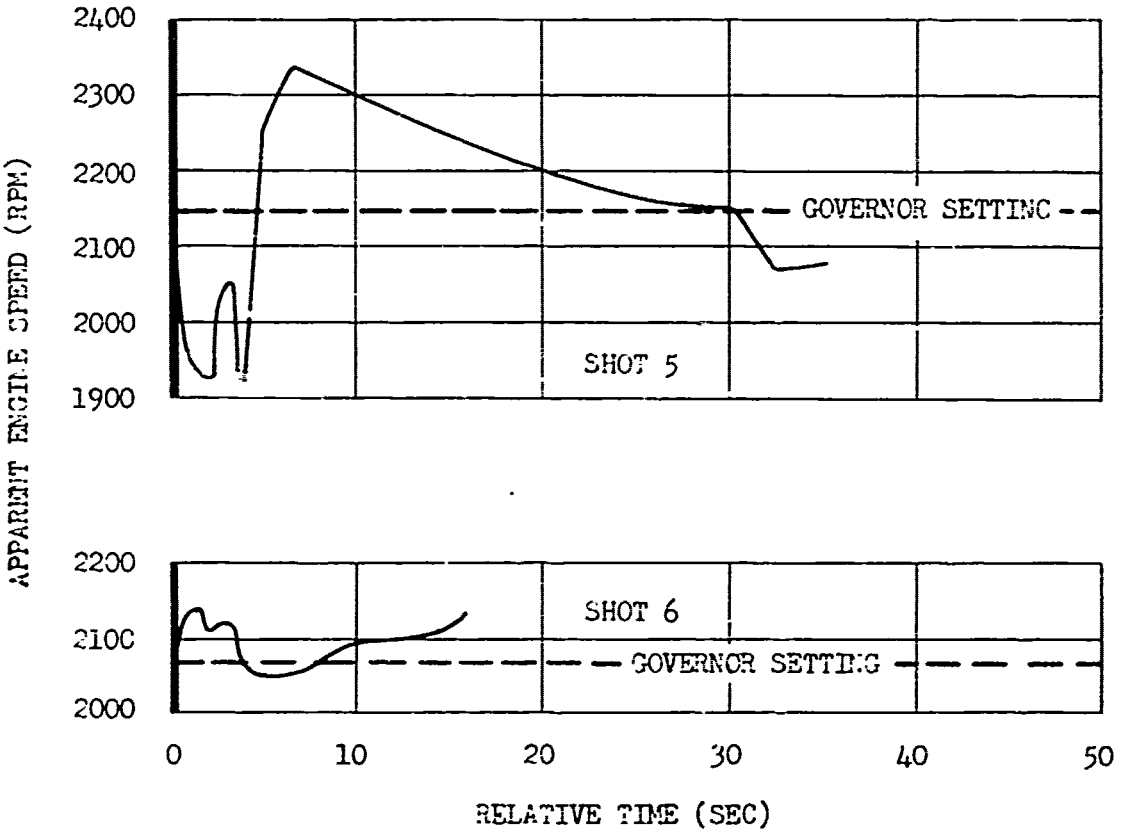

Fig. 5.8 Apparent Engine Speed Change, Shots 5 and 6

ture occurred. Although the engines of the B-36D aircraft appeared to suffer no permanent damage, the effect appears sufficient to warrant further investigation.

CHAPTER 6

CONCLUSIONS AND RECOMMENDATIONS

6.1 CONCLUSIONS

a. Sufficient data are available to determine the responses of a B-36D aircraft to nuclear detonations and to define with reasonable accuracy the maximum delivery capabilities of the aircraft. This does not imply that all of the problems relating to weapon delivery by the B-36D have been solved. As new weapons are developed, or the use of different mission tactics become desirable, it may be necessary to evaluate the adaptability of this aircraft to the particular problem. Even so, it is probable that such a study could be conducted with the test data available from this and previous participations in the nuclear test operations.

b. The data and experience obtained from this experiment will be useful to assist in the establishment of methods applicable to other aircraft for the determination of nuclear effects with relation to weapon delivery capability, structural vulnerability, or lethality problems. Although this particular experiment was confined to the B-36D, data such as the inputs from nuclear detonations received at specific points in space are not unique to this aircraft and thus will add to the overall knowledge applicable to future projects of a similar nature.

c. The specific techniques used during CASTLE to predict thermal inputs and responses were inadequate for accurate, close positioning. This situation reflects the limited amount of useful data available prior to the operation. The data obtained by Project 6.2a should assist in revising the procedures used to calculate thermal effects and should result in more accurate predictions.

d. The formulae and procedures utilized during Operation CASTLE to predict blast effects at overpressures less than 1.0 psi are satisfactory. In general, good correlation was obtained between measured and predicted values.

e. White paint, as used on the B-36D test aircraft, effectively reduces the temperature rise of the skin panels exposed to thermal radiation as long as the paint film itself is not destroyed by this thermal radiation. This paint successfully withstood the thermal radiation conditions encountered on the CASTLE shots. The energy received

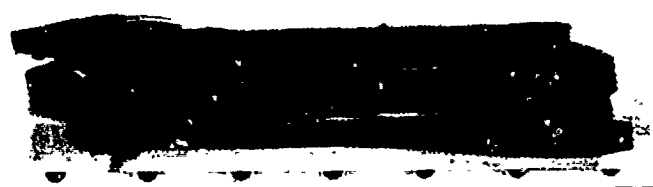

during Shot 5, at the particular incidence angle of exposure, was sufficient to scorch some of the paint. Therefore, this may be considered as the threshold of paint damage.

f. The protective curtains covering the Plexiglas windows provided satisfactory crew protection from the thermal radiation.

g. The generation of smoke inside of the aircraft during the thermal phase has a deleterious effect upon the mental attitude of the crew members. Although no fire was detected, the presence of smoke in the aft crew compartment of the aircraft did increase the apprehension of some of the crew members. This mental state is very undesirable for proper operation of the aircraft.

h. Aircraft fire warning systems can be energized by the thermal radiation. This phenomenon, in itself, is not considered serious except that the warning system is for a short time incapable of detecting an actual fire. However, the consequences of an unfavorable human reaction to the indication of the system could endanger the safety of the aircraft and crew since, with the protective curtains covering the Plexiglas windows, visual observation of the engines and associated structure is not feasible.

i. The blast wave can affect the tail-pipe temperature of operating jet engines and also affect the speed of propeller-coupled reciprocating engines for tail-to aircraft orientations. There seems to be an undefined critical parameter for the effect upon the jet engines since the phenomenon only occurred on two shots, while the reciprocating engines were affected on every shot.

j. The method used by the B-36D crew to position the aircraft at a point in space at a prescribed time was satisfactory.

k. The methods used, in lieu of the Raydist, for the subsequent determination of the position of the aircraft were acceptable but not of the desired accuracy. The radar "map" of the area, as photographed from the radar screen, appeared distorted, thus making the determination of the track of the aircraft difficult.

l. The instrumentation system and procedures used in conjunction with this experiment were, in general, satisfactory. There were, however, some details in which improvement was indicated.

6.2 RECOMMENDATIONS

a. The data obtained from this experiment should be used to verify or modify existing methods of predicting the effects of nuclear detonations on the B-36D type aircraft, thus leading to the establishment of the optimum weapon delivery capabilities of the aircraft.

b. The data and information obtained from this experiment should be made available to those agencies concerned with similar problems such as weapon delivery capabilities, vulnerabilities, or lethalities of other types of aircraft. In addition, the data and information relating the phenomenology of a nuclear detonation to a point in space should be made available as part of the general information which is helpful in analyzing past results from, or planning future participation in, a nuclear test program such as CASTLE.

c. The techniques utilized during Operation CASTLE to predict the

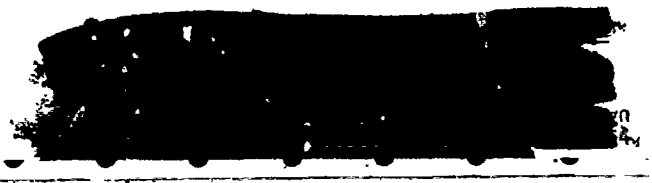

thermal effects of nuclear detonations on aircraft should be improved. This includes both phases of the problem, namely the prediction of the thermal energy at a point in space from a given detonation and the prediction of the temperature rise of a given skin panel of an aircraft at that point in space.

d. A suitable white paint or a similar protective coating should be used, where needed, to reduce the thermal effects upon aircraft operating in the vicinity of a nuclear detonation. To effect this reduction the coating must remain intact throughout the expected temperature rise and other adverse flight conditions; furthermore, the desired protective properties of reflection and conductive insulation should be relatively unaffected during radiant exposure.

e. The protective curtains for covering the Plexiglas windows should be used by aircraft operating in the vicinity of a nuclear detonation; however, an improvement can be made by using a different method or material to assemble the various pieces into a particular curtain. The thread used on the curtains tested during CASTLE burned and allowed the pieces to separate during the thermal phase of Shot 5.

f. Rubber gaskets or other materials which may produce smoke or other undesirable effects within the crew compartment of the aircraft should be protected from the thermal radiation or removed from contact with surfaces which may be heated by thermal radiation. Furthermore, the inside surfaces of the skin covering of the aircraft, particularly under the crew compartment decks should be kept free of oil, grease, or other material which may smoke or burn.

g. The possible effects of the blast wave upon powerplant operation should be investigated. If applicable, this investigation should include jet engines, reciprocating engines and turbo-prop combinations. For engines,operating at or near a critical speed or power setting, the effects of the blast wave may be more serious than the observations of this experiment indicate.

h. A detailed briefing on the probable effects of a nuclear detonation, especially details such as smoke, fire warning system actuation, engine speed change, and feel of the blast wave, should precede any mission where flight in the vicinity of a nuclear detonation is anticipated. A detailed publication based on the past experiences of pilots and aircrews participating in these nuclear tests would be helpful.

i. The following details of instrumentation for this type of test program should be improved:

1. Protecting instrumentation from salt-atmosphere corrosion. Better techniques are needed for moistureproofing wiring, switches, plugs, strain gages, recording equipment, and other devices made of materials susceptible to corrosion.
2. Methods of operating recorders and associated equipment. The development of a reliable, fully automatic sequence of operations, initiated by one control well in advance of detonation time would be more desirable than the manual method utilized for this experiment; however, the reliability of this system must be at least equivalent to that of the system

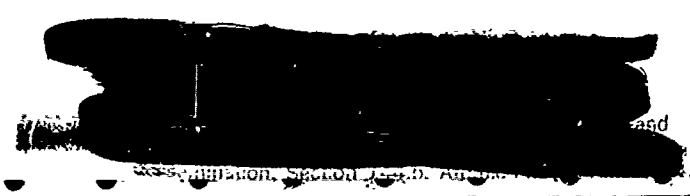

described in this report.

It should be noted that, at this writing, many of these recommendations have been acted upon, and improvements are now in effect. At the close of the field phase of the experiment and during the evaluation of the data, the conclusions, upon which these recommendations are based, became apparent. Since the planning of future tests and operations was in progress at that time, it was desirable to disseminate the information, on a preliminary basis, in advance of this report. As a result, these data became useful for Operation TEAPOT and in the planning for Operation REDWING. These data were also made available to the operational units of the Air Force and various contractors who required the information for the performance of their duties.

APPENDIX A

OSCILLOGRAPH CHANNEL DETAILS

TABLE A.1 - Oscillograph Channel Details, Recorder No. 1

No.	Channel Description	Galvanometer
1	Timing Signal, 100 cps sine wave	7-218
2	Overpressure, fuselage Sta. 391 in., left side, Statham gage	7-215
3	Total bending, left wing Sta. 1062 in.	7-215
4	Total bending, left wing Sta. 604 in.	7-215
5	Total bending, left wing Sta. 390 in.	7-215
6	Acceleration, fuselage Sta. 208.5 in.	7-225
7	Total bending, left wing Sta. 110 in.	7-215
8	Total bending, left stabilizer Sta. 62 in.	7-215
9	Acceleration, fuselage Sta. 1772 in.	7-225
10	Bending, fuselage Sta. 1293 in.	7-215
11	Acceleration, fuselage Sta. 907 in., left side	7-225
12	Acceleration, fuselage Sta. 907 in., right side	7-225
13	Total bending, right stabilizer Sta. 62 in.	7-215
14	Total bending, right wing Sta. 390 in.	7-215
15	Bending, fuselage Sta. 1597 in.	7-215
16	Bending, fuselage Sta. 1037 in.	7-215
17	Pressure, left stabilizer Sta. 359 in.	7-215
18	Voltage monitor, bridge balance no. 1	7-223

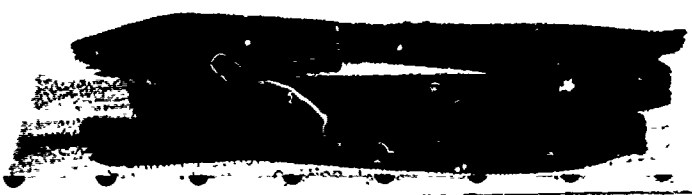

TABLE A.2 - Oscillograph Channel Details, Recorder No. 2

No.	Channel Description	Galvanometer
1	Timing signal, 100 cps sine wave	7-218
2	Temperature, thermocouple cold junction, aft fuselage	7-218
3	Temperature, thermocouple cold junction, left wing	7-218
4	Temperature, left stabilizer Sta. 310 in. (Shot 1) Temperature, left stabilizer Sta. 313 in. (Shots 2, 3, 4, 5, 6)	7-218 7-218
5	Temperature, left stabilizer Sta. 310 in., under stringer (Shot 1) Temperature, left elevator Sta. 144.5 in. (Shots 2, 3, 4, 5, 6)	7-218 7-218
6	Temperature, left stabilizer Sta. 310 in., on stringer (Shot 1) Temperature, left elevator Sta. 312 in. (Shots 2, 3, 4, 5, 6)	7-218 7-218
7	Temperature, left wing Sta. 1270 in. (Shot 1) Temperature, left wing Sta. 1106 in. (Shots 2, 3, 4, 5, 6)	7-218 7-218
8	Temperature, left wing Sta. 1270 in., under stringer (Shot 1) Temperature, left wing Sta. 1068 in., stiffener (Shots 2, 3, 4, 5, 6)	7-218 7-218
9	Temperature, left wing Sta. 1270 in., on stringer (Shot 1) Temperature, left wing Sta. 1068 in., flange (Shots 2, 3, 4, 5, 6)	7-218 7-218
10	Radiant exposure no. 1 (Shots 1, 2, 3, 4, 5) Blank for Shot 6	7-215 ---
11	Radiant exposure no. 4 (Shots 1, 2, 3, 4, 5) Blank for Shot 6	7-215 ---
12	Irradiance no. 1 (Shot 1) Irradiance no. 2 (Shots 2, 3, 4, 5) Blank for Shot 6	7-215 7-225 ---
13	Temperature, left wing Sta. 1095 in. (Shot 1) Temperature, left wing Sta. 1068 in., skin (Shots 2, 3, 4, 5, 6)	7-218 7-218
14	Radiant exposure no. 3 (Shots 1, 2, 3, 4, 5) Blank for Shot 6	7-218 ---
15	Temperature, aft compartment air (Shots 1, 2, 3) Radiant exposure no. 5 (Shots 4, 5, 6)	7-225 7-218
16	Temperature, specimen in aft lower left blister	7-218
17	Blank for Shot 1 Temperature, fuselage Sta. 1898.5 in. (Shots 2, 3, 4, 5, 6)	--- 7-218
18	Voltage monitor, bridge balance no. 2	7-223

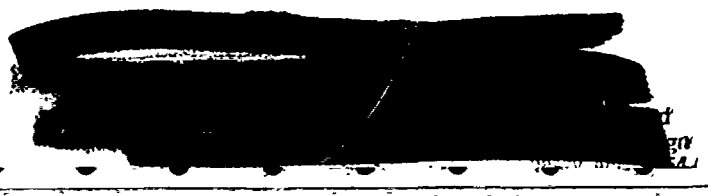

TABLE A.3 - Oscillograph Channel Details, Recorder No. 3

No.	Channel Description	Galvanometer
1	Timing signal, 100 cps sine wave	7-218
2	Elevator deflection	7-218
3	Overpressure, fuselage Sta. 391 in., right side, Statham gage	7-215
4	Acceleration, fuselage Sta. 661.5 in.	7-225
5	Overpressure, fuselage Sta. 391 in., right side, Wiancko gage	7-223
6	Acceleration, left wing Sta. 576.5 in.	7-225
7	Blank for Shots 1, 2, and 3 Total bending, left stabilizer Sta. 153 in. (Shots 4, 5, 6)	--- 7-215
8	Pressure, fuselage Sta. 1287.5 in., bomb bay differential	7-215
9	Acceleration, left wing Sta. 1052 in.	7-225
10	Blank for Shot 1 Angular acceleration, fuselage Sta. 904 in. (Shots 2, 3, 4, 5, 6)	--- 7-225
11	Pressure, fuselage Sta. 1294.5 in., surface pressure	7-215
12	Acceleration, left wing Sta. 375.5 in.	7-225
13	Pressure, left wing Sta. 1270 in.	7-223
14	Acceleration, fuselage Sta. 1319.5 in.	7-225
15	Overpressure, fuselage Sta. 391 in., left side, Consolidated gage	7-223
16	Angular acceleration, fuselage Sta. 904 in. (Shot 1) Blank for Shots 2 and 3 Total bending, left stabilizer Sta. 224 in. (Shot 4, 5, 6)	7-225 --- 7-215
17	Blank for Shots 1, 2, 3, 4 Temperature, jet engine no. 3 tail pipe (Shots 5, 6)	--- 7-215
18	Voltage monitor, bridge balance no. 3	7-223

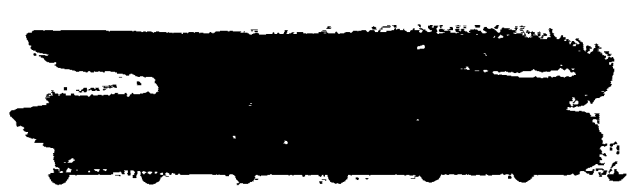

TABLE A.4 - Oscillograph Channel Details, Recorder No. 4

No.	Channel Description	Galvanometer
1	Timing signal, 100 cps sine wave	7-218
2	Radiant exposure no. 2 (Shots 1, 2, 3, 4, and 5) Blank for Shot 6	7-215 ---
3	Bending, right stabilizer Sta. 144 in., front spar	7-215
4	Shear, left stabilizer Sta. 62 in., front spar	7-215
5	Shear, left stabilizer Sta. 62 in., rear spar	7-215
6	Bending, right stabilizer Sta. 62 in., front spar	7-215
7	Bending, right stabilizer Sta. 62 in., rear spar	7-215
8	Shear, right stabilizer Sta. 62 in., front spar	7-215
9	Shear, right stabilizer Sta. 62 in., rear spar	7-215
10	Bending, right stabilizer Sta. 144 in., rear spar	7-215
11	Shear, right stabilizer Sta. 144 in., front spar	7-215
12	Shear, right stabilizer Sta. 144 in., rear spar	7-215
13	Bending, left stabilizer Sta. 62 in., front spar	7-215
14	Bending, left stabilizer Sta. 62 in., rear spar	7-215
15	Bhangmeter timing signal	7-218
16	Blank for Shots 1, 2, and 3 Radar slant range (Shots 4, 5, and 6)	--- 7-215
17	Irradiance no. 3 (Shots 1, 2, 3, 4, and 5) Blank for Shot 6	7-215 ---
18	Voltage monitor, bridge balance no. 4	7-223

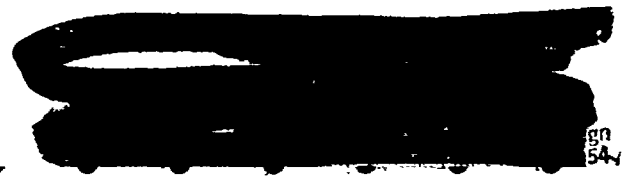

REFERENCES

1. Fink, D. J., General Design Considerations for Aircraft in the Vicinity of a Nuclear Burst, WADC TR 53-238, July 1953, SECRET-RESTRICTED DATA.

2. Levy, L. et al., The Effects of Atomic Explosions on Aircraft, WADC TR 52-244, Volumes I through VII, 1952-1953, SECRET-RESTRICTED DATA.

3. Coulbert, C. D., Ishimoto, T., Problems in Predicting Thermal Radiation from an Atomic Bomb, WADC TR 52-215, April 1953, SECRET-RESTRICTED DATA.

4. Purkey, G. F., Blast Effects on B-36 Type Aircraft in Flight, W.T. 750, Operation UPSHOT-KNOTHOLE, Project 5.3, January 1954, SECRET-RESTRICTED DATA.

5. Coulbert, C. D., O'Brien, P. F., Atmospheric Transmission of Thermal Radiation from Nuclear Weapons to Aircraft, WADC TR 53-212, September 1953, SECRET-RESTRICTED DATA.

6. Streets, L. B., Basic Characteristics of Thermal Radiation from an Atomic Detonation, AFSWP 503, November 1953, SECRET-RESTRICTED DATA.

7. Chapman, R. M., Seavey, M. H., Preliminary Report on the Attenuation of Thermal Radiation from Atomic Weapons, AFCRC-TN 54-25, November 1954, SECRET-RESTRICTED DATA.

8. Ambrosio, A., Bussell, B., MacInnes, W. F., Temperature Distributions in a Typical Aircraft Structure Due to Transient External Heating, WADC TR 52-216, Vol. I, April 1953, UNCLASSIFIED.

9. Ambrosio, A., Ishimoto, T., Temperature Distributions in a Typical Aircraft Structure Due to Transient External Heating, WADC TR 52-216, Vol. II, August 1953, UNCLASSIFIED.

10. Bethe, Hans, Blast Waves, Los Alamos Scientific Laboratory LA-1021, Volume 7, Part 4, August 1947, SECRET-RESTRICTED DATA.

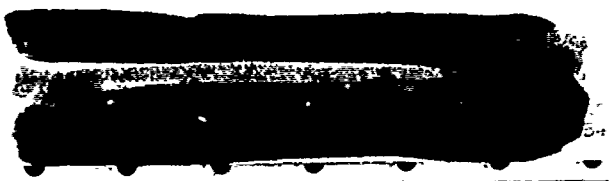

11. Lampson, C. W., Curve of Peak Overpressure Versus Slant Range, Ballistics Research Laboratory LAB-J-57C, 9 December 1949, SECRET-RESTRICTED DATA.

12. Fink, D. J., Kane, J. M., Handbook for the Computation of Dynamic Gust Loads Received by a B-50D Airplane Subjected to the Shock Wave of a Nuclear Explosion, WADC TR 53-176, July 1953, SECRET-RESTRICTED DATA.

13. Broido, A., et al., Thermal Radiation from a Nuclear Detonation, WT-543, Operation TUMBLER-SNAPPER, Project 8.3, March 1953, SECRET-RESTRICTED DATA.

14. Andrews, C. R., Capacitance Welding Technique for the Installation of Thermocouples, WADC TR 53-289, UNCLASSIFIED.

15. Lucier, J., Measurement of Peak Temperatures with Thermal Sensitive Indicators, WADC TR 53-471, June 1954, UNCLASSIFIED.

16. Schlei, E. J., James, G. T., Breidenbach, L. J., Effects of Thermal and Blast Forces from Nuclear Detonations on Basic Aircraft Structures and Components, WT-766, Operation UPSHOT-KNOTHOLE, Project 8.1a, March 1954, SECRET-RESTRICTED DATA.

17. Skopinski, T., Aiken, W., Jr., Huston, W., Calibration of Strain-Gage Installations in Aircraft Structures for the Measurement of Flight Loads, NACA Technical Note 2993, August 1953, UNCLASSIFIED.

18. Hastings Instrument Co., Inc., Hampton, Virginia; literature describing Raydist (Radio location system).

19. Miller, G. C., Data Results, CASTLE, Project 6.2a, WADC Technical Note WCLS-55-10, February 1954, SECRET-RESTRICTED DATA.

20. Gilbert, H. K., Kingsley, N. E., Operation CASTLE, Summary Report of the Commander Task Unit 13, Preliminary Report ITR-934, June 1954, SECRET-RESTRICTED DATA.

21. Los Alamos Scientific Laboratory, The Effects of Atomic Weapons, The Combat Forces Press, Washington, D. C., August 1950, UNCLASSIFIED.

22. Hurty, W. C. et al., Thermal Radiation Measurements at Project IVY, Preliminary Report 53-P3, Operation IVY, February 1953, SECRET-RESTRICTED DATA.

23. Andrews, C. R., Strain Gage Installation Procedures, Memorandum Report UD-102, University of Dayton, May 1954, UNCLASSIFIED.

24. Miller, G. C., Westerheide, J. R., Blast and Thermal Effects on B-36 Aircraft in Flight, Preliminary Report ITR-925, Operation CASTLE, Project 6.2a, May 1954, SECRET-RESTRICTED DATA.

DISTRIBUTION

Military Distribution Categories 5-21 and 5-30

ARMY ACTIVITIES

Asst. Dep. Chief of Staff for Military Operations, D/A, Washington 25, D. C. ATTN: Asst. Executive (R&SW)	1
Chief of Research and Development, D/A, Washington 25, D. C. ATTN: Special Weapons and Air Defense Division	2
Chief of Ordnance, D/A, Washington 25, D. C. ATTN: ORDTX-AR	3
Chief Signal Officer, D/A, P&O Division, Washington 25, D. C. ATTN: SIGOP	4–6
The Surgeon General, D/A, Washington 25, D. C. ATTN: Chief, R&D Division	7
Chief Chemical Officer, D/A, Washington 25, D. C.	8–9
The Quartermaster General, D/A, Washington 25, D. C. ATTN: Research and Development Div.	10
Chief of Engineers, D/A, Washington 25, D. C. ATTN: ENGNB	11–15
Chief of Transportation, Military Planning and Intelligence Div., Washington 25, D. C.	16
Commanding General, Continental Army Command, Ft. Monroe, Va.	17–19
President, Board #1, Headquarters, Continental Army Command, Ft. Sill, Okla.	20
President, Board #2, Headquarters, Continental Army Command, Ft. Knox, Ky.	21
President, Board #3, Headquarters, Continental Army Command, Ft. Benning, Ga.	22
President, Board #4, Headquarters, Continental Army Command, Ft. Bliss, Tex.	23
Commanding General, U. S. Army Caribbean, Ft. Amador, C. Z. ATTN: Cml. Off.	24
Commander-in-Chief, Far East Command, APO 500, San Francisco, Calif. ATTN: ACofS, J-3	25–26
Commanding General, U. S. Army Europe, APO 403, New York, N. Y. ATTN: OPOT Div., Combat Dev. Br.	27–28
Commanding General, U. S. Army Pacific, APO 958, San Francisco, Calif. ATTN: Cml. Off.	29–30
Commandant, Command and General Staff College, Ft. Leavenworth, Kans. ATTN: ALLLS(AS)	31–32
Commandant, The Artillery and Guided Missile School, Ft. Sill, Okla.	33
Secretary, The Antiaircraft Artillery and Guided Missile School, Ft. Bliss, Tex. ATTN: Maj George D. Breitegan, Dept. of Tactics and Combined Arms	34
Commanding General, Army Medical Service School, Brooke Army Medical Center, Ft. Sam Houston, Tex.	35
Director, Special Weapons Development Office, Headquarters, CONARC, Ft. Bliss, Tex. ATTN: Capt T. E. Skinner	36
Commandant, Walter Reed Army Institute of Research, Walter Reed Army Medical Center, Washington 25, D. C.	37
Superintendent, U. S. Military Academy, West Point, N. Y. ATTN: Prof. of Ordnance	38
Commandant, Chemical Corps School, Chemical Corps Training Command, Ft. McClellan, Ala.	39
Commanding General, Research and Engineering Command, Army Chemical Center, Md. ATTN: Deputy for RW and Non-Toxic Material	40–41
Commanding General, Aberdeen Proving Grounds, Md. (inner envelope). ATTN: RD Control Officer (for Director, Ballistic Research Laboratories)	42–43
Commanding General, The Engineer Center, Ft. Belvoir, Va. ATTN: Asst. Commandant, Engineer School	44–46

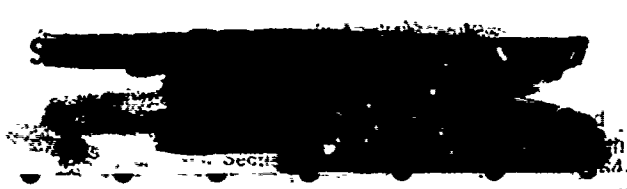

Commanding Officer, Engineer Research and Development Laboratory, Ft. Belvoir, Va. ATTN: Chief, Technical Intelligence Branch 47
Commanding Officer, Picatinny Arsenal, Dover, N. J. ATTN: ORDBB-TK 48
Commanding Officer, Frankford Arsenal, Philadelphia 37, Pa. ATTN: Col. Tewes Kundel 49
Commanding Officer, Army Medical Research Laboratory, Ft. Knox, Ky. 50
Commanding Officer, Chemical Corps Chemical and Radiological Laboratory, Army Chemical Center, Md. ATTN: Tech. Library 51–52
Commanding Officer, Transportation R&D Station, Ft. Eustis, Va. 53
Director, Technical Documents Center, Evans Signal Laboratory, Belmar, N. J. 54
Director, Waterways Experiment Station, PO Box 631, Vicksburg, Miss. ATTN: Library 55
Director, Armed Forces Institute of Pathology, Walter Reed Army Medical Center, 6825 16th Street, N. W., Washington 25, D. C. 56
Director, Operations Research Office, Johns Hopkins University, 7100 Connecticut Ave., Chevy Chase, Md., Washington 15, D. C. 57
Commanding General, Quartermaster Research and Development Command, Quartermaster Research and Development Center, Natick, Mass. ATTN: CBR Liaison Officer 58–60

NAVY ACTIVITIES

Chief of Naval Operations, D/N, Washington 25, D. C. ATTN: OP-36 61–62
Chief of Naval Operations, D/N, Washington 25, D. C. ATTN: OP-03EG 63
Director of Naval Intelligence, D/N, Washington 25, D. C. ATTN: OP-922V 64
Chief, Bureau of Medicine and Surgery, D/N, Washington 25, D. C. ATTN: Special Weapons Defense Div. 65
Chief, Bureau of Ordnance, D/N, Washington 25, D. C. 66
Chief, Bureau of Ships, D/N, Washington 25, D. C. ATTN: Code 348 67–68
Chief, Bureau of Yards and Docks, D/N, Washington 25, D. C. ATTN: D-440 69
Chief, Bureau of Supplies and Accounts, D/N, Washington 25, D. C. 70
Chief, Bureau of Aeronautics, D/N, Washington 25, D. C. 71–72
Chief of Naval Research, Department of the Navy, Washington 25, D. C. ATTN: Code 811 73
Commander-in-Chief, U. S. Pacific Fleet, Fleet Post Office, San Francisco, Calif. 74
Commander-in-Chief, U. S. Atlantic Fleet, U. S. Naval Base, Norfolk 11, Va. 75
Commandant, U. S. Marine Corps, Washington 25, D. C. ATTN: Code A03H 76–79
President, U. S. Naval War College, Newport, R. I. 80
Superintendent, U. S. Naval Postgraduate School, Monterey, Calif. 81
Commanding Officer, U. S. Naval Schools Command, U. S. Naval Station, Treasure Island, San Francisco, Calif. 82
Commanding Officer, U. S. Fleet Training Center, Naval Base, Norfolk 11, Va. ATTN: Special Weapons School 83
Commanding Officer, U. S. Fleet Training Center, Naval Station, San Diego 36, Calif. ATTN: (SPWP School) 84
Commanding Officer, Air Development Squadron 5, VX-5, U. S. Naval Air Station, Moffett Field, Calif. 85
Commanding Officer, U. S. Naval Damage Control Training Center, Naval Base, Philadelphia 12, Pa. ATTN: ABC Defense Course 86
Commanding Officer, U. S. Naval Unit, Chemical Corps School, Army Chemical Training Center, Ft. McClellan, Ala. 87
Commander, U. S. Naval Ordnance Laboratory, Silver Spring 19, Md. ATTN: EE 88
Commander, U. S. Naval Ordnance Laboratory, Silver Spring 19, Md. ATTN: EH 89
Commander, U. S. Naval Ordnance Laboratory, Silver Spring 19, Md. ATTN: R 90
Commander, U. S. Naval Ordnance Test Station, Inyokern, China Lake, Calif. 91
Officer-in-Charge, U. S. Naval Civil Engineering Res. and Evaluation Lab., U. S. Naval Construction Battalion Center, Port Hueneme, Calif. ATTN: Code 753 92
Commanding Officer, U. S. Naval Medical Research Inst., National Naval Medical Center, Bethesda 14, Md. 93
Director, Naval Air Experimental Station, Air Material Center, U. S. Naval Base, Philadelphia, Pa. 94
Director, U. S. Naval Research Laboratory, Washington 25, D. C. ATTN: Mrs. Katherine H. Cass 95

Director, The Material Laboratory, New York Naval Shipyard, Brooklyn, N. Y. 96
Commanding Officer and Director, U. S. Navy Electronics Laboratory, San Diego 52, Calif. ATTN: Code 4223 97
Commanding Officer, U. S. Naval Radiological Defense Laboratory, San Francisco 24, Calif. ATTN: Technical Information Division 98–101
Commanding Officer and Director, David W. Taylor Model Basin, Washington 7, D. C. ATTN: Library 102–103
Commander, U. S. Naval Air Development Center, Johnsville, Pa. 104
Commanding Officer, Clothing Supply Office, Code 1D-0 3rd Avenue and 29th St., Brooklyn, N. Y. 105

AIR FORCE ACTIVITIES

Asst. for Atomic Energy, Headquarters, USAF, Washington 25, D. C. ATTN: DCS/O 106
Director of Operations, Headquarters, USAF, Washington 25, D. C. ATTN: Operations Analysis 107
Director of Plans, Headquarters, USAF, Washington 25, D. C. ATTN: War Plans Div. 108
Director of Research and Development, Headquarters, USAF, Washington 25, D. C. ATTN: Combat Components Div. 109
Director of Intelligence, Headquarters, USAF, Washington 25, D. C. ATTN: AFOIN-IB2 110–111
The Surgeon General, Headquarters, USAF, Washington 25, D. C. ATTN: Bio. Def. Br., Pre. Med. Div. 112
Deputy Chief of Staff, Intelligence, Headquarters, U. S. Air Forces Europe, APO 633, New York, N. Y. ATTN: Directorate of Air Targets 113
Commander, 497th Reconnaissance Technical Squadron (Augmented), APO 633, New York, N. Y. 114
Commander, Far East Air Forces, APO 925, San Francisco, Calif. 115
Commander-in-Chief, Strategic Air Command, Offutt Air Force Base, Omaha, Nebr. ATTN: Special Weapons Branch, Inspector Div., Inspector General 116
Commander, Tactical Air Command, Langley AFB, Va. ATTN: Documents Security Branch 117
Commander, Air Defense Command, Ent AFB, Colo. 118
Commander, Wright Air Development Center, Wright-Patterson AFB, Dayton Ohio. ATTN: WCRRN, Blast Effects Research 119–120
Commander, Air Research and Development Command, PO Box 1395, Baltimore, Md. ATTN: RDDN 121
Commander, Air Proving Ground Command, Eglin AFB, Fla. ATTN: Adj./Tech. Report Branch 122
Director, Air University Library, Maxwell AFB, Ala. 123–124
Commander, Flying Training Air Force, Waco, Tex. ATTN: Director of Observer Training 125–132
Commander, Crew Training Air Force, Randolph Field, Tex. ATTN: 2GTS, DCS/O 133
Commandant, Air Force School of Aviation Medicine, Randolph AFB, Tex. 134–135
Commander, Wright Air Development Center, Wright-Patterson AFB, Dayton, Ohio. ATTN: WCOSI 136–141
Commander, Air Force Cambridge Research Center, LG Hanscom Field, Bedford, Mass. ATTN: CRQST-2 142–143
Commander, Air Force Special Weapons Center, Kirtland AFB, N. Mex. ATTN: Library 144–146
Commandant, USAF Institute of Technology, Wright-Patterson AFB, Dayton, Ohio. ATTN: Resident College 147
Commander, Lowry AFB, Denver, Colo. ATTN: Department of Armament Training 148–149
Commander, 1009th Special Weapons Squadron, Headquarters, USAF, Washington 25, D. C. 150
The RAND Corporation, 1700 Main Street, Santa Monica, Calif. ATTN: Nuclear Energy Division 151–152
Commander, Second Air Force, Barksdale AFB, La. ATTN: Operations Analysis Office 153
Commander, Eighth Air Force, Westover AFB, Mass. ATTN: Operations Analysis Office 154
Commander, Fifteenth Air Force, March AFB, Calif. ATTN: Operations Analysis Office 155
Commander, Western Development Div. (ARDC), P. O. Box 262, Inglewood, Calif. ATTN: WDSIT, Mr. R. G. Veitz 156

[redacted]

OTHER DEPARTMENT OF DEFENSE ACTIVITIES

Asst. Secretary of Defense, Research and Development, D/[illegible], Washington 25, D. C. ATTN: Tech. Library. 157

U. S. Documents Officer, Office of the U. S. National Military Representative, SHAPE, APO 55, New York, N. Y. 158

Director, Weapons Systems Evaluation Group, OSD, Rm 2E1006, Pentagon, Washington 25, D. C. 159

Armed Services Explosives Safety Board, D/D, Building T-7, Gravelly Point, Washington 25, D. C. 160

Commandant, Armed Forces Staff College, Norfolk 11, Va. ATTN: Secretary 161

Commanding General, Field Command, Armed Forces Special Weapons Project, PO Box 5100, Albuquerque, N. Mex. 162–167

Commanding General, Field Command, Armed Forces Special Weapons Project, PO Box 5100, Albuquerque, N. Mex. ATTN: Technical Training Group 163–169

Chief, Armed Forces Special Weapons Project, Washington 25, D. C. ATTN: Documents Library Branch 170–178

ATOMIC ENERGY COMMISSION ACTIVITIES

U. S. Atomic Energy Commission, Classified Technical Library, 1901 Constitution Ave., Washington 25, D. C. ATTN: Mrs. J. M. O'Leary (for DMA) 179–181

Los Alamos Scientific Laboratory, Report Library, PO Box 1663, Los Alamos, N. Mex. ATTN: Helen Redman 182–183

Sandia Corporation, Classified Document Division, Sandia Base, Albuquerque, N. Mex. ATTN: Martin Lucero 184–188

University of California Radiation Laboratory, PO Box 808, Livermore, Calif. ATTN: Margaret Edlund 189–191

Weapon Data Section, Technical Information Service Extension, Oak Ridge, Tenn. 192

Technical Information Service Extension, Oak Ridge, Tenn. (surplus) 193–220

[redacted]